ISBN 978-82-471-9306-8 (printed ver.)
ISBN 978-82-471-9323-5 (electronic ver.)
ISSN 1503-8181

Viggo Lauritz Norum

Doctoral Thesis

Doctoral Theses at NTNU, 2008:160

Viggo Lauritz Norum

Analysis of Ignition and Combustion in Otto Lean-Burn Engines with Prechambers

NTNU
Norwegian University of
Science and Technology

Theses at NTNU, 2008:160

NTNU

NTNU
Norwegian University of
Science and Technology
Thesis for the degree of
doktor ingeniør
Faculty of Engineering Science and Technology
Department of Marine Technology

NTNU
Norwegian University of
Science and Technology

Viggo Lauritz Norum

Analysis of Ignition and Combustion in Otto Lean-Burn Engines with Prechambers

Thesis for the degree of doktor ingeniør

Trondheim, June 2008

Norwegian University of
Science and Technology
Faculty of Engineering Science and Technology
Department of Marine Technology

NTNU
Norwegian University of
Science and Technology

NTNU
Norwegian University of Science and Technology

Thesis for the degree of doktor ingeniør

Faculty of Engineering Science and Technology
Department of Marine Technology

ISBN ISBN 978-82-471-9306-8 (printed ver.)
ISBN ISBN 978-82-471-9323-5 (electronic ver.)
ISSN 1503-8181

Theses at NTNU, 2008:160

Printed by Tapir Uttrykk

Analysis of Ignition and Combustion in Otto Lean-Burn Engines with Prechambers

Viggo L. Norum

May 6, 2008

Abstract

Otto-engines in which the combustion chamber has richer fuel/air mix close to the ignition source and leaner charge further away from the ignition source are often called "stratified charge engines". Stratified charge can be used to increase the combustion speed in an internal combustion engine and thereby enable the engine to run on a fuel/air mix that would normally burn too slowly or not burn at all. The use of prechambers is one way to obtain stratified charge.

This thesis presents and uses methods for studying a prechamber more or less independently from the rest of the engine.

When the prechamber is studied like an engine of itself, then the output of the "engine" is not mechanical power, but rather one or more hot jets into the main chamber. "Prechamber efficiencies" can be defined based on how much of the initial chemical energy is delivered as kinetic or thermal energy into the main chamber. Models of other important characteristics including the jet length and duration are also presented and used.

Acknowledgments

Advisor: Thanks to my advisor; Prof. Harald Valland for help and support during all stages of the study. In particular thanks for not pushing too hard during times when studying prechambers seemed to be the least interesting thing to do.

During the time of the study I have worked 10 years with design of automotive transmissions and robotic actuators at the companies "LuK Norge AS" and "Kongsberg Devotek AS" in addition to getting married, building a house and getting three kids.

Helpers: Thanks to Dr.Ing. students at the department of marine engineering, NTNU. Thanks to Dr.Ing. Tor Øyvind Ask and Dr.Ing. Vilmar Æsøy for ideas to the constant volume combustion rig with prechamber. Thanks to Dr.Ing. Hallvard Paulsen for help with reluctant computers and for help with the optical equipment used with the constant volume combustion rig. Thanks to Dr.Ing. Rune Nordrik at Ulstein Bergen / Rolls-Royce Marine for help getting started with the study.

Thanks to "Christian Michelsen Research" in Bergen, for making their highly advanced camera available.

Thanks to the laboratory staff at Marintek for building the CVC-rig and for instrumenting and operating the medium speed engine.

Thanks to my wife Elisabeth.

Funding: Thanks to Ulstein Bergen / Rolls-Royce Marine — the only internal combustion engine manufacturer still producing Diesel and Otto engines in Norway, and to The Norwegian Research Council for providing financial funding for this work.

Contents

List of Figures

List of Tables

Nomenclature

$\dot{m}$	Mass flow [kg/s]
c_v	Specific heat capacity at constant volume [J/(kg K)]
E_{pi}	Thermal energy delivered to the prechamber jet
E_{pk}	Kinetic energy [J] delivered to the prechamber jet
h	Specific enthalpy [J/kg]
h_c	Specific enthalpy of combustion [J/kg]
h_{jet}	Stagnation enthalpy of gas leaving the nozzle, relative to the gas in the main chamber
HR	Accumulated net heat release [J]
L_{jet}	Length [m] of hot jet
m	Mass [kg]
$\dot{m}_{noz}$	Mass flow through the prechamber nozzle [kg/s]
p	Pressure [Pa]
P_{pk}	Kinetic power [W] delivered to the prechamber jet
P_{pt}	Thermal power delivered to the prechamber jet
$ROHR_c$	Characteristic net rate of heat release [W]
T	Temperature [K]

t	Time
$t_{p>}$	Time when the prechamber pressure becomes larger than the pressure in the main chamber.
u	Specific internal energy [J/kg]
v_{noz}	Velocity [m/s] of flow at exit of nozzle
BMEP	Brake mean effective pressure
CFD	Computational Fluid Dynamics
LHV	Lower heating value of a fuel or a fuel/air mix [J/kg]
MCR	Maximum continuous rating
α	Shape parameter for heat release
η_k	Prechamber kinetic efficiency [-]
η_t	Prechamber thermal efficiency [-]
λ	Air/fuel mass ratio relative to stoichiometric air/fuel ratio
$_{1,\ 2}$	Zones in the the two zone model
$_c$	Combusted
$_j$	Jet
$_m$	Main combustion chamber
$_p$	Prechamber
$_u$	Uncombusted (not yet combusted)

Chapter 1

Introduction

1.1 Background

Internal combustion engines continue to be the best alternative for a number of power generation applications. This thesis "Analysis of ignition and combustion in Otto lean burn engines with prechambers" is a contribution to the development of more efficient and more environmental friendly internal combustion engines.

This study focuses on the performance of prechambers used in internal combustion engines burning a very lean charge (much air and little fuel). The process inside the prechamber is very essential to understand in order to be able to design a good internal combustion engine of this type.

Very lean premixed charge gives lower peak combustion temperature and less NO_x. The use of prechambers is one way to achieve stable and fast combustion of very lean charge.

1.2 Objective of this thesis

Objective #1: To define variables that describes the performance of prechambers — so that it will be easier to study the prechamber independently from the rest of the internal combustion engine. Such performance variables should quantify:

- **The desired output** of the prechamber.
- **Efficiency,** that is ratio of desired output per invested input.
- **Harmful bi-products** of the process of converting the invested input to the desired output.

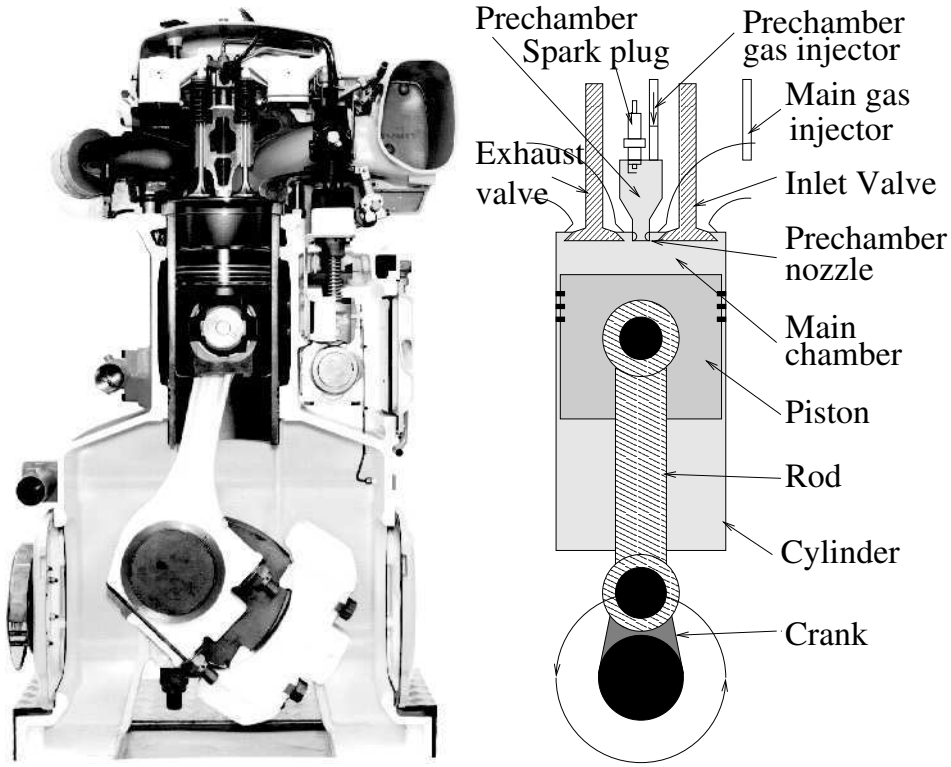

Figure 1.1: Cut away photo of a medium speed engine to the left. Schematic internal parts of an Otto lean burn engine with prechamber to the right. The prechamber is drawn larger than in real engines for illustration purposes. The cylinder diameter of the engine in the picture is 280 mm.

Objective #2: Use experiments with engine and combustion rig to investigate the the validity of the defined performance variables.

Objective #3: To explore how the performance of prechambers is influenced by the geometry. For example: What happens to the performance of the prechamber if the ignition source is moved closer to the nozzle than what is indicated in figure 1.1.

1.3 Lean burn at high load

Using very lean charge and getting much power out of the engine may seem like a contradiction, but it is possible when using turbo charging.

The main components of air is nitrogen and oxygen — two gases which are harmless and vital when they occur in the form of a mix of gaseous N_2 and O_2 in air. Combustion at very high temperatures, as is normally the

case in internal combustion engines, cause reactions between nitrogen and oxygen, resulting in nitrogen oxides NO_x. Nitrogen oxides are toxic and cause environmental damages.

One way to reduce the production of NO_x is to lower maximum combustion temperature. Lowering the maximum temperature can be done by reducing the fraction of fuel in the charge, and by burning a well mixed charge. Otto engines burn pre-mixed charge, while in Diesel engines the fuel and air is mixed during the combustion. The phrase "*Otto lean burn engine with prechamber*", as used in the title of this thesis, refers to piston engines burning a charge consisting of air and a very small fraction of fuel — relative air/fuel ratio λ of approx. 2 or higher. Leaner charge gives lower combustion temperature.

The primary reason for using lean combustion in stead of stoichiometric at high engine load is to:

- Reduce the maximum temperature of combustion and thus reduce the emissions of nitrogen oxides and other harmful products.

Lean combustion also implies some advantages besides lower NO_x emissions:

- Less problems with knocking combustion, the potential of turbo charging thereby increases. Lowering the fuel fraction in the charge while maintaining the same charge pressures would lower the output power of the engine. Increasing the charge pressure compensates for the lower fuel fraction.

- The engine power can be regulated more with fuel supply in stead of throttling. The scavenging loss at part load can thereby be reduced. This is currently the main reason for using lean combustion in automotive engines.

- Less thermal load on critical engine components.

There are also some fundamental problems associated with lean combustion:

- It is difficult to ignite a lean mixture. A lean mixture requires more ignition energy than a stoichiometric mixture.

- The flame speed is lower in lean charges than in stoichiometric charges. This implies a risk for insufficient combustion time and uncompleted combustion. This increases emissions of hydrocarbon and carbon monoxide.

- Exploitation of the increased turbo charging potential must be done with care. If the charge pressure should drop (e.g. due to change in engine load, compressor surge or other reasons), then the fuel delivery must be reduced simultaneously, in some cases very quickly, in order to avoid knocking combustion.

1.4 Prechamber and lean combustion

Very lean charge is so hard to ignite and burns so slowly that one need a more powerful ignition source than a conventional spark plug. A prechamber in an Otto engine works like an amplifier for the spark plug and cause ignition to occur almost simultaneously over a larger volume in the main combustion chamber. See figure 1.1 for an introduction to the internal parts of an Otto lean burn engine with prechamber.

The work process of an Otto engine with prechamber is shown in figure 1.2. The prechamber is filled with a very rich charge (often pure fuel if the fuel is in gas phase) during the intake stroke, see figure 1.2(1). The gas in the prechamber is diluted into an easily ignitable mix when lean charge from the main chamber is pressed into the prechamber during the compression stroke, see figure 1.2(3). The combustion in the prechamber rises the temperature and pressure inside the prechamber. The higher pressure causes jets of warm/burning gas to flow into the main chamber and ignite the lean main charge, see figure 1.2(4). Figure 1.3 also shows this, but with a simpler geometry of the combustion chambers.

The flow through the prechamber nozzles changes direction during combustion in the main chamber as shown in figure 1.2(5), and it changes direction again during the expansion stroke as shown in figure 1.2(6).

Lean charges burn slowly and there is only a limited time available to complete the combustion before the piston goes too far down or the remaining fuel/air mixture auto-ignites with a bang (as in knocking combustion).

Otto engines with prechambers are sometimes called “fast burn engines” due to the dramatic effect prechambers have on the combustion speed.

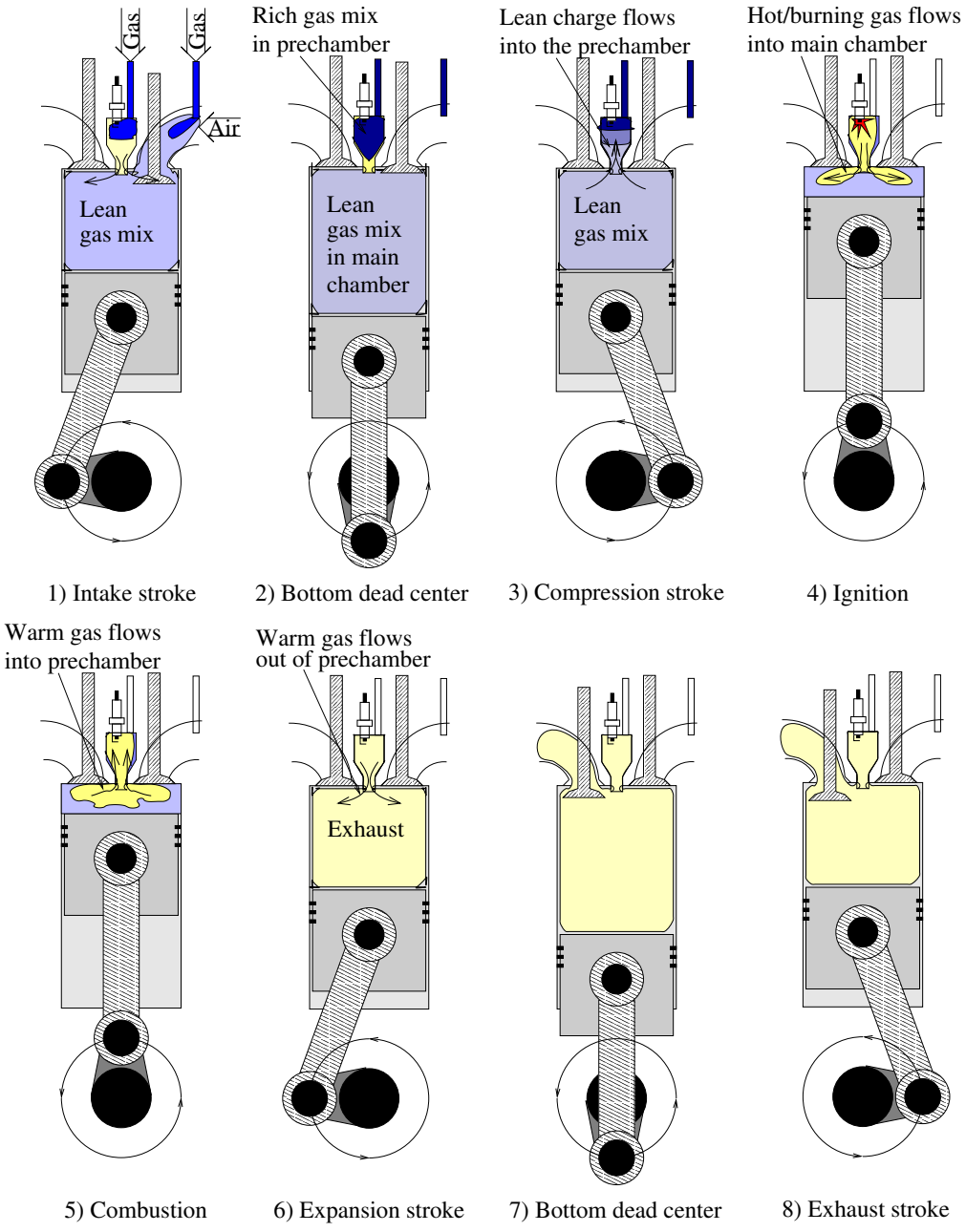

Figure 1.2: The process inside an Otto lean burn engine with prechamber. One can see that the flow through the nozzle shifts direction several times during a four stroke cycle.

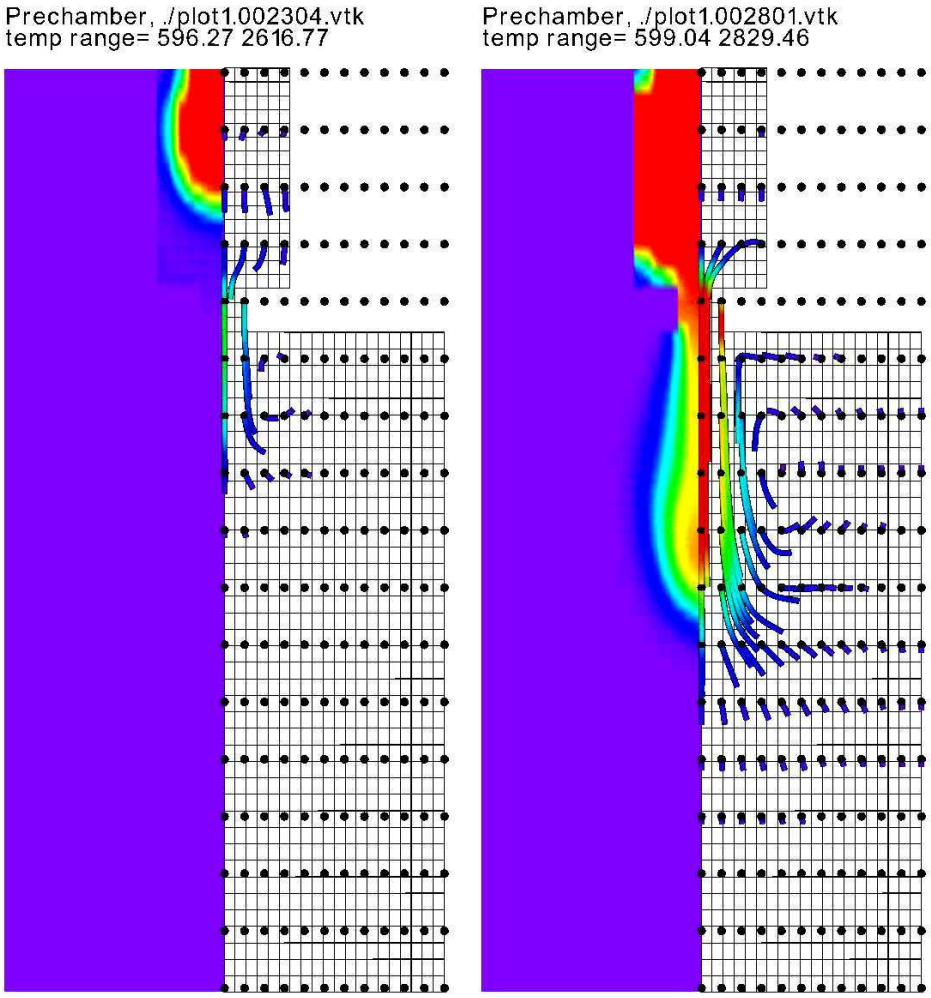

Figure 1.3: Temperature and velocity of flow in an axis-symmetrical combustion chamber with prechamber (upper square), a single nozzle and main chamber (lower square). The temperature is shown as colors in the left parts of the chambers and nozzle, while the flow is shown as streamlines in the right parts. The length and color of the streamlines vary with the velocity. In the first stages of the combustion there is only combustion within the prechamber (left illustration). Later, the combustion reaches the nozzle, and the jet temperature increases (right figure). The figures are made on basis of preliminary CFD results and should only be used as illustrations, not as exact facts. In particular the temperature range is wrong as real gas properties are not used.

Chapter 2

Literature study of prechambers

2.1 Introduction

This chapter will start with a short historical summary of prechambers in order to get familiar the terminology and learn how prechambers are used.

After the historical summary follows section 2.3 with a description of the work cycle in a 4-stroke prechamber engine from air intake through combustion to exhaust stroke with references to literature with more details about observed phenomena in the work cycle.

Finally follows introduction to mathematical modeling techniques known from literature, in particular some that are to be used later in this thesis.

2.2 Evolution of prechambers

One of the main challenges when making internal combustion engines is to get a quick and controlled combustion. Prechambers have been used as a means to increase the combustion rate. Three main types of prechambers have been used throughout the history [Heywood, 1988, p447]. The prechamber types are presented in figure 2.1.

The earliest stratified charge engines with prechamber found in literature is an engine made by Harry R. Ricardo, see figure 2.2, the engine is described in patents and in a SAE paper [Ricardo, 1922].

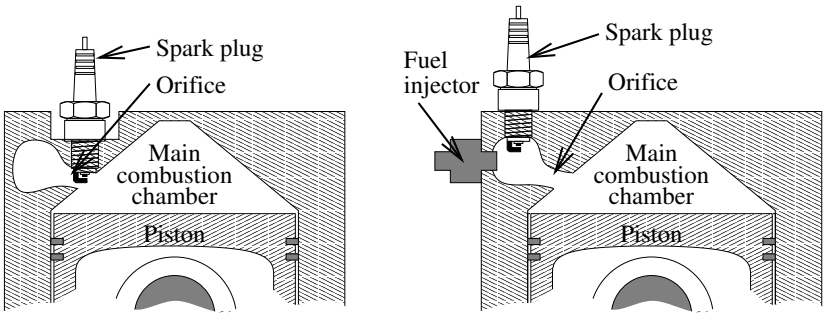

a) Turbulence generating torch cell

b) Auxiliary fuel injector, no scavenging

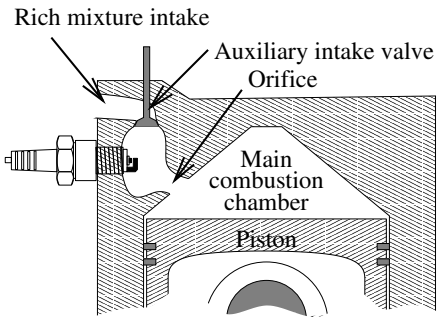

c) With auxiliary intake valve

Figure 2.1: Types of prechambers

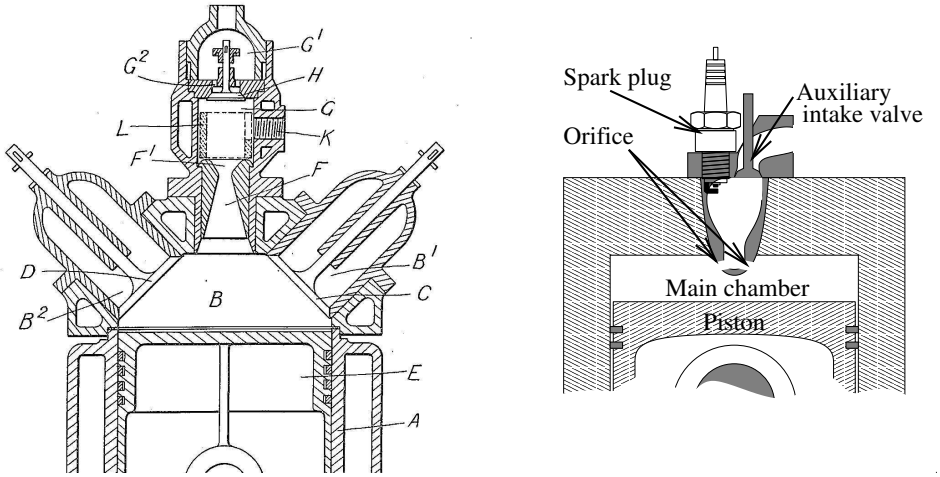

Figure 2.2: To the left: Ricardo's cylinder head of a stratified charge engine, drawing from U.S. patent 1,271,942 filed February 1916. To the right: Recent, centrally placed prechamber with "pepper pot" nozzle, this prechamber is drawn larger than actual size (it should be smaller compared to the piston size).

Ricardo's engine has several striking similarities with current engines, see figure 2.2:

- Centrally placed prechamber with spark plug.
- The auxiliary intake valve is a plain one-way valve operated by the pressure difference between the auxiliary intake manifold and the combustion chambers.

Some of the main differences between Richardo's engine and a modern engine used for electric power generation are:

- Modern prechamber engines are normally turbocharged. Turbocharging compensates for the low heating value of the lean charge.
- One important discovery was reported by Gussak et al. [1963]: Sharp edges of the nozzle make extra turbulence and faster combustion. Modern prechambers seem to have sharp edged nozzles while Ricardo's used an aerodynamically shaped nozzle. Using several smaller nozzles in stead of one larger nozzle enhances this effect. This type of nozzles are also called "pepper pot nozzle" for obvious reasons.
- New prechambers are generally smaller.

- The use of gaseous fuel in prechamber engines solves a couple of Ricardo's problems:

    1. There will be no problem evaporating the fuel in the rich mixture in the prechamber. No auxiliary carburetor is needed — pure fuel can be supplied through the auxiliary valve.
    2. As the gaseous fuel supply has higher pressure than the charge air pressure there is no need for retained intake valve opening to develop the required pneumatic forces to open the auxiliary intake valve.

The recent development of prechambers targets to optimize towards smaller prechambers. It is desirable to make prechambers as small as possible due to the negative impact prechambers have on the efficiency of the engine (increased heat loss) and formation of pollutants due to high combustion temperature inside the prechamber. Simultaneously the development of the main combustion charge goes towards leaner mixtures for the reasons of reducing pollution. As the prechambers are becoming smaller, the energy in the prechamber jets are reduced, but at the same time the charge is becoming leaner and more energy is needed to ignite it.

2.3 Following the process inside the engine

2.3.1 Intake stroke

At the beginning of the intake stroke, both the prechamber and the main chamber contain a mix of exhaust and charge. If the ratio of nozzle area / prechamber volume is small, then the prechamber can be assumed to contain only exhaust. During the intake stroke the prechamber is filled with a rich charge and the main chamber is filled with a lean charge. This filling sets up a flow field inside in both chambers. The shapes and magnitude of the flow field depends on the internal geometry of the engine and the engine speed. The properties and state of the charge and the exhaust back pressure also influences the flow field.

The large scale motions named "swirl" and "tumble", that is circulating flows about a vertical and a horizontal axis respectively (assuming vertical cylinder), see figure 2.4. Swirl and tumble is normally assumed to prevail throughout the compression and affect the combustion.

Some lean burn engines use a main gas valve which is open during only a fraction of the intake stroke, the charge in the main chamber of those engines will have large spatial variations in air fuel ratio. In large scale analyzes (i.e.

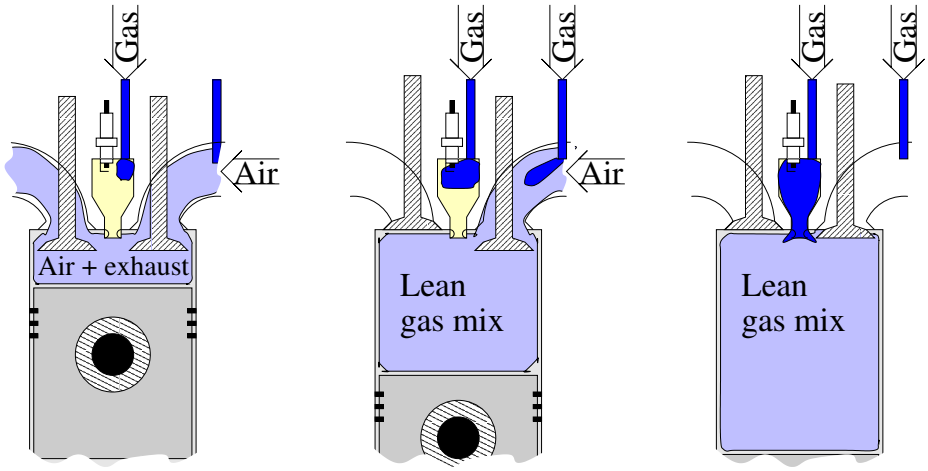

Figure 2.3: The intake stroke of the Otto engine with prechamber

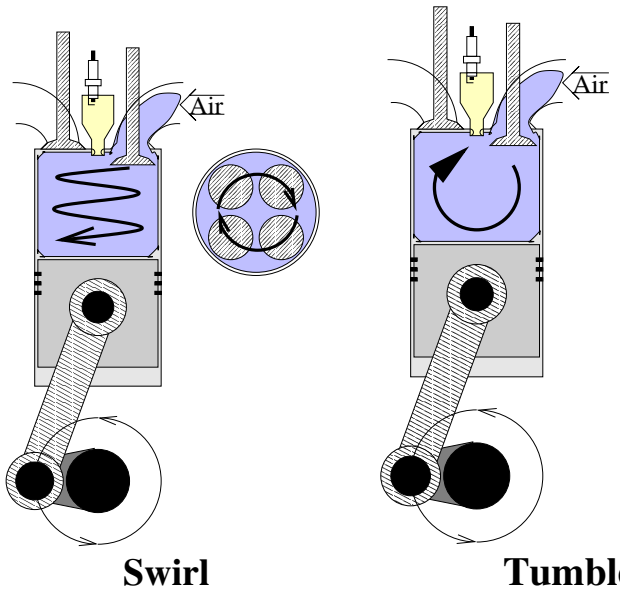

Figure 2.4: Schematic swirl and tumble motions during intake stroke.

one and two zone models) it is often assumed that these inhomogeneities disappear during the compression. Some engine types which can grouped under the name "stratified charge engines", exploit the variations in air fuel ratio to large degree, the same is valid for prechamber engines. The assumption of homogeneous charge is thus inadequate both for stratified charge engines and engines with prechamber. On the other hand, some models assume homogeneous charge in the prechamber, and a different but also homogeneous charge in the main chamber [Hires et al., 1976].

When using turbo or compressor charging, the main charge is normally cooled before entry into the combustion chamber in order to avoid knocking combustion. The rich prechamber charge on the other hand is in some cases heated before entry in order to give faster combustion in the prechamber, this can be done because knocking combustion in the prechamber is less likely to occur as the combustion pressure and temperature is reduced as gas flow out the nozzle. The temperature in the prechamber is also reduced by heat conduction to the prechamber walls, this cooling effect is large due to the small size of prechambers. Some prechamber designs have a prechamber liner insulated from the body of the cylinder head in order to reduce the cooling of the prechamber charge.

2.3.2 Compression stroke

The compression cause flow from the main chamber into the prechamber. Experience and common sense have shown that the lean charge flowing into the prechamber during the compression should be directed away from the spark plug in order to provide an ignitable mix in the vicinity of the spark.

Another method providing fast combustion in the prechamber is to direct the nozzle(s) so that a that a high degree of swirl and / or tumble is introduced in the prechamber.

Wolff et al. [1997] use an experimental setup with a constant volume combustion rig with a transparent quartz prechamber to study the flow and mixing inside the prechamber.

Dexter and Ennemoser [1995] use CFD to calculate the flow in the prechamber during the compression. Nordrik et al. [1989] (unpublished?) also describes and presents a CFD program to calculate the flow and mixing in prechambers.

Experience has shown that the mixing process inside the prechamber during the compression stroke has large influence on the performance when running on very lean charge. Dexter and Ennemoser [1995] shows that tumble flows in the main chamber induce a flow pattern inside the prechamber and how this flow pattern govern the blending process inside a symmetric

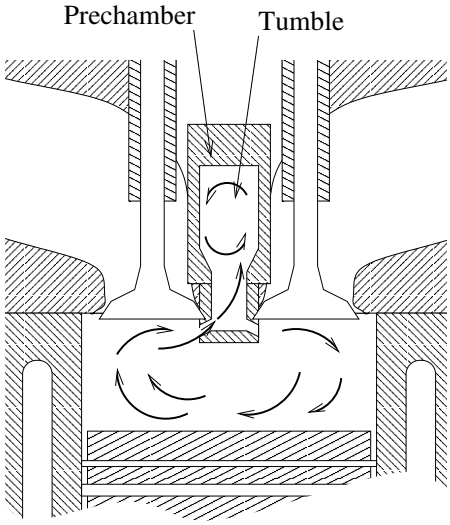

Figure 2.5: Schematic induced tumble in a symmetric prechamber during compression stroke.

centrally placed prechamber with a "pepper pot" type nozzle (a very commonly used type of prechamber), see figure 2.5. It is also shown that a change in the inlet angle of the fuel into the prechamber may more or less revert the tumble flow.

2.3.3 Ignition in the prechamber

The spark ignition follows the same thermodynamic laws in prechambers as in most SI engines, but the the mixture inside the prechamber often has larger spatial variations in Air/Fuel ratio than is normally found in SI engines. Models for the ignition process are described in (for example) Griffiths and Barnard [1995], Glassman [1996] and Nordrik [1993].

The spark causes a small flame kernel with high temperature. The initial flame growth is governed by heat release by combustion and heat transfer from the combustion products to both a "preheat zone" in the fuel/air mixture and to the electrodes of the spark plug.

A minimum ignition energy E_{min} is needed in order to initiated the combustion. E_{min} can be estimated as:

$$E_{min} = \pi d_q^2 \frac{\kappa}{S_u}(T_b - T_u). \tag{2.1}$$

Where d_q is the quenching distance, κ is the heat transfer coefficient, S_u is

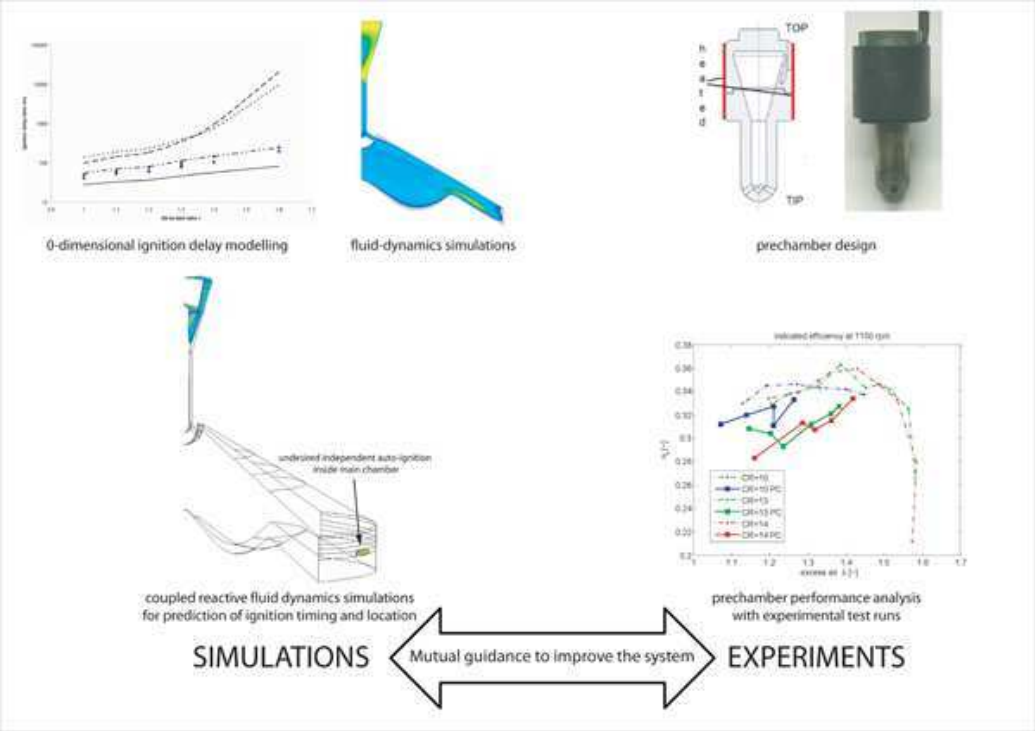

Figure 2.6: Poster published on Internet by Heyne Stefan at "Industrial Energy Systems Laboratory (LENI)" under the title "Prechamber Auto-Ignition in Stationary Gas Engines"

the laminar burn speed, T_b is the temperature of the combustion products and T_u is the temperature of the fuel/air mixture.

Recent research on NO_x-reduction in automotive engines [Lavy et al., 2000] and others have published that controlled auto ignition (CAI) or Homogeneous Charge Compression-Ignition (HCCI) can give a reduction of NO_x by a factor between 10 and 100. Auto-ignition inside the prechamber of stationary gas engines is also being developed, see for example figure 2.6 or Wunsch et al. [2007]. The temperature of the walls in the prechamber (and maybe also the nozzle and the residual exhaust gas inside the prechamber?) elevates the temperature inside the prechamber so that auto ignition occurs inside the prechamber and not at the exhaust valve or at the main chamber's side of the prechamber nozzle. Maybe this could be combined with heat capacitive prechamber lining similar to what was present in some of Richardo's first prechambers.

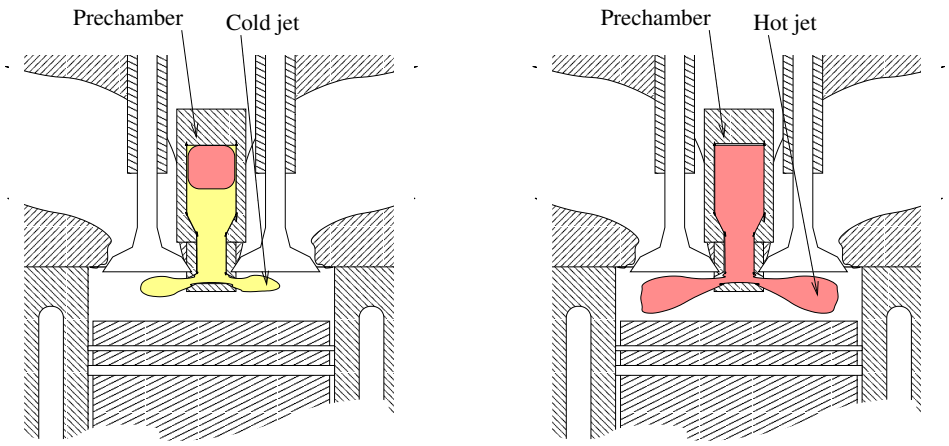

Figure 2.7: The the charge in the prechamber burns and sends first jets of uncombusted charge, then warm / burning jets into the main chamber.

2.3.4 Ignition in main combustion chamber

As the combustion in the prechamber transforms chemically stored energy into thermal energy, the pressure in the prechamber will increase.

Let $t_{p>}$ define the time at which the pressure in the prechamber becomes higher than the pressure in the main chamber. At this time (or after a negligible delay), the flow through the nozzle shifts direction and the desired jet into the main chamber is thereby started.

At a certain time, t_{fn} the flame front will reach the nozzle. From $t_{p>}$ until t_{fn}, the jet will consist of "cold" charge, after t_{fn} one may assume that the jet consist of warm combustion products. See figure: 2.7.

Little relevant literature is found within the subject of "ignition by a hot reacting jet in internal combustion engines", but more peripheral articles can be found, for example: Phillips [1972] is about ignition of a premixed charge by a transient turbulent jet of hot inert gas, it describes experiments is at atmospheric conditions and considers safety and "safe gaps" to avoid ignition. In despite of it's intended application, both the time scale and size are not far off those in an engine, and also the presented Schlieren pictures in [Phillips, 1972] show a high degree of similarity with pictures presented in chapter 6 of this thesis.

2.3.5 Combustion in the main chamber

There are two pressure peaks in the prechamber for each combustion cycle. Two pressure peaks may also cause two peaks of high temperature in the

prechamber. The first peak is during combustion in the prechamber, the other peak is during combustion in the main chamber. As the charge in the main chamber burns, the pressure in the main chamber increases and cause flow into the prechamber though the nozzles.

2.4 Formation of nitrogen oxides

The main reason for using a very lean charge in the combustion is to reduce the NO_x. Chemical formulas and reaction rates from literature shows that the formation of NO_x deepens on temperature level and duration at high temperature.

Very lean premixed charge gives lower peak combustion temperature and less NO_x. The use of prechambers is one way to achieve stable and fast combustion of very lean charge, but the combustion in the prechamber is done at high temperatures and is (at least for some engines) found to be the main source of NO_x in lean burn engines with prechamber. Both Hires et al. [1976] and Chrisman and Freen [1994] report that the majority of NO_x is formed in the prechamber (not in the main combustion chamber) when the relative air/fuel ratio λ in the main chamber is high.

The NO_x-reactions become slower as the temperature sinks during the expansion stroke. Hires et al. [1976] use 1800 K as the temperature for full freeze of NO_x-reactions.

It is common practice, and in some cases also required according to international regulations, to calculate the mass of NO_x as if every NO_x-molecule is NO_2.

2.5 Cycle by cycle variations

Spark ignition engines (and also auto-ignited engines) are known for having cycle by cycle variations to the cylinder pressure [Heywood, 1988]. Heywood gives three reasons for cycle by cycle variations, quote:

1. The variations in gas motion in the cylinder during combustion, cycle-by-cycle

2. The variations in the amounts of fuel, air, and recycled exhaust gas supplied to a given cylinder each cycle

3. Variations in mixture composition within the cylinder each cycle — especially near the spark plug — due to variations in mixing between air, fuel, recycled exhaust gas, and residual gas

Cycle by cycle variations are very undesired. The cycle by cycle variations are expected to increase with a) leaner charge, b) more inhomogeneous charge, c) less spark energy and d) lower temperature.

Cycle by cycle variations can be observed in experimental studies with a lean burn engine with prechamber in section 5.4 and with a constant volume combustion rig in section 6.3 of this thesis.

2.6 Summary of prechamber experience

We have now had a look at historical prechambers and followed the process inside the engine from the intake stroke to the combustion in the main combustion chamber. Along the way we have learned that:

- Very fast combustion of the prechamber charge is essential. The methods to achieve this include:
  - The charge in the prechamber should be warm, either as a result of the nozzle being hot and heating the lean charge flowing into the prechamber, and / or as a result of preheating the rich charge, and / or as a result using isolating liner inside the prechamber.
  - The mixture in the vicinity of the spark is essential. Direct the lean flow into the prechamber during the compression away from the spark plug.
  - The turbulence inside the prechamber is important, the more turbulence the faster combustion. The flow into the prechamber during the scavenging and compression strokes should be used to increase the turbulence. Sharp edges on the nozzles makes more turbulence in the prechamber.
- The jets should reach far into the main combustion chamber so that the flames have a shorter way to propagate to complete the combustion of the lean charge.

2.7 Combustion modeling

It is possible to model the combustion process in a prechamber (and also in the main chamber) based on equations of

- conservation of mass
- conservation of energy

- conservation of volume
- reaction rate
- gas properties

The combustions chambers can be divided into zones (or control volumes), where a zone represents a fraction of the volume of a combustion chamber. The gas states are assumed to be uniform within a zone. The simplest (and often most inaccurate) is to use a single zone for the whole combustion chamber. Chrisman and Freen [1994] reports on the use of coupled "single zone" model, one zone for the prechamber, one for the main chamber, one for the intake port and one for the exhaust port, each zone is connected to the next through a nozzle.

A slightly more advanced alternative to "single zone models" are "two zone models". In "two zone models" the combustion chamber is divided into two zones, one containing uncombusted charge and the other containing combustion products. Two coupled equation sets of the same form as in the single zone model is used as governing equations in the two zone model. Hires et al. [1976] use two coupled two zone model for simulation of Otto engines with prechamber. Valland [1984] use a two zone model. Experiments with two zone models are also presented in this thesis.

The main advantages of "two zone models" over "single zone models" are:

- The temperature in the combusted zone is predicted more accurately, therefore one can expect the formation of NO_x to be more accurate also.
- When the flame reaches the nozzle, then the density of the flow through the nozzle changes. A single zone model can not predict the change in density and therefore the calculated flow through the nozzle will be less accurate when using a single zone model.
- The temperature of the jet out of the prechamber is predicted more accurately, therefore one can expect that the ignition in the main chamber can be predicted more accurately.

In computational fluid dynamics or "CFD" there are a high number of zones. Equations of momentum and turbulence are used to connect the zones. Results from "CFD" will not be presented in this thesis.

2.7.1 Heat transfer

Heat transfer to/from the charge occurs during all stages of the process. The heat transfer is not only important for the thermal load on the parts (with respect to over heating or cracking), but also with respect the the combustion process inside the prechamber.

It was mentioned is section 2.3.1 that some prechambers have a liner insulated from the body of the cylinder head in order to reduce the cooling of the prechamber charge before ignition. Such liner or inserts into the prechamber could also be used to cool the charge during and after combustion and thereby reduce the generation of NO_x in the prechamber. This is mentioned here just as an idea for future investigation — it will not be explored in this report.

Several models for the heat transfer exists. Most models use an average flow velocity as input to a formula for estimation of heat transfer coefficient between the charge and the walls in the combustion chamber. In this thesis will be explored an alternative method using measurement of pressure and the characteristics of the nozzle between the chambers to calculate the net heat release in the prechamber. The method of using the nozzle does only give good result when there is high flow velocity through the nozzle.

2.7.2 Transient jets

Hot transient jets are the the desired output of a prechamber. Analysis of the jets are slightly outside the scope of this thesis — the thesis is mainly about the process inside the prechamber, but a jet model helps to visualize the output of calculation models. Understanding of governing processes of transient jets is of course essential for the understanding of ignition and combustion in engines with prechambers.

Three groups of transient jet models are described in literature. They can be grouped after the number of spatial dimensions in which the states are stored.

1. Zero dimensional models where all results are functions of time, initial state, geometry of nozzle and other known parameters.

2. One dimensional models, with spatial discretization along the center axis of the jet.

3. Multi dimensional models. These are two and three dimensional simulations using computational fluid dynamics.

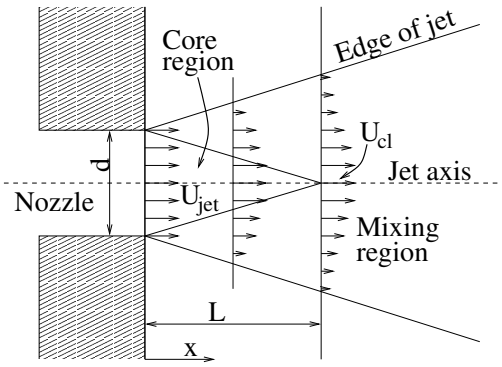

Figure 2.8: Dent jet mixing model

The different models should of course give the same results, but higher accuracy and more information can be expected from the more complex models.

The advantage of zero dimensional models is that they are easier to use than the others — no spatial integration, and often also the integration in time can be done algebraically once and for all, resulting simple formulas for the jet's spread angle and length as a function of time.

Zero dimensional models have traditionally been used in description of spray, especially diesel injection in internal combustion engines. Although developed for spray, these models are often applicable for gas jets also. Some spray models define a breakup length for the liquid core. The liquid core section must of course be dropped when the model is used on gas jet.

One of the first zero dimensional oil spray models was presented by Schweitzer [1937]. Research is still done in order to find a good and relatively simple universal spray model. Schihl et al. [1996] presents an analysis of zero dimensional spray models and he also presented his own model. Schihl's model builds on earlier work by Dent [1971], Hiroyasu and Arai [1980], Wakuri et al. [1960], Chikahisa and Murayama [1995] and others. Dent's model is based on gas jet mixing theory, and fits well for the purpose of modeling of ignition in prechamber-engines. The mixing model is shown in Figure 2.8. The modeling starts by assuming a velocity profile where the center velocity is reciprocal to the distance from the nozzle:

$$\frac{U_{cl}}{U_{jet}} = \frac{L}{x} \tag{2.2}$$

and also assuming a spread angle as given by:

$$\tan\theta = \frac{d}{2L} = 0.125\sqrt{\frac{\rho_{main}}{\rho_{jet}}}. \tag{2.3}$$

U_{jet} and ρ_{jet} are the velocity and density calculated by the nozzle equation. The fixed factor 0.125 in the equation seems a bit odd, as common sense says that the spread angle should really depend on the nozzle shape or turbulence energy of the flow. Inserting $\dot{x} = U_{cl}$ into equation 2.2 gives:

$$\frac{\dot{x}}{U_{jet}} = \frac{L}{x} \tag{2.4}$$

which is a differential equation with the solution:

$$x(t) = 2\sqrt{U_{jet} L \cdot t} \tag{2.5}$$

which is a model for the penetration length of a transient jet when U_{jet} and L are constant (which they are not in the case of a prechamber jet).

This jet model will be used later in this document together with a two zone combustion model.

2.8 Summary of literature study

In the literature were found several techniques that will be used in this thesis, in particular:

- Pressure measurements in combustion chambers, also in prechambers, of running engines.
- Two-zone combustion models and models of transient jets.
- Constant volume combustion rigs, also some with prechambers.
- Combustion chambers with windows where flames can be observed either directly or through for example Schlieren technique.

Parameters that characterizes the performance of a prechamber alone were difficult to find in the literature. It is clear that the desired output of a prechamber is a hot jet that can ignite a very lean charge in the main chamber, but how to quantify the ability to ignite the main charge without testing the prechamber in an engine? Answers to this question will be explored in the next chapters.

Chapter 3

Performance of prechambers

3.1 Introduction

One of the objectives of the thesis is to define variables that describes the performance of prechambers. Since the definitions of such prechamber performance variables are hard to find in the literature, the definitions will have to be made here. The performance variables should identify and quantify:

- **The desired output** of the prechamber.
- **Harmful bi-products** of the process inside the prechamber.
- **Efficiency** — the ratio of desired output per invested input or per harmful bi-product.

3.2 Desired output of a prechamber

Performance can be presented as quantification of the desired output, examples of such are "top speed" of a vehicle, "maximum continuous power rating (MCR)" of a power plant or of a generator set.

The purpose of a prechamber in an Otto engine is to deliver a warm burning jet into the main chamber so that the main charge is ignited. In addition to the temperature of the jet, the jet also increase the combustion speed by introducing higher flow velocity (both large scale and turbulence) into the main chamber. One can expect that a prechamber that produce more of a desired output will give faster combustion in the main chamber of in an engine than a prechamber that produces less.

It is hereby suggested that the performance variables used to describe the output of the prechamber should quantify:

- The kinetic power and energy delivered to the jet. More kinetic power and energy means that the jet will reach respectively faster and further into the main chamber and the jet will generate more turbulence.
- Length and/or volume of the hot jet. Length or volume may be an alternative to using kinetic energy as a performance variable.
- Thermal power and energy delivered to the jet. More thermal power and energy means that the jet will cause respectively faster and more stable ignition of the main charge.

More complete expressions for calculation of the variables described above will be presented in later sections of this chapter.

The duration of the jet can also be used as a measure of the output from prechambers. It is expected that a prechamber with shorter duration of the jet will often better than one with longer duration of the jet.

3.3 Harmful bi-products from a prechamber

The main harmful bi-product from the prechamber is normally NO_x when charge in the prechamber is close to stoichiometric and therefore the combustion temperature becomes so high that NO_x is generated. One can quantify NO_x either by mass or by volume:

- Mass, calculating every NO_x molecule as if it was NO_2, for example as micrograms per combustion.
- By volume fraction in gas flow out of the prechamber, for example as ppm (parts per million). In other words: Count how many NO_x molecules there are per million molecules that exits from the prechamber.

If one choose to use volume fraction (ppm), then it may be useful to give one value for the hot jet and another value for the exhaust gas exiting from the prechamber during scavenging.

If one choose to use mass, then it may be useful to split the total mass of NO_x into groups according to the origin of the NO_x — when and where it was generated. One would expect that there are two temperature peaks in the prechamber for each combustion cycle — the first one during combustion in the prechamber, the other one during combustion in the main chamber.

There may be different methods for reduction of NO_x during these two phases, therefore it could be useful to have two different parameters quantifying the NO_x.

3.4 Efficiency of a prechamber

An *efficiency* is normally defined as the useful output of a machine divided by the "cost" of the input to the machine. The invested input to a prechamber can be considered to be the value, either monetary value or heat value, of the gas burnt in the prechamber. Efficiencies are often presented as dimensionless ratios (for example the efficiency of a gear is mechanical power on output shaft divided by mechanical power on input shaft), but it can also be have a dimension, for example miles per gallon or gram CO_2 per kilometer for a vehicle.

Dimensionless efficiencies (energy out/energy in) can be used to compare prechambers of different geometries and sizes. The input to the prechamber is a combustible charge, the useful output is a warm jet. The charge has a heating value LHV. The jet has kinetic and thermal energy. With this as a starting point we may define thermal efficiency and kinetic efficiency of the prechamber:

- η_t prechamber thermal efficiency, hereby defined as thermal energy delivered to the jet, divided by the reaction energy initially present in the prechamber charge.
- η_k prechamber kinetic efficiency, hereby defined as kinetic energy delivered to the jet, divided by the reaction energy initially present in the prechamber charge.

One can argue that mass of fuel burnt in the prechamber of a modern Otto lean burn engine is small compared to the total mass of fuel and therefore has little influence on the total efficiency of the engine. When the mass of fuel burnt in the prechamber is so small that it is negligible compared to the total mass, then it does not make sense to optimize the prechamber design towards maximum thermal or kinetic efficiency — other design goal may be much more important.

3.5 Alternative efficiencies of a prechamber

The major harmful bi-product of the combustion in the prechamber is NO_x, therefore: The cost of the "input" to a prechamber can be considered to be the

NO_x produced in the prechamber (as an alternative to heat value as used in previous section). If one should define an efficiency for a prechamber similar to "gram CO_2 per kilometer for a vehicle", then that could be "micrograms NO_x per Joule jet energy". Any of the prechamber output parameters; P_{pk}, E_{pk}, P_{pt} and E_{pt} (and maybe also L_{jet} and V_{jet} at a certain time after ignition) can be divided by the mass of NO_x to make an "efficiency".

Other efficiencies and ratios can also be defined for a prechamber, similarly as for the main chamber, for example scavenging efficiency and trapping efficiency.

3.6 Notation

The different zones in the chambers are hereby labeled with mnemonic subscripts. The subscripts will be used also with other variables than volume.

V_p The volume of the prechamber, $V_p = V_{pu} + V_{pc}$

V_{pu} The not yet combusted volume in the prechamber, i.e. in ahead of the flame front.

V_{pc} The combusted volume of the prechamber, i.e. behind the flame front.

V_m The volume of the main chamber $V_m = V_{mu} + V_{mc}$

V_{mu} The not yet combusted volume in the main chamber, i.e. ahead of the flame front.

V_{mc} The combusted volume of the main chamber, i.e. behind the flame front.

V_{jet} The volume of the jet.

t_{ig} Time of ignition in the prechamber.

$t_{p>}$ Time when the prechamber pressure becomes higher than the pressure in the main chamber.

t_{NOX1} Time when the temperature in the combusted zone has reached a temperature so that formation of NO_x starts.

t_{fn} Time when the flame reaches the prechamber nozzle.

t_{pr} Time when the pressure ratio between the two chambers, p_p/p_m is is highest.

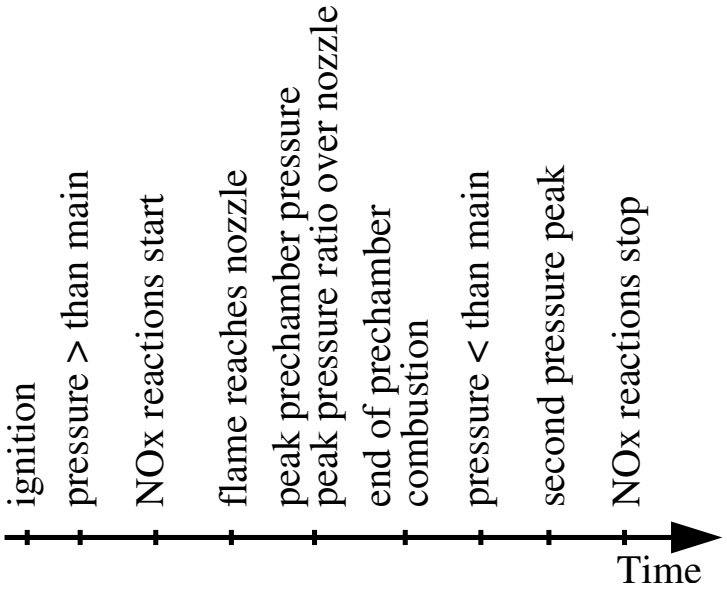

Figure 3.1: Events in prechamber process.

$t_{p<}$ Time when the prechamber pressure becomes lower than the pressure in the main chamber.

t_{NOX2} Time when the temperature in the combusted zone becomes so low than the NO_x reactions are halted.

The ordering of the events may deviate slightly from what is shown in figure 3.1. The subscripts will also be used on other variables than time.

3.7 Kinetic prechamber power and energy

Let the kinetic prechamber power be defined as:

$$P_{pk} = \frac{1}{2}\dot{m}v_{noz}^2, \tag{3.1}$$

where $\dot{m}$ is the mass flow through the nozzle and v_{noz} is the velocity at the outlet of the nozzle. Both $\dot{m}$ and v_{noz} are functions of time.

Let the kinetic prechamber energy be the kinetic power integrated over time as:

$$E_{pk} = \int_{t_{p>}}^{t_{p<}} P_{pk} dt, \tag{3.2}$$

P_{pk} and E_{pk} should be possible to calculate during numerical simulation of prechambers. It is also possible to use measured pressure in the chambers of a real engine as input to simulation models — such models will be used in the next chapters.

3.8 Thermal power and energy delivered to the jet

Let the thermal power delivered to the jet be defined as:

$$P_{pt} = \dot{m} h_{jet} \tag{3.3}$$

where h_{jet} is the stagnation enthalpy of the gas leaving the nozzle relative to the enthalpy the gas in the main chamber.

Let the thermal jet energy be the kinetic power integrated over time as:

$$E_{pt} = \int_{t_{p>}}^{t_{p<}} P_{pt} dt \tag{3.4}$$

3.9 Length and volume of the jet

Recall the zero dimensional jet model presented in the literature study (previous chapter):

$$x(t) = 2\sqrt{v_{jet} \cdot L \cdot t} \tag{3.5}$$

where x the length of the jet as a function of time.

Applying the superposition principle to the jet and inserting the expression for L gives the following expression for the hot jet length when v_{noz} and ρ are not constant:

$$L_{jet}(t) = \max_{\tau=t_{fn}}^{t} \sqrt{16 \cdot d \sqrt{\frac{\rho_{jet}(\tau)}{\rho_{main}(\tau)}} v_{noz}(\tau) \cdot (t-\tau)}. \tag{3.6}$$

If the combustion in the prechamber is of relatively short duration (short compared to crank speed of the engine and short compared to combustion in main chamber), then ρ_{main} can be assumed to be constant during the prechamber combustion. Note that as τ is larger or equal to t_{fn} (the time the flame reaches the nozzle), this means that only the hot jet length is estimated.

A formula estimating the volume of the jet can also be developed using the same method as for the jet length. Assuming that the jet length x is much larger than the core length L and using the formula for volume of a cone:

$$V_{jet}(t) = \max_{\tau=t_{fn}}^{t} \left[2\pi \left(\frac{\rho_{jet}(\tau)}{\rho_{main}} \right)^{1/4} [d \cdot v_{noz}(\tau) \cdot (t-\tau)]^{3/2} \right]. \tag{3.7}$$

3.10 Characteristic prechamber time

A characteristic time can be defined in several ways, depending on what is the purpose of defining it. Since we are aiming at the output of the prechamber, one could for example use the "center of gravity" method with respect to prechamber jet power E_{pt}:

$$\tau_{cg} = \frac{1}{E_{pt}} \int_{t_{p>}}^{t_{p<}} (t - t_{p>}) \dot{m} h_{jet} dt, \tag{3.8}$$

or one could define another characteristic time defined as: "thermal energy delivered to the jet" divided by "maximum power delivered to the jet":

$$\tau_{max} = \min_{t_{p>}}^{t_{p<}} \frac{E_{pt}}{\dot{m} h_{jet}} \tag{3.9}$$

τ_{max} describes the duration of the peak power. τ_{max} will be used in the calculations in the following chapters.

3.11 Discussion and conclusions

A set of performance parameters for prechambers have been defined. The performance parameters are grouped into three categories as:

- **The desired output** of the prechamber:
  - P_{pk} and E_{pk} are respectively kinetic power and kinetic energy delivered to the jet.
  - P_{pt} and E_{pt} are respectively thermal power and thermal energy delivered to the jet.
  - L_{jet} and V_{jet} are length and volume of the hot jet.
  - τ_{cg}, τ_{max} are two slightly different definitions of characteristic durations for the transfer of thermal power to the jet.
- **Harmful bi-products** of the process in the prechamber: NO_x is the main harmful bi-product. It can be quantified by
  - Mass, as micrograms per combustion. For further details the mass of NO_x can split further into groups according to in which phase of combustion it was generated.
  - Volume, as parts per million in the gas flowing out of the prechamber. For further details it can be split into groups according to when the gas exits from the prechamber; with the hot jet, during the expansion stroke or with the scavenging.
- **Efficiency** — the ratio of desired output per invested input can be defined in two ways according to what one regards as the "investment", the fuel or the NO_x-bi-product.
  - The values for E_{pk} and E_{pt} can be divided by the lower heat value of the fuel present in the prechamber at the time of ignition and make respectively kinetic and thermal prechamber efficiency.
  - Any of the prechamber output parameters; P_{pk}, E_{pk}, P_{pt} and E_{pt} (and maybe also L_{jet} and V_{jet} at a certain time after ignition) can be divided by the mass of NO_x to make an "efficiency".

The performance parameters should be possible to calculate on the basis of both experimental studies and on numerical/computational experiments.

It is too early to say if these are a correct and complete set of performance variables which can be used to fully evaluate the performance of prechambers, but at least they can and will be used as a starting point for prechamber studies in the following chapters.

Chapter 4

Two zone prechamber model

4.1 Introduction

The targets of this is chapter are:

- To develop mathematical models of a prechamber and calculate the performance variables introduced in chapter 3.
- To evaluate, by perturbation of the input parameters to the model, how the performance variables are influenced by geometry of the prechamber.

Recalling the performance variables:

- **The desired output** of the prechamber:
  - Kinetic power and kinetic energy delivered to the jet.
  - Thermal power and thermal energy delivered to the jet.
  - Length and volume of the hot jet.
  - Characteristic durations of the jet.
- **Harmful bi-products** of the process in the prechamber: NO_x is the main harmful bi-product. It can be quantified by mass or by volume fraction.
- **Efficiency** — the ratio of desired output per invested input can be defined in two ways according to what one regards as the "investment", the fuel or the NO_x-bi-product.
  - Kinetic and thermal prechamber efficiency.

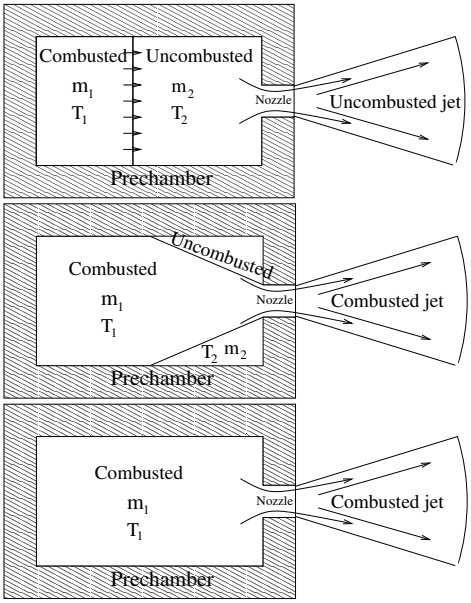

Figure 4.1: The three stages of the two zone prechamber model

– Any of the prechamber output parameters; can be divided by the mass of NO_x to make an "efficiency".

It was selected to use a two zone combustion model — one zone for the charge (fuel and air) and one zone for the combustion products. The two zones are separated by a flame front. The gas composition and state is simplified to be uniform throughout each zone. The two zone model is the simplest combustion model that can predict the temperature of the jet and combustion products in the prechamber with a reasonable accuracy. The temperature of the combustion products is important because it governs the production of NO_x.

Three stages of the two zone prechamber model are shown in figure 4.1:

1. After ignition but before the flame reaches the nozzle.
2. After the flame reaches the nozzle but before combustion ends.
3. After the end of combustion.

4.2 Mathematical models

Two different models will be used here, one with pressure as input an one with combustion rate parameters. The basis for the two models are the same, but

the equations are slightly re-organized depending of what is used as input. Common for both models are the following description of the geometry of the prechamber:

- V_p, volume of prechamber
- V_{ff}, volume fraction combusted when the flame reaches the nozzle
- A_{noz}, total area of the nozzle, all holes together
- C_{noz}, nozzle discharge coefficient
- $\#_{noz}$, number of nozzles to distribute A_{noz} over.

Initial state and the properties of the working fluid in both zones are also needed. Also a model for the reaction rate is needed. In the next sections will be presented two models of the reaction rate: One model with shape parameters for the heat release and another model using measured pressure in stead.

4.2.1 Model using measured pressure as input

The mathematical equations for a two zone model of a prechamber are described in this section. Use the gas state equation:

$$p\,V = m\,R\,T$$

Differentiate it, assume R = R(p,T) and get:

$$\frac{\dot{p}}{p}(1 - \frac{p}{R}\frac{\partial R}{\partial p}) - \frac{\dot{T}}{T}(1 + \frac{T}{R}\frac{\partial R}{\partial T}) - \frac{\dot{m}}{m} + \frac{\dot{V}}{V} = 0 \tag{4.1}$$

Also use the energy equation on differential form for an open, homogeneous system where u = u(p,T):

$$m\frac{\partial u}{\partial p}\dot{p} + mc_v\dot{T} + u\dot{m} + p\dot{V} = \dot{Q} + \Sigma h_i\dot{m}_i \tag{4.2}$$

Finally use the continuity relation:

$$\dot{m} = \Sigma\dot{m}_i \tag{4.3}$$

For zone 2, the values of $\partial R/\partial p$, $\partial u/\partial p$, and $\partial R/\partial T$ are negligible. Apply equations 4.1, 4.2 and 4.3 to the two zones. The equation system can then be sorted into matrix form as:

$$\begin{bmatrix} \frac{1}{m_1} & (\frac{1}{T_1} + \frac{1}{R_1}\frac{\partial R}{\partial T}) & 0 & 0 & -\frac{1}{V_1} \\ u_1 - h_2 & m_1 c_{v,1} & 0 & 0 & p \\ 0 & 0 & \frac{1}{m_2} & \frac{1}{T_2} & \frac{1}{V_2} \\ 0 & 0 & u_2 - h_2 m_2 c_{v,2} & & -p \\ 1 & 0 & 1 & 0 & 0 \end{bmatrix} \begin{bmatrix} \dot{m}_1 \\ \dot{T}_1 \\ \dot{m}_2 \\ \dot{T}_2 \\ \dot{V}_1 \end{bmatrix} = \begin{bmatrix} \frac{\dot{p}}{p} - \frac{\dot{p}}{R_1}\frac{\partial R_1}{\partial p} \\ \dot{Q}_1 - m_1\frac{\partial u_1}{\partial p}\dot{p} + \dot{m}_{1,noz}(h_2 - h_1) \\ \frac{\dot{p}}{p} \\ \dot{Q}_2 \\ -\dot{m}_{1,noz} - \dot{m}_{2,noz} \end{bmatrix} \tag{4.4}$$

The pressure and pressure gradient appears as excitation in the right side of equation 4.4. This equation is valid both before and after the flame reaches the nozzle. $\dot{m}_{1,noz}$ and $\dot{m}_{2,noz}$ are flow through the nozzle from zone one and two respectively. The flow through the nozzle is calculated with a nozzle equation assuming quasi-steady state in the nozzle.

The coefficients of equation 4.4 are implemented in Fortran code as:

```
a(:,1)=(/         1, 1+T1*RT1/R1,          0,         0,  -1/V1,         dpp/pp-dpp*Rp1/R1 /)
a(:,2)=(/(u1-h2)*m1,   T1*m1*cv1,          0,         0,     pp, Q1-m1*up1*dpp+mf1*(h2-h1) /)
a(:,3)=(/         0,          0,          1,         1,   1/V2,                    dpp/pp /)
a(:,4)=(/         0,          0, (u2-h2)*m2, T2*m2*cv2,    -pp,                        Q2 /)
a(:,5)=(/        m1,          0,         m2,         0,      0,                -mf1-mf2 /)
```

The complete source code is included in appendix A.

The computer program takes all flow from zone one (uncombusted) until a selected fraction (called V_{ff}) of the prechamber volume has combusted,

thereafter all nozzle flow comes from zone two (combusted). There are always some irregularities in the calculated ROHR at the switching point, this indicates that the real switching between uncombusted and combusted nozzle flow is a somewhat gradual process, not on/off as in the simulation program.

By trying different values for V_{ff} one can find the correct value for V_{ff} as the V_{ff} that gives the least irregularities at the switching point.

4.2.2 Model with assumed function for heat release

An alternative two zone model of a prechamber are described in this section. This model can be used if the pressure in the combustion chambers are unknown.

If the pressure is unknown, then the pressure gradient must move over to the left side in equation 4.4, while the mass gradients must move to the right side. This results in the following equation system:

$$\begin{bmatrix} -\frac{1}{T_1} - \frac{\partial R}{R_1 \partial T} & 0 & \frac{1}{V_1}\frac{1}{p} - \frac{\partial R_1}{R_1 \partial p} \\ m_1 c_{v,1} & 0 & p \quad m_1 \frac{\partial u_1}{\partial p} \\ 0 & \frac{1}{T_2} & \frac{1}{V_2} \quad -\frac{1}{p} \\ 0 & m_2 c_{v,2} - p & 0 \end{bmatrix} \begin{bmatrix} \dot{T}_1 \\ \dot{T}_2 \\ \dot{V}_1 \\ \dot{p} \end{bmatrix} = \begin{bmatrix} \frac{\dot{m}_1}{m_1} \\ \dot{Q}_1 + \dot{m}_{1,noz}(h_2 - h_1) + \dot{m}_1(h_2 - u_1) \\ -\frac{\dot{m}_2}{m_2} \\ \dot{Q}_2 + \dot{m}_2(h_2 - u_2) \end{bmatrix} \tag{4.5}$$

Heat release The heat is released into zone 1. The rate of heat release is used to calculate the mass flows $\dot{m}_1$ and $\dot{m}_2$ as:

$$\dot{m}_1 = \frac{ROHR_1}{h_c} - \dot{m}_{1,noz}$$

$$\dot{m}_2 = -\frac{ROHR_1}{h_c} - \dot{m}_{2,noz}$$

where h_c is the heat value of the charge and $\dot{m}_{1,noz}$ and $\dot{m}_{2,noz}$ are the flow through the nozzle from respectively zone 1 and 2.

The net rate of heat release is assumed to be a known function of the state variables. The "known function" used in the calculations presented here is:

$$ROHR_1 = ROHR_c(\frac{V_1}{V_p})^{\alpha_1}(\frac{V_2}{V_p})^{\alpha_2} \tag{4.6}$$

where $ROHR_c$ is an assumed characteristic rate of heat release, V_1 and V_2 are the combusted and uncombusted volumes, α_1 is shape parameter for the flame initiation and α_2 is shape parameter for the flame extinction. A plot including shape parameters are shown in figure 4.2.

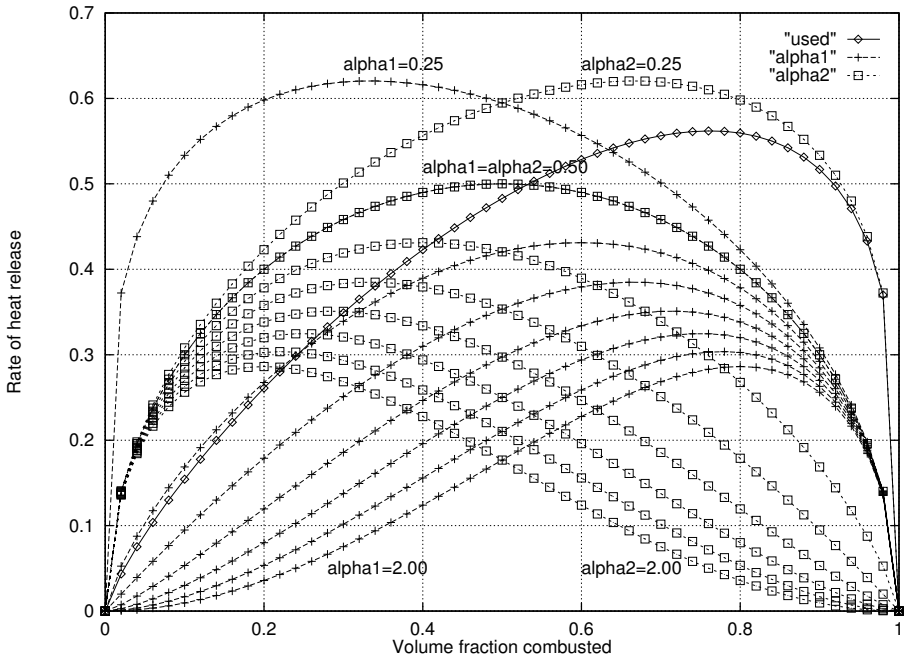

Figure 4.2: Rate of heat release as a function of combusted volume. The line marked "used" is the one used in the simulations. The lines marked "alpha1" all have varying α_1 and constant $\alpha_2 = 0.5$. The lines marked "alpha2" all have $\alpha_1 = 0.5$ and varying α_2.

Larger $ROHR_c$ gives a higher and shorter rate of heat release curve. Shorter because larger heat release consumes the charge faster. $ROHR_c$ should be selected so that it gives a reasonable fast combustion.

Both α_1 and α_2 are intended to be in the range 0.1 — 2.0, smaller values give respectively quick initiation and extinction, larger values give respectively longer ignition delay and slow extinction. Following the logic that the combustion speed is proportional to the flame surface area, and assuming a spherical flame, α_1 should have the value 2/3. This value neglects the self accelerating effects of combustion depending on temperatures, turbulence and heat conduction. α_1 must be adjusted upwards to account for these effects.

α_2 depends on the shape of the prechamber, α_2 should be small if the prechamber is designed so that the flame is supposed to extinct against the prechamber walls simultaneously in all directions.

$\alpha_1 = 0.8$ and $\alpha_2 = 0.25$ appears to be a good starting point for further adjustment.

4.3 Gas properties

The temperature in the combustion products in the prechamber will reach more than 1500 K. Dissociation is significant in this temperature range. Therefore a gas model including equilibrium reactions was used. The gas properties used in the simulations come from Zacharias [1966], using fuel-air equivalence ratio = 0 for the charge (thus pure dry air) and 1 for the products (stoichiometric exhaust gas).

The calculation of gas properties assumes a fuel on the form C_nH_{2n} and dry air. Methane, the main component of natural gas has 4 hydrogen per carbon atom and does therefore not comply with the formula C_nH_{2n}, but this approximation is believed to be better than ignoring dissociation .

4.4 Initial values

The simulation is to be started right after the spark ignition. m_{tot} and T_2 can then be calculated from the charge state and properties, prechamber volume and compression ratio.

The initial m_1 is the mass covered by the initial flame core. Assuming the initial flame core has a volume of 8 mm^3 and thus $m_1 = \frac{8 \text{ mm}^3}{V_p} m_{tot}$. A small flame core will lead to a long "ignition delay", the length will also depend on the assumed rate of heat release function, in particular on α_1.

The initial T_1 is the spark temperature which is assumed to be 2500 K.

The initial T_1 has little influence on the simulation, as initial mass in zone 1 is small.

4.5 Nozzle

The flow through the nozzles/orifices is calculated according to equations 4.7 to 4.11.

$$p_r = max(\frac{p_{main}}{p_{pre}}, (\frac{2}{k+1})^{\frac{k}{k-1}}) \quad (4.7)$$

$$\psi = \sqrt{\frac{k}{k-1}(p_r^{\frac{2}{k}} - p_r^{\frac{k+1}{k}})} \quad (4.8)$$

$$c_{avg} = c_d \cdot \psi \cdot \sqrt{2 \cdot R \cdot T} \quad (4.9)$$

$$\rho = \frac{p_{pre}}{R \cdot T} \quad (4.10)$$

$$\dot{m} = A_n \cdot \rho \cdot c_{avg} \quad (4.11)$$

where c_{avg} is average flow velocity over the area of the orifice. Equation 4.7 contains the expression for critical pressure ratio as given by equation (3.67) in Øverli [1992]. Equation 4.8 is same as equation (3.64) in Øverli [1992]. A nozzle discharge coefficient c_d (with assumed value of 0.5 for nozzle with sharp edges) is used in calculation of average flow velocity c_{avg} in equation 4.9.

4.6 Results from two zone model

A "reference" prechamber is run through the model first, then parameters are changed one by one to see what the effect of the change is. Some key input values for the reference simulation is given in table 4.1. A summary of results with perturbations of the input is shown in table 4.2. Plots of the results can be found in figures on the following pages.

V_p	16.00	ml
A_n	48.00	mm^2
$\#_{noz}$	6	-
V_{ff}	0.7	
$ROHR_c$	1.0	MW
T_1	2500	K
T_2	750	K

Table 4.1: Some of the input values used for the reference simulation, a complete listing of the input can be found in appendix B.1.

Perturbation	η_t	η_k	t_{pc}	L_{jet} 5 ms
Reference	41%	0.6%	0.9 ms	0.20 m
$V_{ff} = 1.0$	18%	0.4%	0.4 ms	0.20 m
$V_{ff} = 0.0$	74%	0.7%	1.8 ms	0.16 m
$A_n = 96.0mm^2$	31%	0.3%	0.5 ms	0.22 m
$A_n = 24.0mm^2$	51%	0.8%	1.6 ms	0.17 m

Table 4.2: Summary of perturbations and results. The input to the reference simulation is given in table 4.1. Making the shape of the prechamber so that the flame reaches the nozzle late ($V_{ff} = 1.0$), has the negative effect of decreasing the thermal and kinetic efficiencies of the prechamber. Making the shape of the prechamber so that the flame reaches the nozzle early ($V_{ff} = 0.0$), has the negative effect of increasing the duration of the discharge from the prechamber and reducing the length of the jets at a given time, here 5 ms after ignition.

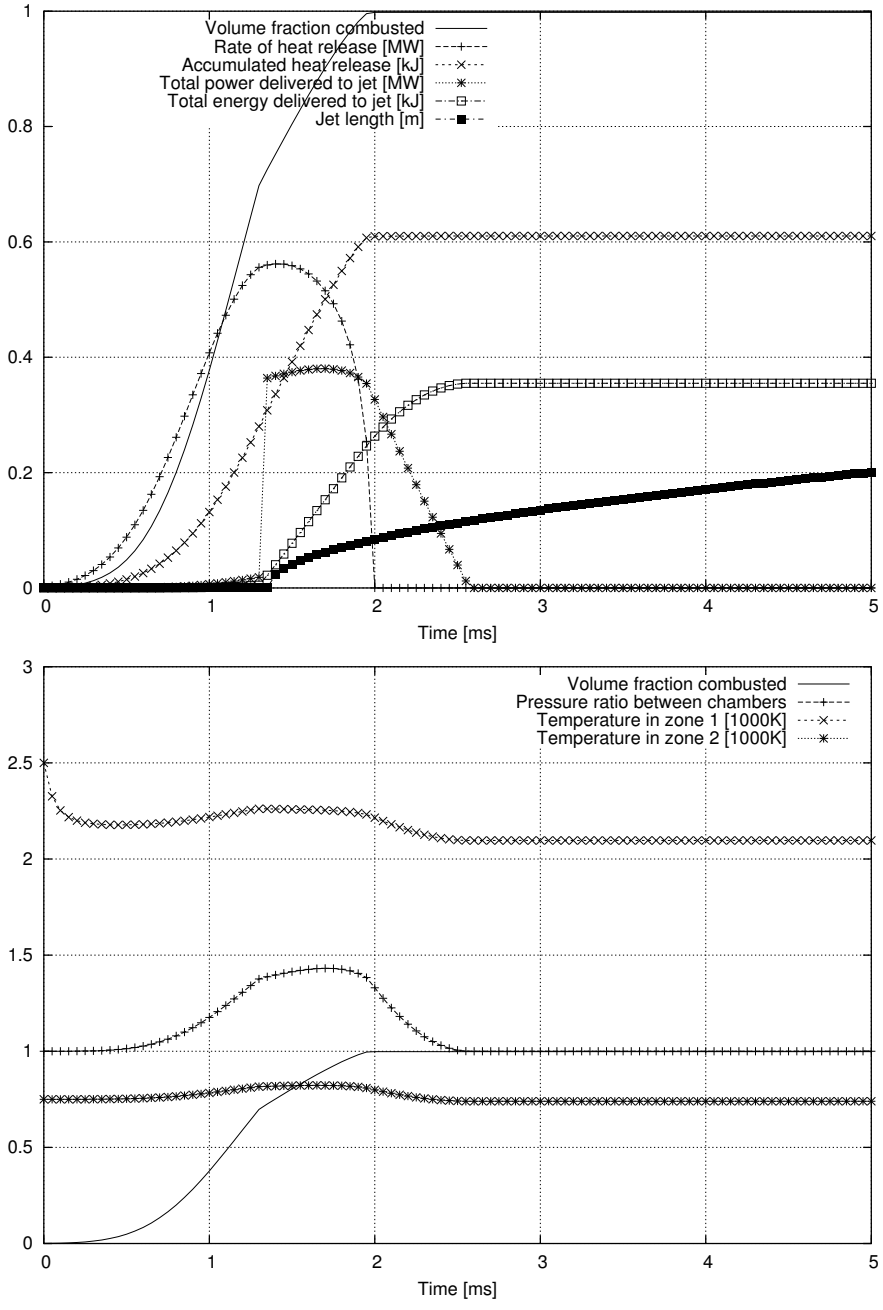

Figure 4.3: Two zone reference simulation

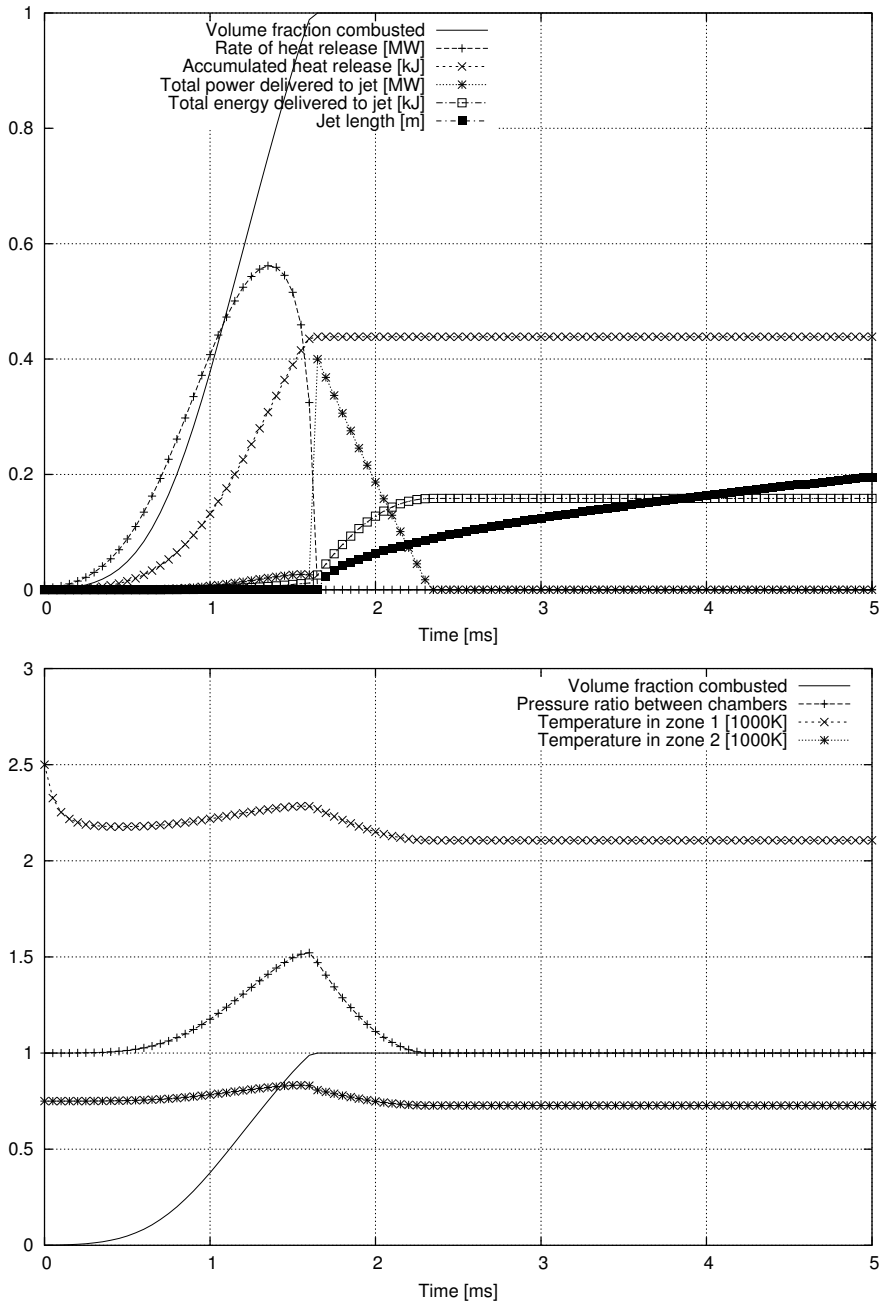

Figure 4.4: Increasing V_{ff} to 1.0. This means that the flame reaches the nozzle at the same time as the end of the combustion in the prechamber.

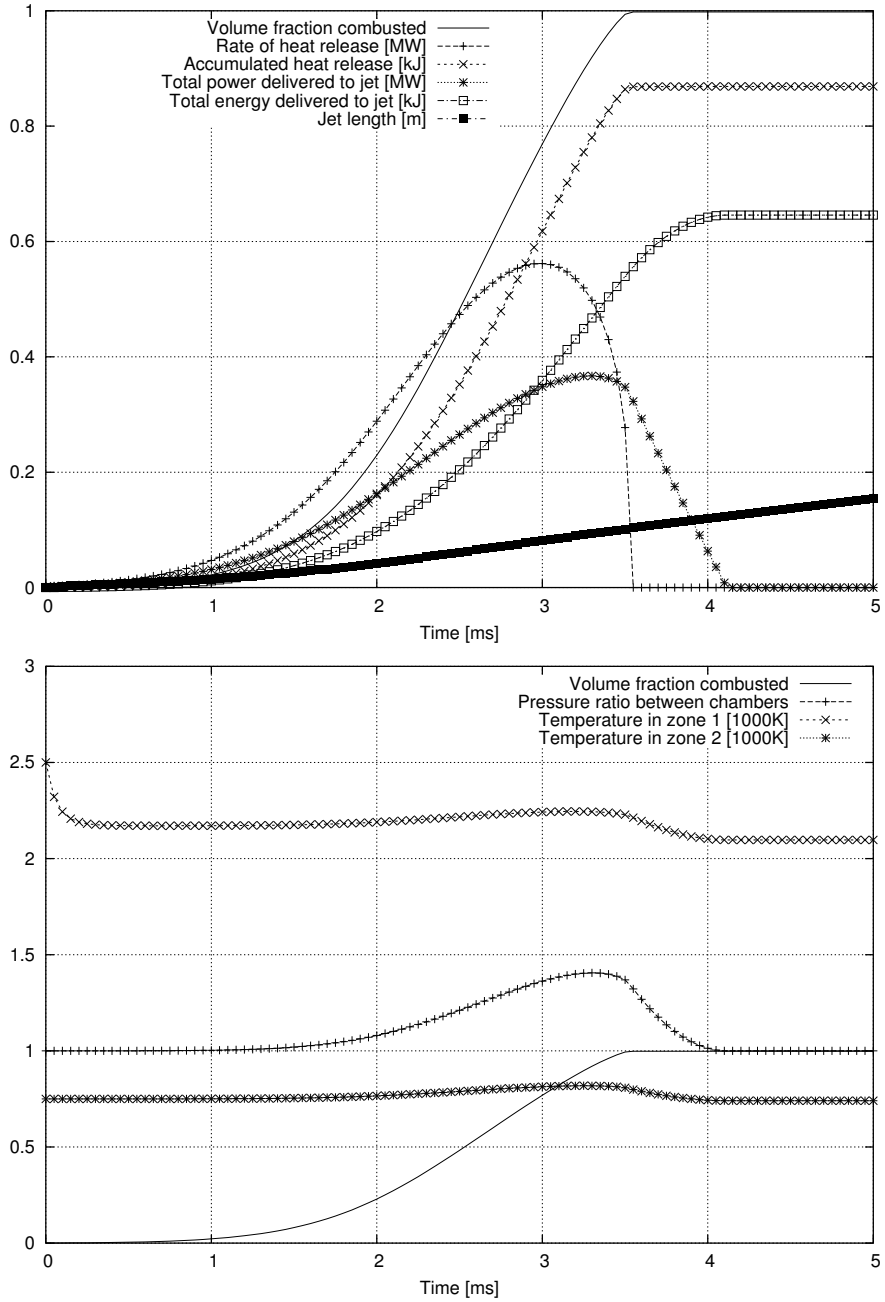

Figure 4.5: Results from the two zone model when $V_{ff} = 0.0$. This means that the flame reaches the nozzle at the time of ignition, this would be the case if the charge is ignited close to the nozzle.

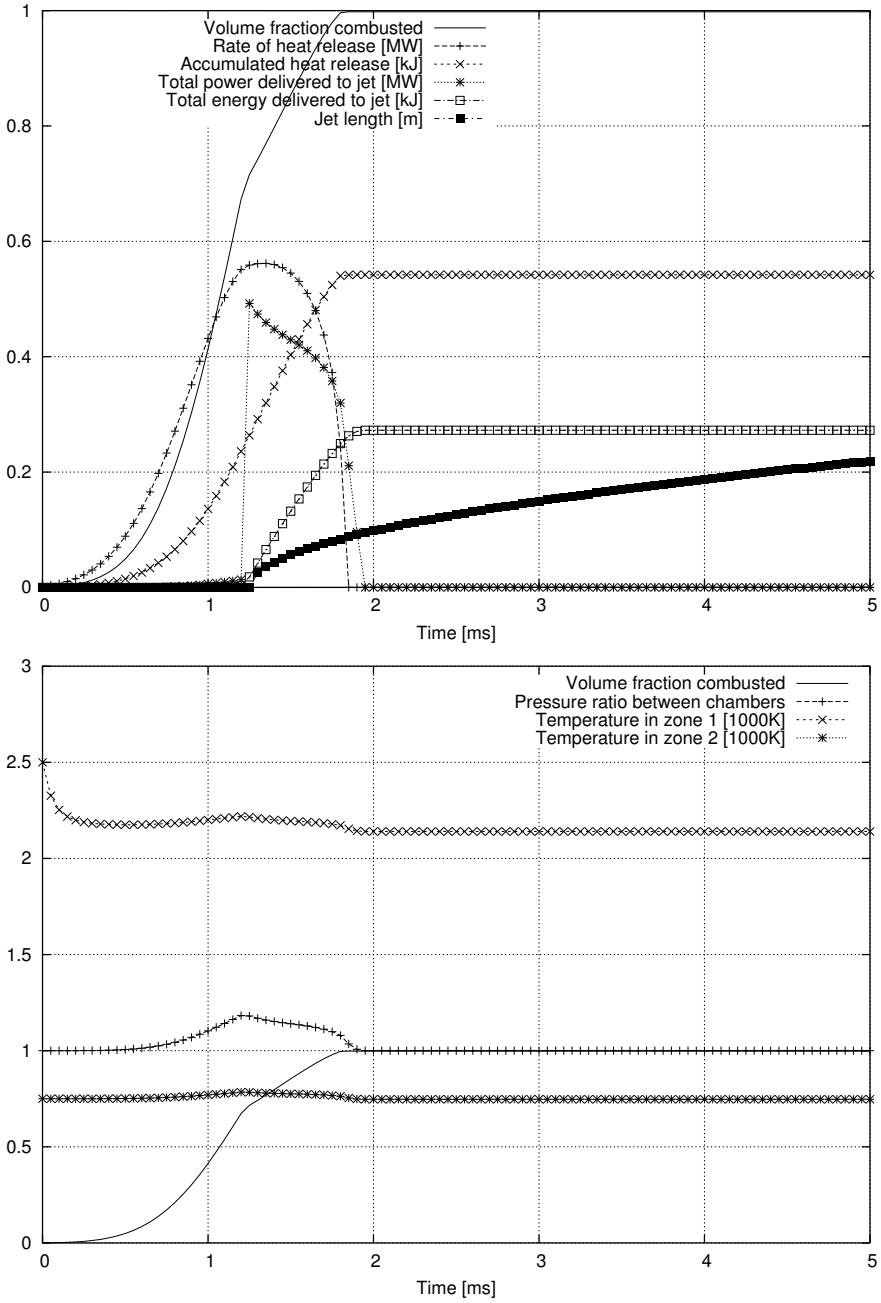

Figure 4.6: Results from the two zone model when the nozzle area is doubled, $A_n = 96$ mm^2.

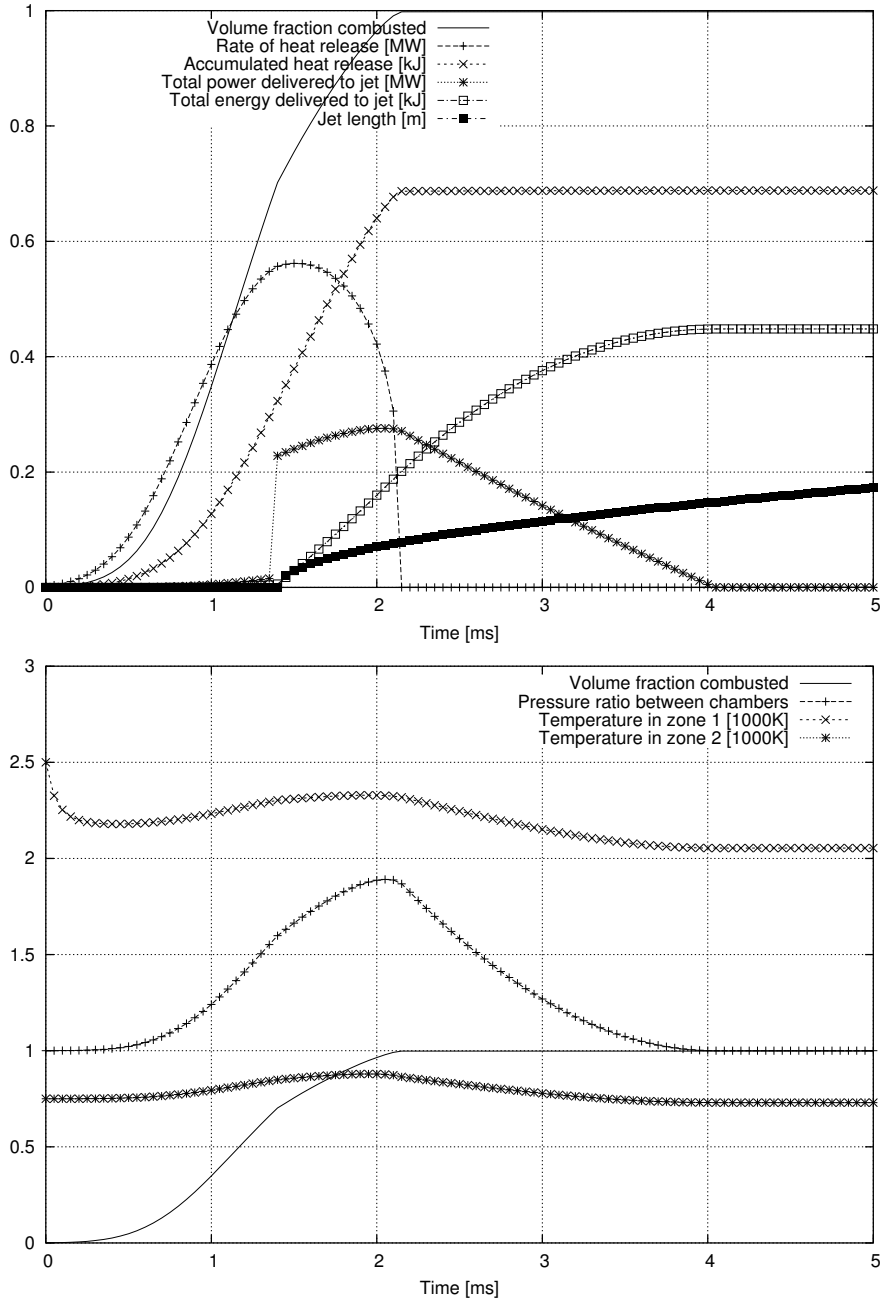

Figure 4.7: Results from the two zone model when the nozzle area is halved, $A_n = 24$ mm^2.

4.7 Validation of computer program

In addition to the simplifications done in the model, one may also consider the possibility for "bugs" in the computer program. One way of code validation is to use calculated pressure from the program with assumed shape of ROHR as input to the program that use pressure as input. This is a way of first calculating a result then using the inverse function to calculate the first input values. This has been done and the results can be seen in figure 4.8. There are no significant difference between the two results, this means that if there is a bug in the one program, then an inverse bug is present in the other program.

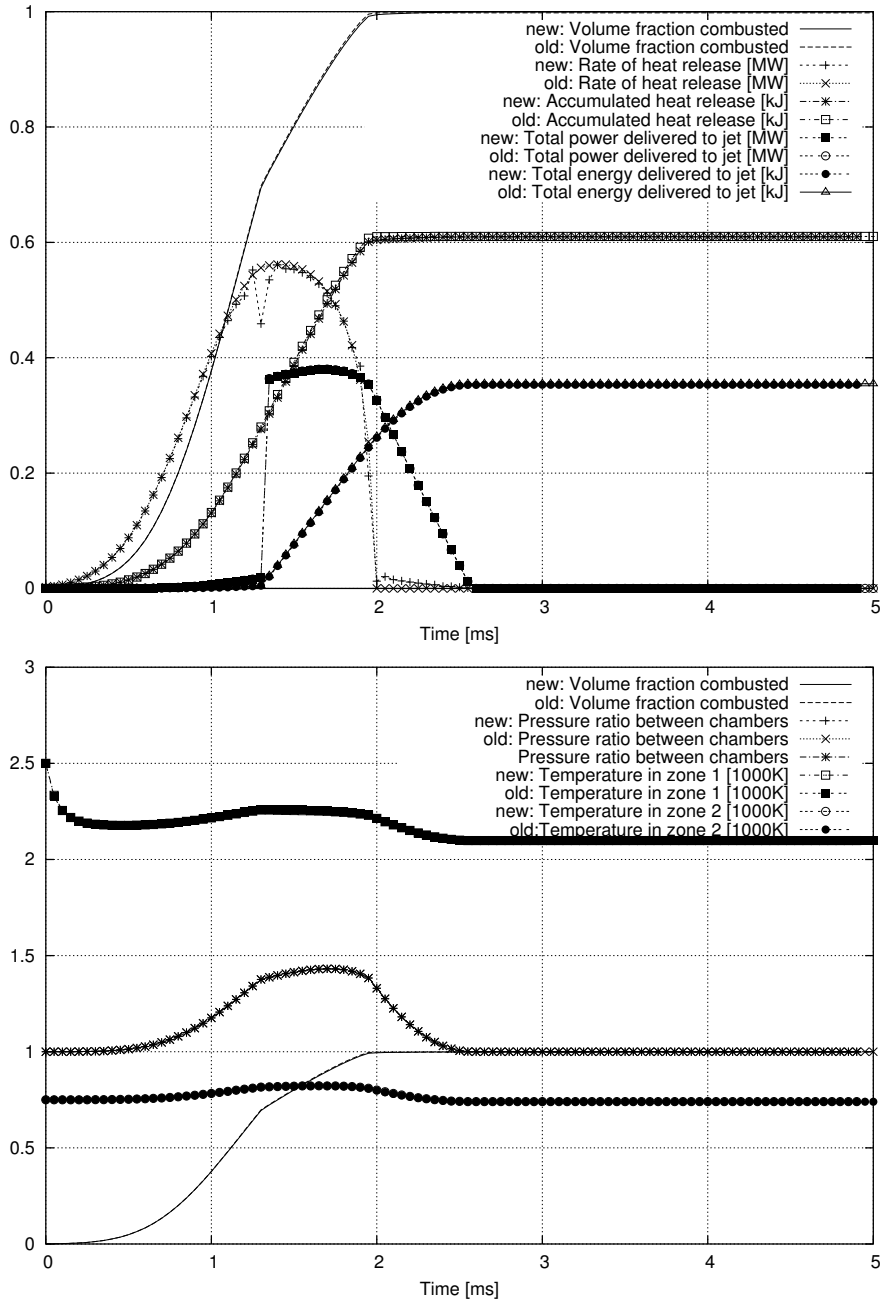

Figure 4.8: Results from two simulations, the one marked "new" uses pressure calculated by the other "old" as input. There is a small difference exactly where the nozzle flow switches from uncombusted to combusted.

4.8 Summary of numerical two-zone models

The first objective of this chapter was to develop and present ways to calculate a list parameters that describes the performance of prechambers. The target is only partially fulfilled as the presented models do not calculate all the desired parameters: Two numerical two-zone models of the prechamber are presented, implemented and used to calculate all of the parameters presented under the heading "desired output" in addition to thermal and kinetic efficiency of a prechamber, while the paramenters presented under the headings "Harmful bi-products" are not calculated.

The second objective of this chapter was to evaluate, by perturbation of the input parameters to the model, how the performance variables are influenced by geometry of the prechamber. The perturbations included changing the effective area of the nozzle and the timing of when the flame reaches the nozzle. The results are presented as graphs (function of time) and summarized in table 4.2.

There are two reasons why the implemented models do not calculate the generated NO_x.

1. In order calculate mass of NO_x generated in the prechamber it is neccessary to include the combustion in the main chamber and also the expansion stroke (untill the temperature in the prechamber are so low that the NO_x-reactions freeze) into the calculation models. It can be argued that it is outside the scope of this thesis to include so much of the process outside the prechamber.

2. The target (objective) has not always been as clearly described as it is now. When the models were made, then it was not clearly defined that calculation of NO_x was desired. Limited time and resources do not allow updating the models at present time.

One of the two presented models use measured pressure in both prechamber and main combustion chamber as inputs. The other model use a given heat release/transfer function as input. The use of the nozzle equation to calculate the net heat release is an obvious limitation of the program using measured pressure as input. This cause the following problems:

1. If the used characteristics of the nozzle is inaccurate, then the calculated heat release will also be inaccurate.

2. The nozzle equation is non-linear. When there is little pressure difference over then nozzle, then the calculated heat release will be very

inaccurate in the sense that a small error the measured pressure will have a large influence on the calculated heat release.

It would be an important improvement if the calculation program used heat transfer coefficients (in stead of the nozzle equation) in the periods when there is little pressure difference over the nozzle.

Chapter 5

Analysis of a running engine

5.1 Introduction

The goal for this experiment is to:

1. Measure the pressure in the prechamber of a running engine. This can be used as a reference for the experiments with a constant volume combustion rig (to be presented in later chapter of this thesis).
2. Use cycle by cycle variations to explore what is the desired behavior/shape of the combustion rate.
3. Use the measured pressure as input to the two-zone model as defined i chapter 4.
4. Use the two-zone model to calculate values for the performance variables defined in section 3.

5.2 Laboratory setup

Engine: "KR-3" — a three cylinder research version of "Bergen type K", the same engine type as shown in picture 5.1. One cylinder was equipped with piezo-electric pressure sensors in both prechamber and main combustion chamber. Engine data is summarized in table 5.1.

Figure 5.1: Cut-away picture of "Bergen type K" medium speed engine.

Cycle	:	Otto 4 stroke turbocharged and inter-cooled.
Bore	:	250 mm
Stroke	:	300 mm
Comp. ratio	:	12
MCR	:	14.25 bar BMEP at 1000 RPM
Efficiency	:	40 % at MCR
Power	:	175 kW/cylinder at MCR
Charge press.	:	2.4 bar at MCR
Fuel	:	Low pressure natural gas
Ignition	:	Capacitive spark in a 16 cm^3 prechamber with six 3 mm diameter nozzles

Table 5.1: Engine data for "KR-3". The values are valid only for this particular research engine and during this experiment.

5.3 Results

All measured results are collected in appendix C. Further analysis of selected measurements are presented in the next sections of this chapter. Measured pressure during a single engine cycle is shown in figure 5.2. Only measurements at high load will be analyzed, as the engine is expected to be used at high load most of the time.

One may observe from figure 5.2 that:

- The pressure in the prechamber is significantly higher than in the main chamber in a period of approximately 10 degrees. At a speed of 1000 RPM, this is equal to 1.7 ms.
- Maximum pressure ratio between chambers is approximately 1.4.

Comparison to other published measurements: Prechamber pressure curves published by Crane and King [1992], using a single cylinder Caterpillar 1Y540 at 1000 RPM, 3.45 bar BMEP with varying prechambers show somewhat longer and period with high prechamber pressure, which may be due to lower BMEP and narrower prechamber orifice: Prechamber pressure is significantly higher than the main chamber pressure for 10 to 20 crank degrees. Prechamber combustion duration: 5 to 8 degrees. Maximum pressure ratio between chambers: 2.5.

Prechamber pressure curves published by Snyder and Dexter [1990], see figure 5.3, using a single cylinder research engine, look similar to the curves recorded on the KR3.

5.4 Cycle by cycle variations

As most spark ignited engines, also this one has cycle by cycle variations in the cylinder (and prechamber) pressure. It might be possible to use the cycle by cycle variations to evaluate how the prechamber performance parameters influence the output of the engine. It is far more convenient to study the difference from one cycle to the next than to do a measurement, then modify the prechamber and attempt to re-create the same conditions for a test with the modified prechamber.

From figures 5.4 and 5.5 one may observe a correlation between fast/early combustion in the prechamber and high maximum pressure in the main chamber. The correlation is due to ignition timing — the piston is on the way down when the peak pressure in the main chamber occurs. The linear regression line in the figure has a correlation coefficient of 0.85.

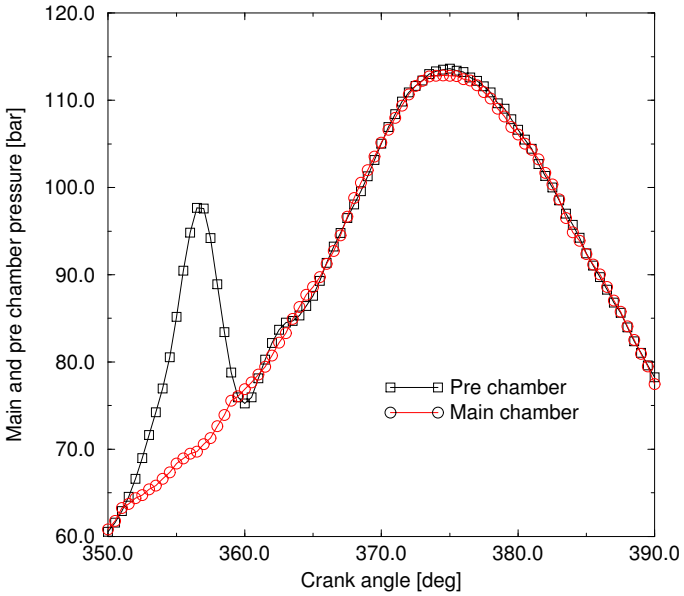

Figure 5.2: Measured pressure in both chambers during parts of a single representative engine cycle at high engine load.

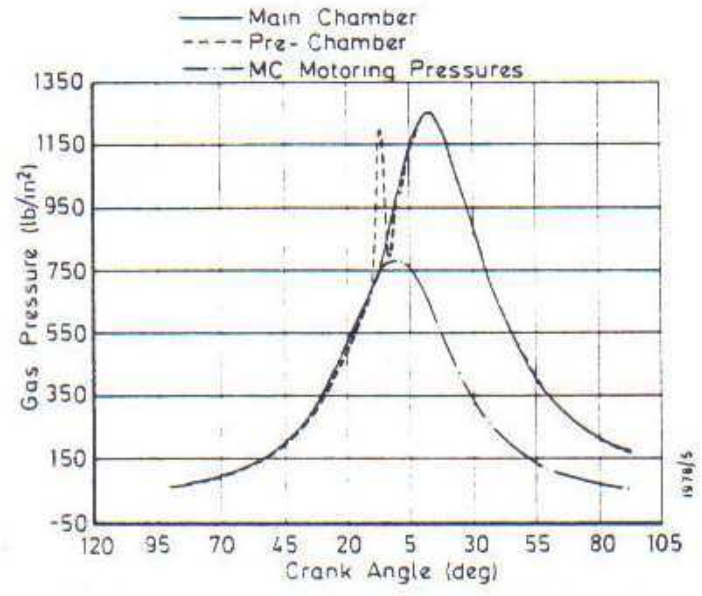

Figure 5.3: Figure from Snyder and Dexter [1990], showing "Pressure diagrams from the single cylinder engine for $\lambda = 1.65$ & timing 13° BTDC". This may be compared to figure 5.2

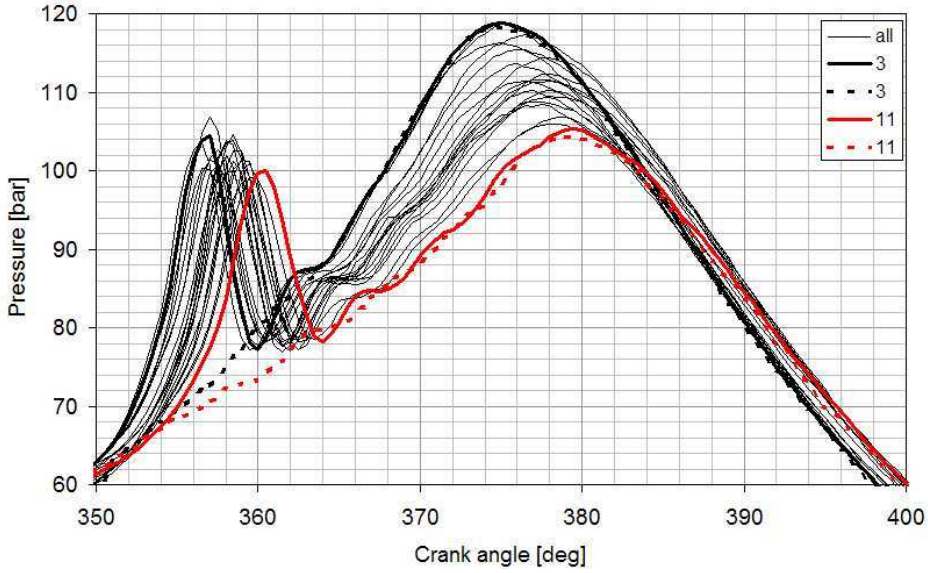

Figure 5.4: Comparing a fast and a slow combustion. Of the 20 recorded cycles, the two highlighted corresponds to cycle #3 (fast) and #11 (slow). Pressure in main chamber is shown with dotted lines.

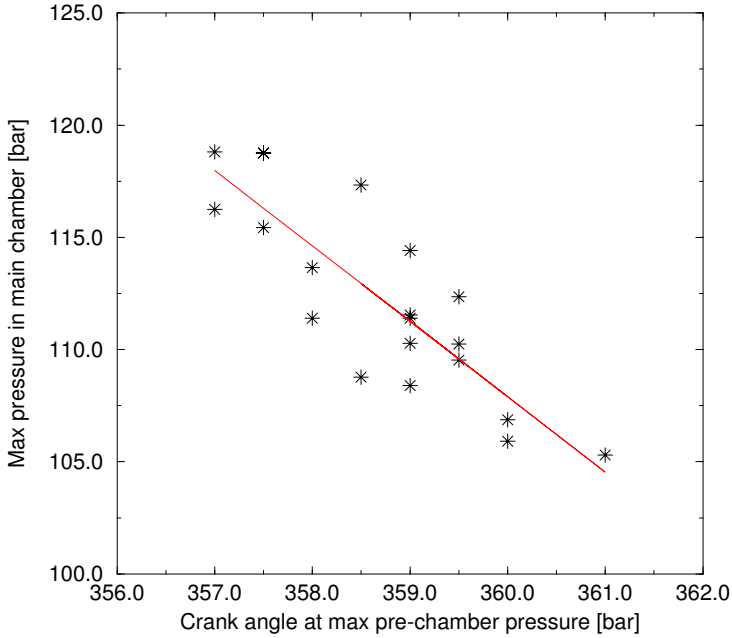

Figure 5.5: Plotting max main cylinder pressure in bar versus position of the prechamber peak in degrees for 20 consecutive cycles.

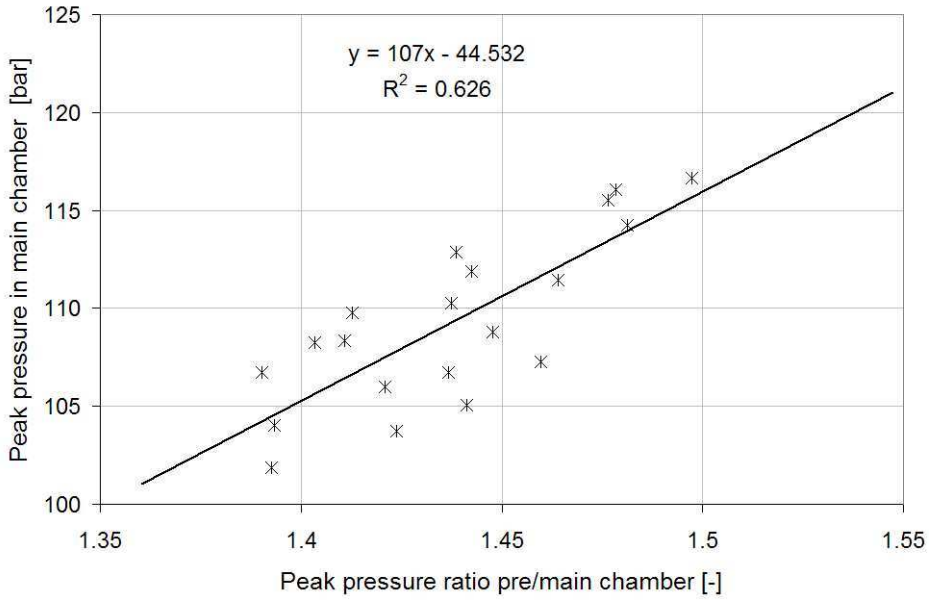

Figure 5.6: Correlation between pressure ratio between the two chambers during combustion in prechamber and maximum pressure in main chamber for 20 consecutive combustions.

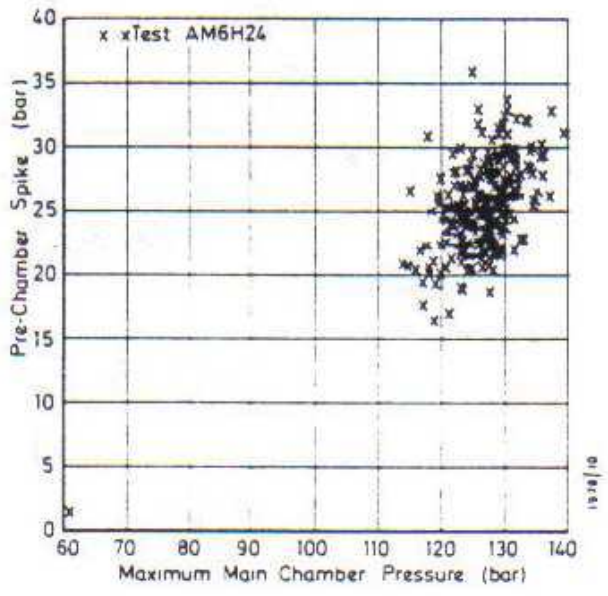

Figure 5.7: Figure from Snyder and Dexter [1990], showing "Correlation for pre-chamber spike height & main-chamber pressure for 300 cycles". This may be compared to figure 5.6

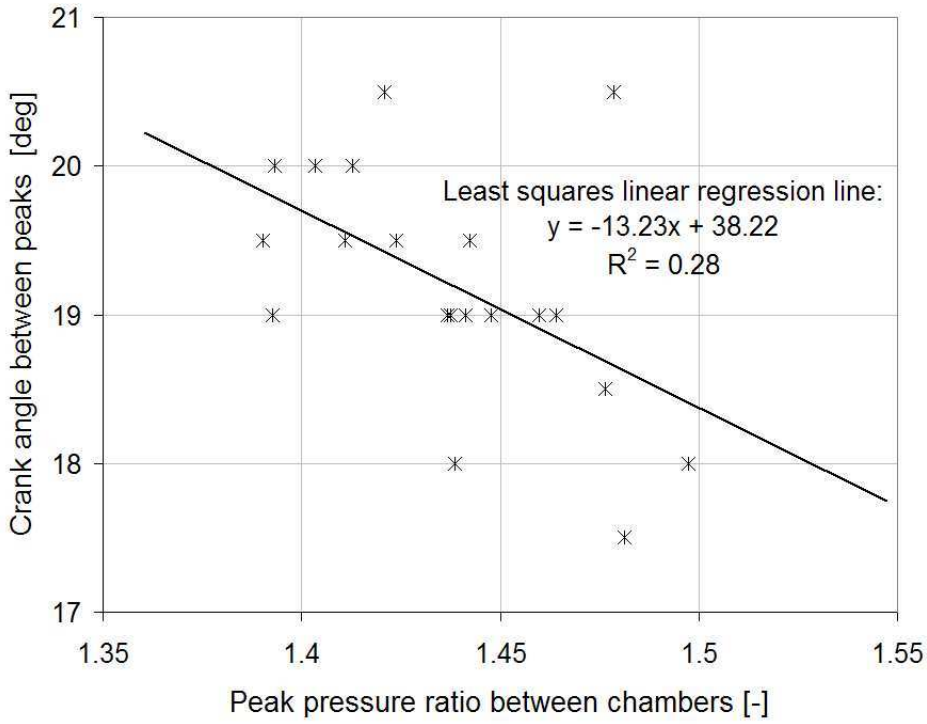

Figure 5.8: Correlation between peak pressure ratio (prechamber/main chamber) and crank angle between max pressure in prechamber and max pressure in main chamber. The stars indicate 20 consecutive combustion cycles.

Correlation between "peak pressure ratio between the two chambers" and "maximum pressure in main chamber" is presented in figures 5.6. This rather good correlation is in contrast to the finding of Snyder and Dexter [1990], see figure 5.7, who found:

> While there is a slight tendency for the peak main chamber to be higher when the pre-chamber spike is high, the data in general shows a random scatter.

The good correlation in the measurements with the KR-3 engine is particularly interesting with respect to the prechamber performance parameters as suggested in section 3 if one let the combustion rate in the main chamber be represented by "peak pressures in main chamber" and let the kinetic and thermal power of the jet be represented by "peak pressure ratio between prechamber and main chamber".

Another, but very weak, correlation is presented in figure 5.8. The correlation line indicates that the cycles with 10% higher pressure in the pre-

chamber will have approx. 10% shorter delay from prechamber peak untill reaching max pressure in the main chamber.

The correlation between "indicated mean effective pressure" and "crank angle between peak pressures in prechamber and main chamber" is close to zero.

The correlation between "cylinder pressure at time of ignition" and "crank angle between peak pressures in prechamber and main chamber" is also close to zero.

One may ask: Which of the traces in figure 5.4 is the most desirable one; cycle #3 with high pressure or #11 with late combustion? The answer to that question depends on the evaluation criterion:

- Thermal load on the combustion chamber: Cycle #11 has both lower peak pressure and lower duration at high pressure. Heat transfer and high temperature is associated with high pressure, therefore it should be safe to assume that cycle #11 is better with respect to lower thermal load on piston and cylinder head.

- Efficiency: Cycle #11 has 3.5 % higher mean effective pressure. The reason for this may be less heat transfer to the walls in the combustion chamber, or it may be caused by variations of the charge composition. If one assume that the charge composition is same, then cycle #11 will have 3.5 % higher efficiency.

- NO_x: Cycle #11 has both lower peak pressure and lower duration at high pressure. High temperature is associated with high pressure. NO_x is generated at high temperature, therefore is should be safe to assume that cycle #11 is better with respect to lower NO_x.

- HC, emission of hydrocarbons though the exhaust: When combustion occurs late, then there is risk of incomplete combustion and emission of HC. One can therefore assume that cycle #3 is better with respect to low emission of HC.

Figure 5.4 illustrates one of the balancing acts of tuning the engine: If the ignition timing had been set later, then one would get more cycles like #3 (and one would reduce thermal load, reduce NO_x and maybe also increase efficiency), but one would also get cycles much slower than #3 and these cycles would have incomplete combustion.

Figure 5.4 also illustrates the benefits of having a fast and stable combustion with little cycle by cycle variations: If the combustion in the main chamber had been faster or if there were less cycle by cycle variations, then

one would probably have used a few degrees later ignition timing in this engine and thereby achieved advantages with respect to thermal load, less NO_x and probably also higher efficiency.

The cause of cycle by cycle variations may be varying spark timing, varying charge composition in the vicinity of the spark, variations in the flow and turbulence near the spark or variations in the charge in the main chamber. More about cycle by cycle variations can be found in for example chapter 9.4 of Heywood [1988].

Snyder et al. [1988] presents another source of cycle by cycle variations. Quote from Snyder et al. [1988]:

> A misfire can occur in an engine if the burning prechamber charge fails to ignite the lean main-chamber charge. Figure 17 (in Snyder's paper) shows movie stills where one of the jets "misfired" in the CVC rig and failed to ignite the main-chamber charge. The flame in direct view did not die out, but combustion was started by other jets. Thus, for this run, only two out of the three pepperpot jets were successful in igniting the main-chamber charge.

The pictures are not included here because the copy is of low quality and difficult to explain. This phenomenon could explain deviations from the regression line in figure 5.5, however the deviations may also be explained by variations in the charge composition in the main chamber.

Also observe the two highlighted cycles in figure 5.9 where two cycles have similar paths in the prechamber combustion, while one is higher in the main chamber and maintains higher pressure during the expansion stroke. This variation may be due to variations in the main chamber charge, or it may be due to a misfiring jet from a prechamber nozzle hole, as described by Snyder et al. [1988], causing incomplete combustion in the main chamber. If it did not maintain higher pressure during expansion stroke, then it would be more likely to be caused by a misfiring jet.

5.5 Other observations

Pressure difference between chambers From figure 5.2 one can observe that the two pressures (as expected) follow each other very closely, except for a few degrees after the ignition.

Direct effect of jet volume: The main chamber pressure does not show a sharp increase when it receives the jet. From this observation one may conclude that this prechamber is so small that the (direct) effect on the

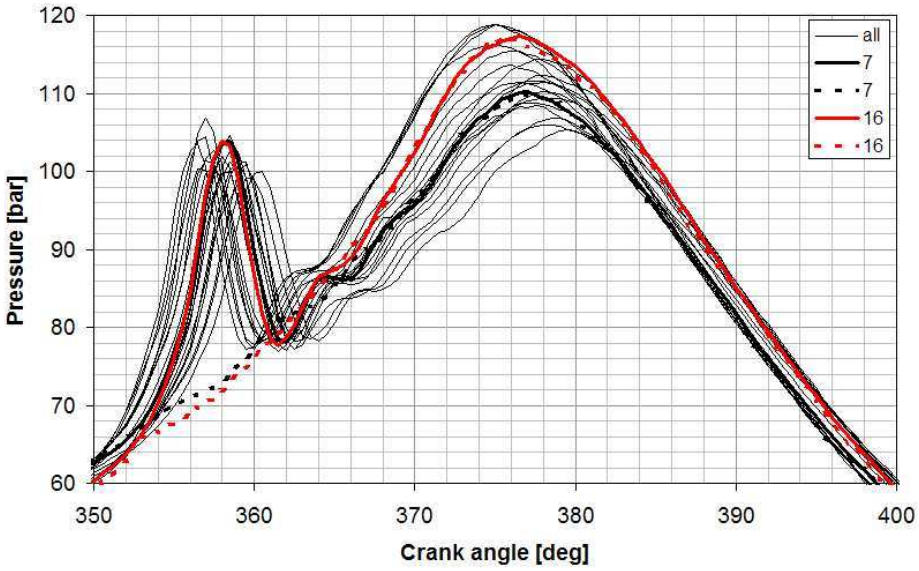

Figure 5.9: Comparing two cycles with similar paths in prechamber, but with different path in main chamber. Of the 20 recorded cycles, the two highlighted corresponds to cycle #7 (low) and #16 (high). Pressure in main chamber is shown with dotted lines.

pressure in the main chamber from the volume flow from the prechamber is negligible.

5.6 Using the two zone model

The calculation models presented in section 4.2.1 may be applied to the measured pressure and the given engine parameters. The following procedure for using the two zone calculation program was used:

1. Make an input file with the engine parameters and a first guess of V_{ff} (volume fraction combusted when flame reaches nozzle) and LHV_{net} (nett heat value [J/kg] for the charge). Select one of the pressure traces (here from figure 5.4) to use as input.

2. Run the program, plot the result, adjust LHV_{net} and run the program again until the volume fraction combusted at the end of combustion is close to unity.

3. There will be a drop/step in the calculated ROHR at the time when the real flame reaches the nozzle. Adjust V_{ff} and re-run the program

until the flame reaches the nozzle at this time.

The result is displayed in figure 5.10. The best fit was found with approximately V_{ff}=90 % , and with a heat value of the charge $LHV_{net} = 1.1$ MJ/kg. This value of LHV_{net} is approximately 40 % of a stoichiometric charge of CH_4 and air with the given intake conditions. 60 % is "missing" due to heat loss, not stoichiometric charge and maybe also higher temperature than expected during the intake stroke. Geometrical deviations may also be a reason, for example: A nozzle discharge coefficient of 0.5 was assumed because the nozzles have sharp edges, if the coefficient is higher, then it would lead to calculation of a higher LHV_{net}.

The thermal and kinetic efficiencies are calculated to respectively 17 % and 0.43 %. Note that these efficiencies are calculated with the given LHV_{net}.

The hot jets are calculated to reach 70 mm into the main chamber 1.2 ms after ignition.

Effect of geometrical variations A change in the nozzle geometry would affect the nozzle discharge coefficient. Figure 5.11 shows the same picture as figure 5.10, but with nozzle discharge coefficient of 0.75. This leads to (according to the procedure described above) $LHV_{net} = 2.0$ MJ/kg or 74 % of a stoichiometric charge of CH_4 and air. In this case the thermal and kinetic efficiencies are calculated to respectively 20 % and 0.84 %. Also note that the calculated combustion temperature is significantly higher when using the higher nozzle discharge coefficient.

Calculating with larger nozzle diameter would have almost the same effect as increasing the discharge coefficient, but it would in have more effect on the jet length.

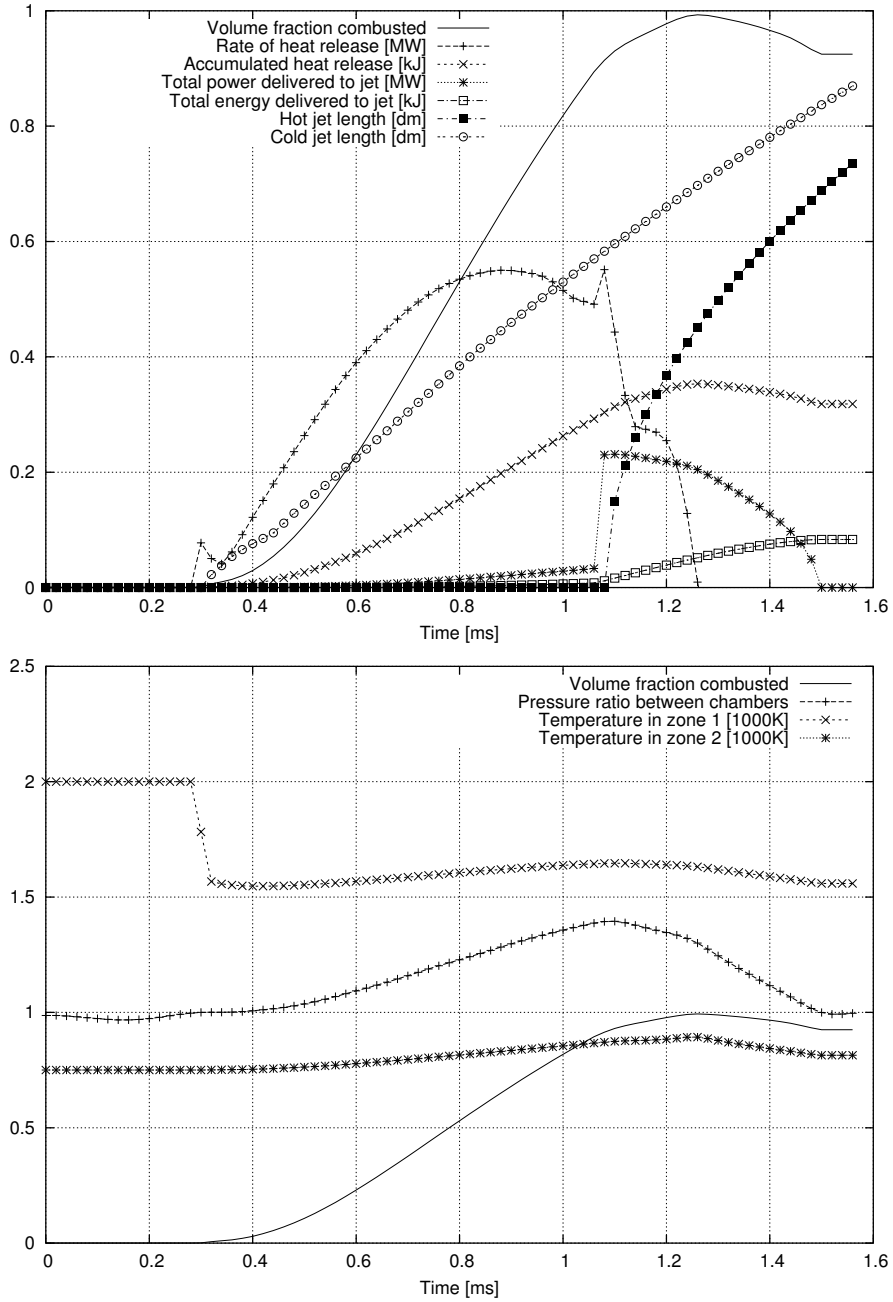

Figure 5.10: Using measured pressures and a simple numerical prechamber model to estimate rate of heat release and jet length. The ignition is at time=0.3 ms. 1 ms = 6 deg of crank angle.

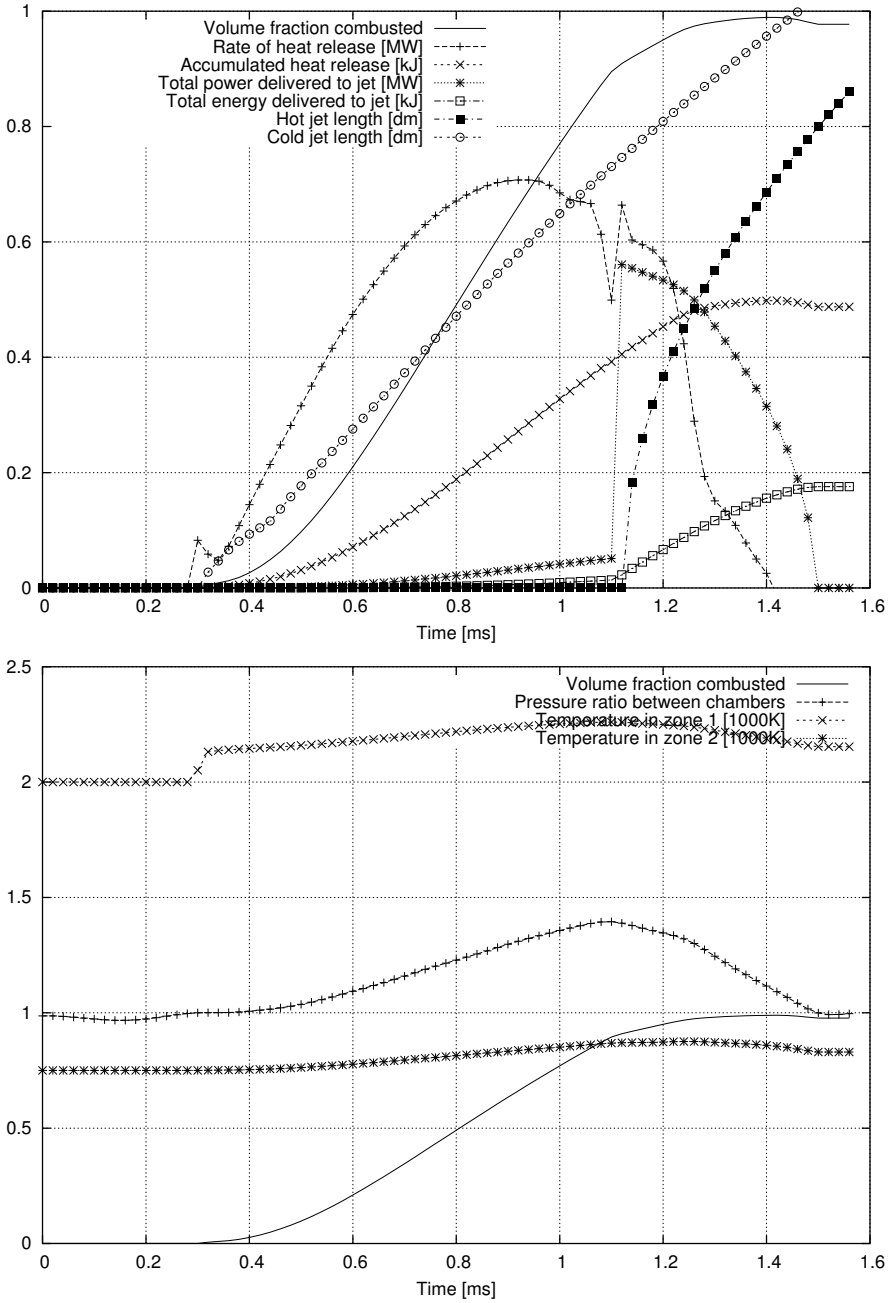

Figure 5.11: Output from two zone model when the nozzle discharge coefficient is increased to 0.75.

5.7 Summary from experiments with medium speed engine

Pressure measurements in both prechamber and main chamber of a spark ignited medium speed engine burning premixed air and natural gas have been completed and analyzed. The pressures and the calculated values are of course only valid for this particular engine.

The results are summarized in the following list.

- The prechamber combustion lasts approximately 1 ms.
- The pressure ratio between the two chambers during combustion in the prechamber is in the range from 1.39 to 1.50.
- Spark ignited engines with prechambers suffer from cycle by cycle variations with several origins. One source of cycle by cycle variation may be that one or more of the hot jets fail, or uses longer time, to ignite the main charge.
- The very rough jet model indicates that the six hot jets from the prechamber reach 70 mm into the main chamber within 1.2 ms after ignition.
- The output of the two zone model is sensitive to geometrical variations, small changes in the nozzle size or shape have large effects on the results.
- In particular the calculated temperature is sensitive to the effetive nozzle area. This means that the calculated temperatures can not be used as input to calculation of NO_x formation.

Cycle by cycle variations are found to be important. Note that none of the suggested prechamber performance parameters introduced in section 3 describes cycle by cycle variations directly. The closest parameter would be the "characteristic prechamber times". It might be wise to include a new "characteristic prechamber time" as a prechamber performance variable with target of describing cycle by cycle variations. It could be defined as duration from ignition (first spark) to peak pressure in prechamber.

The presented correlations support the idea that more power (kinetic or thermal) from the prechamber gives faster combustion in the main chamber. Faster combustion in the main chamber is desired with respect to both engine efficiency and emissions.

5.8 Recommendation for further work

If one varies the charge in the prechamber (so that the prechamber performance is changed), then it should be possible to study the correlation between the suggested prechamber performance parameters and engine performance.

Chapter 6

Experiments with a constant volume combustion rig

6.1 Introduction

The goal for these experiments is to use a constant volume combustion rig (CVC-rig) with prechamber to:

1. Measure pressure in both chambers in the rig and use the pressures as input to the two-zone model as defined i chapter 4.2.1. The two-zone model will then calculate values for the performance variables defined in chapter 3.

2. Visually observe the jet length from the prechamber and compare calculated and observed jet length.

3. Change the geometry of the prechamber and observe how this influences the performance of the prechamber. The results from this has been moved to appendix E.

That the rig has "constant volume" implies that there is no reciprocating piston as would be present in an engine. CVC-rigs without prechamber and Schlieren systems have been used previously at the Department of Marine Engineering, NTNU [Æsøy, 1996, Ask, 1992, Paulsen, 1995]. CVC-rigs are also commonly used elsewhere, and some have also used CVC-rigs in the study of premixed combustion in conjunction with prechambers: Snyder and Dexter [1990], Snyder et al. [1988] and Wolff et al. [1997].

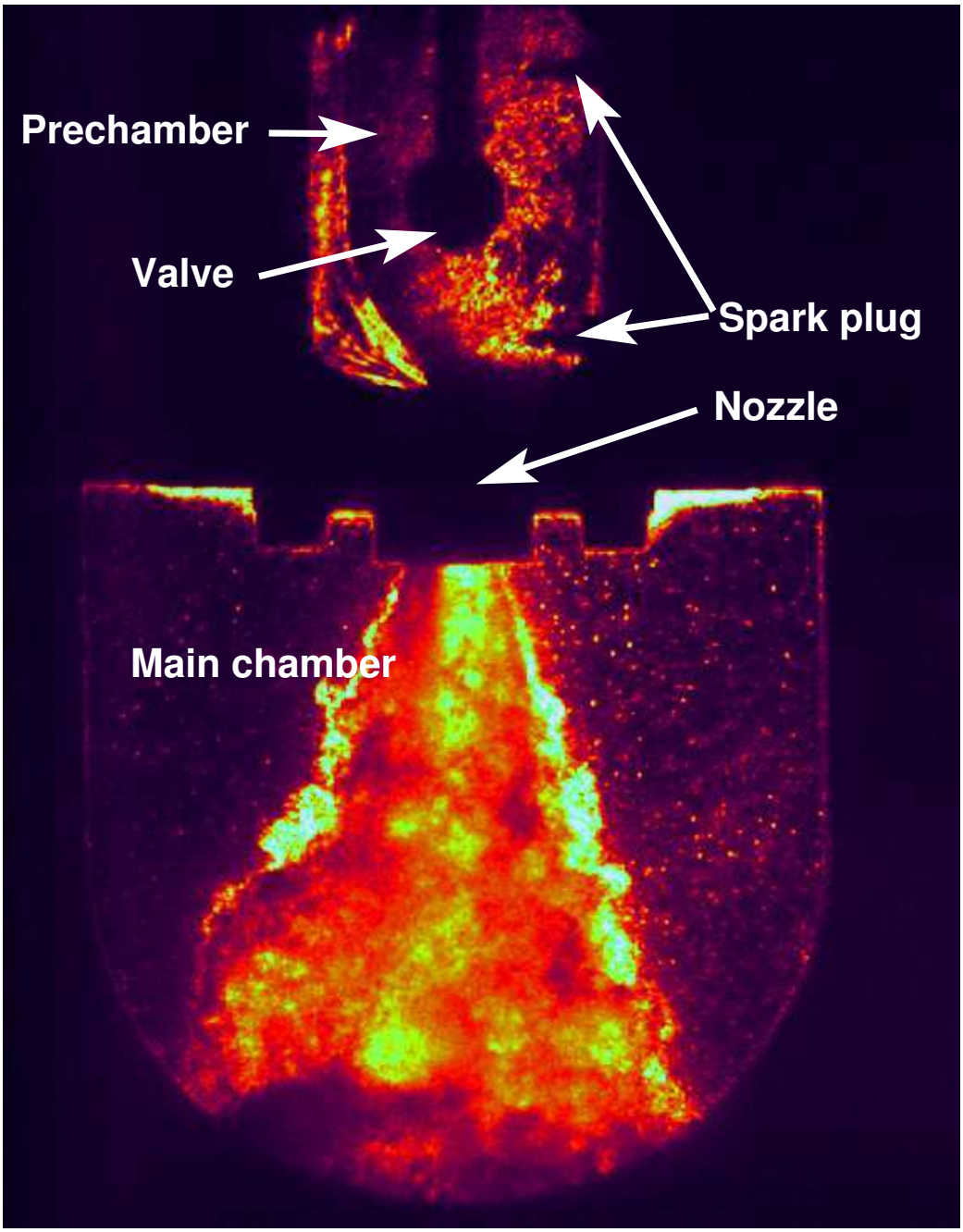

Figure 6.1: Large picture of a prechamber (upper square in picture, size 30 mm x 40 mm) blowing a burning jet into the main combustion chamber. The flame front inside the prechamber is clearly visible. All the "stars" in the picture are results of a previous experiment that burnt soot particles into the glass windows. It is possible to move the valve plunger down so that the opening between the chambers is closed.

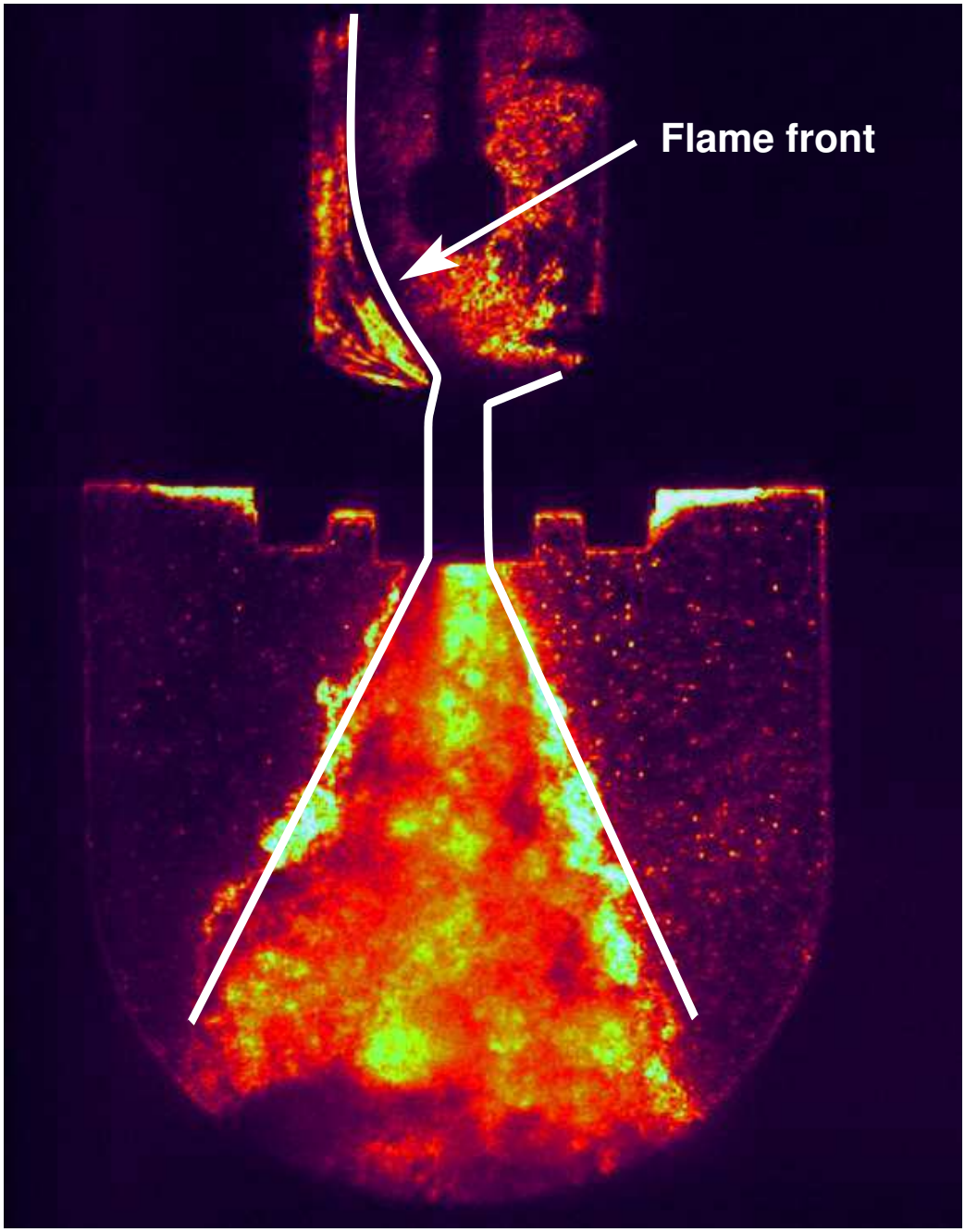

Figure 6.2: Same picture as in previous figure, but with the flame front marked by a white line.

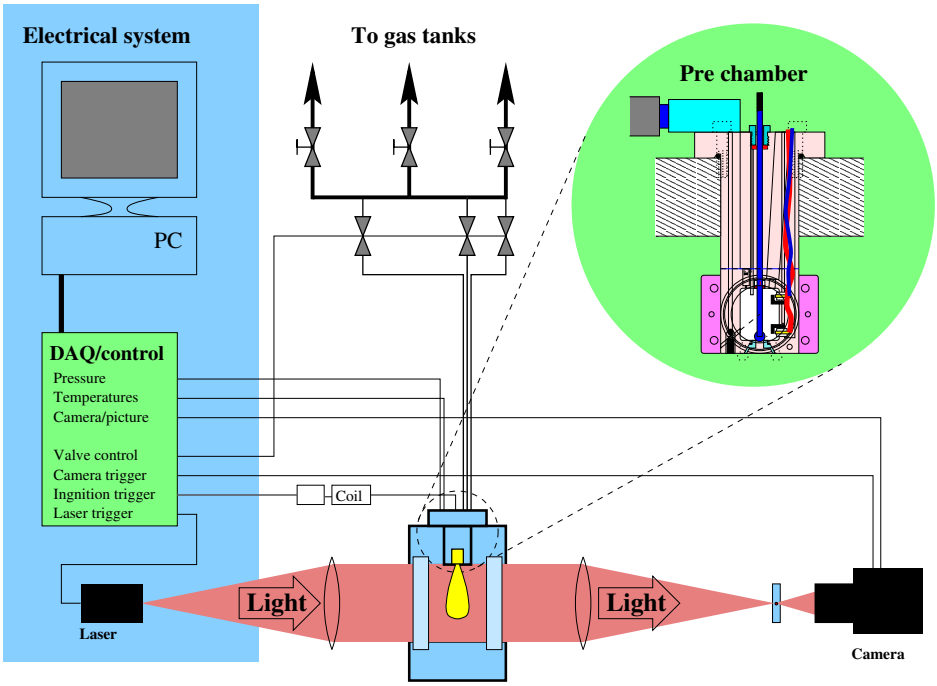

Figure 6.3: Schematic laboratory setup. The combustion chamber is shown in lower, midle part of the figure. A blown up figure of a prechamber is shown in the upper right. The hydraulic system for valve control and the rugged mounting frames are not shown in this figure.

6.2 Laboratory setup

The laboratory setup (see figure 6.3 and 6.4) consists of; the main combustion chamber, prechambers, hydraulic system, Schlieren setup, gas delivery system, ignition system and electronic control and measurement system. More about the hardware can be found in appendix D.

Figure 6.5 shows a screen-shot of the control program of the CVC-rig along with an explanation. The operating sequences are also also described in more detail together with the results from each experiment. A summary of different operating sequences can be found in appendix E.

The measurements available are start pressure in main chamber and pressure development in both chambers.

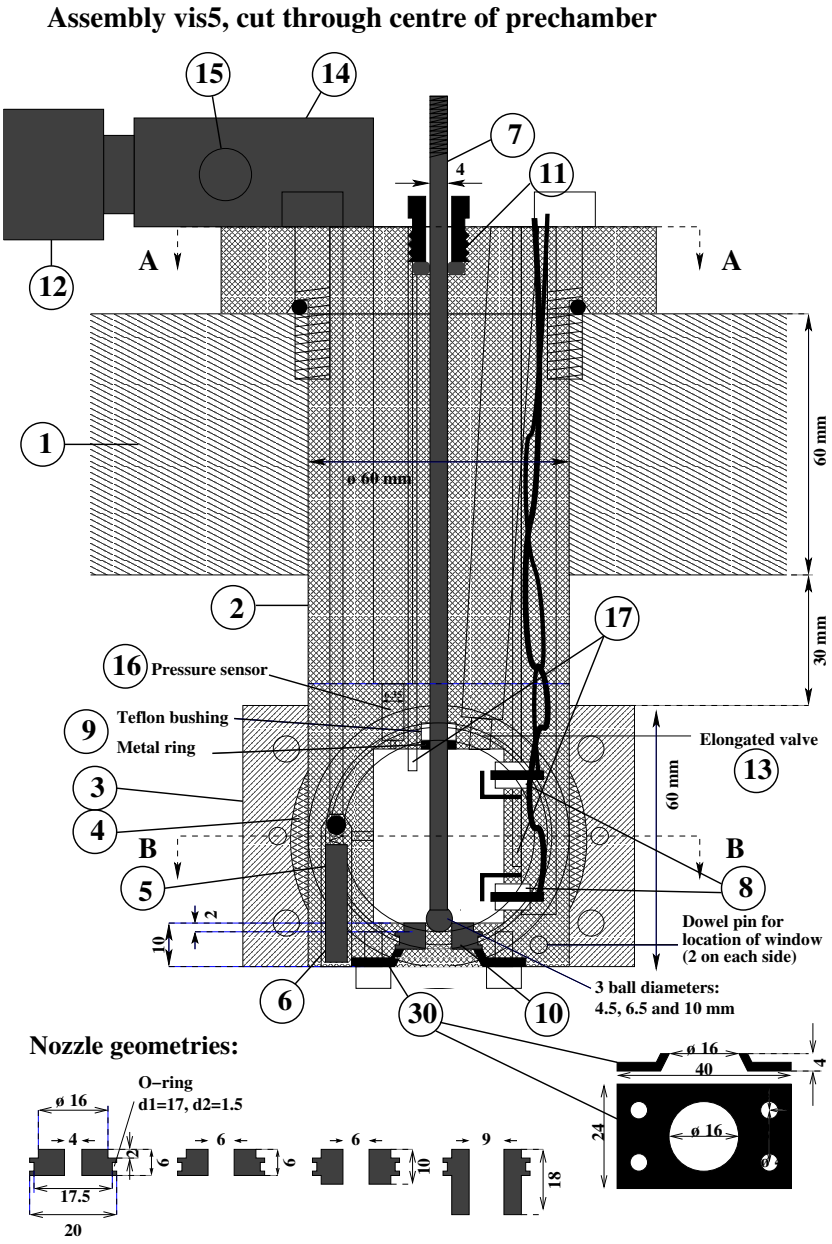

Figure 6.4: Cutaway drawing of prechamber assembly consisting of the following main parts: (1) Main chamber housing, (2) Prechamber housing, (3) Window and holder (two off, one on each side), (5) One way valve for gas supply, (7) Pin for closing then nozzle, (8) Spark plugs, (10) Nozzle, (12) Valve for gas supply, solenoid operated, (13) Exhaust valve, solenoid operated, (14) Gas supply manifold, (16) Pressure sensor, (17) Temperature sensors, (30) Nozzle holder.

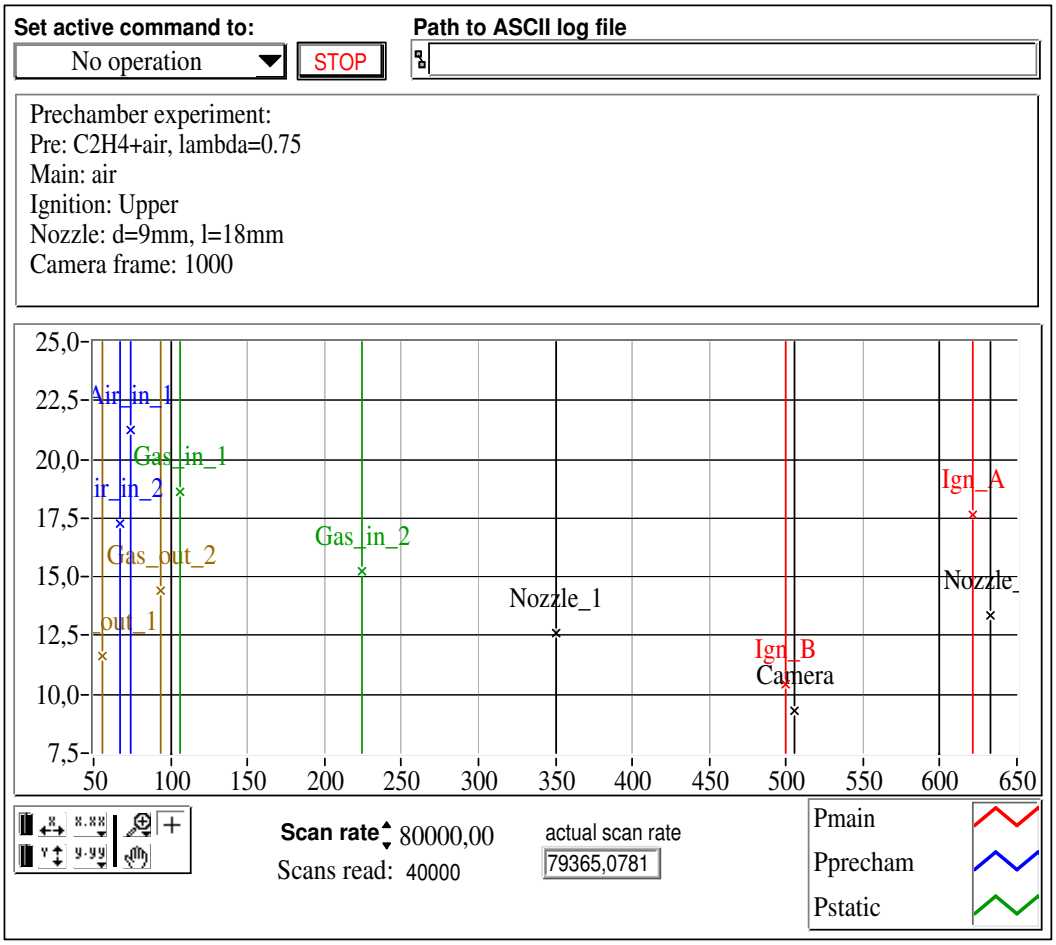

Figure 6.5: Screen-shot of the control program for the CVC-rig. The graph can show pressure [bar] as a function of time [ms] and is also used to program the test sequence. The timing of events can be programmed by clicking and dragging the timing control lines along the horizontal time axis. (The cross on the timing control lines has no other effect than placing the label.) The timing control lines have the following meanings:
Air_in_1 / Air_in_2: Open/close air inlet into the prechamber.
Camera: Trigger the camera. The result will be a single image.
Gas_in_1 / Gas_in_2: Open/close gas inlet into the prechamber.
Gas_out_1 / Gas_out_2: Open/close exhaust towards the atmosphere.
Ign_A / Ign_B: Trigger the ignition at respectively the upper and lower ignition system.
Log_1 / Log_2: Start/stop high speed pressure measurements.
Nozzle_1 / Nozzle_2: Open/close the opening between the prechamber and the main chamber.
The text window above the timing lines contains a short description of the current experiment.

6.3 Experiment 1

Of several series of experiments, only one is selected for presentation in full length here, results from other experiments are shown in appendix E.

The target of this experiment is to measure pressure in both chambers of the CVC-rig, use the measured pressure as input to a calculation model and compare measured and calculated jet length.

Prechamber: Square chamber with windows: 30 x 30 x 40 mm with Ø 9 x 18 mm nozzle (as shown in figure 6.4) and using the upper ignition source.

Gas: Rich $\lambda = 0.75$ mix of C_2H_4 and air. The prechamber contains air at atmospheric pressure at the start of the control sequence, while the main chamber contains air at 8 bar pressure. Rich C_2H_4 and air was chosen because it was found in preliminary experiments that this gas is easy to ignite and has a higher flame speed than CH_4 and air.

The operating sequence is shown in figure 6.6.

Pictures and pressure measurements from this experiment can be found in figures: 6.8 to 6.22.

Measured pressure from the prechamber was used as input the numerical program as presented in section 4.2.1 and used to calculate rate of heat release and jet length. The height of the prechamber is 40 mm, looking at the pictures, one may observe that the cold jet reaches a similar distance (40 mm) at time=3 ms. This is the same as the calculated cold jet length in figure 6.7.

The best fit was found (using the approach as described in section 5.6) to be with approximately V_{ff}=45 %, and with a heat value of the charge $LHV_{net} = 0.6$ MJ/kg (note that this is only half of what was found for the engine in section 5.6). The thermal and kinetic efficiencies are calculated to respectively 46 % and 0.5 %, which can also be compared to the values for the engine.

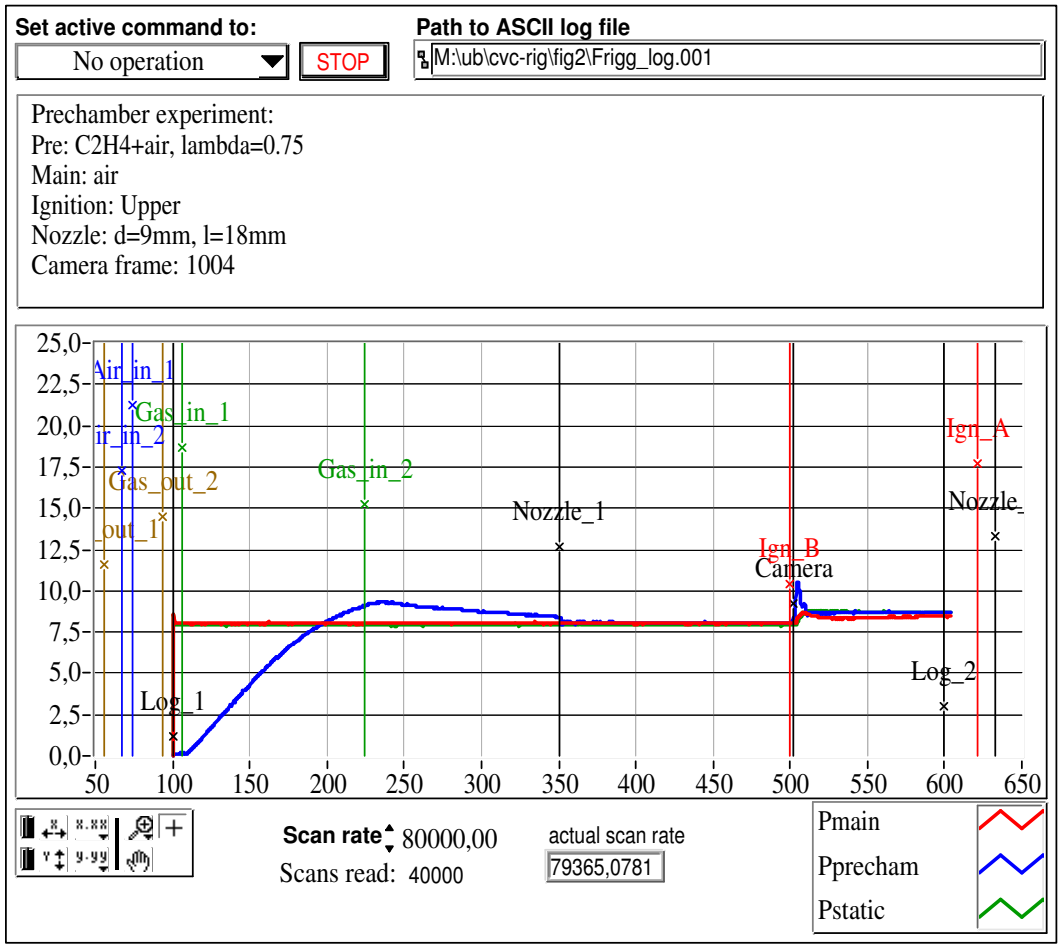

Figure 6.6: Operating sequence for experiment 1. The graph shows also pressure measurements as a result from running the sequence. The inlet valve is opened at time = 100 ms and causes a pressure increase in the prechamber as the prechamber is filled with premixed C_2H_4 and air until the inlet valve is closed at time = 225 ms. The nozzle between the two chambers is opened at time = 350 ms. Ignition is triggered at time = 500 ms. One can see the pressure increase caused by the combustion as a "bump" in the pressure measurement right after time = 500 ms. The graphs presenting the results of the experiments will be zoomed in and showing only the area right after time = 500 ms.

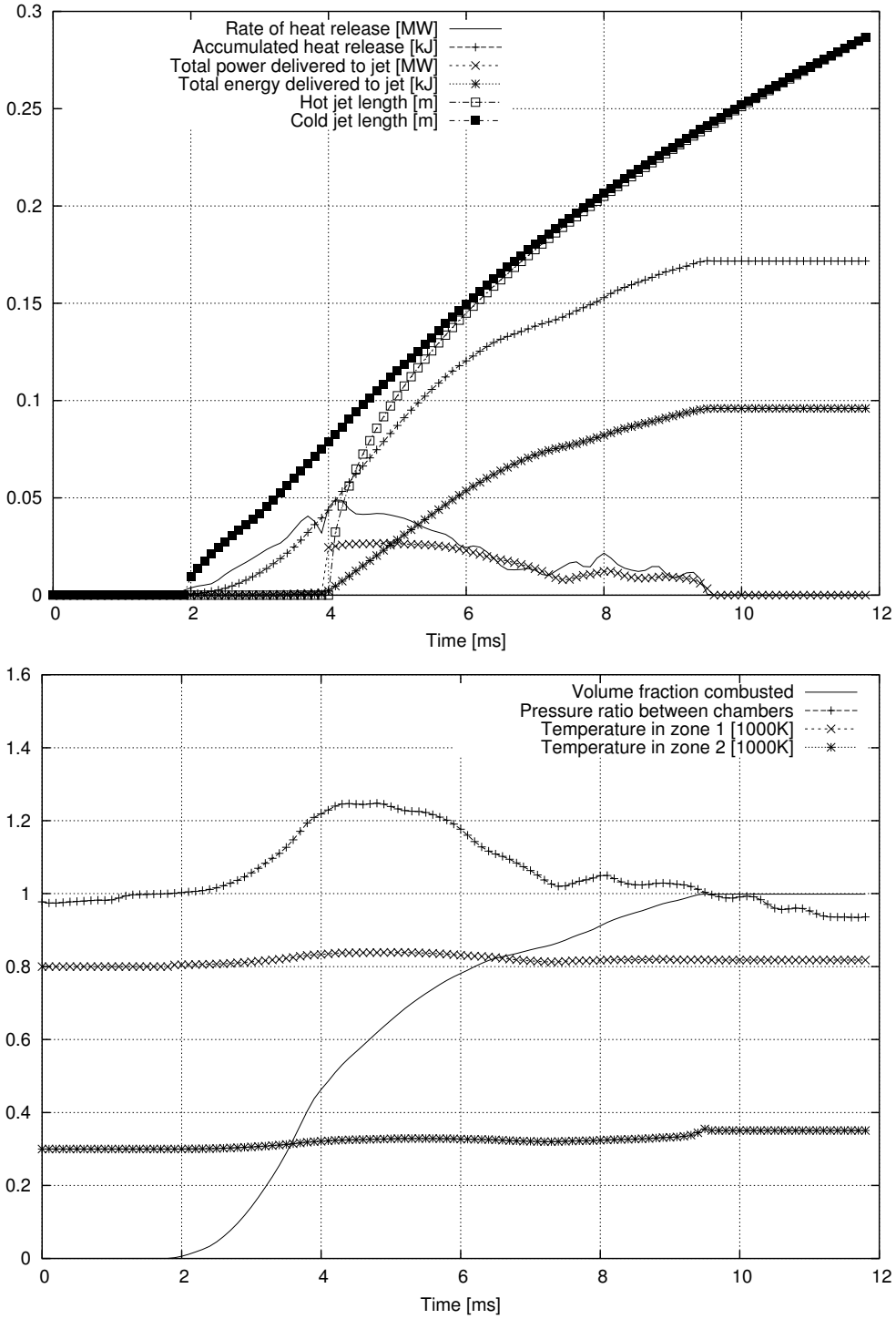

Figure 6.7: Output from calculation of ROHR, etc. Using log file 1006 (see figure 6.20) as input, $V_{ff} = 45$ % and $LHV_{net} = 0.6$ MJ/kg

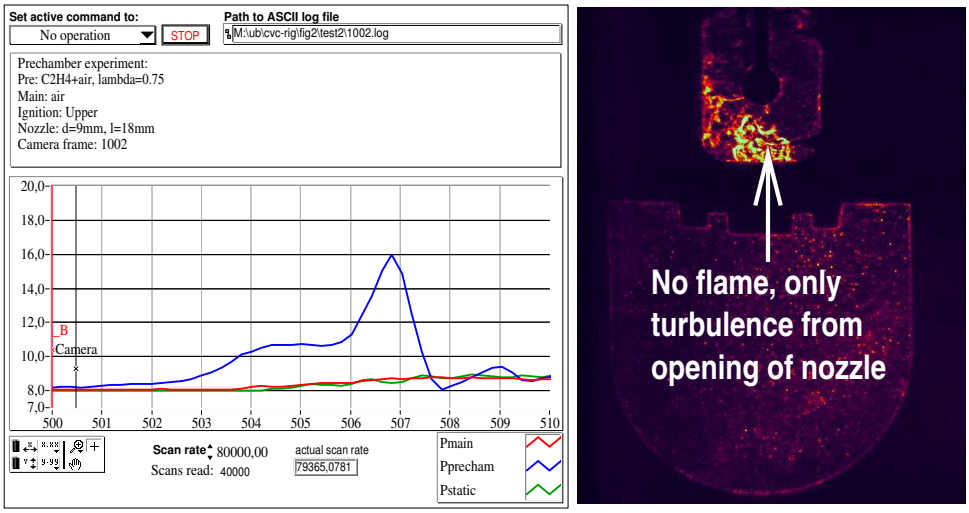

Figure 6.8: Picture is taken 0.5 ms after ignition is triggered. No spark or flame is visible. The control program settings are the same window as shown in figure 6.6, but the time scale window is zoomed so that only a few milliseconds directly after the ignition trigger is visible. The picture is taken at the time indicated by the vertical line marked "Camera" in the program window. Note that there is a large peak in the recorded prechamber pressure close to the end of the combustion.

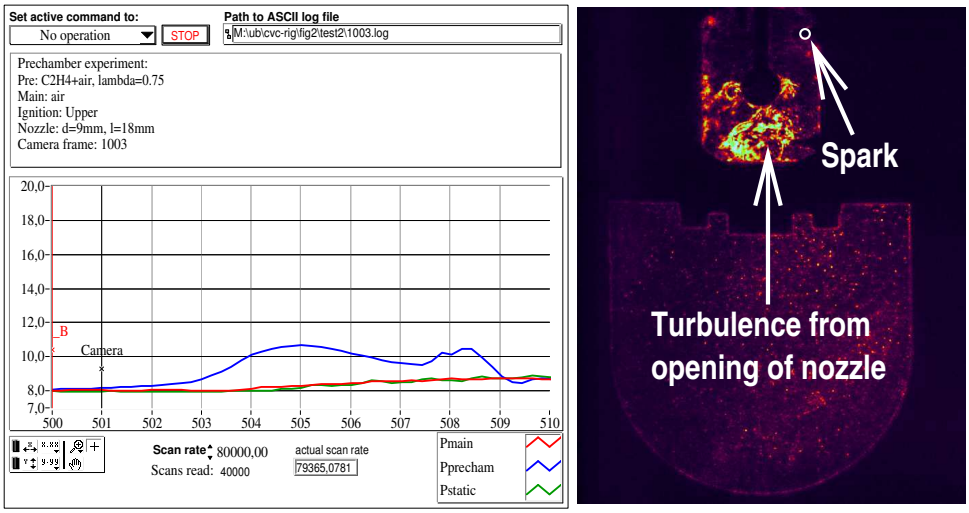

Figure 6.9: The experiment is repeated, but with the picture taken slightly later, now 1.0 ms after ignition trigger. A small spark or flame can be seen at the upper spark plug. Note that the pressure during the first half of the combustion is similar to what was recorded during the previous combustion, but the pressure peak close to the end of combustion is lower.

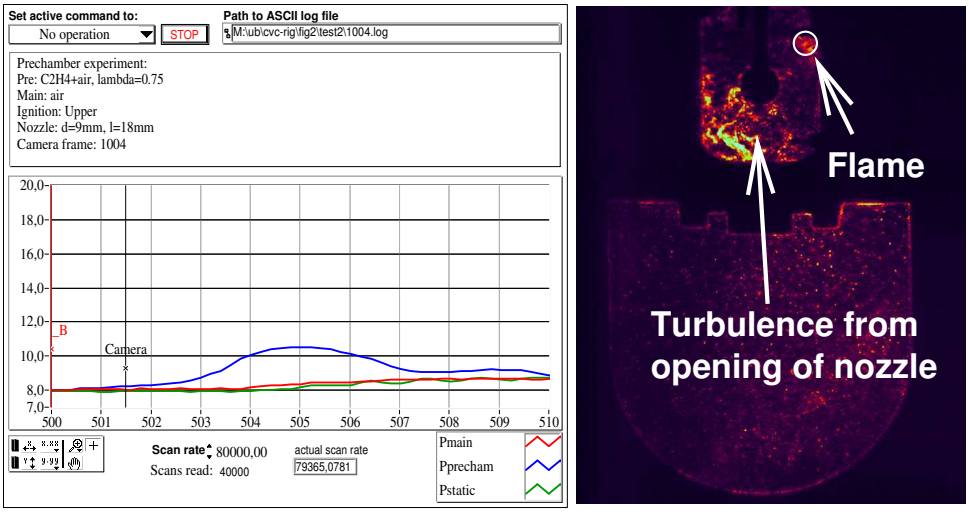

Figure 6.10: The experiment is repeated, now the picture is taken 1.5 ms after ignition trigger. The flame kernel has grown larger compared to the previous picture. Note that the pressure during the first half of the combustion is similar to what was recorded during the previous combustions, but the pressure peak close to the end of combustion has disappeared.

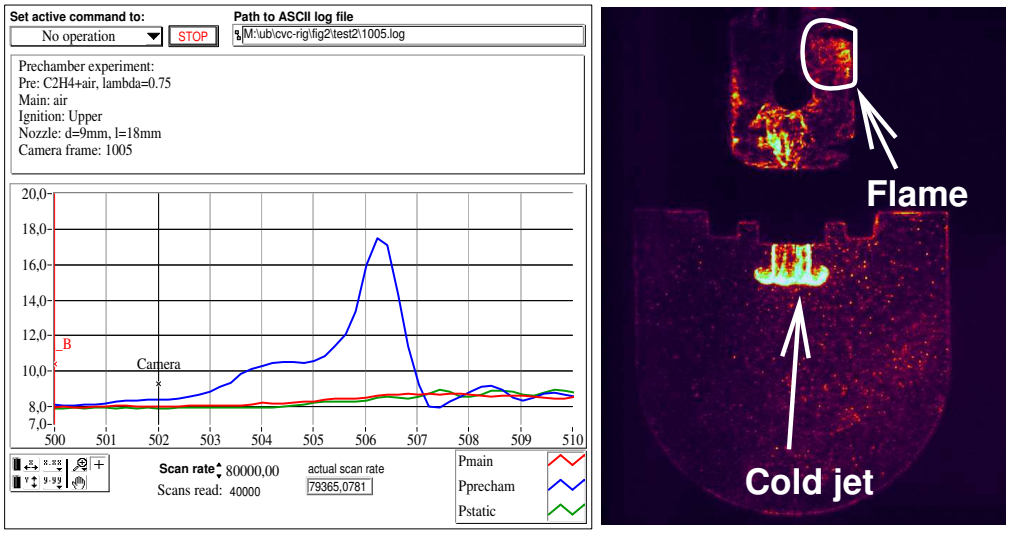

Figure 6.11: The experiment is repeated, now the picture is taken 2.0 ms after ignition trigger. The flame is larger compared to the previous picture and causes a small pressure increase in the prechamber. The pressure gives a flow of "cold" (not combusted) gas from the prechamber into the main chamber. The pressure peak close to the end of combustion is back again.

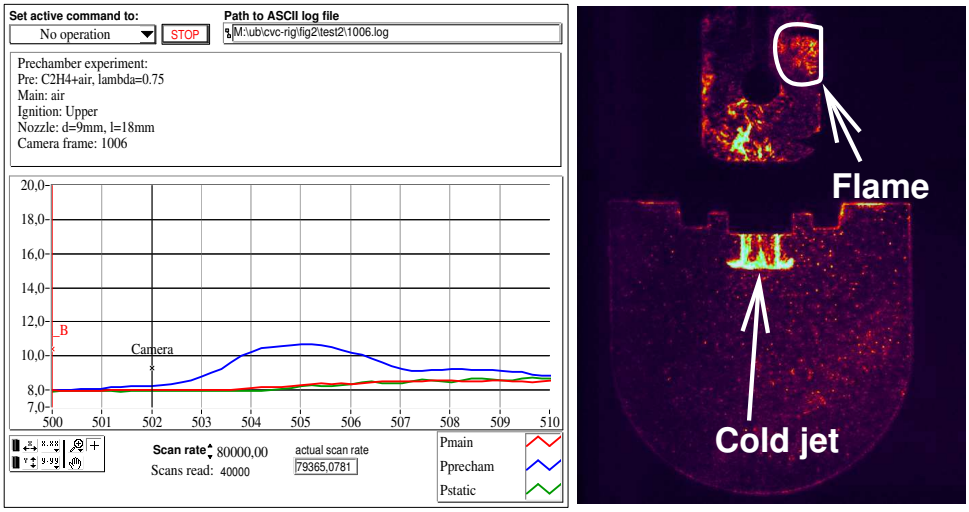

Figure 6.12: The experiment is repeated, the picture is taken at the same timing as in the previous repetition, i.e. 2.0 ms after ignition trigger. The pressure peak close to the end of combustion is gone, but the cold jet early in the combustion is very similar to the one in the previous combustion.

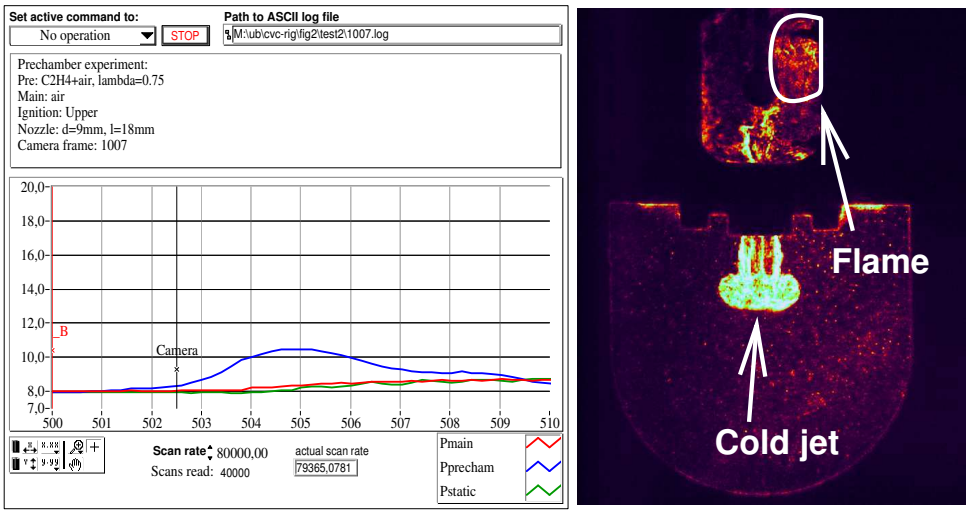

Figure 6.13: The experiment is repeated, now the picture is taken 2.5 ms after ignition trigger.

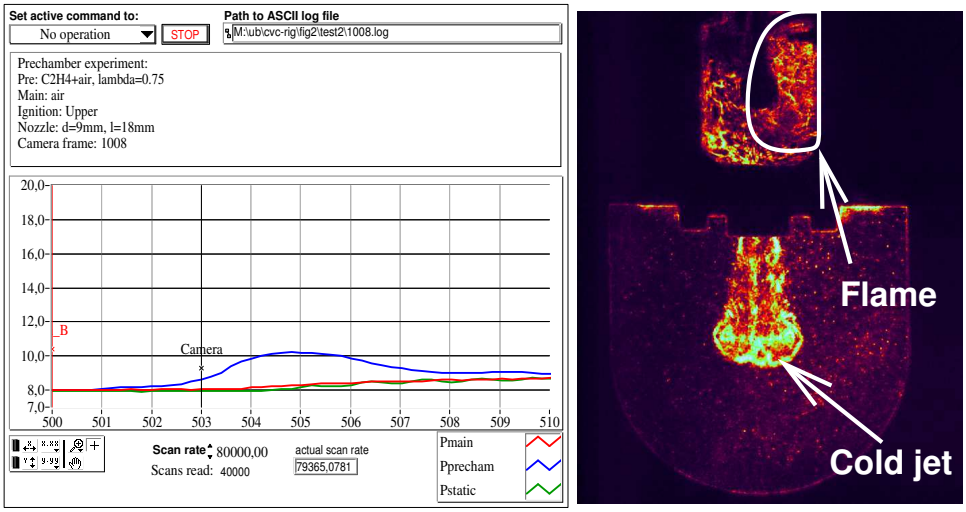

Figure 6.14: The experiment is repeated, now the picture is taken 3.0 ms after ignition trigger. The flame has now almost reached the nozzle between the two chambers.

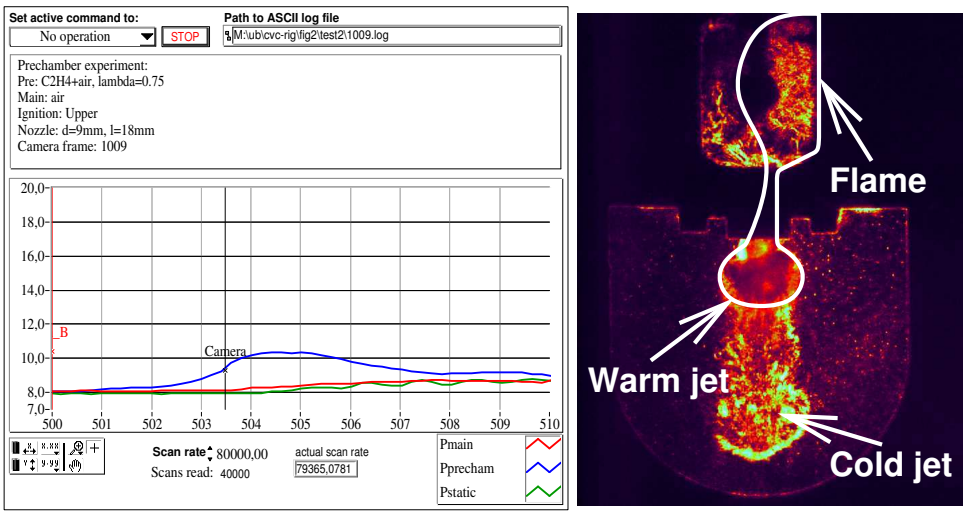

Figure 6.15: The experiment is repeated, now the picture is taken 3.5 ms after ignition trigger. The flame has now almost reached through nozzle and created a 15mm long warm jet into the main chamber. The warm jet ignites the fuel in the cold jet. The combustion of fuel in the cold jet causes the jet spread angle to increase close to the nozzle.

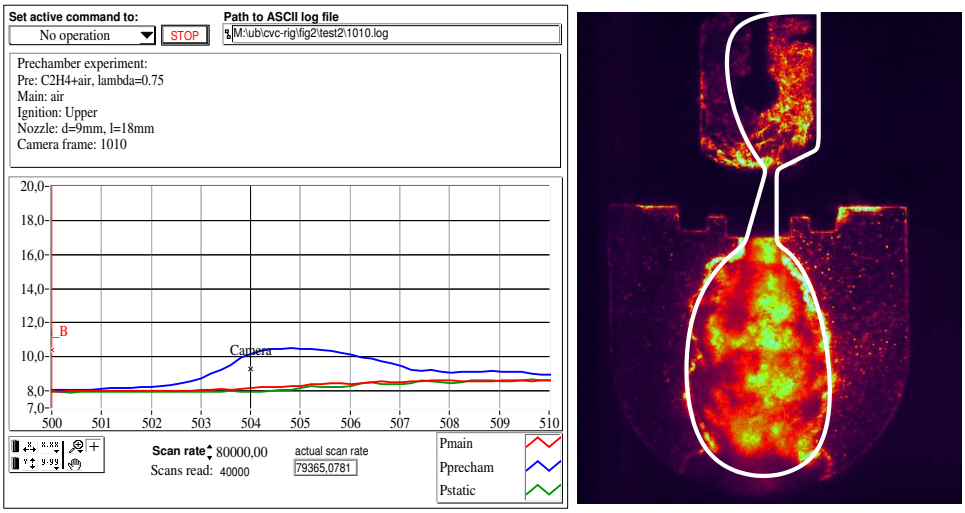

Figure 6.16: The experiment is repeated, now the picture is taken 4.0 ms after ignition trigger. The warm jet ignites the fuel in the cold jet. The combustion of fuel in the cold jet causes the jet spread angle to increase close to the nozzle.

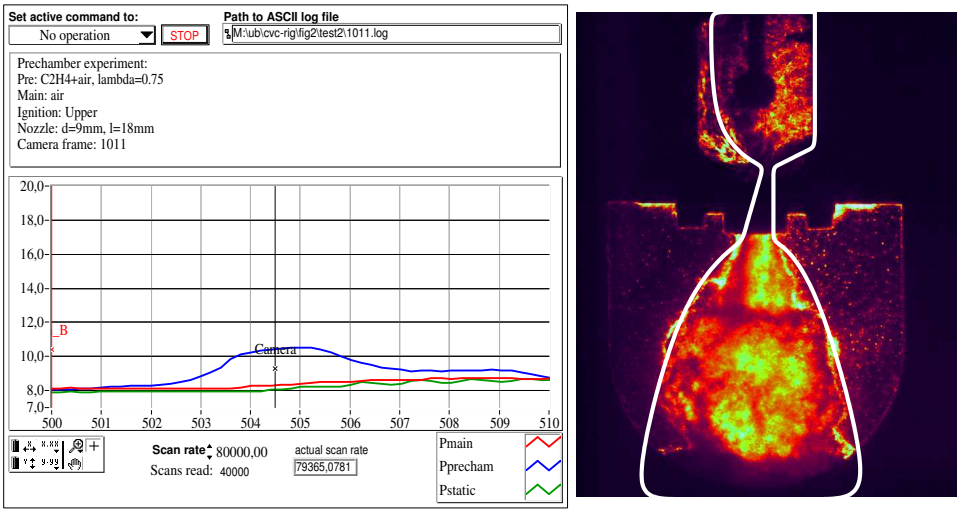

Figure 6.17: Picture taken 4.5 ms after ignition trigger.

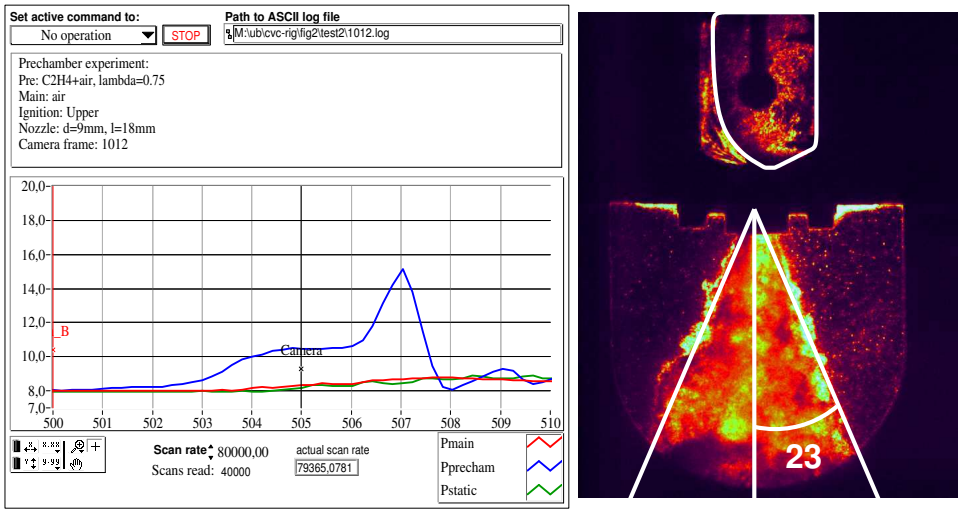

Figure 6.18: The experiment is repeated, now the picture is taken 5.0 ms after ignition trigger. The jet spread angle can be measured to be approximately 23°.

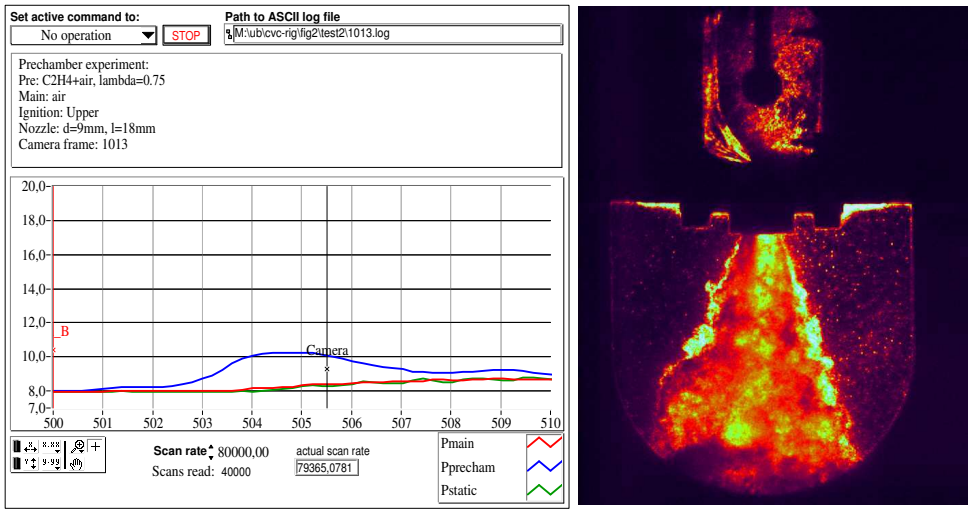

Figure 6.19: Picture taken 5.5 ms after ignition trigger.

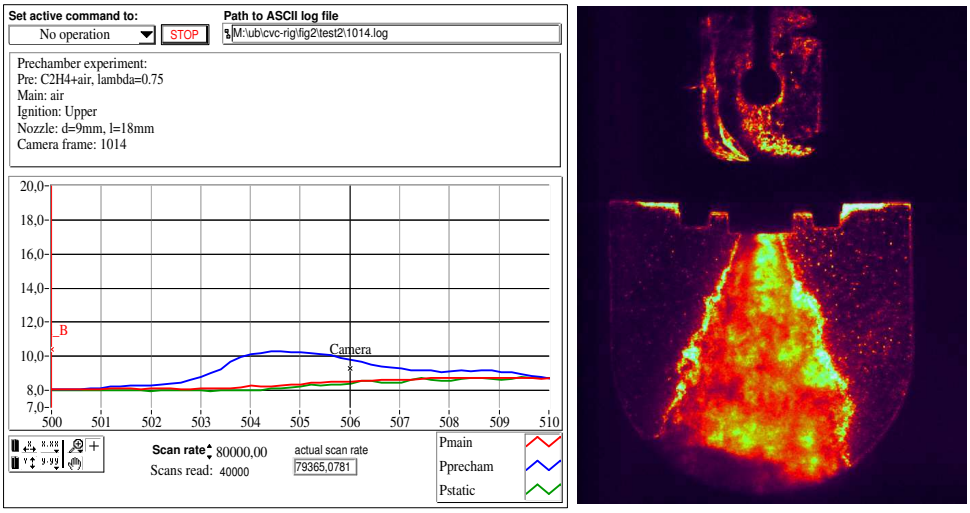

Figure 6.20: Picture taken 6.0 ms after ignition trigger. The surface of the flame is clearly visible inside the prechamber.

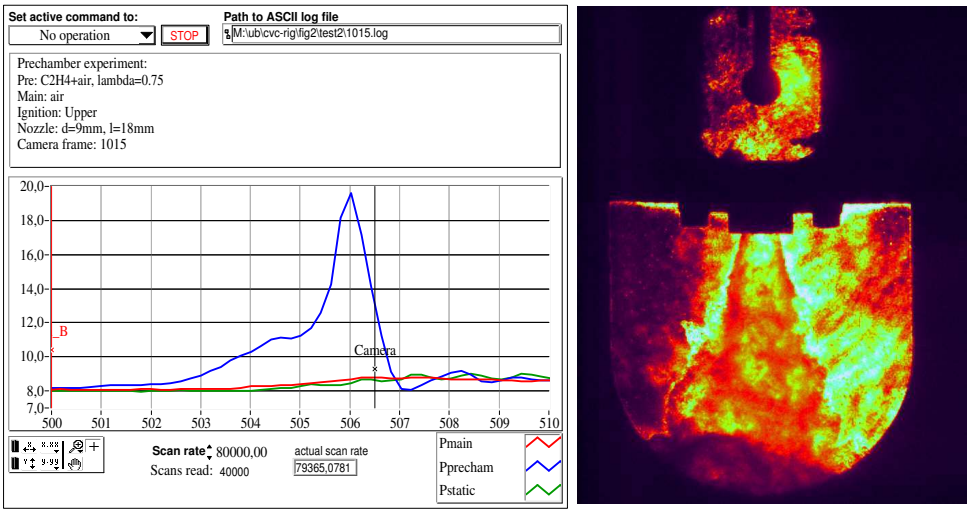

Figure 6.21: Picture taken 6.5 ms after ignition trigger. This picture is taken directly after a knocking combustion. There is no visible flame surface inside the prechamber. Also the gas in the main chamber (to the right from the jet) appears to be affected by the knock.

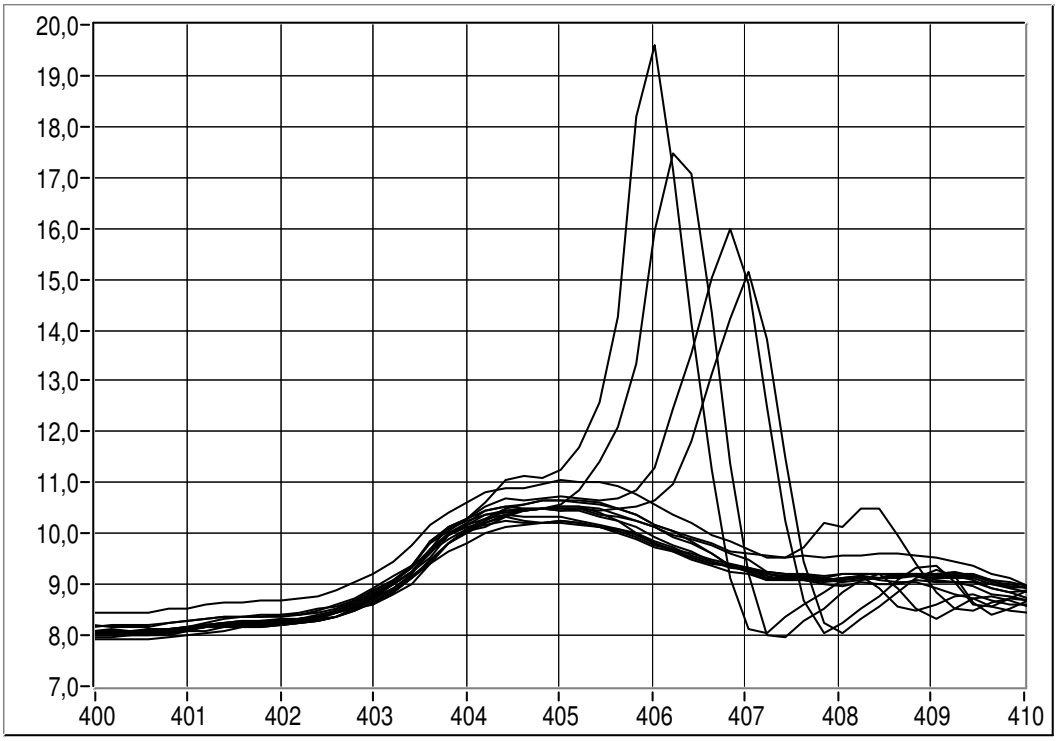

Figure 6.22: Pressure [bar] as a function of time [ms]. 15 prechamber pressures collected into one graph. There is a large difference in pressure at the last stages of the combustion. This is believed to be due to a kind of knocking combustion.

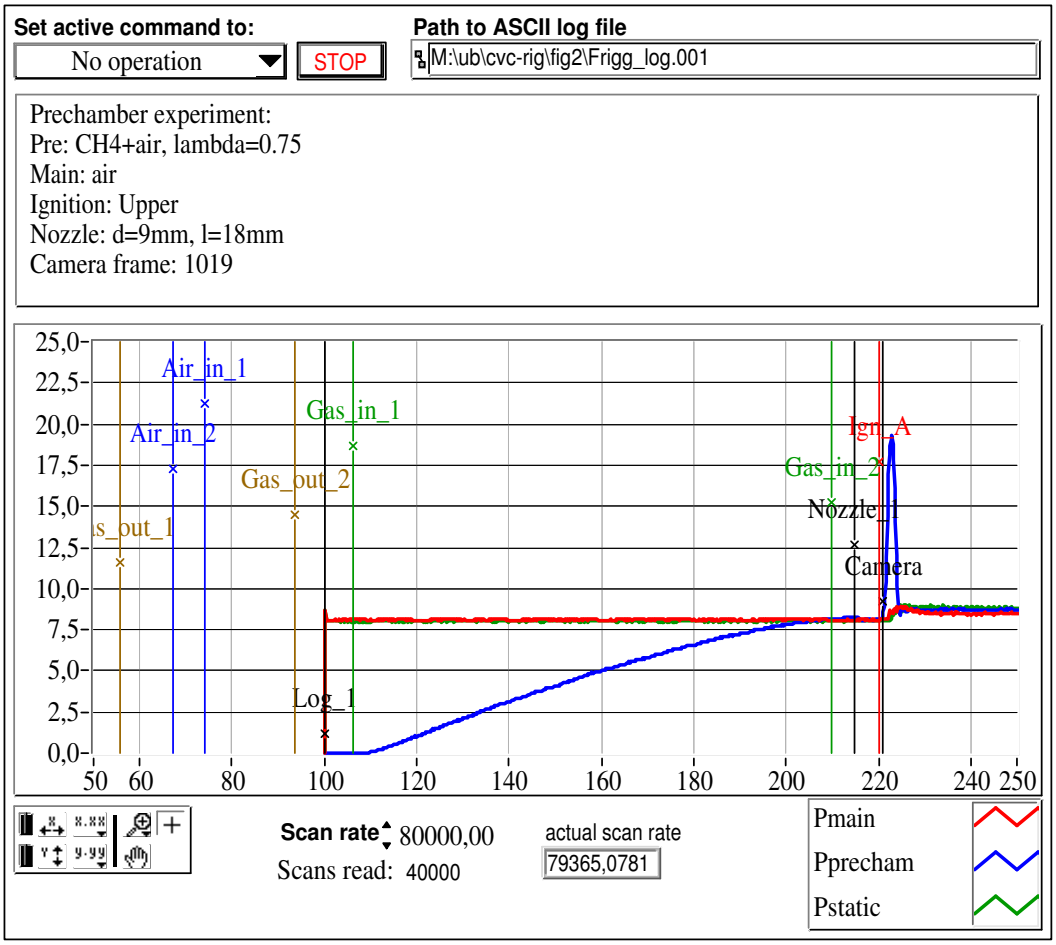

Figure 6.23: Operating sequence for experiment 2, giving higher flow velocity and more turbulence in the prechamber, the filling of the prechamber ends only 10 ms before ignition.

6.4 Experiment 2: Increased flow velocity

The difference from the previous experiment is that a modified operation sequence (as shown in figure 6.23) of the valves gives higher flow velocity and more turbulence during the combustion in the prechamber.

Pictures and pressure measurements from this experiment can be found in section E.4. A collection of recorded prechamber pressure is shown in figure 6.24.

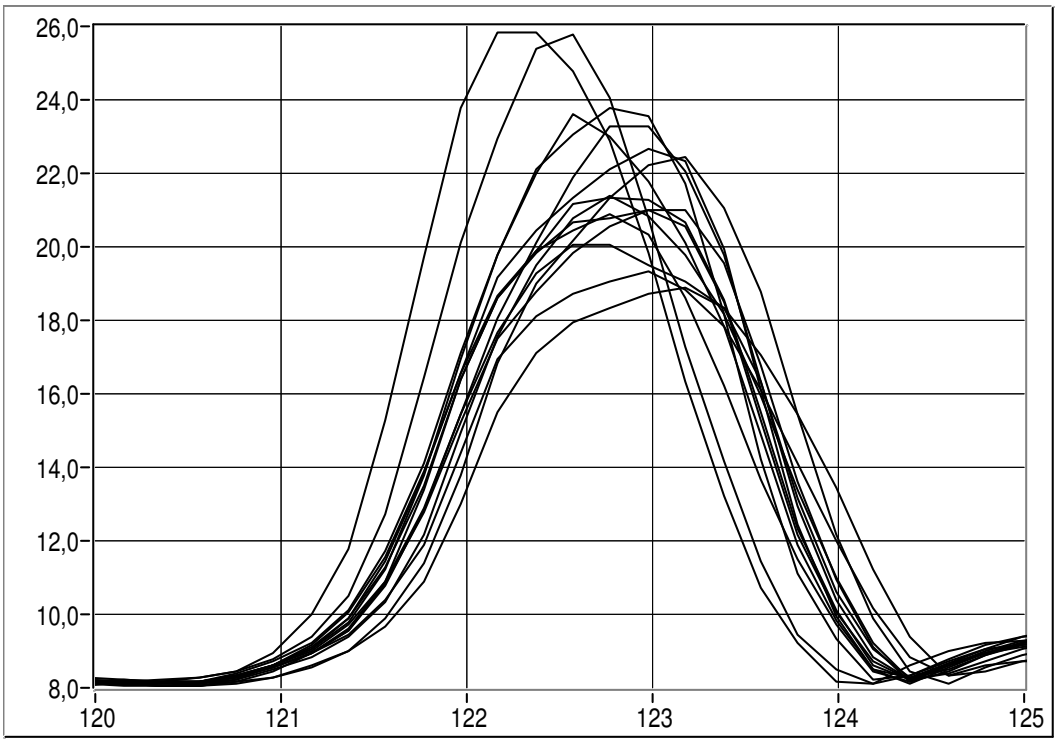

Figure 6.24: Experiment 2, increased flow velocity. Prechamber pressure [bar] from several combustions are collected and shown as functions of time [ms]. This can be compared to figure 6.22 which shows pressure from combustions at lower flow velocity. Note that the time scale is different in the two figures.

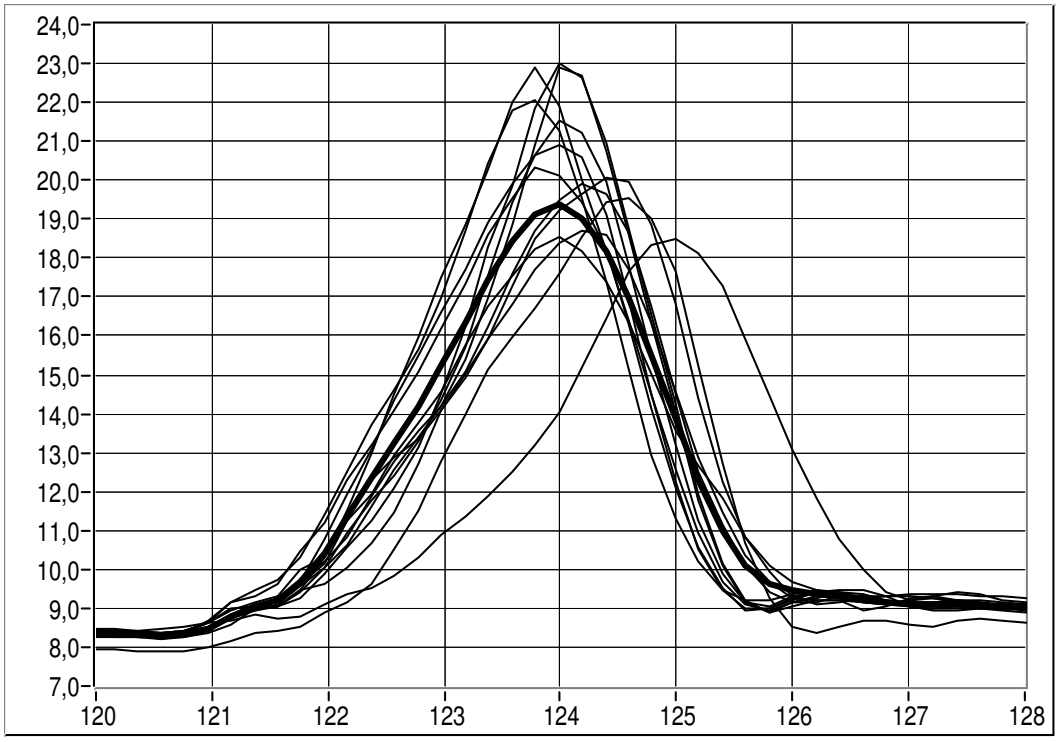

Figure 6.25: Experiment 3, increased flow velocity and lower ignition source. Prechamber pressure [bar] from several combustions are collected and shown as functions of time [ms]. This can be compared to figure 6.24 which shows similar results but using the upper ignition source.

6.5 Experiment 3: Lower ignition source

The only difference from the previous experiment is the location of the ignition. Pictures and pressure measurements from this experiment can be found in section E.5.

When comparing the pressures recorded when using an ignition source far from the nozzle (see figure 6.24) to pressures recorded when using an ignition source close from the nozzle (see figure 6.25), then one can see that the pressures are approximate equal, but the duration is longer when using the ignition source close to the nozzle. This indicates that more volume is flowing through the nozzle when using the ignition source close to the nozzle.

Measured pressure from one combustion was used as input to the two-zone model as defined i chapter 4. The best fit was found (using the approach as described in section 5.6) to be with approximately V_{ff}=10 %, and with a heat value of the charge $LHV_{net} = 1.2$ MJ/kg (note that this is almost same as what was found for the engine in section 5.6). The thermal and kinetic

efficiencies are calculated to respectively 73 % and 0.92 %, which is much higher than the values for the engine (respectively 17 % and 0.43 %) and also higher than the values found when using the constant volume rig with slower combustion and upper ignition source (respectively 46 % and 0.5 %).

6.6 Summary from experiments with combustion rig

A constant volume combustion rig with prechamber has been made. It is possible to visually observe the flame (and also flow when using Schlieren method) in both the main combustion chamber and the prechamber through glass windows. Pressure is measured in both chambers.

Preliminary experiments indicated that a rich $\lambda = 0.75$ mix of C_2H_4 and air give reliable ignition in the prechamber. Some flow velocity (turbulence) is necessary in order to give combustion speed in the same range as observed in an Otto engine with prechamber in section 5. The required flow velocity is achieved by manipulation of the inlet and outlet valves to the prechamber.

Measured pressure was used as input to the two zone combustion model as presented in section 4. The thermal and kinetic efficiency of the prechamber was found to be much higher when using an ignition source close to the nozzle than when using an ignition source far from the nozzle. On the other hand: The combustion in the prechamber has longer duration when igniting close to the nozzle as the flame has to travel upwind in stead of downwind; it is therefore not necessarily so that ignition close to the nozzle is better than ignition close to the nozzle. Another point is that the charge composition in a real engine may be different close to the nozzle than far from the nozzle.

The effects of placing the ignition source closer to the nozzle was also predicted by the perturbations done on the reference two-zone simulation as presented in table 4.2.

It was found to be very difficult to observe the length of the jet coming out of the prechamber when the combustion speed is high. The only comparison between observed and calculated jet length is therefore based on an experiment where there is lower flow velocity and lower flame speed. Calculated and observed jet length was equal, but this is not a complete validation of the jet length calculation as only one comparison of jet lengths was done.

Chapter 7

Summary and conclusions

Three objectives were defined in chapter 1. The following sections contain summaries of results for each of the three objectives.

7.1 Objective #1: Prechamber performance

The first objective of the thesis is to define variables that describe the performance of prechambers — so that it will be easier to study the prechamber independently from the rest of the internal combustion engine.

A set of performance variables are presented in chapter 3. The performance parameters are grouped into the following three categories:

- **The desired output** of the prechamber:
  - P_{pk} and E_{pk} are respectively kinetic power and kinetic energy delivered to the jet.
  - P_{pt} and E_{pt} are respectively thermal power and thermal energy delivered to the jet.
  - L_{jet} and V_{jet} are length and volume of the hot jet.
  - τ_{cg}, τ_{max} are two slightly different definitions of characteristic durations for the transfer of thermal power to the jet.
  - Variation (cycle by cycle) of the time when flame reaches the nozzle
- **Harmful bi-products** of the process in the prechamber: NO_x is the main harmful bi-product. It can be quantified by either mass or volume:

  - Mass, as micrograms per combustion. For further details the mass of NO_x can split into groups according to which phase of combustion it was generated in.
  - Volume, as parts per million in the gas flowing out of the prechamber. For further details it can be split into groups according to when the gas exits from the prechamber; with the hot jet, during the expansion stroke or with the scavenging.

- **Efficiency** — the ratio of desired output per invested input can be defined in two ways according to what one regards as the "investment", the fuel or the NO_x-bi-product.
  - The values for E_{pk} and E_{pt} can be divided by the lower heat value of the fuel present in the prechamber at the time of ignition and make respectively kinetic and thermal prechamber efficiency.
  - Any of the prechamber output parameters; P_{pk}, E_{pk}, P_{pt} and E_{pt} (and maybe also L_{jet} and V_{jet} at a certain time after ignition) can be divided by the mass of NO_x to make an "efficiency".

In addition to these performance variables were found that cycle by cycle variations are important. It is suggested to use the standard deviation of "time from initial spark until the flame reaches the nozzle" as a measure of cycle by cycle variations introduced by the prechamber.

7.2 Objective #2: Validity of performance variables

The second objective of the thesis is to use experiments with engine and combustion rig to investigate the validity of the defined performance variables. Validity includes:

- **Correlation to engine performance:** The presented prechamber performance variables should have significant correlation to the performance of the engine.
- **Availability:** The prechamber performance variables should be possible to measure, directly or indirectly via calculations based on measurement of other variables.
- **Completeness:** The prechamber performance variables should be complete in the sense that they describe the most important features of the prechamber performance.

7.2.1 Correlation to engine performance

No analysis of direct correlation between the prechamber performance variables and engine performance has been presented in the thesis, however in section 5.4 was observed cycle by cycle variations in an engine and it was presented correlation of pressure in the two chambers indicating that faster combustion in the prechamber causes faster combustion in the main chamber. This indicates that if one were to provoke larger variations in the prechamber performance, by for example varying the charge composition in the prechamber, then it should be possible to make correlations between the suggested prechamber performance variables and engine performance.

The following section is a brief discussion of the correlation between the prechamber performance variables and engine performance.

The importance of thermal power and energy of the jet is plausible based on the fact that a minimum energy is needed to ignite the mix of fuel and air (as briefly presented in section 2.3.3).

Kinetic power and energy of the jet: Kinetic energy is necessary to transport the hot jet far enough into the main combustion chamber. One can see from the presented results in table 4.2 that more kinetic energy does not necessarily give a longer jet. It can be expected that more kinetic energy in the jets from the prechamber will give more turbulence in the main chamber and therefore increase the rate of heat release.

Alternatives to kinetic energy may be to use:

- Calculated hot jet length (use for example the presented jet model)
- Momentum delivered to the jet.

The duration of the jet is important because there is limited time available for the combustion. An engine running at high RPM will require faster combustion in both chambers than a motor running at lower RPM. The timing of the jet is also important. Cycle by cycle variation in the timing of the jet has been included as prechamber performance variable.

The thermal or kinetic efficiencies of the prechamber have little influence on the thermal efficiency of the engine as long as a small fraction of the fuel is burnt in the prechamber. However, the efficiency will indirectly influence more important features, for example: A small prechamber with high efficiency can have the same ability to ignite the charge in the main chamber as a larger prechamber with lower efficiency. One can expect the smaller prechamber to produce less of harmful bi-products.

7.2.2 Availability

Numerical two-zone models, and computer programs, that calculates some of the performance variables are presented in chapter 4. It should also be possible to get similar values for the performance variables by processing results from CFD.

The two-zone programs were used independently in numerical experiments and also applied together with measurements of pressure in a running engine and with measurements of pressure in a constant volume combustion rig.

7.2.3 Completeness

No proof is presented showing that the variables listed in section 7.1 give a complete description of performance of a prechamber.

In particular the geometry of the hot jets, relative to the main chamber, is not fully described by length and volume of the jet. Example: The jets may be directed so that some parts of the main combustion chamber are far away from the jets. This will most likely have adverse influence on the engine performance even if this is not described by the suggested prechamber performance variables.

One limitation with respect to trying to describe the performance of a prechamber *independently* of the engine: The state, composition, flow velocity and even the direction of flow velocity (see figure 2.4) in the main chamber during the compression stroke will have influence on the rate of heat release in the prechamber. This means that the prechamber performance variables are not properties of a prechamber alone but rather properties of a prechamber when used in one particular engine, and they will vary also with the operating conditions of that engine.

7.3 Objective #3: Prechamber geometry

The third objective of the thesis is to explore how the performance of prechambers is influenced by the geometry of the prechamber.

Results from simulation with a two-zone model of a prechamber is presented in table 4.2. Two geometry variables were perturbed: The nozzle area and the timing of flame reaching the nozzle. The results indicated that the larger nozzle area gave the longer jets and shorter duration of the combustion. A prechamber geometry designed so that the flame reaches the nozzles late, for example by placing the ignition source far from the nozzles, will shorten the duration of the combustion in the prechamber.

Experiments with different prechamber geometries in combination with a constant volume combustion rig are presented in chapter 6 and appendix E. Placing the ignition source close to the nozzle had the same influence as predicted by the two-zone model.

7.4 Summary from experiments with combustion rig

This section is similar to the summary presented in chapter 6. A constant volume combustion rig with prechamber has been made. Much time and effort were spent making and tuning the combustion rig before reaching reliable operation.

It is possible to visually observe the flame (and also observe flow of charge when using Schlieren method) in both the main combustion chamber and the prechamber through glass windows. Pressure is measured in both chambers.

Preliminary experiments indicated that a rich mix of C_2H_4 and air, at $\lambda = 0.75$, give reliable ignition in the prechamber. Turbulence in the prechamber is necessary in order to give combustion speed in the same range as observed in an Otto engine with prechamber in section 5. The required turbulence is achieved by manipulation of the inlet and outlet valves to the prechamber.

Measured pressure was used as input to the two zone combustion model as presented in section 4. The thermal and kinetic efficiency of the prechamber was found to be much higher when using an ignition source close to the nozzle than when using an ignition source far from the nozzle. On the other hand: The combustion in the prechamber has longer duration when igniting close to the nozzle as the flame has to travel upwind in stead of downwind; it is therefore not necessarily so that ignition close to the nozzle is better than ignition far from the nozzle. Another point is that the charge composition in a real engine vary throughout the prechamber.

The influence of placing the ignition source closer to the nozzle was also predicted by the perturbations done on the reference two-zone simulation as presented in table 4.2.

It was found to be difficult to observe the length of the jet coming out of the prechamber when the combustion speed is high. The only comparison between observed and calculated jet length is therefore based on an experiment with lower flow velocity and lower flame speed in the prechamber. Calculated and observed jet length was equal, but this is not a complete validation of the jet length calculation as only one comparison of jet lengths was done.

7.5 Recommendation for further work

- Include heat transfer models and pollution models in the two zone model, in particular model of NO_x formation.
- Experiment with running engine and pressure measurement in both chambers: Vary the charge in the prechamber (so that the prechamber performance is changed), and study the correlation between the prechamber performance variables and engine performance.
- Use the output from the prechamber two zone model as input to a two zone model of the main chamber. Alternatively make a model with four zones (two in prechamber and two in main chamber). Include pollution models also in the model of the main chamber.
- Further work with CFD is also recommended. In particular one should be able to calculate the prechamber performance variables on the basis of CFD simulations of the prechamber. One should also be able to specify the required performance of a prechamber based on simulations of the main chamber.
- Controlled auto ignition (compression ignition with residual exhaust gas) in the prechamber should be explored further, for example using the methods recommended above.

Appendix A

Two zone simulation program

A.1 Main program

```
!===============================================================================
!   P R E C H A M B E R   integration program                      Fortran
!
!   The main program just performs integration of an initial value problem.
!   The system modelling is implemented in the two_zone module.
!
!   (c) 1998 Viggo L. Norum and NTNU
!===============================================================================
program integration
  use two_zone, only: initialize, dy, write_log, wp, write_report
  implicit none
  real(kind=wp),dimension(10):: y, d1, d2, d3 ! Integration variables
  real(kind=wp):: t, dt, t_end ! Integration time
  integer:: i, j, subcycle, steps
  namelist /integration_config/ t, dt, t_end, subcycle, y
  read(unit=*,nml=integration_config)
  write(unit=*,fmt="(a)") "Echo of input values:"
  write(unit=*,nml=integration_config)
  steps = (t_end-t)/dt
  call initialize( t, y, steps )
  dt=dt/subcycle
  integration_loop: do j=1,steps
     call write_log(t,y,j)
     do i=1,subcycle               ! 4th order Runge Kutta integration
        d1=dy(t,y); y=y+0.5*dt*(d1       ); t=t+0.5*dt  !1st step
        d2=dY(t,y); y=y+0.5*dt*(d2-    d1)              !2nd step
        d3=dY(t,y); y=y+    dt*(d3-0.5*d2); t=t+0.5*dt  !3rd step
        y =y+dt*(dy(t,y)-4*d3+2*d2+d1)/6                !4th step
     end do
  end do integration_loop
  call write_report(t,y)
end program integration
```

A.2 Two zone subprogram with ROHR shape as input

One may link the following module or the next together with the main program depending on what to use as input.

```
!=============================================================================
!   P R E C H A M B E R   module   two_zone                        Fortran
!
!   This module is the part of the program which formulates
!   the prechamber calculation as an initial value problem.
!   Shape parameters for ROHR are used as input.
!
!   (c) 1998 Viggo L. Norum and NTNU
!=============================================================================
module two_zone
  use utilities
  use zach
  implicit none

  type state
     ! Variables in the state vector:
     real(kind=wp):: t,  pp   ! Time and pressure in prechamber
     real(kind=wp):: m1, m2   ! Mass in zone 1 & 2 [kg]
     real(kind=wp):: T1, T2   ! Temperature in zone 1 & 2 [K]
     real(kind=wp):: V1, V2   ! Volume of zone 1 & 2 [m^3]
     real(kind=wp):: Et, Ek   ! Total and kinetic energy delivered to the jet [J]
     real(kind=wp):: HR       ! Accumulated heat release inside prechamber [J]
     ! Variables calculated by the routine "jet_model"
     real(kind=wp):: tip_v
     real(kind=wp):: tip_vol
  end type state
  type(state), save, dimension(:), allocatable:: history

  ! Configuration variables to be read from file:
  real(kind=wp):: alpha1, alpha2 ! ROHR shape parameters
  real(kind=wp):: area   ! Effective nozzle area [m^2] sum
  real(kind=wp):: noz_c  ! Nozzle discharge coefficient
  real(kind=wp):: noz_d  ! Nozzle diameter (used for calc of jet length)
  real(kind=wp):: ROHRc  ! Characteristic rate of heat release [W]
  real(kind=wp):: hc     ! Enthalpy of combustion [J/kg]
  real(kind=wp):: pm     ! Pressure in main chamber [Pa]
  real(kind=wp):: Tm     ! Temperatre in the main chamber [K]
  real(kind=wp):: Vff    ! Volume fraction combusted when flame reaches nozzle
  real(kind=wp):: Vp     ! Volume of prechamber [m^3]
  integer      :: numnoz ! Number of nozzles
  namelist /two_zone_config/ alpha1, alpha2, &
       area, noz_c, noz_d, ROHRc, hc, pm, Tm, Vff, Vp, numnoz


  ! Variables calculated and stored for reporting purposes
  real(kind=wp),save:: Hi     ! Reaction energy of prechamber charge [J]
  real(kind=wp),save:: dEtp   ! Peak total power delivered to the jet [W]

  ! Variables in the state vector and it's derivative:
  real(kind=wp):: pp, dpp  ! Pressure and derivative of pressure in prechamber
  real(kind=wp):: m1, m2, dm1, dm2 ! Mass in zone 1 & 2 [kg] and [kg/s]
  real(kind=wp):: T1, T2, dT1, dT2 ! Temperature in zone 1 & 2 [K] and [K/s]
  real(kind=wp):: V1, V2, dV1, dV2 ! Volume of zone 1 & 2 [m^3] and [m^3/s]
  real(kind=wp):: Et, Ek, dEt, dEk ! Total and kin. jet energy [J] and [W]
  real(kind=wp):: HR, ROHR    ! Heat release inside prechamber [J] and [W]
```

```
  ! Other variables caclulated by the routine "caclulate":
  real(kind=wp):: cf       ! Flow velocity at exit of the nozzle [m/s]
  real(kind=wp):: mf1, mf2 ! Mass flow throgh nozzle [kg/s] frome zone 1 and 2
  real(kind=wp):: t        ! Time [s]
  real(kind=wp):: Tf       ! Temperature at nozzle outlet [K]
  real(kind=wp):: h1,u1,s1,hp1,hT1,hF1,up1,uT1,&
       uF1,sp1,sT1,sF1,Rp1,RT1,RF1,R1,cp1,cv1,k1
  real(kind=wp):: h2,u2,s2,hp2,hT2,hF2,up2,uT2,&
       uF2,sp2,sT2,sF2,Rp2,RT2,RF2,R2,cp2,cv2,k2
  real(kind=wp):: hmi1, hmi2, mi1, mi2, Q1, Q2
  real(kind=wp):: jet_len, jet_vol

contains
  !===========================================================================
  !   P R E C H A M B E R   subroutine   initialize
  !   Purpose: Read configuration prameters and initial values
  !            from file and do some initial caclulations.
  !===========================================================================
  subroutine initialize( time, y, steps )
    real(kind=wp), intent(in):: time
    real(kind=wp), dimension(:), intent(in):: y
    integer, intent(in):: steps
    open(unit=10, file="log.txt", status="replace"); close(unit=10) !Erase log
    open(unit=10, file="pressure.txt", status="replace")
    write(unit=10, fmt=*) steps
    close(unit=10)
    read( unit=*, nml=two_zone_config)
    write(unit=*, nml=two_zone_config)
    allocate(history(steps))
    call unpack( time, y )
    !call calculate
    Hi=m2*hc
    dEtp=0.0_wp
  end subroutine initialize

  !===========================================================================
  !   P R E C H A M B E R   subroutine   calculate
  !   Purpose: Update all module state variables to reflect the values
  !            of the state vector at the time t.
  !===========================================================================
  subroutine calculate
    real(kind=wp),parameter:: 0 = 0.0_wp
    real(kind=wp), dimension(5,4):: a
    call zach3( pp,T1,1._wp,3,h1,u1,s1,hp1,hT1,hF1,up1,uT1,&
         uF1,sp1,sT1,sF1,Rp1,RT1,RF1,R1,cp1,cv1,k1 )
    call zach3( pp,T2,0._wp,3,h2,u2,s2,hp2,hT2,hF2,up2,uT2,&
         uF2,sp2,sT2,sF2,Rp2,RT2,RF2,R2,cp2,cv2,k2 )
    ROHR = heat_release()
    h2=h2+hc; u2=u2+hc; mf1=0.0_wp; mf2=0.0_wp
    if ( V1 < Vff*Vp ) then ! Before flame reaches nozzle
       call nozzle( area, 0.5_wp, pp, T2, R2, cp2, k2, pm, cf, mf2, Tf )
    else ! After flame reached the nozzle
       call nozzle( area, 0.5_wp, pp, T1, R1, cp1, k1, pm, cf, mf1, Tf )
       if (V2 < 1.0e-5_wp * Vp) ROHR = 0.0_wp ! Only one zone (all combusted)
    end if
    dm1 =  ROHR/hc-mf1
    dm2 = -ROHR/hc-mf2
    dEt = mf1*cp1*(Tf-Tm)+mf2*cp2*(Tf-Tm)
    Q1=0; Q2=0;
    a(:,1)=(/ -1/T1-RT1/R1, 0.0_wp,  1/V1, 1/pp+Rp1/R1,                    dm1/m1 /) !T1
    a(:,2)=(/       0.0_wp,  -1/T2, -1/V2,        1/pp,                    dm2/m2 /) !T2
```

```
  a(:,3)=(/       m1*cv1, 0.0_wp,    pp,      m1*up1, Q1+mf1*(h2-h1)+dm1*(h2-u1) /) !V1
  a(:,4)=(/       0.0_wp, m2*cv2,   -pp,      0.0_wp, Q2            +dm2*(h2-u2) /) !pp
  !write(*,fmt="(5g11.2)") (a(:,i),i=1,size(a,2))
  call solve( a )
  dT1=a(5,1); dT2=a(5,2); dV1=a(5,3); dpp=a(5,4); dV2=-dV1
  dEk=0.5*(mf1+mf2)*cf**2
  if (dEt>dEtp) then
     dEtp=dEt
  end if
end subroutine calculate

!=========================================================================
!   P R E C H A M B E R   subroutine   jet_model
!   Purpose: Calculate jet length
!=========================================================================
subroutine jet_model(j)
  integer,intent(in):: j
  real(kind=wp):: rho_jet, rho_main
  rho_jet=pm/(R1*Tf)
  rho_main=12.0
  history(j)%t=t
  if ( V1 < Vff*Vp ) then
     history(j)%tip_v = 0.0_wp
  else
     history(j)%tip_v = sqrt(rho_jet / rho_main) * cf
  end if
  history(j)%tip_vol = (rho_jet / rho_main)**0.25 * cf
  jet_len = 4*sqrt(noz_d*maxval(history(:j)%tip_v * (t-history(:j)%t)))
  jet_vol = 2*pi*noz_d*maxval(history(:j)%tip_vol * (t-history(:j)%t)**1.5)
end subroutine jet_model


!=========================================================================
!   P R E C H A M B E R   subroutine   dy
!   Purpose: Update all module state variables to reflect
!            the values of the state vector y at the time t
!            and return the derivatives of the state vector.
!=========================================================================
function dy( t, y ) result( res )
  real(kind=wp), intent(in):: t
  real(kind=wp), dimension(:),intent(in):: y
  real(kind=wp), dimension(size(y)):: res
  call unpack(t,y)
  call calculate
  res = (/ dpp, dT1, dm1, dV1, dT2, dm2, dV2, ROHR, dEt, dEk /)
end function dy

!=========================================================================
!   P R E C H A M B E R   subroutine   unpack
!   Purpose: Unpack the state vector into individual state variables
!=========================================================================
subroutine unpack(time,y)
  real(kind=wp), intent(in):: time
  real(kind=wp), dimension(:),intent(in):: y
  t=time; pp=y(1); T1=y(2); m1=y(3); V1=y(4); T2=y(5);
  m2=y(6); V2=y(7); HR=y(8); Et=y(9); Ek=y(10)
end subroutine unpack

!=========================================================================
!   P R E C H A M B E R   function   heat_release
!   Purpose: Calculate the heat release.
!=========================================================================
```

```
  function heat_release() result(res)
    real(kind=wp):: res
    real(kind=wp),parameter:: hr_v1 = 0.000_wp
    real(kind=wp),parameter:: hr_v2 = 0.002_wp
    if ( V1/Vp < hr_v1 .or. V2/Vp < hr_v2 ) then
       res=0.0_wp
    else
       res = ROHRc * (V1/Vp)**alpha1 * (V2/Vp)**alpha2
    end if
  end function heat_release

  !=========================================================================
  !   P R E C H A M B E R   subroutine   write_log
  !   Purpose: Write a time series of the results
  !=========================================================================
  subroutine write_log( t, y, j )
    real(kind=wp),intent(in):: t
    real(kind=wp),dimension(:),intent(in):: y
    integer, intent(in):: j
    call unpack( t, y )
    call calculate
    call jet_model(j)
    !write(*,"(4(a,g11.5))") "Time=",t*1000,"    pr=", pp/pm, &
    !     "  jet len=", jet_len, "  jet vol=", jet_vol
    open(unit=10,file="log.txt",status="old",position="append")
    write( unit=10, fmt="(30e15.5e3)" ) 1e3*t, & ! time [ms]
         V1*1e6, V1/Vp, pp*1e-6, pp/pm, &
         mf1+mf2, jet_len, 0.0, 0.0, 0.0, &
         m1, T1*1e-3, m2, T2*1e-3, HR*1.0e-3, &          ! column 11..20:
         Et*1e-3, Ek*1e-3, 0.0, 0.0, 0.0, &              !    state vector
         dm1, dT1*1e-6, dm2, dT2*1e-6, ROHR*1e-6, &      ! column 21..30:
         dEt*1e-6, dEk*1e-6, jet_len, 0.0, 0.0           !    derivatives
    close(unit=10)
    open(unit=10,file="pressure.txt",status="old",position="append")
    write( unit=10, fmt=* ) t, pp, pm
    close(unit=10)
  end subroutine write_log

   !=========================================================================
   !   P R E C H A M B E R   subroutine   write_report
   !   Purpose: Write a report after end of simulation
   !=========================================================================
   subroutine write_report( t, y )
      real(kind=wp),intent(in):: t
      real(kind=wp),dimension(:),intent(in):: y
      call unpack( t, y )
      call calculate
      write( unit=*,fmt="(a)" ) "Summary of results:"
      write( unit=*,fmt="(a,f8.2,a)" ) "eta_t", 100*Et/Hi  ," %"
      write( unit=*,fmt="(a,f8.2,a)" ) "eta_k", 100*Ek/Hi  ," %"
      write( unit=*,fmt="(a,f8.2,a)" ) "  T_e",1000*Et/dEtp," ms"
   end subroutine write_report
end module two_zone
```

A.3 Two zone subprogram with pressure as input

One may link this module or the previous one together with the main program depending on what to use as input.

```
!=============================================================================
!   P R E C H A M B E R   module   two_zone                          Fortran
!
!   This module is the part of the program which formulates
!   the prechamber calculation as an initial value problem.
!   Measured pressure is used as input to the calculation.
!
!   (c) 1998 Viggo L. Norum and NTNU
!=============================================================================
module two_zone
  use utilities
  use zach
  use nag_spline_1d, only: nag_spline_1d_comm_wp => nag_spline_1d_comm_dp, &
       nag_spline_1d_auto_fit, nag_spline_1d_eval
  implicit none

  type state
     ! Variables in the state vector:
     real(kind=wp):: t,  pp   ! Time and pressure in prechamber
     real(kind=wp):: m1, m2   ! Mass in zone 1 & 2 [kg]
     real(kind=wp):: T1, T2   ! Temperature in zone 1 & 2 [K]
     real(kind=wp):: V1, V2   ! Volume of zone 1 & 2 [m^3]
     real(kind=wp):: Et, Ek   ! Total and kinetic energy delivered to the jet [J]
     real(kind=wp):: HR       ! Accumulated heat release inside prechamber [J]
     ! Variables calculated by the jet model
     real(kind=wp):: tip_v    ! Hot jet tip velocity [m/s]
     real(kind=wp):: tip_vc   ! Cold jet tip velocity [m/s]
     real(kind=wp):: tip_vol  ! Hot jet volume [m^3]
  end type state
  type(state), save, dimension(:), allocatable:: history

  ! Configuration variables to be read from file:
  real(kind=wp):: area   ! Brute nozzle area [m^2]
  real(kind=wp):: noz_c  ! Nozzle discharge coefficient
  real(kind=wp):: noz_d  ! Nozzle diameter [m]
  real(kind=wp):: hc     ! Enthalpy of combustion [J/kg]
  real(kind=wp):: pm     ! Pressure in main chamber [Pa]
  real(kind=wp):: Tm     ! Temperatre in the main chamber [K]
  real(kind=wp):: Vff    ! Volume fraction combusted when flame reaches nozzle
  real(kind=wp):: Vp     ! Volume of prechamber [m^3]
  namelist /two_zone_config/ area, noz_c, noz_d, hc, pm, Tm, Vff, Vp

  ! Variables calculated and stored for reporting purposes
  real(kind=wp),save:: Hi     ! Reaction energy of prechamber charge [J]
  real(kind=wp),save:: dEtp   ! Peak total power delivered to the jet [W]

  ! Variables in the state vector and it's derivative:
  real(kind=wp):: pp, dpp  ! Pressure and derivative of pressure in prechamber
  real(kind=wp):: m1, m2, dm1, dm2 ! Mass in zone 1 & 2 [kg] and [kg/s]
  real(kind=wp):: T1, T2, dT1, dT2 ! Temperature in zone 1 & 2 [K] and [K/s]
  real(kind=wp):: V1, V2, dV1, dV2 ! Volume of zone 1 & 2 [m^3] and [m^3/s]
  real(kind=wp):: Et, Ek, dEt, dEk ! Total and kin. jet energy [J] and [W]
  real(kind=wp):: HR, ROHR    ! Heat release inside prechamber [J] and [W]

  ! Other variables caclulated by the routine "caclulate":
```

```
  real(kind=wp):: cf       ! Flow velocity at exit of the nozzle [m/s]
  real(kind=wp):: mf1,mf2  ! Mass flow throgh nozzle [kg/s] from zone 1 and 2
  real(kind=wp):: t        ! Time [s]
  real(kind=wp):: Tf       ! Temperature at nozzle outlet [K]
  real(kind=wp):: h1,u1,s1,hp1,hT1,hF1,up1,uT1,&
       uF1,sp1,sT1,sF1,Rp1,RT1,RF1,R1,cp1,cv1,k1
  real(kind=wp):: h2,u2,s2,hp2,hT2,hF2,up2,uT2,&
       uF2,sp2,sT2,sF2,Rp2,RT2,RF2,R2,cp2,cv2,k2
  real(kind=wp):: Q1, Q2

  real(kind=wp):: jet_len, jet_vol, jet_len_cold
  type(nag_spline_1d_comm_wp):: pp_spline, pm_spline
contains
  !=============================================================================
  !   P R E C H A M B E R   subroutine   initialize
  !   Purpose: Read configuration prameters and initial values
  !            from file and do some initial caclulations.
  !=============================================================================
  subroutine initialize( time, y, steps )
    real(kind=wp), intent(in):: time
    real(kind=wp), dimension(:), intent(in):: y
    integer, intent(in):: steps
    real(kind=wp),dimension(:),allocatable:: t_log, pp_log, pm_log
    integer:: n,i
    open(unit=10, file="log.txt", status="replace"); close(unit=10) !Erase log
    read( unit=*, nml=two_zone_config)
    write(unit=*, nml=two_zone_config)
    allocate(history(steps))
    open(unit=10, file="pressure.txt", status="old")
    read(unit=10, fmt=*) n
    allocate( t_log(n), pp_log(n), pm_log(n) )
    read(unit=10,fmt=*) (t_log(i), pp_log(i), pm_log(i), i=1,n)
    close(unit=10)
    call nag_spline_1d_auto_fit("c", t_log, pp_log, 0.8_wp, pp_spline)
    call nag_spline_1d_auto_fit("c", t_log, pm_log, 0.5_wp, pm_spline)
    call unpack( time, y )
    Hi=m2*hc
    dEtp=0.0_wp
  end subroutine initialize

  !=============================================================================
  !   P R E C H A M B E R   subroutine   calculate
  !   Purpose: Update all module state variables to reflect the values
  !            of the state vector at the time t.
  !=============================================================================
  subroutine calculate
    real(kind=wp), dimension(6,5):: a
    integer:: i
    call nag_spline_1d_eval(pp_spline,t,pp,sd1=dpp)
    call nag_spline_1d_eval(pm_spline,t,pm)
    call zach3( pp,T1,1.0_wp,3,h1,u1,s1,hp1,hT1,hF1,up1,uT1,&
         uF1,sp1,sT1,sF1,Rp1,RT1,RF1,R1,cp1,cv1,k1 )
    call zach3( pp,T2,0.0_wp,3,h2,u2,s2,hp2,hT2,hF2,up2,uT2,&
         uF2,sp2,sT2,sF2,Rp2,RT2,RF2,R2,cp2,cv2,k2 )
    h2=h2+hc
    u2=u2+hc
    if ( V1 < Vff*Vp ) then ! Before flame reaches nozzle
       !write(*,*) "STATE 1"
       call nozzle( area, noz_c, pp, T2, R2, cp2, k2, pm, cf, mf2, Tf )
       mf1=0
       dEt = mf2*cp2*(Tf-Tm)
    else ! After flame reached the nozzle
```

```
     call nozzle( area, noz_c, pp, T1, R1, cp1, k1, pm, cf, mf1, Tf )
     mf2=0
     dEt = mf1*cp1*(Tf-Tm)
  end if
  Q1=0.0_wp; Q2=0.0_wp
  if (pp<pm) dpp=0.0_wp
  a(:,1)=(/     1.0_wp, 1+T1*RT1/R1,    0.0_wp,    0.0_wp, -Vp/V1,         dpp/pp-dpp*Rp1/R1 /) !m1
  a(:,2)=(/ (u1-h2)*m1,   T1*m1*cv1,    0.0_wp,    0.0_wp,  Vp*pp, Q1-m1*up1*dpp+mf1*(h2-h1) /) !T1
  a(:,3)=(/    0.0_wp,      0.0_wp,     1.0_wp,    1.0_wp,  Vp/V2,                     dpp/pp /) !m2
  a(:,4)=(/    0.0_wp,      0.0_wp, (u2-h2)*m2, T2*m2*cv2, -Vp*pp,                         Q2 /) !T2
  a(:,5)=(/        m1,      0.0_wp,         m2,    0.0_wp, 0.0_wp,                -mf1-mf2 /) !V1
  !write(*,fmt="(6g14.5)") (a(:,i),i=1,size(a,2))
  call solve2( a )
  !write(*,fmt="(5g14.5)") a(6,:)
  dm1=a(6,1)*m1; dT1=a(6,2)*T1; dV1=a(6,5)*Vp
  dm2=a(6,3)*m2; dT2=a(6,4)*T2; dV2=-dV1
  ROHR=(dm1+mf1)*hc
  dEk=0.5*(mf1+mf2)*cf**2
  if (dEt>dEtp) then
     dEtp=dEt
  end if
end subroutine calculate

!=========================================================================
!   P R E C H A M B E R   subroutine   jet_model
!   Purpose: Calculate jet length
!=========================================================================
subroutine jet_model(j)
  integer,intent(in):: j
  real(kind=wp):: rho_jet, rho_main
  rho_jet=pm/(R1*Tf)
  rho_main=12.0
  history(j)%t=t
  if ( V1 < Vff*Vp ) then
     history(j)%tip_v = 0.0_wp
     history(j)%tip_vol = 0.0_wp
  else
     history(j)%tip_v = sqrt(rho_jet / rho_main) * cf
     history(j)%tip_vol = (rho_jet / rho_main)**0.25 * cf
  end if
  history(j)%tip_vc = sqrt(rho_jet / rho_main) * cf
  !write(*,"(3(a,g11.5))") "Time=",t*1000,"   tip_v=", history(j)%tip_v, "  cf=",cf
  jet_len      = 4*sqrt( noz_d * maxval(history(:j)%tip_v  * (t - history(:j)%t)) )
  jet_len_cold = 4*sqrt( noz_d * maxval(history(:j)%tip_vc * (t - history(:j)%t)) )
  jet_vol = 2*pi*noz_d*maxval(history(:j)%tip_vol * (t-history(:j)%t)**1.5)
end subroutine jet_model

!=========================================================================
!   P R E C H A M B E R   subroutine   dy
!   Purpose: Update all module state variables to reflect
!            the values of the state vector y at the time t
!            and return the derivatives of the state vector.
!=========================================================================
function dy( t, y ) result( res )
  real(kind=wp), intent(in):: t
  real(kind=wp), dimension(:),intent(in):: y
  real(kind=wp), dimension(size(y)):: res
  call unpack(t,y)
  call calculate
  res = (/ ROHR, dT1, dm1, dV1, dT2, dm2, dV2, ROHR, dEt, dEk /)
end function dy
```

```
  !=============================================================================
  !   P R E C H A M B E R   subroutine   unpack
  !   Purpose: Unpack the state vector into individual state variables
  !=============================================================================
  subroutine unpack(time,y)
    real(kind=wp), intent(in):: time
    real(kind=wp), dimension(:),intent(in):: y
    t=time; pp=y(1); T1=y(2); m1=y(3); V1=y(4); T2=y(5);
    m2=y(6); V2=y(7); HR=y(8); Et=y(9); Ek=y(10)
  end subroutine unpack

  subroutine write_log( t, y, j )
    real(kind=wp),intent(in):: t
    real(kind=wp),dimension(:),intent(in):: y
    integer, intent(in):: j
    call unpack( t, y )
    call calculate
    call jet_model(j)
    write(*,"(7(a,g12.5))") "Time=",t*1000,"    pr=", pp/pm, &
         "  jet len=", jet_len, "  jet vel=", cf, "  dm1=", dm1, "  dm2=",dm2, "  ROHR=", ROHR
    open(unit=10,file="log.txt",status="old",position="append")
    write( unit=10, fmt="(30e15.5e3)" ) 1e3*t, & ! time [ms]
         V1*1e6, V1/Vp, pp*1e-6, pp/pm, &
         mf1+mf2, jet_len, jet_len_cold, 0.0, 0.0, &
         m1, T1*1e-3, m2, T2*1e-3, HR*1.0e-3, &          ! column 11..20:
         Et*1e-3, Ek*1e-3, 0.0, 0.0, 0.0, &              !    state vector
         dm1, dT1*1e-6, dm2, dT2*1e-6, ROHR*1e-6, &      ! column 21..30:
         dEt*1e-6, dEk*1e-6, 0.0, 0.0, 0.0               !    derivatives
    close(unit=10)
  end subroutine write_log

   !=============================================================================
   !   P R E C H A M B E R   subroutine   write_report
   !   Purpose: Write a report after end of simulation
   !=============================================================================
   subroutine write_report( t, y )
      real(kind=wp),intent(in):: t
      real(kind=wp),dimension(:),intent(in):: y
      call unpack( t, y )
      call calculate
      write( unit=*,fmt="(a)" ) "Summary of results:"
      write( unit=*,fmt="(a,f8.2,a)" ) "eta_pt",100*Et/Hi," %"
      write( unit=*,fmt="(a,f8.2,a)" ) "eta_pk",100*Ek/Hi," %"
      write( unit=*,fmt="(a,f8.2,a)" ) "  T_ce",1000*Et/dEtp,  " ms"
   end subroutine write_report
end module two_zone
```

A.4 Utility subprograms

```
!=============================================================================
!   P R E C H A M B E R   module   "utilities"                      Fortran
!
!   This module contains mathematical and thermodynamical
!   procedures used by the two zone prechamber simulation program.
!
!   (c) 1998 Viggo L. Norum and NTNU
!=============================================================================
module utilities
   implicit none
```

```
   integer,parameter:: wp=selected_real_kind(p=12,r=30) ! Numerical precision
   real(kind=wp):: pi=3.14159265358979323844_wp
contains
   !=============================================================================
   !   M A T H   subroutine   solve
   !   Purpose: Solve a system of linear equations.
   !=============================================================================
   subroutine solve(a)  ! with max column pivot
      real(kind=wp),intent(in out):: a(:,:)
      integer:: i,j,n,m
      n=size(a,2)
      forward: do i=1,n-1
               m=sum(maxloc(abs(a(i,i:))))+i-1; a(:,(/i,m/))=a(:,(/m,i/))
               forall (j=i+1:n) a(i+1:,j)=a(i+1:,j)-a(i,j)/a(i,i)*a(i+1:,i)
      end do forward
      back: do i=n,1,-1
               a(n+1:,i)=(a(n+1:,i)-matmul(a(n+1:,i+1:),a(i+1:n,i)))/a(i,i)
      end do back
   end subroutine solve

   !=============================================================================
   !   P R E C H A M B E R   subroutine   solve2
   !   Purpose: Solve a system of linear equations,
   !   implemented as a call to NAG's library
   !=============================================================================
   subroutine solve2(a)  ! with max column pivot
     use nag_gen_lin_sys
     real(kind=wp),intent(in out):: a(:,:)
     real(kind=wp):: aa(size(a,2),size(a,2)), b(size(a,2))
     aa=transpose(a( :size(a,2),:))
     b =a(  size(a,1),:)
     call nag_gen_lin_sol(aa,b)
     a(  size(a,1),:)=b
   end subroutine solve2

   !=============================================================================
   !   T H E R M O   Subroutine   nozzle
   !
   !   Given the throat area of the nozzle, the inlet and outlet
   !   gas properties, this function returns the mass flow through
   !   the nozzle.  Isentropic flow and perfect gass is asumed.
   !
   !   If the pressure ratio exceeds the critical value,
   !   the speed is set to sonic speed.
   !=============================================================================
   subroutine nozzle( area, c, p1, T, R, cp, k, p2, cf, mf, Tf )
      real(kind=wp),intent(in):: area ! brute nozzle area [m^2]
      real(kind=wp),intent(in):: c    ! nozzle discharge coeffieicent
      real(kind=wp),intent(in):: p1   ! chamber 1 pressure
      real(kind=wp),intent(in):: T
      real(kind=wp),intent(in):: R
      real(kind=wp),intent(in):: cp
      real(kind=wp),intent(in):: k
      real(kind=wp),intent(in):: p2  ! chamber 2 pressure
      real(kind=wp),intent(out):: cf ! Flow velocity [m/s] (average over area)
      real(kind=wp),intent(out):: mf ! Mass flow [kg/s]
      real(kind=wp),intent(out):: Tf ! Outlet temperature [K]
      real(kind=wp):: pr, rho
      if (p2>p1) then
         cf=0
         mf=0
         Tf = T ! Wrong ?
```

```
      else
         pr  = max( p2 / p1, (2/(k+1))**(k/(k-1)) )
         cf  = c * sqrt( R*T*2.0_wp * k / (k-1) * ( pr**(2/k) - pr**( (k+1)/k )))
         !cf  = sqrt( 2.0_wp * k / (k-1)* ( pr**k - pr**( (k+1)/k )))
         Tf  = T ! Wrong ?
         rho = p1/( R * Tf )
         mf  = cf * rho * area
         !mf  = p1 / sqrt( R * T ) * area * cf
      end if
   end subroutine nozzle
end module utilities
```

A.5 Gas properties

The routine for calculation of gas properties is taken directly from a Fortran 77 code programed by Harald Valland. The only modification is the that the code is placed inside a Fortran 90 module and that the floating point variable size/kind is selectable with "real(kind=wp)::". It is included here in order to have the whole two zone simulation program documented (with the exception of NAG's spline-fitting routines which are used to interpolate the measured pressure when pressure is used as input).

```
      module zach
      use utilities, only: wp
      contains
      subroutine ZACH3(p,T,F,DCO,h,u,s,hp,hT,hF,up,uT,uF,sp,sT,sF,
     &                 Rp,RT,RF,R,cp,cv,k)
c ....................................................................
c ... This routine calculates the thermodynamic gas properties of com-
c     bustion gases using Zacharias formulae. The fuel is CnH2n and the
c     air is dry atmospheric air. Only lean mixtures are considered.
c ....................................................................
c ... Reference: Friedemann Zacharias: Analytische Darstellung  der
c     thermodynamischen Eigenschaften von Verbrennungsgasen.
c     Dissertation TU Berlin 1966.
c ....................................................................
c ... Input parameters:
c     p     pressure [Pa]
c     T     temperature [K]
c     F     fuel air equivalence ratio [-] (F = 1/lambda)
c     DCO   control parameter:
c           DCO= 0  ideal gas properties with real gas correction
c              = 1  correction for lower stage dissiciation added
c              = 2  correction for upper stage dissociation added
c ... Output parameters:
c     h     specific enthalpy [J/kg]
c     u     specific internal energy [J/kg]
c     s     specific entropy [J/kgK]
c     hp,hT,hF  partial derivatives of H with respect to p,T,F.
c     up,uT,uF  partial derivatives of U with respect to p,T,F.
c     sp,sT,sF  partial derivatives of S with respect to p,T,F.
c     Rp,RT,RF  partial derivatives of R with respect to p,T,F.
c     R     gas constant [J/kgK]
c     cp    specific heat at constant pressure [J/kgK]
c     cv    specific heat at constant volume [J/kgK]
c     k     ratio of specific heats: k=cp/cv
c
c ... Note:
c     Units according to SI:
c     energy: [J]   mass: [kg]   pressure: [Pa]=[N/m2]  temperature: [K]
c ....................................................................
```

```
c ... Programmed by: H. Valland, NTH, Trondheim, 1968
c     Restructured: 98-02-16/hv :: derivatives of entropy included
c     Restructured: 98-11-18/hv :: collection of terms
c ..................................................................
      implicit none
      integer DC0
      real(kind=wp):: p,T,F,h,u,s
      real(kind=wp):: hp,hT,hF,up,uT,uF,sp,sT,sF,Rp,RT,RF,R,cp,cv,k
      real(kind=wp):: EP0,EP1,EP2,EP3,EP4,EP5,EP6,FC0,FC1,FC2,FC3,FC4,
     &     FC6,FC7,FC8,FC6T,FC6V,FC7T,FC7P,FC8T,FC8V
      real(kind=wp):: PP,TT,TT2,V,LNPP,LNT,LNT2,PB,PBT,PBV,
     &     PC,PCV,Y,YV,YT,YP,EXPY,A,AV,B0,B0V,D,DV
      real(kind=wp):: AZ,AZP,AZV,AH,AHP,AHV,AS,ASP,ASV
      real(kind=wp):: BZ,BZT,BZP,BZV,BH,BHT,BHP,BHV
      real(kind=wp):: ZZ,ZZP,ZZT,ZZV,ZR,ZRP,ZRT,ZRV
      real(kind=wp):: Z1,Z1P,Z1T,Z1V,Z2,Z2P,Z2T,Z2V
      real(kind=wp):: HH,HHP,HHT,HHV,H0,H0T,H0V,    HR,HRT,HRV,HRP
      real(kind=wp):: H1,H1P,H1T,H1V,H2,H2T,H2V,H2P
      real(kind=wp):: SS,SSP,SST,SSV,S0,S0T,S0V,S0P,SR,SRT,SRV,SRP
      real(kind=wp):: S1,S1P,S1T,S1V,S2,S2T,S2V,S2P
      real(kind=wp):: fs
c ..................................................................
c ... Test if input parameters are out of range.
      if((p .lt. 100. .or. p .gt. 1.E8)  .or.
     &   (T .lt. 200. .or. T .gt. 6000.) .or.
     &   (F .lt.   0. .or. F .gt.    1.))then
         PRINT*,'   ZACH:  INPUT PARAMETERS OUT OF RANGE:'
         PRINT*,'   p = ',p,'   T = ',T,'   F = ',F
         go to 9999
      endif
c ..................................................................
c ... Input accepted.
c ..................................................................
c     In this section, compute ideal gas properties of gas mixture,
c     adding correction for real-gas behaviour at high density.
c ..................................................................
      fs=0.067671
      FC0=1.019716E-5
      TT=.001*T
      PP=FC0*p
      V=(1.-F)/(1.+.0698*F)
c      V=(1.-F)/(1.+fs*F)
      LNPP=LOG(PP)
      TT2=TT*TT
c
      A= 2.77105E-4 -.900711E-4*V
      B0=6.42217E-4 -.98367E-4*V
      D=.8868E-2    -.6131E-2*V
c
      AV= -.900711E-4
      B0V=-.98367E-4
      DV= -.6131E-2
c
      FC6 = EXP(D/TT2)/TT
      FC6T=-EXP(D/TT2)/TT2*(1.0+2.0*D/TT2)
      FC6V= DV*EXP(D/TT2)/TT
      FC7 =PP/TT
      FC7T=-PP/TT2
      FC7P=1.0/TT
      FC8 =1.+D/TT2
      FC8V=DV/TT2
      FC8T=-2.0*D/(TT2*TT)
```

```
c .....................................................................
c --- Compressibility function:
c
      ZR = FC7*(B0-A*FC6)
c      ZRT=-FC7*(B0-A*FC6*2.0*FC8)/TT
      ZRT=-FC7*(B0-2.0*A*FC6*(1.-D/TT2))/TT
      ZRV= FC7*(B0V-FC6*(AV+DV*A/TT2))
      ZRP= (B0-A*FC6)/TT
c
      ZZ =1.0+ZR
      ZZT=    ZRT
      ZZV=    ZRV
      ZZP=    ZRP
c .....................................................................
c --- Enthalpy function
c
      H0=     +3.514956    -.005026*V
     &    +TT*(+.131438    -.383504*V
     &    +TT*(+.477182    +.185214*V
     &    +TT*(-.287367    -.694862E-1*V
     &    +TT*(+.742561E-1 +.164041E-1*V
     &    +TT*(-.916344E-2 -.204537E-2*V
     &    +TT*(+.439896E-3 +.101610E-3*V))))))
c
      H0T=          +.131438    -.383504*V
     &    +TT*(2.0*(+.477182    +.185214*V)
     &    +TT*(3.0*(-.287367    -.694862E-1*V)
     &    +TT*(4.0*(+.742561E-1 +.164041E-1*V)
     &    +TT*(5.0*(-.916344E-2 -.204537E-2*V)
     &    +TT*(6.0*(+.439896E-3 +.101610E-3*V))))))
c
      H0V=     -.005026
     &    +TT*(-.383504
     &    +TT*(+.185214
     &    +TT*(-.694862E-1
     &    +TT*(+.164041E-1
     &    +TT*(-.204537E-2
     &    +TT*(+.101610E-3))))))
c
      HR =+FC7*(B0-2.0*A*FC6*FC8)
      HRT=+FC7T*(B0-2.0*A*FC6*FC8)+FC7*(-2.0*A)*(FC6T*FC8+FC6*FC8T)
      HRP= HR/PP
      HRV=+FC7*(B0V-2.0*(AV*FC6*FC8+A*FC6V*FC8+A*FC6*FC8V))
c
      HH =H0 +HR
      HHT=H0T+HRT
      HHP=   +HRP
      HHV=H0V+HRV
c .....................................................................
c --- Entropy function:
c
      PB=     +2.972979    +.553140*V
     &    +TT*(+.583837E-1 -.485001*V
     &    +TT*(+.871349    +.698183E-1*V
     &    +TT*(-.451556    -.287720E-2*V
     &    +TT*(+.109164    -.693663E-3*V
     &    +TT*(-.129754E-1 +.920231E-4*V
     &    +TT*(+.608234E-3 -.299679E-5*V))))))
c
      PBT=         (+0.583837E-1 -0.485001*V)
     &    +TT*(2.0*(+0.871349    +0.698183E-1*V)
     &    +TT*(3.0*(-0.451556    -0.287720E-2*V)
```

```
     &    +TT*(4.0*(+0.109164    -0.693663E-3*V)
     &    +TT*(5.0*(-0.129754E-1 +0.920231E-4*V)
     &    +TT*6.0*( +0.608234E-3 -0.299679E-5*V)))))
c
      PBV=     +.553140
     &    +TT*(-.485001
     &    +TT*(+.698183E-1
     &    +TT*(-.287720E-2
     &    +TT*(-.693663E-3
     &    +TT*(+.920231E-4
     &    +TT*(-.299679E-5))))))
c
      PC =-.805214+V*(-.400981+V*(.576989+V*.060056))
      PCV=-0.400981+V*(1.153978+0.180168*V)
c
      LNT=LOG(1000.*TT)
      S0 =(3.5566-0.0659*V)*LNT-LNPP+PB-PC
      S0T=(3.5566-0.0659*V)/TT+PBT
      S0P=-1.0/PP
      S0V=(-0.0659)*LNT+PBV-PCV
c
      SR =-A*FC7*FC6*FC8
      SRT=-A*(FC7T*FC6*FC8+FC7*FC6T*FC8+FC7*FC6*FC8T)
      SRP=-A*FC7P*FC6*FC8
      SRV=-FC7*(AV*FC6*FC8+A*FC6V*FC8+A*FC6*FC8V)
c
      SS =S0 +SR
      SST=S0T+SRT
      SSP=S0P+SRP
      SSV=S0V+SRV
c ....................................................................
c ....................................................................
      if(DC0 .gt. 0)then
c ...    Correction for lower stage dissociation.
         LNT2=LOG(TT/1.65)
         EP0=EXP(.007*LNPP)
         EP1=EXP(.0115*LNPP)
         EP2=EXP(-.03453*LNPP)
         EP3=EXP(-.103*LNPP)
         EP4=EXP(-.127*LNPP)
         EP5=EXP(-.0212*LNPP)
         EP6=EXP(-.306*TT)
         FC1=-.51*EP3-.14+(.12-.29*EP4)*LNT2
         FC2=(1.-V)*(1.-(1.-V)*(1.-V)*(1.-V)*.2772)*.9088*EP5
         FC3=(.573+.083*LNPP)*EP6
         FC4=15.*EXP(FC1*LNT2)
         Y=FC4-6.9078-FC2+FC3
         YT=FC4*(FC1+LNT2*(.12-.29*EP4))/TT-.306*FC3
         YP=(FC4*LNT2*(.05253*EP3+.03683*EP4*LNT2)
     &       +FC2*.0212+.083*EP6)/PP
         YV=(1.-(1.-V)*(1.-V)*(1.-V)*1.1088)*.9088*EP5
         EXPY=EXP(Y)
c
c --- Compressibility correction:
         AZ =(.420-.193*V)*EP0
         AZP=AZ*.007/PP
         AZV=-.193*EP0
         BZ =1.0+EXPY/TT
         BZT=(YT*TT-1.0)*EXPY/TT2
         BZP=EXPY*YP/TT
         BZV=EXPY*YV/TT
c
```

```
         Z1 =AZ/BZ
         Z1T=(   -Z1*BZT)/BZ
         Z1P=(AZP-Z1*BZP)/BZ
         Z1V=(AZV-Z1*BZV)/BZ
c
         ZZ =ZZ +Z1
         ZZT=ZZT+Z1T
         ZZP=ZZP+Z1P
         ZZV=ZZV+Z1V
c ..................................................................
c --- Enthalpy correction:
         AH =(25.9-11.*V)*EP1
         AHV=-11.*EP1
         AHP=AH*.0115/PP
         BH =TT*BZ
         BHT=BZ+TT*BZT
         BHP=TT*BZP
         BHV=TT*BZV
c
         H1 =AH/BH
         H1T=(   -H1*BHT)/BH
         H1P=(AHP-H1*BHP)/BH
         H1V=(AHV-H1*BHV)/BH
c
         HH =HH +H1
         HHT=HHT+H1T
         HHP=HHP+H1P
         HHV=HHV+H1V
c ..................................................................
c --- Entropy correction:
         AS =(8.179-3.726*V)*EP2
         ASV=-3.726*EP2
         ASP=AS*(-0.03453)/PP
c
         S1 =AS/BZ
         S1T=(   -S1*BZT)/BZ
         S1P=(ASP-S1*BZP)/BZ
         S1V=(ASV-S1*BZV)/BZ
c
         SS =SS +S1
         SST=SST+S1T
         SSP=SSP+S1P
         SSV=SSV+S1V
      endif
c ..................................................................
c ..................................................................
      if(DCO .eq. 2)then
c ...    Correction for upper stage dissociation.
         EP0=EXP(-.05648*LNPP)
         EP1=EXP(-.045*LNPP)
         Y=18.0972-2.43*TT*EP1
         YT=-2.43*EP1
         YP=-2.43*TT*EP1*(-.045/PP)
         EXPY=EXP(Y)
c
c --- Compressibility correction:
         AZ =0.774-.119*V-(.0128+.005*V)*LNPP
         AZV=-.119-.005*LNPP
         AZP=-(.0128+.005*V)/PP
         BZ =1.0+EXPY/TT
         BZT=(YT*TT-1.0)*EXPY/TT2
         BZP=EXPY*YP/TT
```

```
c
         Z2 =AZ/BZ
         Z2T=(   -Z2*BZT)/BZ
         Z2P=(AZP-Z2*BZP)/BZ
         Z2V=(AZV       )/BZ
c
         ZZ =ZZ +Z2
         ZZT=ZZT+Z2T
         ZZP=ZZP+Z2P
         ZZV=ZZV+Z2V
c ..................................................................
c --- Enthalpy correction:
         AH =86.5-3.065*LNPP-14.35*V
         AHP=-3.065/PP
         AHV=-14.35
         BH =TT*BZ
         BHT=BZ+TT*BZT
         BHP=TT*BZP
c
         H2 =AH/BH
         H2T=(   -H2*BHT)/BH
         H2P=(AHP-H2*BHP)/BH
         H2V=(AHV       )/BH
c
         HH =HH +H2
         HHT=HHT+H2T
         HHP=HHP+H2P
         HHV=HHV+H2V
c ..................................................................
c --- Entropy function correction:
         AS =(14.512*EP0-2.434*V)
         ASP=AS*(-0.05648)/PP
         ASV=-2.434*EP0
c
         S2 =AS/BZ
         S2T=(   -S2*BZT)/BZ
         S2P=(ASP-S2*BZP)/BZ
         S2V=(ASV)/BZ
c
         SS =SS +S2
         SST=SST+S2T
         SSP=SSP+S2P
         SSV=SSV+S2V
      endif
c ..................................................................
c ..................................................................
c ... Calculation of properties and partial derivatives.
c ..................................................................
c ... Constants applied:
c        FC1 = R0/M
c        FC2 = (1/M)*dM/dF
c        FC3 = dV/dF
c ..........
      FC1=8314.7*(.333333*F+4.7732)/(9.3517*F+138.25)
      FC2=-1.44575/((.333333*F+4.7732)*(9.3517*F+138.2500))
      FC3=-(1.0+fs)/((1.+fs*F)*(1.+fs*F))
      R=FC1*ZZ
      h=FC1*T*HH
      s=FC1*SS
      u=h-R*T
c .........
      Rp=FC1*ZZP*FC0
```

```
      RT=FC1*ZZT*.001
      RF=FC1*(ZZV*FC3-ZZ*FC2)
c .........
      up=FC1*T*(HHP-ZZP)*FC0
      uT=FC1*(HH-ZZ+TT*(HHT-ZZT))
      uF=FC1*T*((HHV-ZZV)*FC3-(HH-ZZ)*FC2)
c .........
      hp=FC1*T*HHP*FC0
      hT=FC1*(HH+TT*HHT)
      hF=FC1*T*(HHV*FC3-HH*FC2)
c .........
      sp=FC1*SSP*FC0
      sT=FC1*SST*0.001
      sF=FC1*(SSV*FC3-SS*FC2)
c .........
      cp=hT
      cv=uT+up*(R/T+RT)/(R/p-Rp)
      k=cp/cv
c ..................................................................
 9999 continue
      RETURN
      END subroutine
      end module zach
```

Appendix B

Input files to two zone program

The input file is formated as two Fortran namelists, one namelist for the configuration of the prechamber, and one for initial values and configuration of the integration routine. The input file is written by a preprocessor program, but the values are also easy to change "by hand" using a text editor.

B.1 Reference simulation

```
&INTEGRATION_CONFIG
   T        =  0.0,
   DT       =  5.0E-05,
   T_END    =  1.0E-02,
   SUBCYCLE =  100,
   Y        =  6.0E+06   2.5E+03   6.5479232047856364E-08   8.0E-09
      7.5E+02   4.3524558585883086E-04   1.5992E-05  0.0  0.0  0.0
/
&TWO_ZONE_CONFIG
   ALPHA1 = 0.8,
   ALPHA2 = 0.25,
   AREA   = 4.8E-05,
   NOZ_C  = 0.5,
   NOZ_D  = 3.1915382432114E-3,
   ROHRC  = 1.0E+06,
   HC     = 2.0E+06,
   PM     = 6.0E+06
   TM     = 7.50E+02,
   VFF    = 0.7,
   VP     = 1.6E-05,
   NUMNOZ = 6
/
```

Appendix C

Data from measurements on a prechamber engine

This chapter contains the measured data and plots generated by Marintek's measurements and analysis software: "Tango". It is included just for those specially interested in engine data and emmisions and should be skipped by others. The next pages contain Norwegian text.

TESTPROTOKOLL UBE KR3 GASS

Model: /tmp_mnt/home/immhp1/c/viggon/ub/kr3/krg_norum
Reg.no.: 2 Date: 9 Apr 97 Time: 14:22:16

Motor og driftsdata

Hn_M	[MJ/Kg]	49.48			
BMEP	[bar]	4.11	Gassforbruk	[g/s]	10.04
BMIP	[bar]		Gassforbruk_V.n	[m^3/s]	0.00
Pmax	[bar]		Energiforbruk_s	[MJ/kWh]	14.66
fi(Pmax)	[deg]		Energiforbruk_s.ISO	[MJ/kWh]	13.93
Turtall motor	[rpm]	806	Virkningsgrad	[%]	24.6
Moment	[Nm]	1446	Paadrag gassventil	[deg]	Not Ava
Akseleffekt	[kW]	122	AFR styresignal	[%]	Not Ava
Fortenningsvinkel	[deg]	Not Ava	Paadrag luftspjeld	[%]	Not Ava
Vol_eff.	[]	0.88			

Luft - Avgass

Barometerstand	[mbar]	997	Trykkfall l.m.dyse	[mbar]	2.3
Lufttetthet	[kg/m^3]	1.16	Luftmengde	[kg/s]	0.35
Lufttemp.f.l.m.dyse	[C]	25.9	Luftmengde_V.n	[m^3/s]	0.27
Lufttemp. f. lader	[C]	36.1	Luftforbruk_s	[kg/kWh]	10.36
Lufttemp. e. lader	[C]	56.8	Avgassmengde vaat	[kg/h]	1300
Lufttemp. receiver	[C]	33.6	Lambda MFlow	[]	2.05
Eksostemp. e. syl.1	[C]	264	Lambda O2	[]	2.86
Eksostemp. e. syl.2	[C]	397	Lambda CO2	[]	3.06
Eksostemp. e. syl.3	[C]	502	Lambda_tot	[]	2.19
Eksostemp. f. turbin	[C]	404	Turtall turbolader	[rpm]	16599
Eksostemp. e. turbin	[C]	318	Turtall turbolader_300K	[rpm]	16348
Gasstemp. f. motor	[C]	18.42	Trykk luftreceiver	[bar]	1.18
Gasstrykk inn	[bar]	7.18	Trykk avgassreceiver	[bar]	1.13
Gasstrykk hoved	[bar]	1.40	Trykkforhold o. lader	[]	1.19
Gasstrykk forkammer	[bar]	1.20	Adiab. virkn.gr. lader	[]	0.00

Emisjonsdata

NOx vaat	[ppm]	78.5	Spec_NOx_corr	[g/kWh]	1.26
HC vaat	[ppm]	3842.0	Spec_HC	[g/kWh]	58.71
CO torr	[ppm]	1149.3	Spec_CO	[g/kWh]	10.83
CO2 torr	[%]	3.5	Spec_CO2	[g/kWh]	526.00
O2 torr	[%]	14.1			
HC 5% O2	[mg/nm^3]	16725	Corr_NOx	[]	0.95
CO 5% O2	[mg/nm^3]	3365	Corr_wet	[]	0.92
NOx 5% O2	[mg/nm^3]	377			

Kj.vann - Sm.oljedata

Kj.v..temp. f. motor	[C]	72.8	Sj.v.temp. inn	[C]	17.3
Kj.v.temp. e. motor	[C]	74.3	Sj.v.temp. f. sm.o.kj.	[C]	17.9
Sm.o.temp. f. motor	[C]	53.7	Sj.v.temp. f. f.v.kj.	[C]	19.5
Sm.o.temp. e. motor	[C]	58.6	Sj.v.temp. ut	[C]	20.9

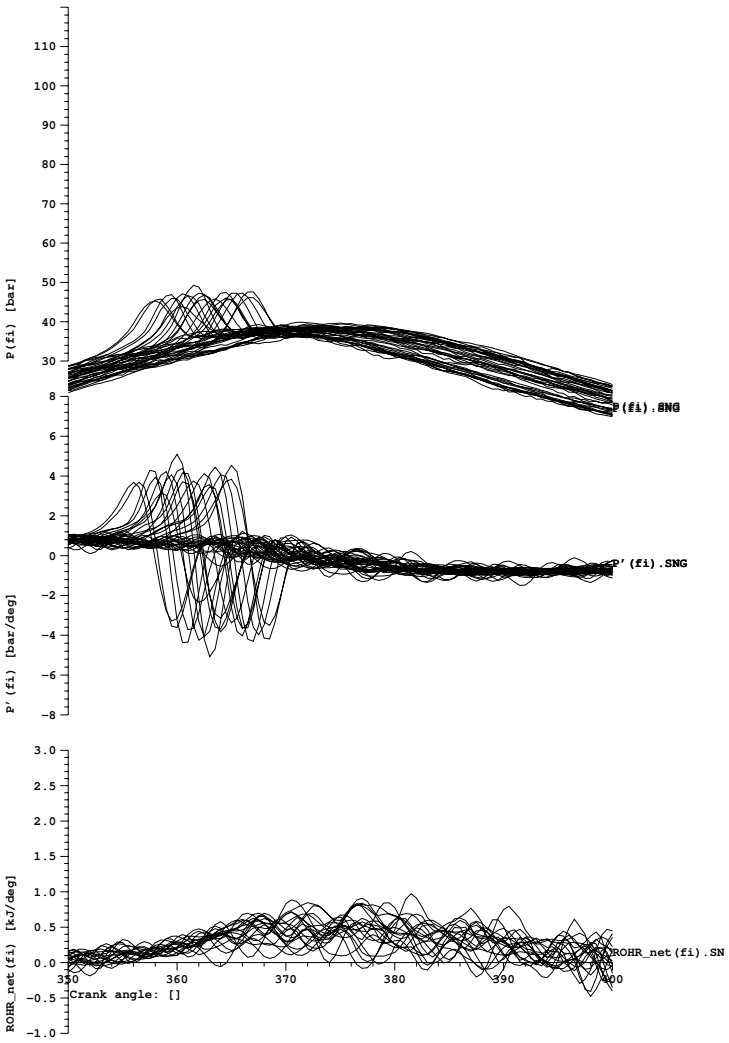
P(fi) [bar]
P(fi).SNG
P'(fi) [bar/deg]
P'(fi).SNG
ROHR_net(fi) [kJ/deg]
ROHR_net(fi).SN
Crank angle: []

TESTPROTOKOLL UBE KR3 GASS

Model: /tmp_mnt/home/immhp1/c/viggon/ub/kr3/krg_norum
Reg.no.: 3 Date: 9 Apr 97 Time: 14:48:01

Motor og driftsdata

Hn_M	[MJ/Kg]	49.48			
BMEP	[bar]	14.25	Gassforbruk	[g/s]	26.80
BMIP	[bar]		Gassforbruk_V.n	[m^3/s]	0.01
Pmax	[bar]		Energiforbruk_s	[MJ/kWh]	9.08
fi(Pmax)	[deg]		Energiforbruk_s.ISO	[MJ/kWh]	8.54
Turtall motor	[rpm]	1003	Virkningsgrad	[%]	39.7
Moment	[Nm]	5009	Paadrag gassventil	[deg]	Not Ava
Akseleffekt	[kW]	526	AFR styresignal	[%]	Not Ava
Fortenningsvinkel	[deg]	Not Ava	Paadrag luftspjeld	[%]	Not Ava
Vol_eff.	[]	0.95			

Luft - Avgass

Barometerstand	[mbar]	998	Trykkfall l.m.dyse	[mbar]	15.5
Luftttetthet	[kg/m^3]	1.16	Luftmengde	[kg/s]	0.90
Lufttemp.f.l.m.dyse	[C]	26.8	Luftmengde_V.n	[m^3/s]	0.70
Lufttemp. f. lader	[C]	56.0	Luftforbruk_s	[kg/kWh]	6.17
Lufttemp. e. lader	[C]	149.8	Avgassmengde vaat	[kg/h]	3344
Lufttemp. receiver	[C]	52.9	Lambda MFlow	[]	1.97
Eksostemp. e. syl.1	[C]	553	Lambda O2	[]	2.02
Eksostemp. e. syl.2	[C]	554	Lambda CO2	[]	1.91
Eksostemp. e. syl.3	[C]	539	Lambda_tot	[]	1.90
Eksostemp. f. turbin	[C]	587	Turtall turbolader	[rpm]	35679
Eksostemp. e. turbin	[C]	416	Turtall turbolader_300K	[rpm]	34060
Gasstemp. f. motor	[C]	14.44	Trykk luftreceiver	[bar]	2.40
Gasstrykk inn	[bar]	6.96	Trykk avgassreceiver	[bar]	2.09
Gasstrykk hoved	[bar]	2.28	Trykkforhold o. lader	[]	2.44
Gasstrykk forkammer	[bar]	2.09	Adiab. virkn.gr. lader	[]	0.00

Emisjonsdata

NOx vaat	[ppm]	155.9	Spec_NOx_corr	[g/kWh]	1.51
HC vaat	[ppm]	529.7	Spec_HC	[g/kWh]	4.83
CO torr	[ppm]	421.7	Spec_CO	[g/kWh]	2.26
CO2 torr	[%]	5.8	Spec_CO2	[g/kWh]	488.35
O2 torr	[%]	11.2			
HC 5% O2	[mg/nm^3]	1605	Corr_NOx	[]	0.96
CO 5% O2	[mg/nm^3]	860	Corr_wet	[]	0.87
NOx 5% O2	[mg/nm^3]	522			

Kj.vann - Sm.oljedata

Kj.v..temp. f. motor	[C]	81.3	Sj.v.temp. inn	[C]	17.7
Kj.v.temp. e. motor	[C]	84.3	Sj.v.temp. f. sm.o.kj.	[C]	18.9
Sm.o.temp. f. motor	[C]	55.2	Sj.v.temp. f. f.v.kj.	[C]	20.9
Sm.o.temp. e. motor	[C]	61.4	Sj.v.temp. ut	[C]	27.2

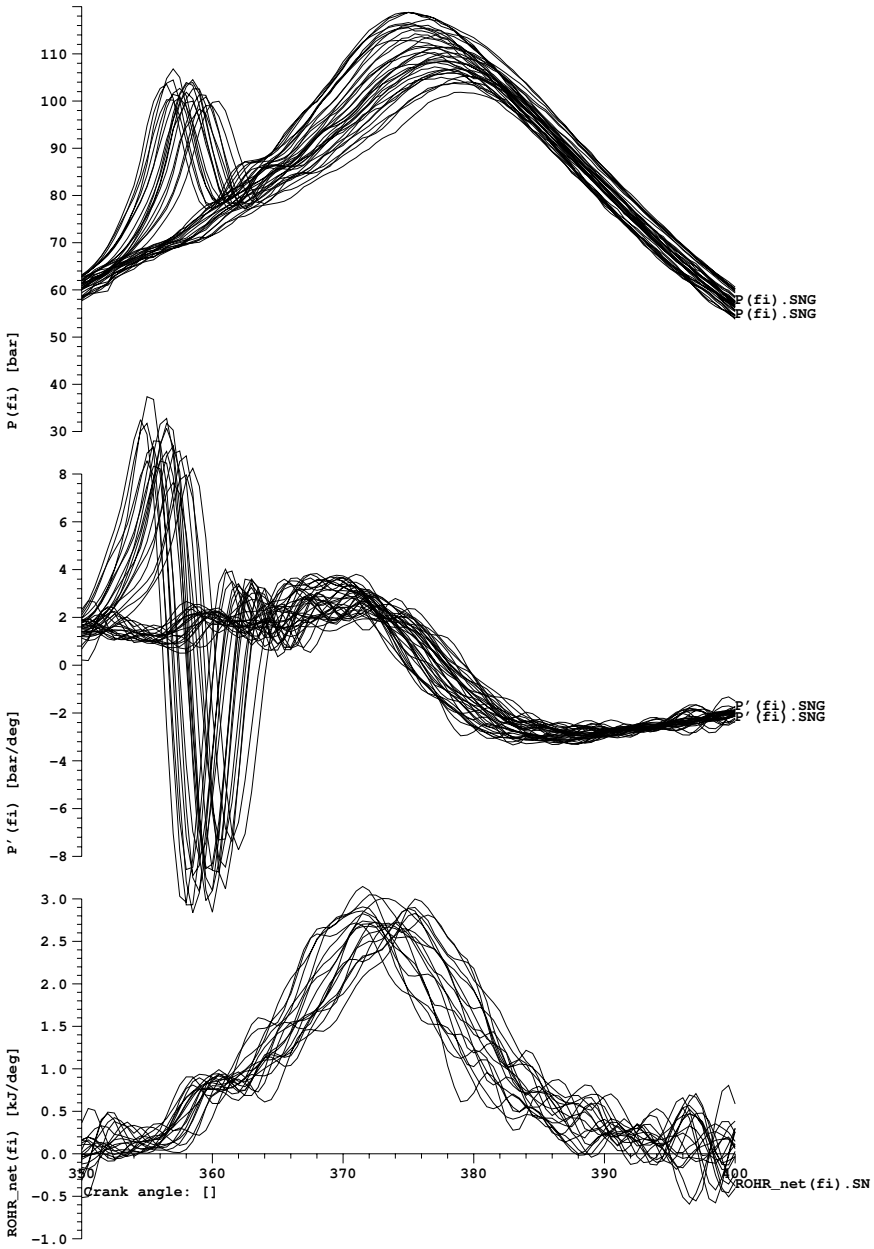
P(fi) [bar]
P(fi).SNG
P(fi).SNG
P'(fi) [bar/deg]
P'(fi).SNG
P'(fi).SNG
ROHR_net(fi) [kJ/deg]
ROHR_net(fi).SN
Crank angle: []

TESTPROTOKOLL UBE KR3 GASS

Model: /tmp_mnt/home/immhp1/c/viggon/ub/kr3/krg_norum
Reg.no.: 4 Date: 9 Apr 97 Time: 14:54:09

Motor og driftsdata

Hn_M	[MJ/Kg]	49.48			
BMEP	[bar]	8.00	Gassforbruk	[g/s]	17.42
BMIP	[bar]		Gassforbruk_V.n	[m^3/s]	0.00
Pmax	[bar]		Energiforbruk_s	[MJ/kWh]	10.49
fi(Pmax)	[deg]		Energiforbruk_s.ISO	[MJ/kWh]	9.88
Turtall motor	[rpm]	1004	Virkningsgrad	[%]	34.3
Moment	[Nm]	2813	Paadrag gassventil	[deg]	Not Ava
Akseleffekt	[kW]	296	AFR styresignal	[%]	Not Ava
Fortenningsvinkel	[deg]	Not Ava	Paadrag luftspjeld	[%]	Not Ava
Vol_eff.	[]	0.93			

Luft - Avgass

Barometerstand	[mbar]	997	Trykkfall l.m.dyse	[mbar]	6.5
Luftttetthet	[kg/m^3]	1.16	Luftmengde	[kg/s]	0.58
Lufttemp.f.l.m.dyse	[C]	27.0	Luftmengde_V.n	[m^3/s]	0.45
Lufttemp. f. lader	[C]	49.9	Luftforbruk_s	[kg/kWh]	7.11
Lufttemp. e. lader	[C]	101.3	Avgassmengde vaat	[kg/h]	2165
Lufttemp. receiver	[C]	44.5	Lambda MFlow	[]	1.97
Eksostemp. e. syl.1	[C]	491	Lambda O2	[]	2.13
Eksostemp. e. syl.2	[C]	505	Lambda CO2	[]	2.06
Eksostemp. e. syl.3	[C]	552	Lambda_tot	[]	1.95
Eksostemp. f. turbin	[C]	553	Turtall turbolader	[rpm]	26378
Eksostemp. e. turbin	[C]	416	Turtall turbolader_300K	[rpm]	25420
Gasstemp. f. motor	[C]	14.63	Trykk luftreceiver	[bar]	1.55
Gasstrykk inn	[bar]	7.11	Trykk avgassreceiver	[bar]	1.40
Gasstrykk hoved	[bar]	1.68	Trykkforhold o. lader	[]	1.56
Gasstrykk forkammer	[bar]	1.49	Adiab. virkn.gr. lader	[]	0.00

Emisjonsdata

NOx vaat	[ppm]	173.4	Spec_NOx_corr	[g/kWh]	1.93
HC vaat	[ppm]	1032.9	Spec_HC	[g/kWh]	10.84
CO torr	[ppm]	554.3	Spec_CO	[g/kWh]	3.45
CO2 torr	[%]	5.4	Spec_CO2	[g/kWh]	524.35
O2 torr	[%]	11.7			
HC 5% O2	[mg/nm^3]	3300	Corr_NOx	[]	0.96
CO 5% O2	[mg/nm^3]	1191	Corr_wet	[]	0.88
NOx 5% O2	[mg/nm^3]	612			

Kj.vann - Sm.oljedata

Kj.v..temp. f. motor	[C]	80.0	Sj.v.temp. inn	[C]	17.9
Kj.v.temp. e. motor	[C]	82.2	Sj.v.temp. f. sm.o.kj.	[C]	18.7
Sm.o.temp. f. motor	[C]	54.9	Sj.v.temp. f. f.v.kj.	[C]	21.0
Sm.o.temp. e. motor	[C]	61.4	Sj.v.temp. ut	[C]	24.8

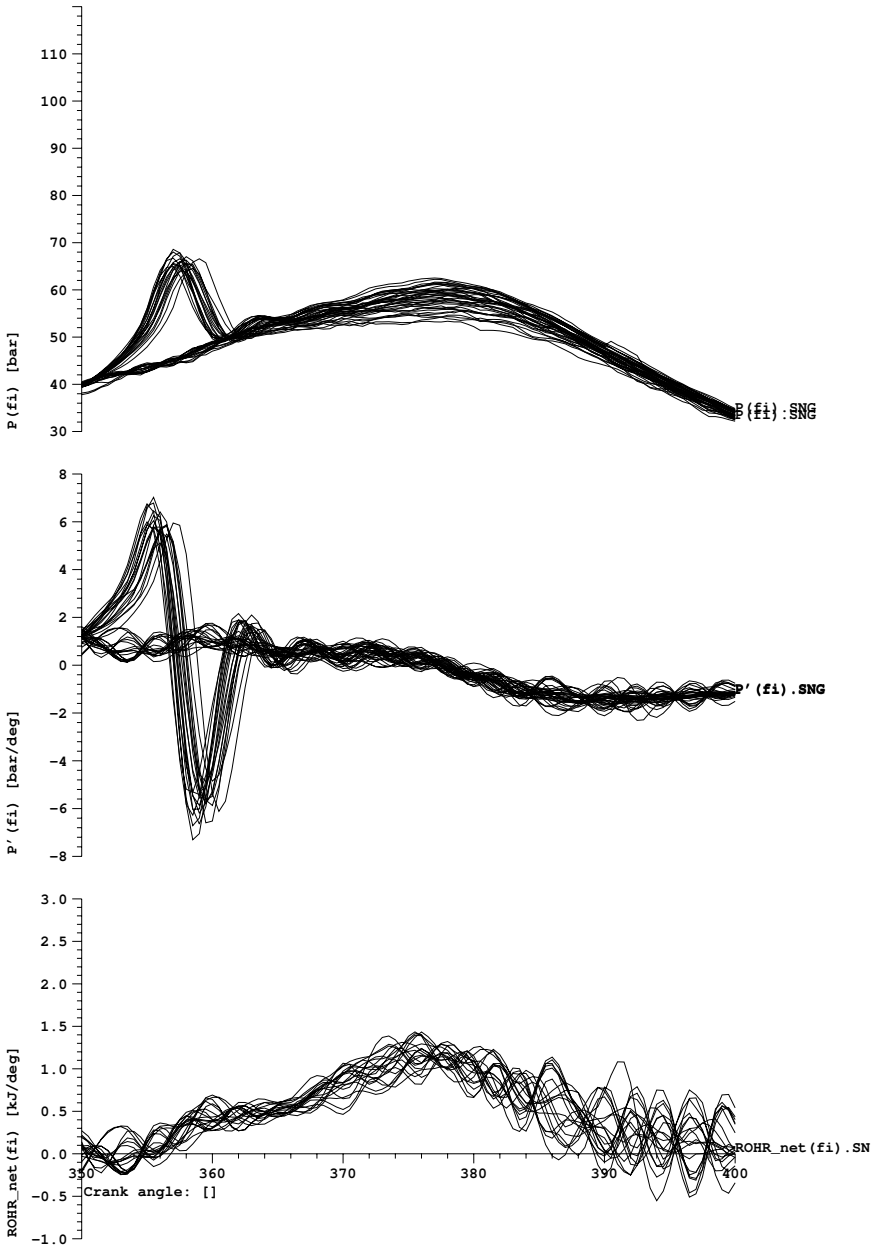
P(fi) [bar]
110
100
90
80
70
60
50
40
30
P(fi).SNG
P'(fi) [bar/deg]
8
6
4
2
0
−2
−4
−6
−8
P'(fi).SNG
ROHR_net(fi) [kJ/deg]
3.0
2.5
2.0
1.5
1.0
0.5
0.0
−0.5
−1.0
ROHR_net(fi).SN
350
360
370
380
390
400
Crank angle: []

TESTPROTOKOLL UBE KR3 GASS

Model: /tmp_mnt/home/immhp1/c/viggon/ub/kr3/krg_norum
Reg.no.: 6 Date: 9 Apr 97 Time: 15:03:22

Motor og driftsdata

Hn_M	[MJ/Kg]	49.48			
BMEP	[bar]	3.97	Gassforbruk	[g/s]	12.84
BMIP	[bar]		Gassforbruk_V.n	[m^3/s]	0.00
Pmax	[bar]		Energiforbruk_s	[MJ/kWh]	15.62
fi(Pmax)	[deg]		Energiforbruk_s.ISO	[MJ/kWh]	14.72
Turtall motor	[rpm]	1002	Virkningsgrad	[%]	23.1
Moment	[Nm]	1396	Paadrag gassventil	[deg]	Not Ava
Akseleffekt	[kW]	146	AFR styresignal	[%]	Not Ava
Fortenningsvinkel	[deg]	Not Ava	Paadrag luftspjeld	[%]	Not Ava
Vol_eff.	[]	0.90			

Luft - Avgass

Barometerstand	[mbar]	997	Trykkfall l.m.dyse	[mbar]	3.9
Luftttetthet	[kg/m^3]	1.16	Luftmengde	[kg/s]	0.45
Lufttemp.f.l.m.dyse	[C]	26.3	Luftmengde_V.n	[m^3/s]	0.35
Lufttemp. f. lader	[C]	42.7	Luftforbruk_s	[kg/kWh]	11.12
Lufttemp. e. lader	[C]	69.8	Avgassmengde vaat	[kg/h]	1674
Lufttemp. receiver	[C]	39.4	Lambda MFlow	[]	2.07
Eksostemp. e. syl.1	[C]	328	Lambda O2	[]	2.76
Eksostemp. e. syl.2	[C]	425	Lambda CO2	[]	2.91
Eksostemp. e. syl.3	[C]	532	Lambda_tot	[]	2.16
Eksostemp. f. turbin	[C]	452	Turtall turbolader	[rpm]	19860
Eksostemp. e. turbin	[C]	355	Turtall turbolader_300K	[rpm]	19357
Gasstemp. f. motor	[C]	15.57	Trykk luftreceiver	[bar]	1.23
Gasstrykk inn	[bar]	7.16	Trykk avgassreceiver	[bar]	1.21
Gasstrykk hoved	[bar]	1.48	Trykkforhold o. lader	[]	1.23
Gasstrykk forkammer	[bar]	1.27	Adiab. virkn.gr. lader	[]	0.00

Emisjonsdata

NOx vaat	[ppm]	60.4	Spec_NOx_corr	[g/kWh]	1.04
HC vaat	[ppm]	3535.6	Spec_HC	[g/kWh]	57.97
CO torr	[ppm]	1149.8	Spec_CO	[g/kWh]	11.58
CO2 torr	[%]	3.7	Spec_CO2	[g/kWh]	593.18
O2 torr	[%]	13.9			
HC 5% O2	[mg/nm^3]	14813	Corr_NOx	[]	0.95
CO 5% O2	[mg/nm^3]	3240	Corr_wet	[]	0.91
NOx 5% O2	[mg/nm^3]	279			

Kj.vann - Sm.oljedata

Kj.v..temp. f. motor	[C]	79.3	Sj.v.temp. inn	[C]	17.3
Kj.v.temp. e. motor	[C]	80.7	Sj.v.temp. f. sm.o.kj.	[C]	18.1
Sm.o.temp. f. motor	[C]	54.3	Sj.v.temp. f. f.v.kj.	[C]	20.2
Sm.o.temp. e. motor	[C]	60.2	Sj.v.temp. ut	[C]	22.2

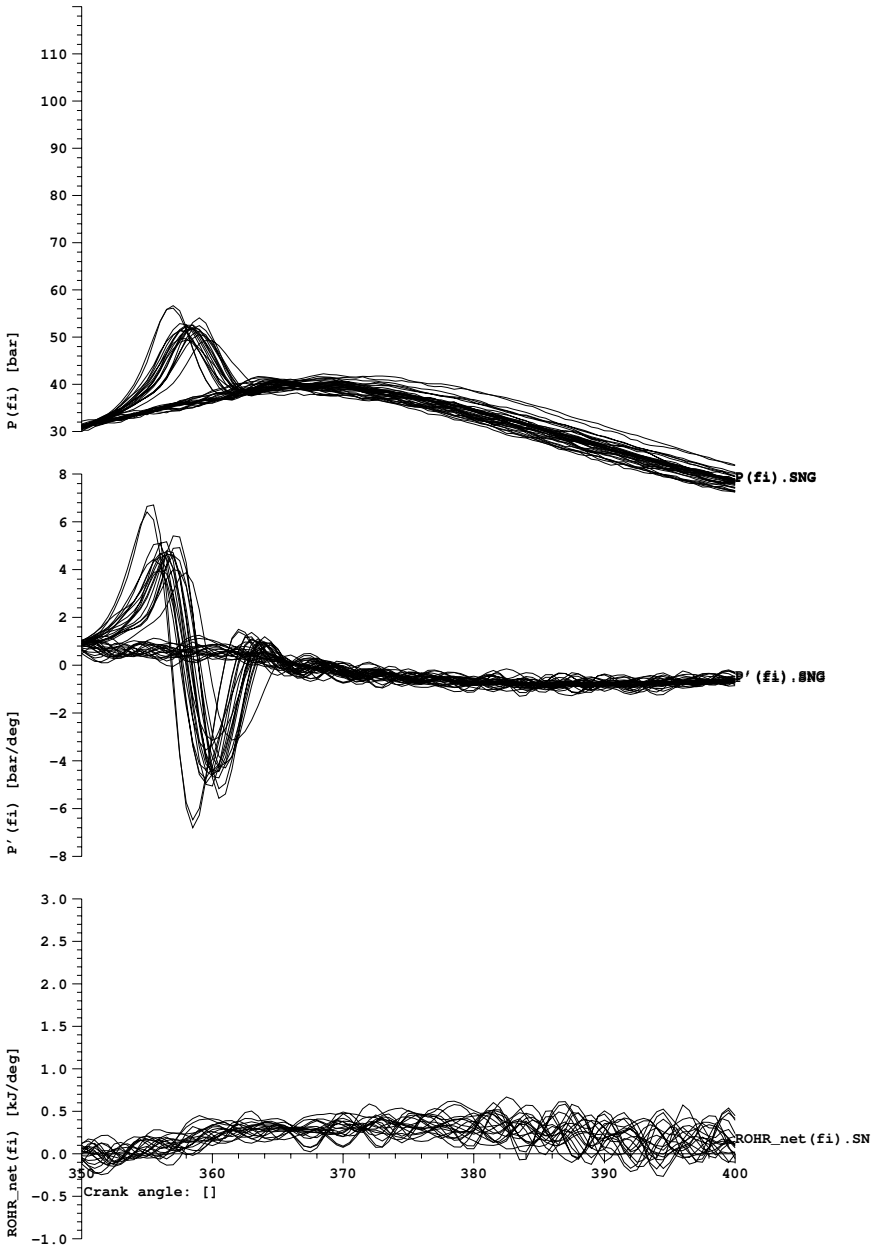
P(fi) [bar]
P(fi).SNG
P'(fi) [bar/deg]
P'(fi).SNG
ROHR_net(fi) [kJ/deg]
ROHR_net(fi).SN
Crank angle: []

Appendix D

New experimental equipment

This section is a more detailed description of the equipment used during the experiments described in section 6. The laboratory setup (see figure D.1) consists of; the bomb, prechambers, hydraulic system, Schlieren setup, gas delivery system, ignition system and electronic control and measurement system. Each subsystem will be described in the next pages.

A constant volume combustion rig (also called CVC-rig or "bomb") has been equipped with prechambers of varying geometry and a hydraulic device to close and open the nozzle between the chambers. The CVC-rig and the prechambers have temperature transducers and piezo-electric pressure transducers, in addition the rig and one of the prechambers have windows allowing visual sight straight through the rig. A Schlieren system as described in appendix Fis used to photograph the gas flow and combustion.

The bomb has been used in numerous experiments by Marintek and Marine Engineering, NTNU. The bomb is basically a stainless steel cylinder, 200 mm internal diameter, and 100 mm length. The cylinder has eight radial holes, 60 mm in diameter for mounting various equipment. The prechamber is mounted in one of the radial holes. The ends of the cylinder are sealed with 30 mm thick stainless steel plates fastened with eight 25 mm bolts. The end plates have windows so it is possible to see straight through the bomb.

Prechambers, three cylindrical prechambers (labeled "c") and one with square cross-section (labeled "s"): "c16/60", "c22/30", "c32/45" and "s30/40", the two numbers are respectively diameter (or sides in the square) and length in mm. The square chamber (see figure D.2) has two glass walls so that it is possible to see straight trough it. All prechambers used here have an inlet valve, an outlet valve, two ignition points, a pressure transducer, two temperature transducers and a

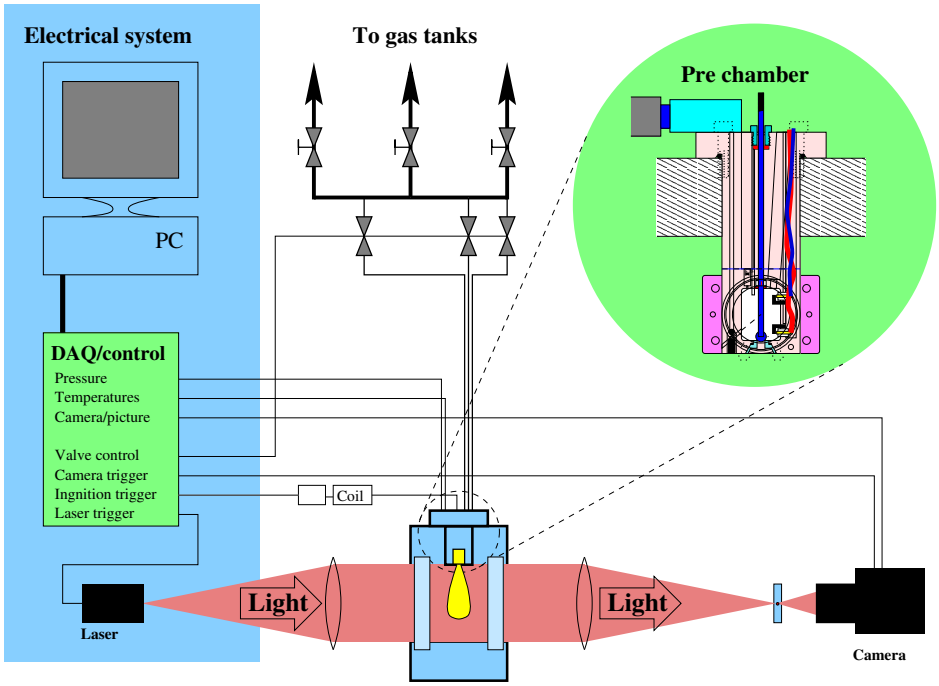

Figure D.1: Schematic laboratory setup. The bomb is shown in lower, midle part of the figure. A blown up figure of a prechamber is shown in the upper right. The hydraulic system for valve control and the rugged mounting frames are not shown in this figure.

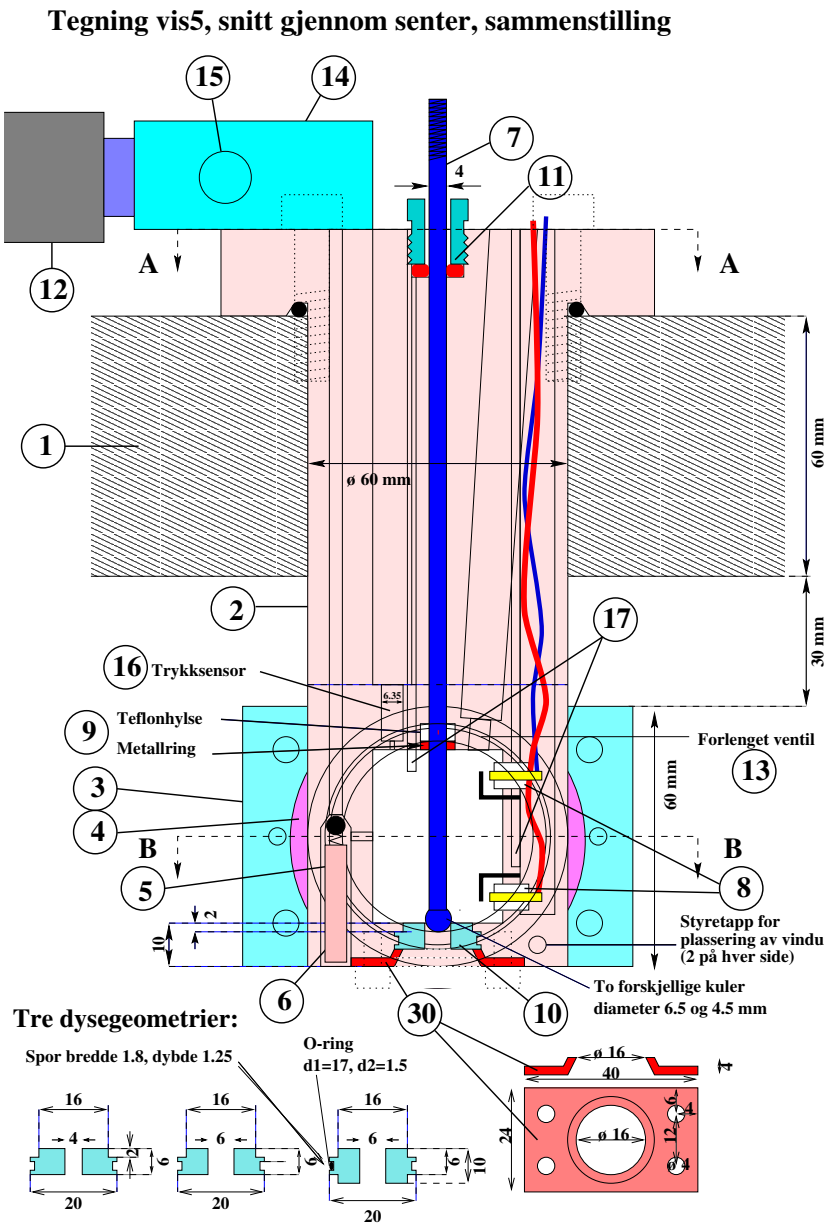

Figure D.2: Cutaway drawing of prechamber assembly consisting of the following main parts: (1) Bomb housing, (2) Prechamber housing, (3) Window and holder (two off, one on each side), (5) One way valve for gas supply, (7) Pin for closing then nozzle, (8) Spark plugs, (10) Nozzle, (12) Valve for gas supply, solenoid operated, (13) Exhaust valve, solenoid operated, (14) Gas supply manifold, (16) Pressure sensor, (17) Temperature sensors, (30) Nozzle holder.

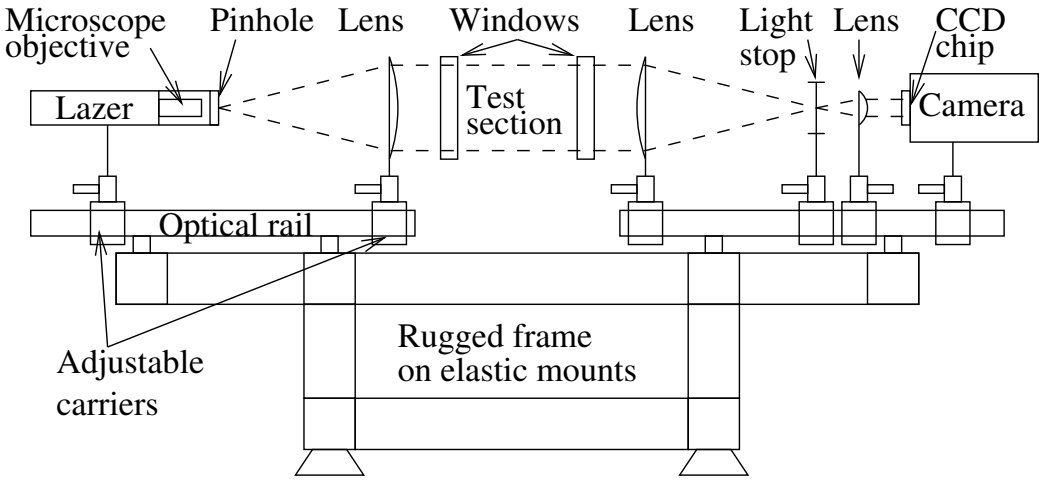

Figure D.3: Schematic Schlieren setup with lenses.

set of interchangeable nozzles. The nozzles are placed centrally in the cylinder end (centrally in the square for "s30/40"). All the nozzles have one single round hole with sharp edges. The nozzles are numbered in a similar scheme as the prechamber: "n4/4", "n6/4", "n6/6", "n6/10", "n9/6" and "n9/18".

Hydraulic system for closing and opening the prechamber nozzle. In order to know the exact charge composition in the prechamber at the time of ignition, it is necessary to close the nozzle during the filling process of the prechamber. Real engines does not have means for closing the nozzle between the chambers. The nozzle is opened with high accuracy and high speed. The pin closing the nozzle can be removed up to 30 mm in 2 ms, and with an acceleration of approximately 15000 m/s^2.

Schlieren setup consisting of laser, microscope objective, pinhole, lenses, optical mounting rails, adjustable carriers, a heavy frame for mounting the bomb and the optical equipment, a video camera with "line rate" accuracy triggering, an old PC with frame-grabber and software for image manipulation. A Schlieren setup is sketched in figure D.3.

Figure 6.1 shows example Schlieren images. The prechamber, which is the bright square in the top half of the picture, is 40 mm high and 30 mm wide. The round knob on the top is the valve for closing the nozzle. The nozzle is closed when the knob is pushed down through the prechamber onto the nozzle which is in the middle of the dark bar between the two chambers. The pin beside the knob is a temperature

sensor. The two pins on the right side of the prechamber are spark plugs. When using prechambers without glass, the prechamber is lifted up so that more of the jet is visible.

Gas delivery system Pipelines, valves and pressure bottles for mixing gas. Fuel and air may be mixed in the bottles or in the bomb. The valves are shut before the experiments start and there are flame traps between the bomb and the bottles in order to avoid combustion inside the bottles. As an additional safety precaution, the fuel/air mixtures are at relatively low pressure.

The valves leading gas into and out of the prechamber are electrically operated by solenoids so that it's possible to use high precision valve timing to generate turbulence inside the prechamber.

Ignition system. One ignition system for the prechamber and one for the main chamber to use for two stage combustion. Type: Bosch transistor controlled with coils. The coils are charged in 5 ms and produces a powerful spark visible for 2 ms at atmospheric conditions. The prechamber spark plugs are made of 1.2 mm wire and have 1 mm spark gap.

Electronic control and measurement system consisting of home made circuits, National Instruments' data acquisition and control boards and an old IBM PC. It controls valves for gas inlet to the prechamber, gas outlet from the prechamber, ignition, hydraulic system for the nozzle, triggering of the camera, and it records and displays temperature and pressure measurements.

Figures on the next pages shows the blueprints of the prechambers. All drawings have been scaled to fit page size.

D.1 Prechambers without windows

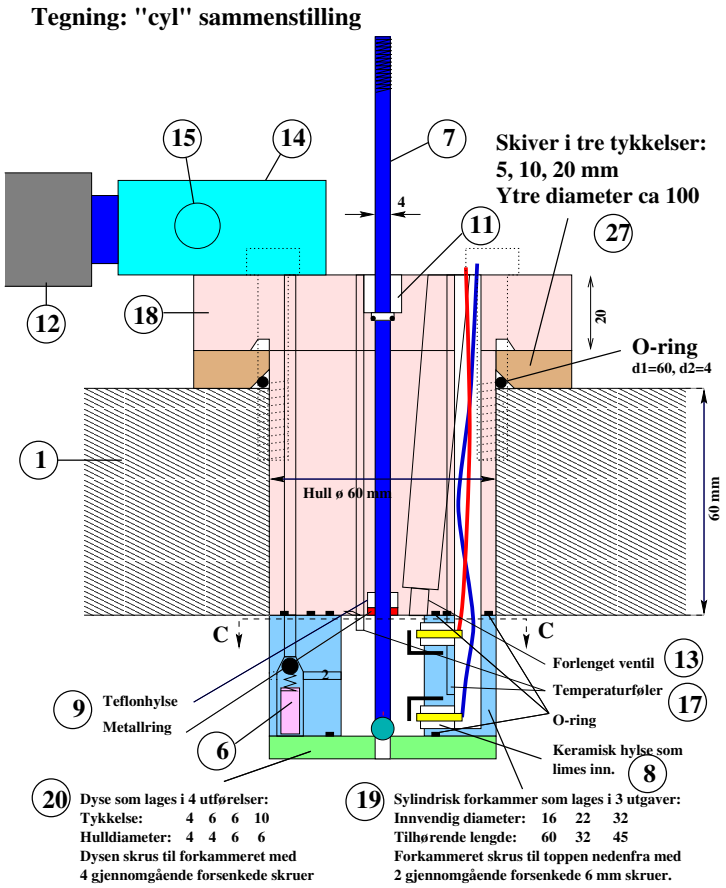

Tegning: "cyl4", snitt 45 grader fra siden.

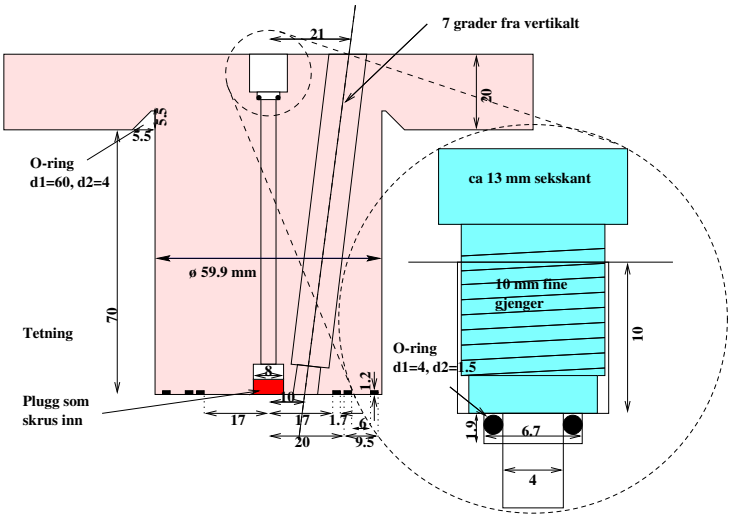

Snitt øverst, nytt forsøk.

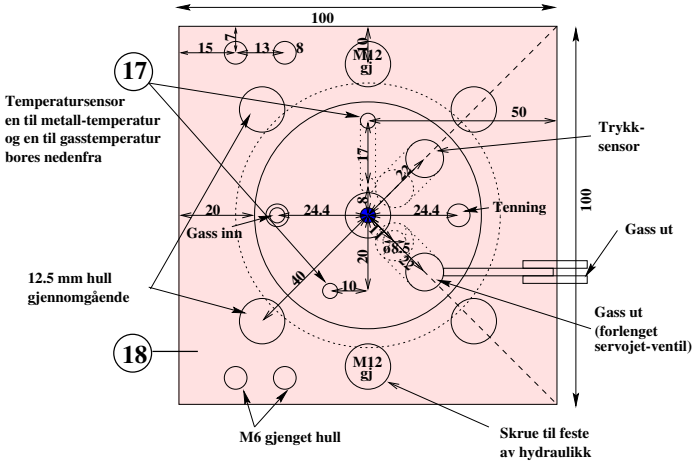

Tegning: "cyl2"

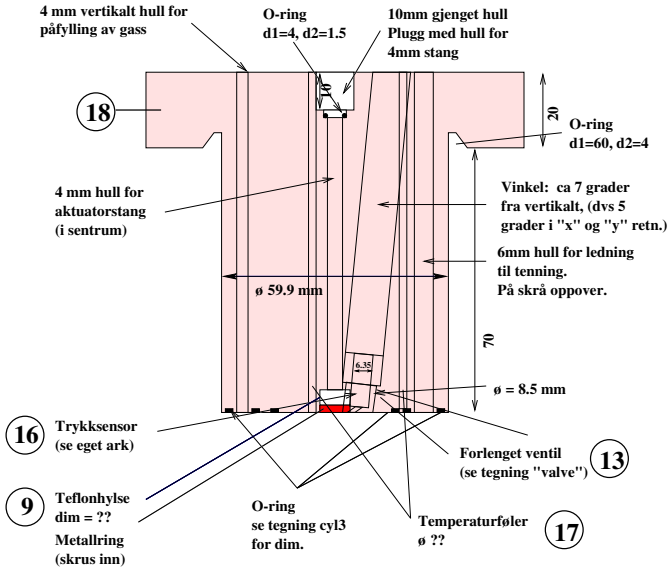

Snitt øverst. Se tegning "cyl3" for snitt nederst

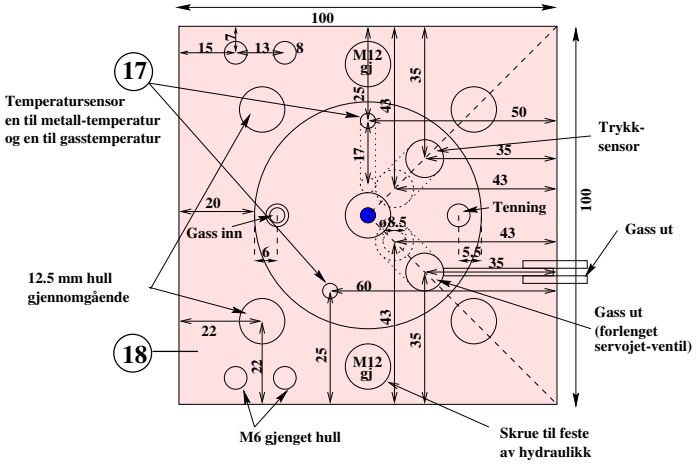

Tegning: cyl3

(19)

Sylindrisk forkammer som lages i 3 utgaver:
Innvendig diameter D: 16 22 32
Tilhørende lengde L: 60 32 45
Forkammeret skrus til toppen nedenfra med 2 gjennomgående forsenkede 6 mm skruer.

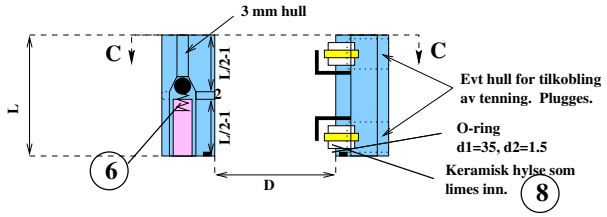

Snitt C-C (mellom forkammer og topp):

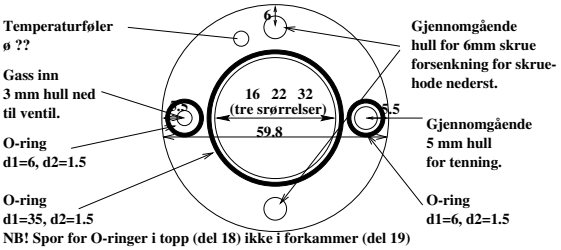

NB! Spor for O-ringer i topp (del 18) ikke i forkammer (del 19)
Se dysegeometri for snitt nederst på forkammeret.

Fire dysegeometrier for kammer uten gjennomsyn: (20)

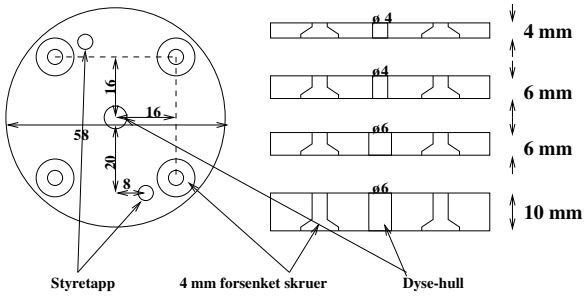

Tegning:
"manif"

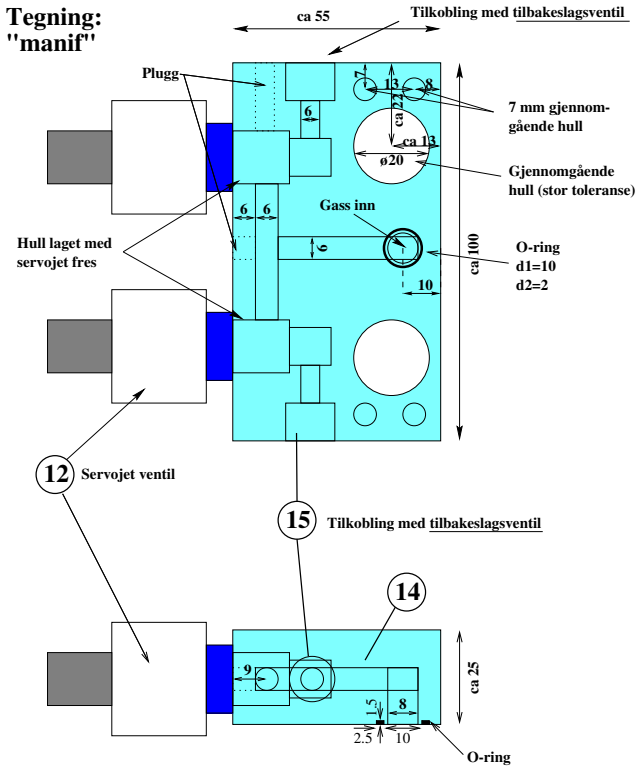

Forlengelse av Servo-Jet ventil:

Opprinnelig ventil slik den kommer fra fabrikken (denne skal ikke lages her):

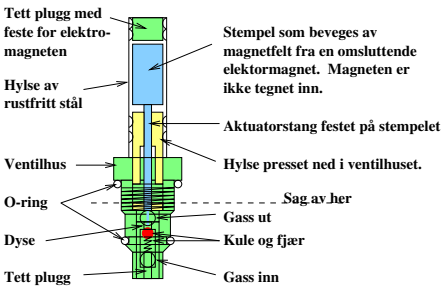

Forlengelsen utføres ved at man kapper ventilen i to et par millimeter oppå gjengepartiet (uten å skade aktuatorstangen). Den øvre delen benyttes som den er, mens den nedre delen dreies ned og gjenges. Det må lages en forlengelse til aktuatorstangen. Det skal med andre ord IKKE lages en ny øvre del til ventilen men kun en forlengelse til den ORIGINALE aktuatorstangen.

Nedre del av ventilen:

Opprinnelig: **Modifisert:**

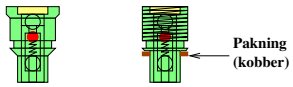

Forlengelse til aktuatorstangen:

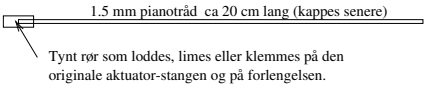

D.2 Hydraulic mechanism

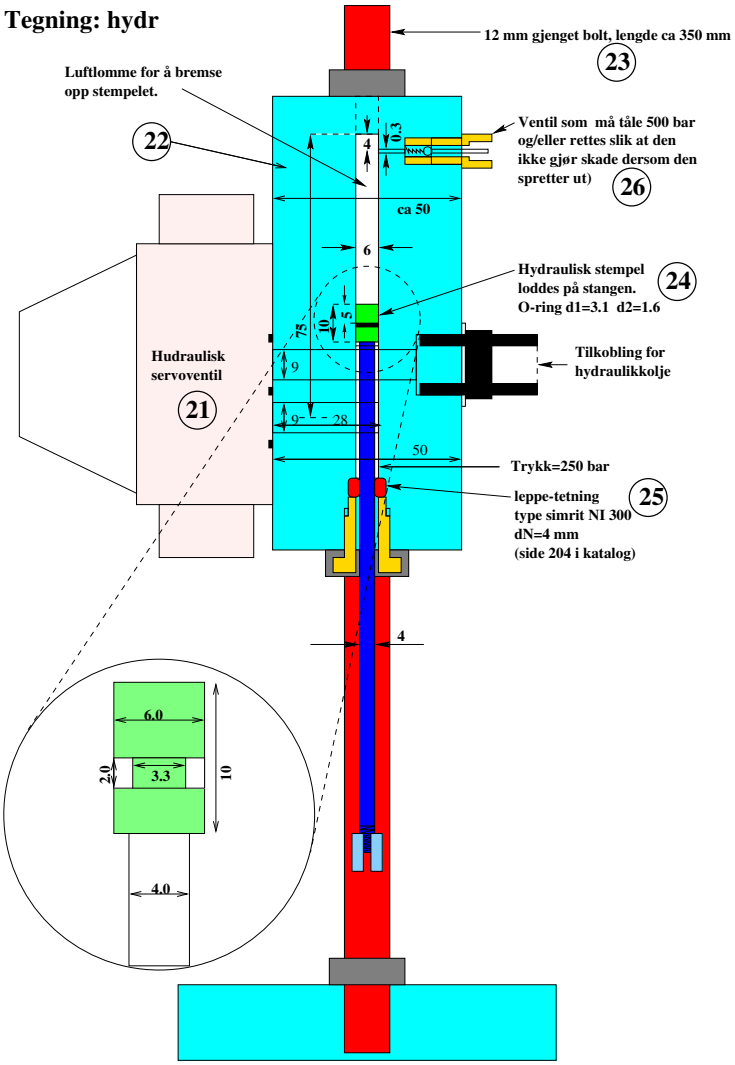

Tegning:
hydr2

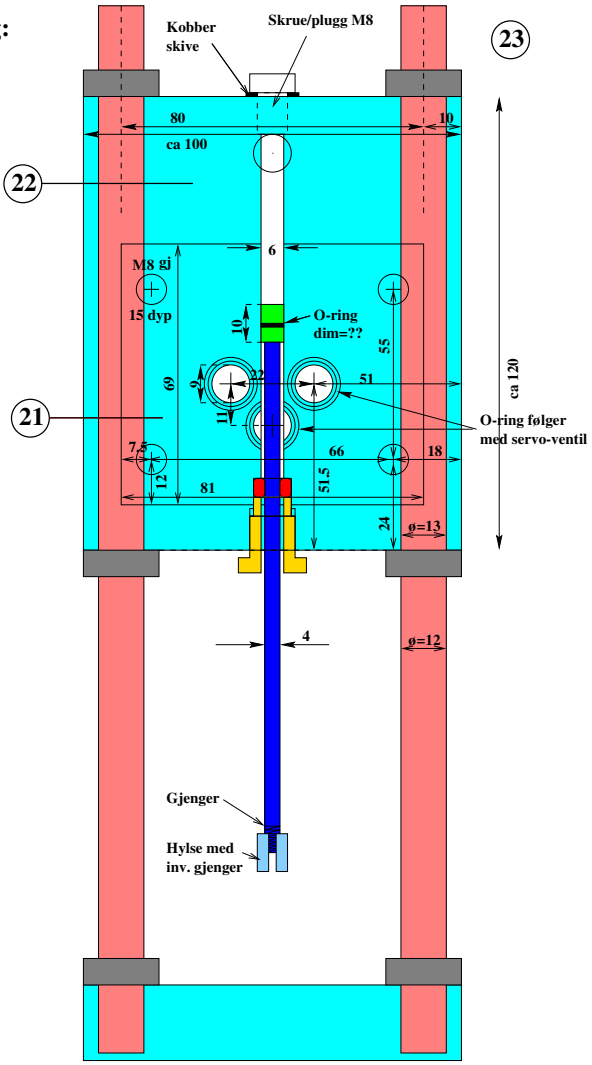

Tegning: hydr3

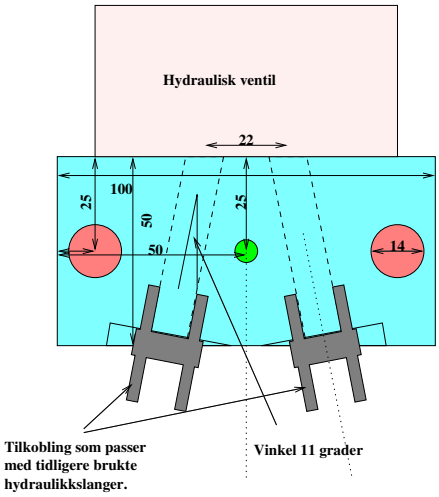

Tegning: rod

Det skal lages to stenger, en med ca 4.5mm kule og en med ca 6.5mm kule

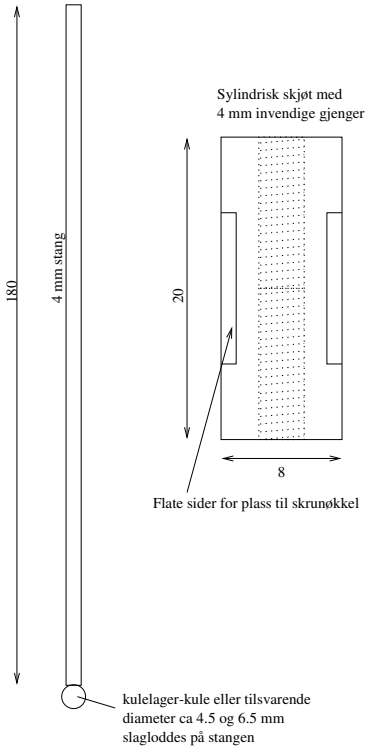

D.3 Prechambers with windows

Snitt gjennom senter, sammenstilling vis3:

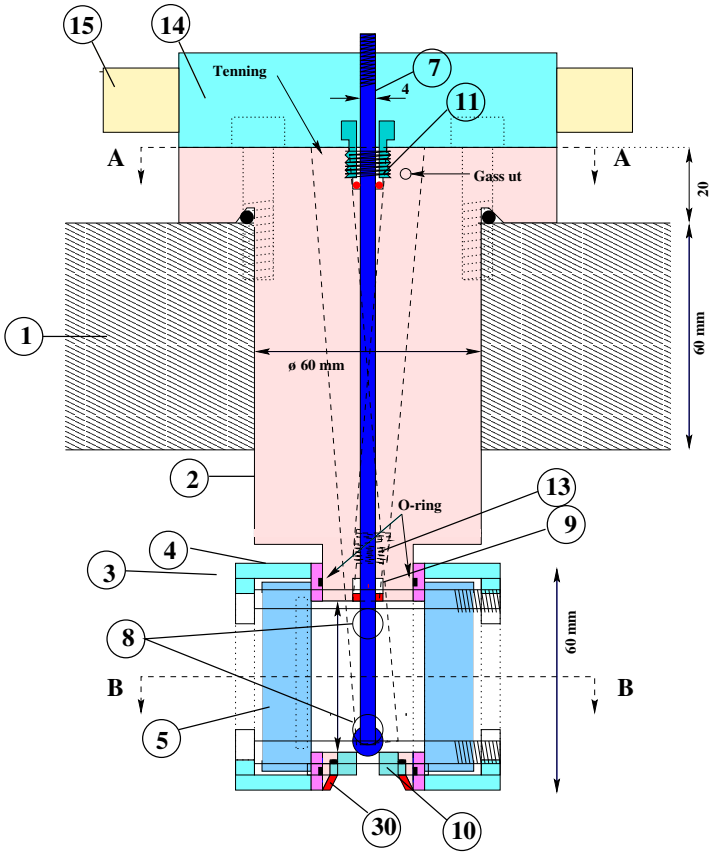

Tegning vis5, snitt gjennom senter, sammenstilling

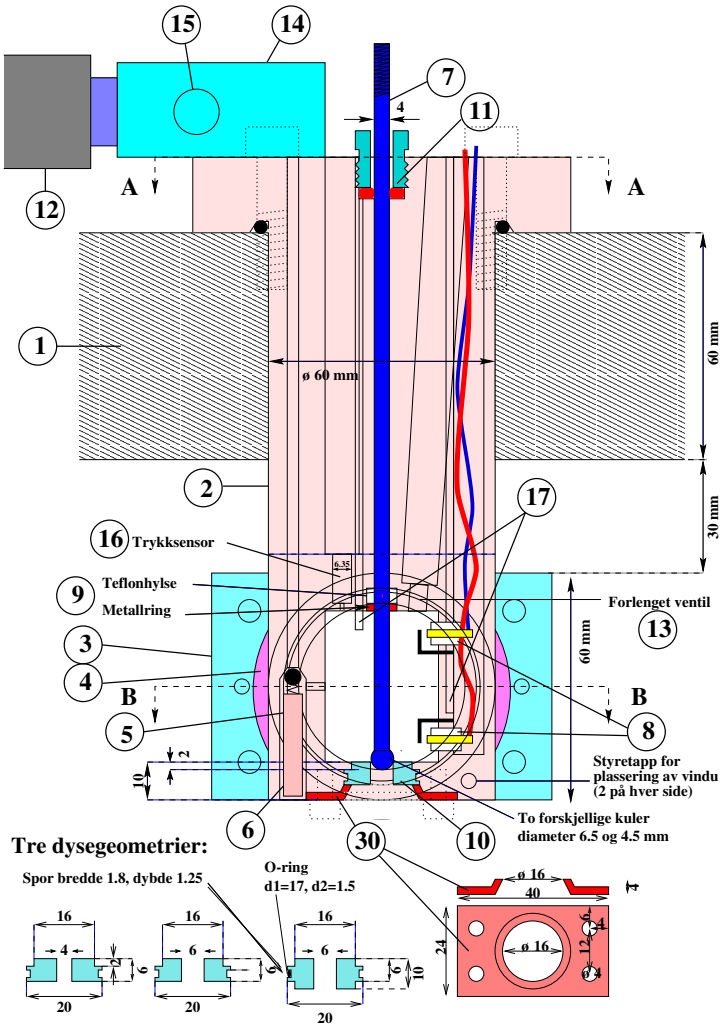

Snitt A-A
vis4 sammenstilling

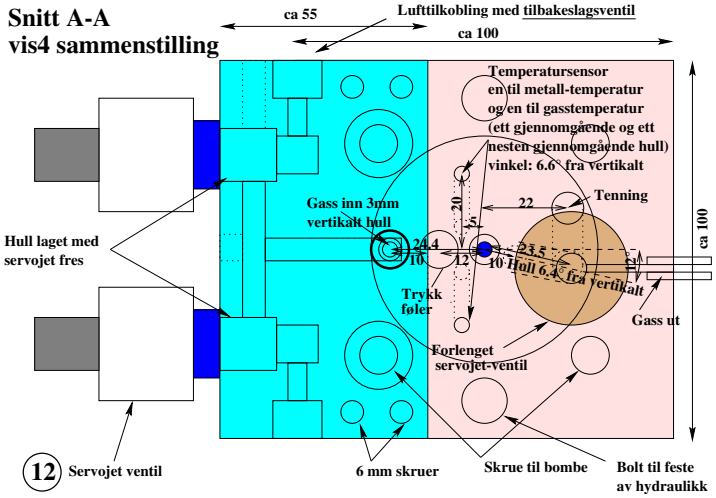

Snitt B-B

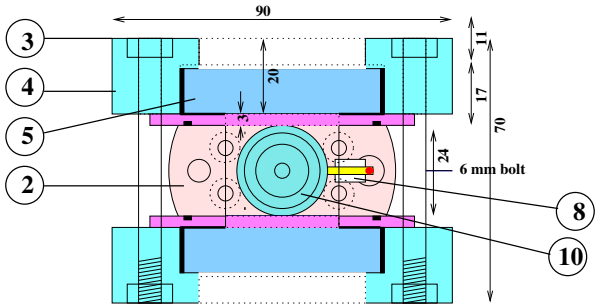

Snitt gjennom senter, tegning vis7:

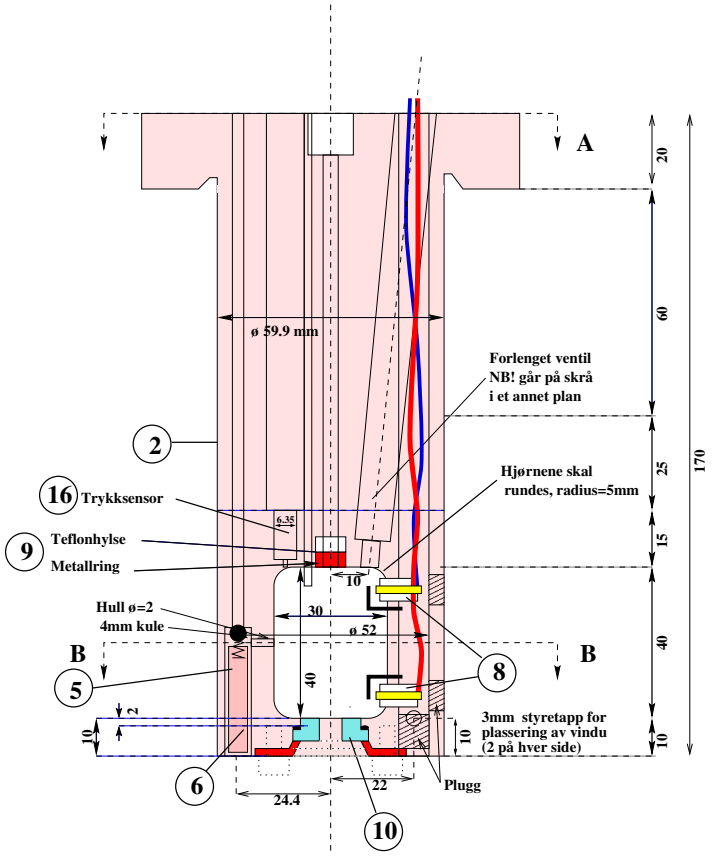

Snitt gjennom senter, tegning vis8:

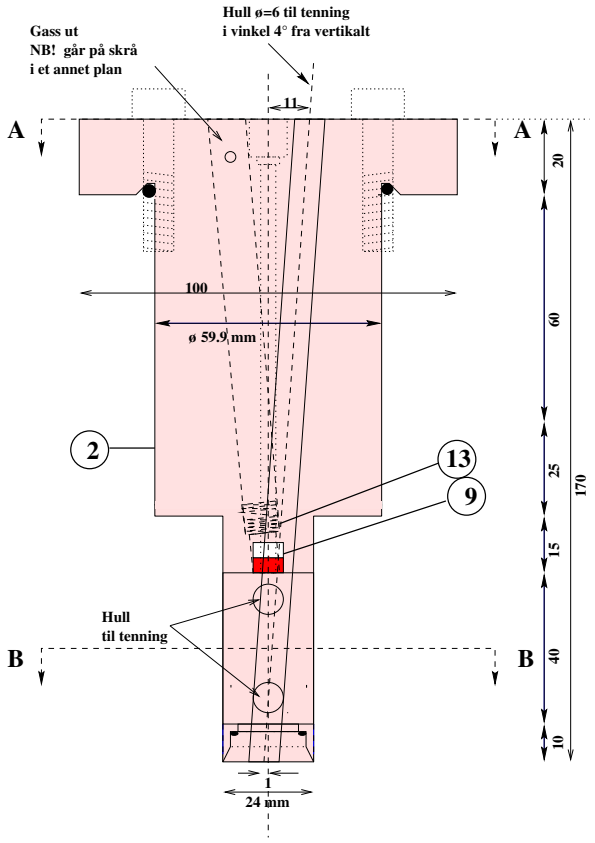

3 Ytre del av glass-holder: Tegning: vis9

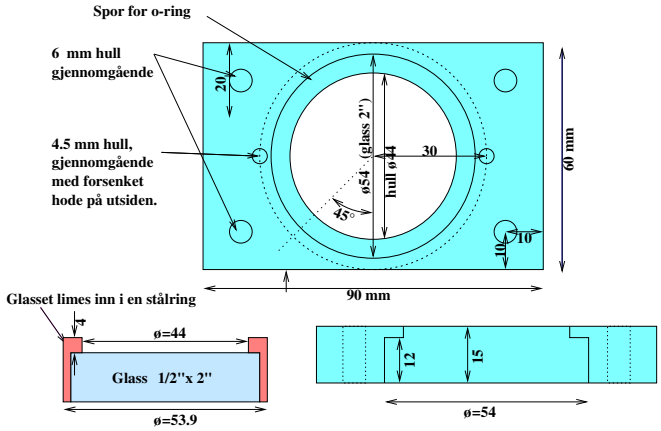

4 Indre del av glass-holder:

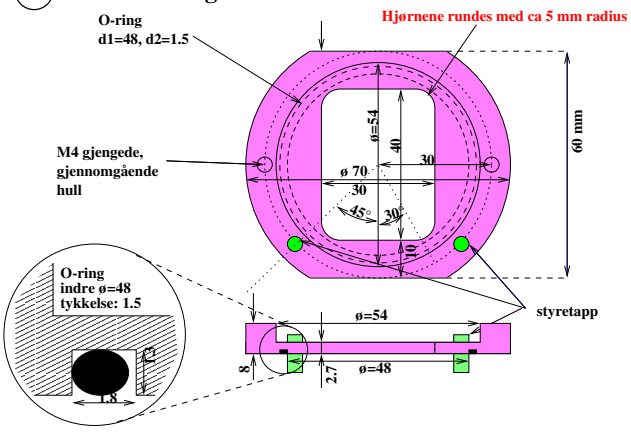

Appendix E

Data from CVC-rig experiment

This chapter contains additional description of experiments and results from experiments with a constant volume combustion rig with prechamber (the equipment presented in appendix D). A few selected experiments are presented in chapter 6, other experiments are presented here in the appendix without much explanation (what you see is what you get).

E.1 Ignition duration and nozzle opening

This section describes a function test of the ignition and nozzle opening mechanism. The result was that the ignition starts less than 1 ms after it's triggered. The spark is visible for at least for 1 ms.

The nozzle mechanism is able to move the nozzle needle 24 mm in less than 3 ms, when starting from closed position. There is an additional delay of 4 to 5 ms before the nozzle mechanism starts to move.

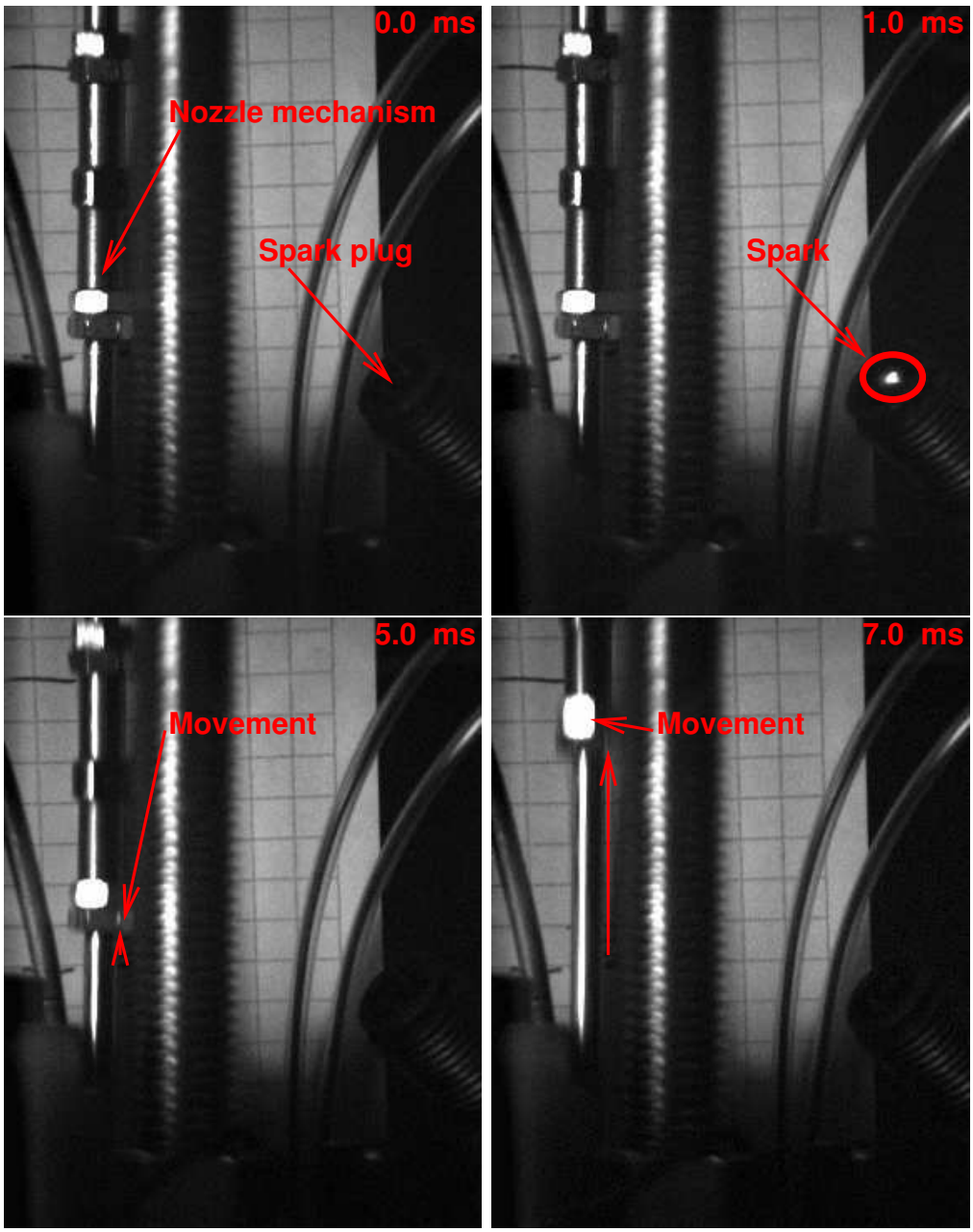

Figure E.1: Pictures taken 0, 1, 5, and 7 ms after triggering of the ignition, showing a spark plug (lower right) and parts of the nozzle opening mechanism located on the top of the combustion chamber.

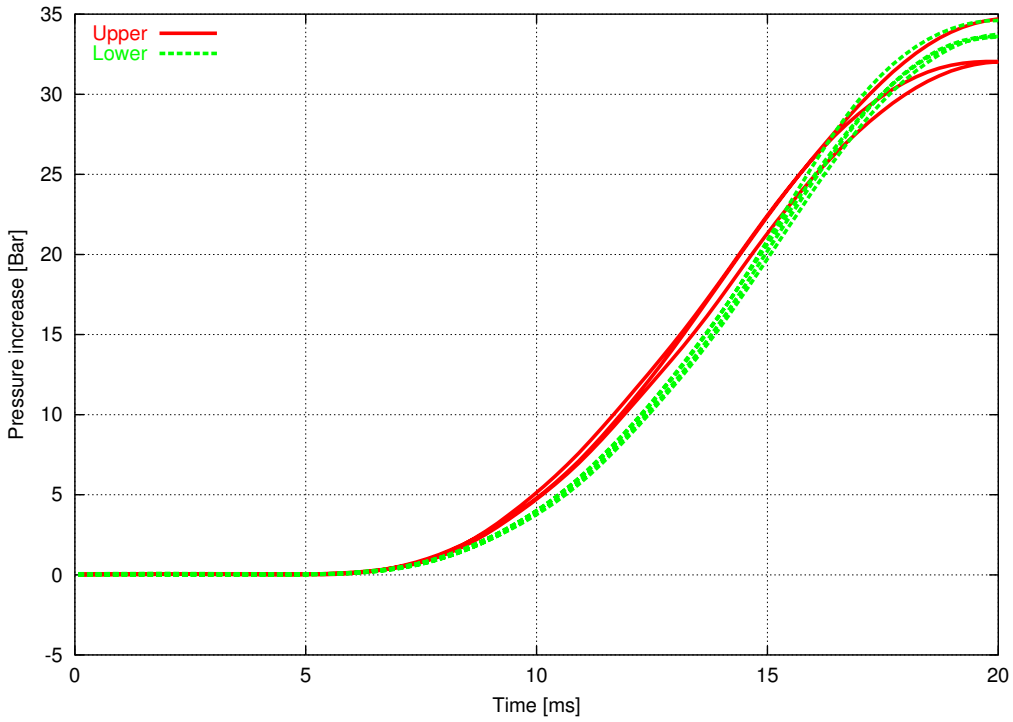

Figure E.2: Pressure measurements from ignition at upper and lower ignition point.

E.2 Combustion in a closed prechamber

Gas "EM" (lean C2H4+air see table E.2) , operating sequence: 1) Flush with "EM", 2) Close nozzles, 3) Wait 100 ms, 4) Ignite without opening the nozzle between the combustion chambers.

Abr.	*Description*	*Purpose*
Op:	The nozzle is kept open. The prechamber is flushed with a premixed gas. Ignition simultaneously with the the flushing is stooped.	Function test of the equipment. The flushing should provide repeatable flow.
Cl:	The nozzle is kept closed. The prechamber is flushed with a premixed gas. The outlet valve is closed 50 ms before the ignition, and the inlet valve is closed simultaneously with the ignition.	Check if the combustion speed is symmetric with respect to upper and lower ignition point.
No:	Opening nozzle, same as "Cl" but the prechamber nozzle is opened 1 ms to 50 ms before the ignition. Both chambers have roughly the same initial pressure.	Create repeatable prechamber combustion for study of the jet.
In:	Inflow, the prechamber is flushed with fuel at low pressure, the main chamber is filled to higher pressure. The prechamber is left to calm for 500 ms before the nozzle is opened. Ignition 10 ms after opening the nozzle.	Create more realistic mixing and turbulence patterns in the prechamber.
Ts:	Two stage combustion, similar as "In", except the main chamber is filled with a mix containing $CO + O_2 + N_2$ and ignited.	Give more engine like conditions with respect to temperature.

Table E.1: Description of operating sequences to be used in the experiments.

Abr.	*Description*
Air:	Compressed air or sometimes a mix of 21 % O_2, 79 % N_2
CH_4:	Compressed methane
MM:	Stoichiometric mix of CH_4 and air
EM:	Lean $\lambda = 1.4$ mix of C_2H_4 and air
EM2 :	Rich $\lambda = 0.75$ mix of C_2H_4 and air
OM:	A mix of xx% CH_4, xx % air and xx % O_2
CM:	A mix of 27.53 % CO, 21.09 % O_2 and 21.09 % air which is used for two stage combustion. The exhaust gas of this mix contains 21% O_2. The combustion does not blur the windows with condense.

Table E.2: Gases used in the CVC-rig experiments. All the gases and pipelines are at room temperature (293 K).

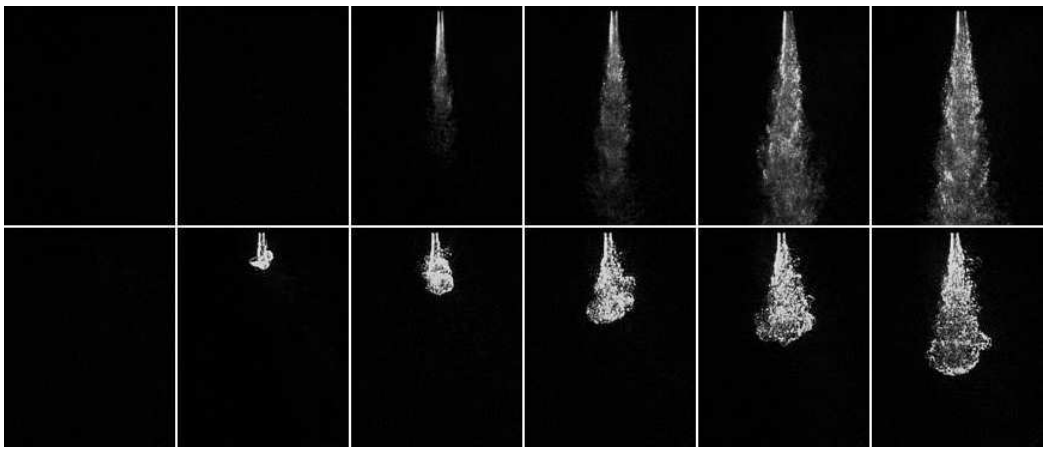

Figure E.3: Schlieren pictures of prechamber jets. The pictures are taken at 1 ms intervals, starting 1 ms after ignition. The upper ignition point is used in the upper picture series, the lower ignition point in the lower series. The largest cylindrical prechamber (diameter = 32 mm, length = 45 mm, see section D) and a nozzle of 4 mm diameter and 6 mm length.

E.3 Prechamber jet into atmosphere

This experiment was mainly a preliminary function test of the equipment. The combustion is so slow that very little pressure is built up even though the nozzles area / prechamber volume ratio is almost an order of magnitude lower than in a real engine.

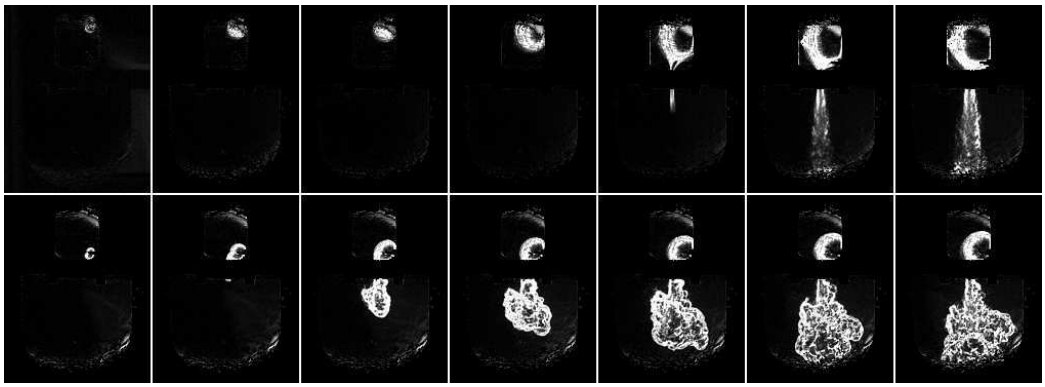

Figure E.4: Nozzle diameter = 6 mm, length = 10 mm.

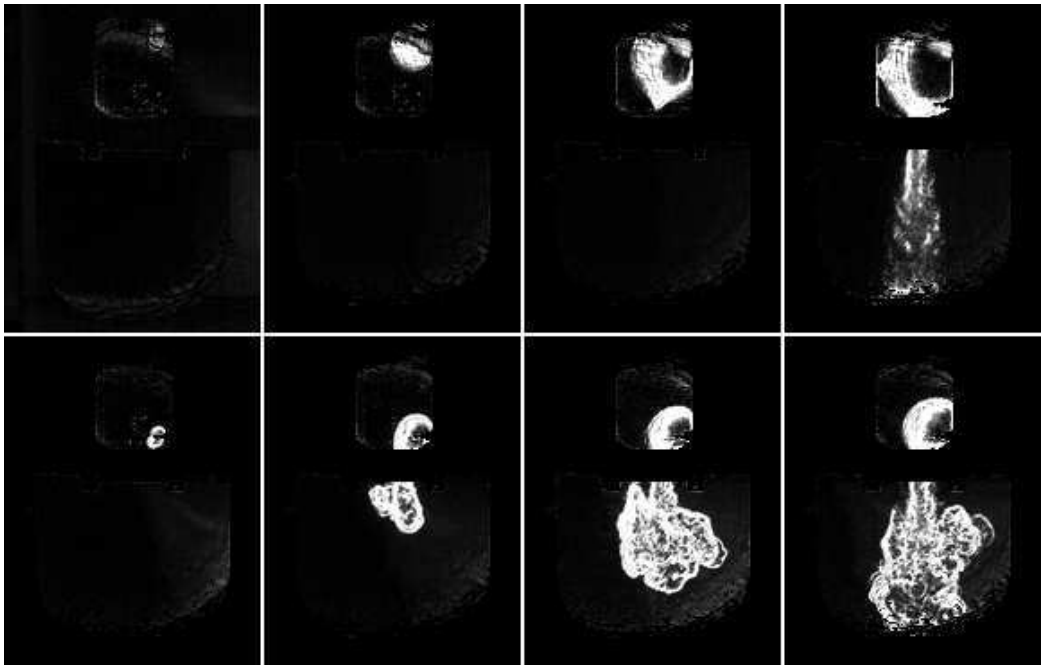

Figure E.5: Nozzle diameter = 6 mm, length = 4 mm. Pictures taken 1, 3, 5 and 7 ms after ignition

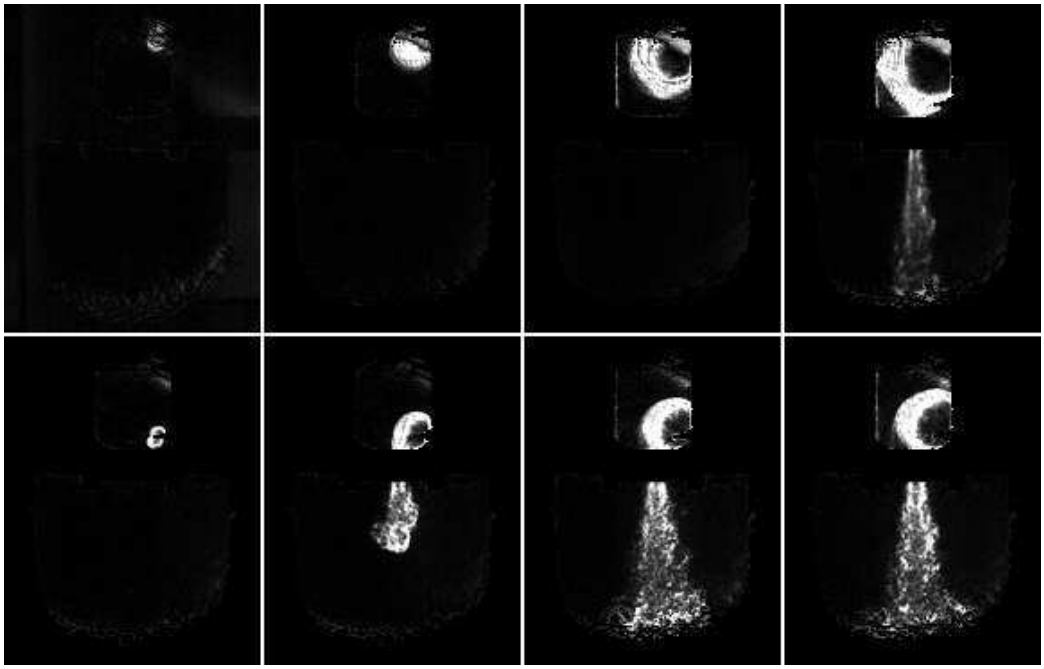

Figure E.6: Nozzle diameter = 4 mm, length = 4 mm. Pictures taken 1, 3, 5 and 7 ms after ignition

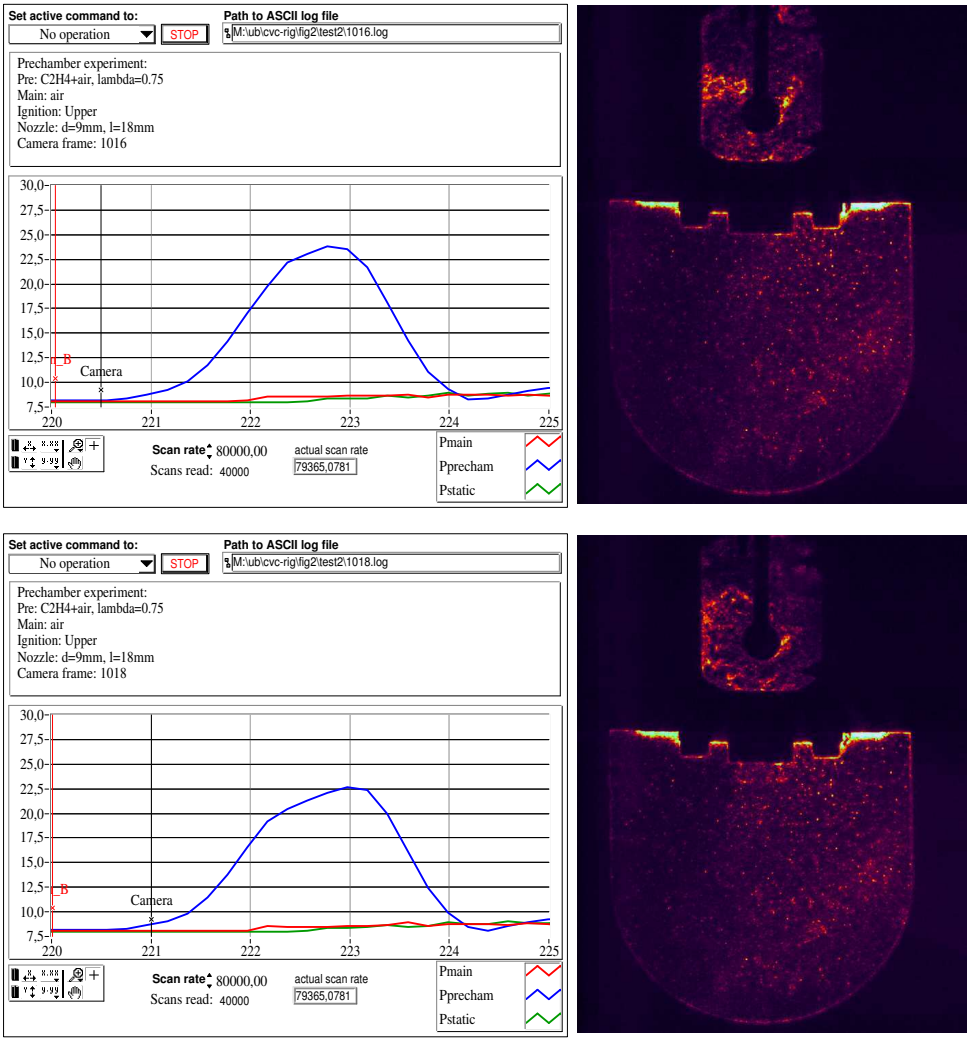

E.4 Experiment 2, more turbulence

Experiment 1 (with less turbulence and slower combustion) and also a summary of experiment 2 are presented in chapter 6. The target of this experiment is the same as in experiment 1. The difference from the experiment 1 is that a modified operation sequence of the valves gives higher flow velocity more turbulence during the combustion in the prechamber.

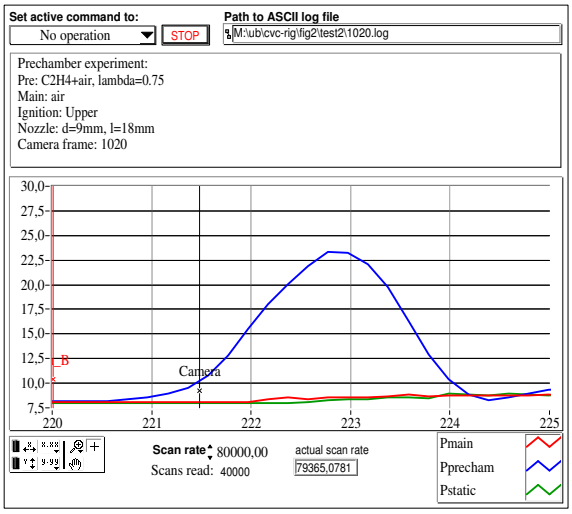
Set active command to:
No operation
STOP
Path to ASCII log file
M:\ub\cvc-rig\fig2\test2\1020.log
Prechamber experiment:
Pre: C2H4+air, lambda=0.75
Main: air
Ignition: Upper
Nozzle: d=9mm, l=18mm
Camera frame: 1020
30,0
27,5
25,0
22,5
20,0
17,5
15,0
12,5
10,0
7,5
B
Camera
220
221
222
223
224
225
Scan rate 80000,00
Scans read: 40000
actual scan rate
79365,0781
Pmain
Pprecham
Pstatic

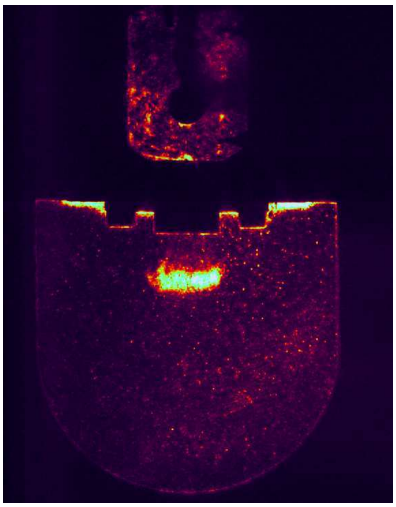

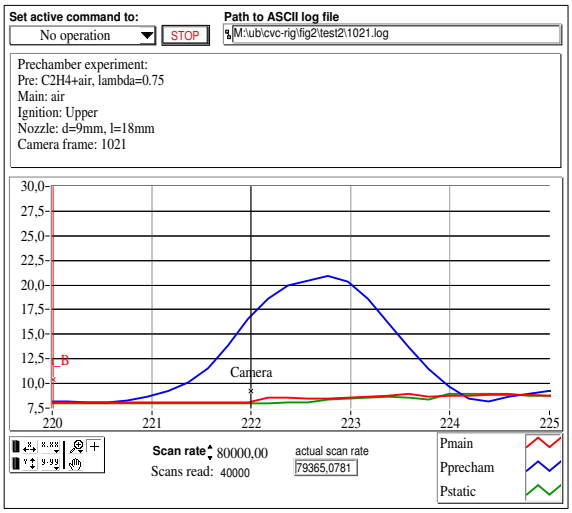
Set active command to:
No operation
STOP
Path to ASCII log file
M:\ub\cvc-rig\fig2\test2\1021.log
Prechamber experiment:
Pre: C2H4+air, lambda=0.75
Main: air
Ignition: Upper
Nozzle: d=9mm, l=18mm
Camera frame: 1021
30,0
27,5
25,0
22,5
20,0
17,5
15,0
12,5
10,0
7,5
B
Camera
220
221
222
223
224
225
Scan rate 80000,00
Scans read: 40000
actual scan rate
79365,0781
Pmain
Pprecham
Pstatic

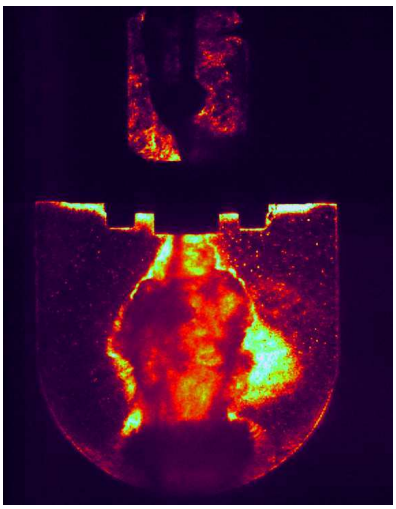

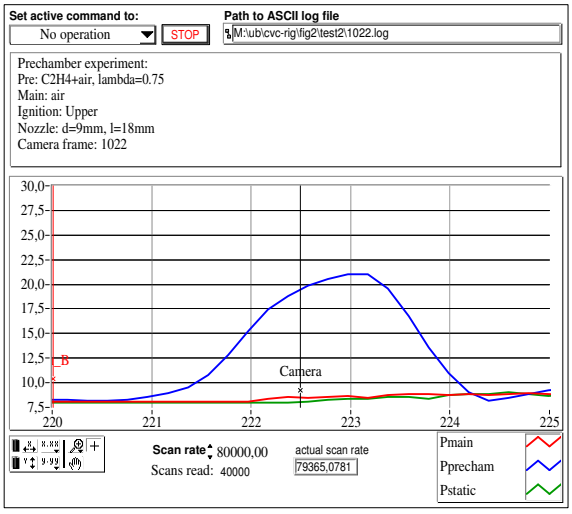
Set active command to:
No operation
STOP
Path to ASCII log file
M:\ub\cvc-rig\fig2\test2\1022.log
Prechamber experiment:
Pre: C2H4+air, lambda=0.75
Main: air
Ignition: Upper
Nozzle: d=9mm, l=18mm
Camera frame: 1022
30,0
27,5
25,0
22,5
20,0
17,5
15,0
12,5
10,0
7,5
B
Camera
220
221
222
223
224
225
Scan rate 80000,00
Scans read: 40000
actual scan rate
79365,0781
Pmain
Pprecham
Pstatic

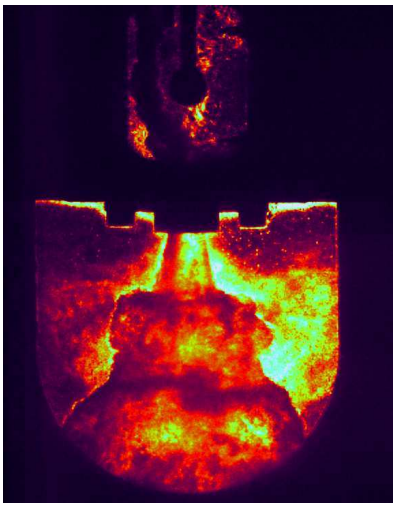

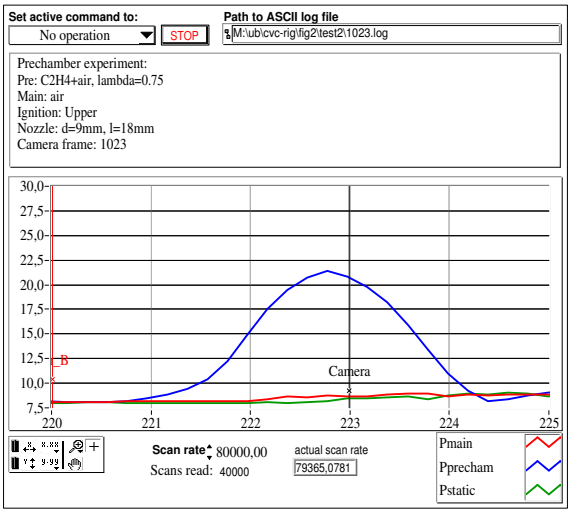
Set active command to:
No operation
STOP
Path to ASCII log file
M:\ub\cvc-rig\fig2\test2\1023.log
Prechamber experiment:
Pre: C2H4+air, lambda=0.75
Main: air
Ignition: Upper
Nozzle: d=9mm, l=18mm
Camera frame: 1023
30,0
27,5
25,0
22,5
20,0
17,5
15,0
12,5
10,0
7,5
B
Camera
220
221
222
223
224
225
Scan rate 80000,00
Scans read: 40000
actual scan rate
79365,0781
Pmain
Pprecham
Pstatic

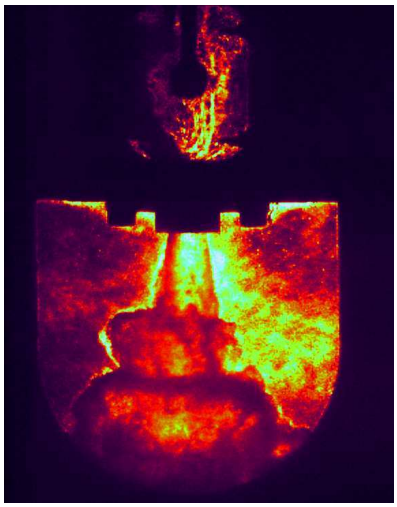

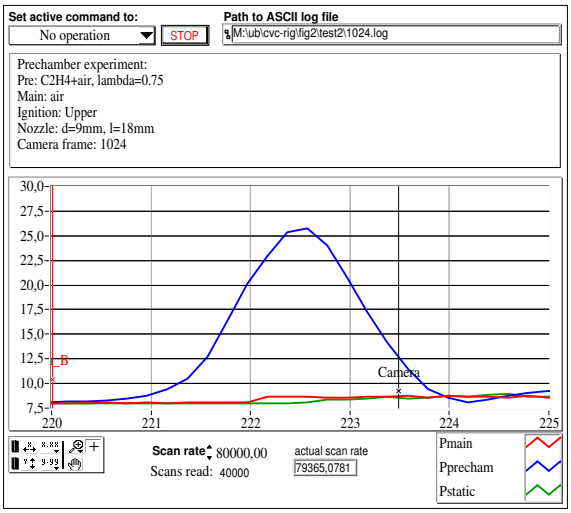
Set active command to:
No operation
STOP
Path to ASCII log file
M:\ub\cvc-rig\fig2\test2\1024.log
Prechamber experiment:
Pre: C2H4+air, lambda=0.75
Main: air
Ignition: Upper
Nozzle: d=9mm, l=18mm
Camera frame: 1024
30,0
27,5
25,0
22,5
20,0
17,5
15,0
12,5
10,0
7,5
B
Camera
220
221
222
223
224
225
Scan rate 80000,00
Scans read: 40000
actual scan rate
79365,0781
Pmain
Pprecham
Pstatic

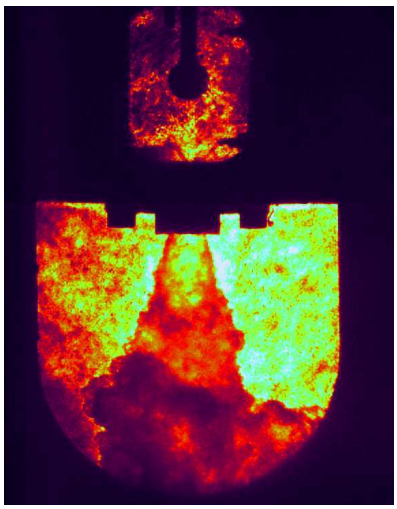

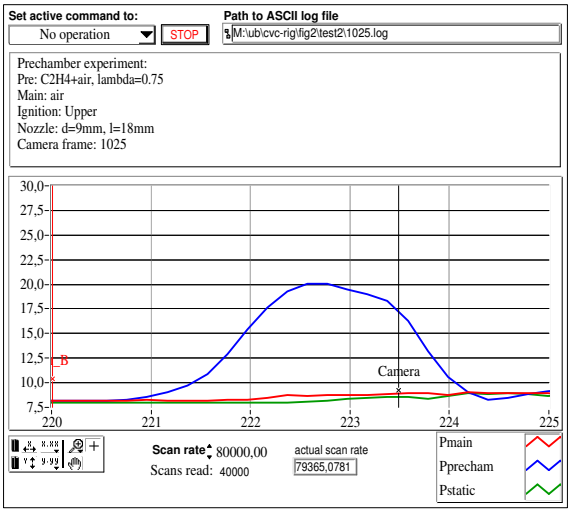
Set active command to:
No operation
STOP
Path to ASCII log file
M:\ub\cvc-rig\fig2\test2\1025.log
Prechamber experiment:
Pre: C2H4+air, lambda=0.75
Main: air
Ignition: Upper
Nozzle: d=9mm, l=18mm
Camera frame: 1025
30,0
27,5
25,0
22,5
20,0
17,5
15,0
12,5
10,0
7,5
B
Camera
220
221
222
223
224
225
Scan rate 80000,00
Scans read: 40000
actual scan rate
79365,0781
Pmain
Pprecham
Pstatic

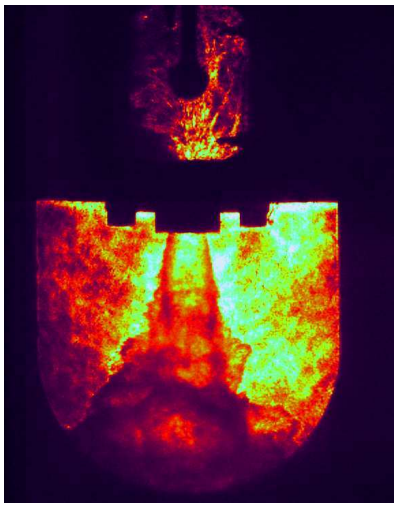

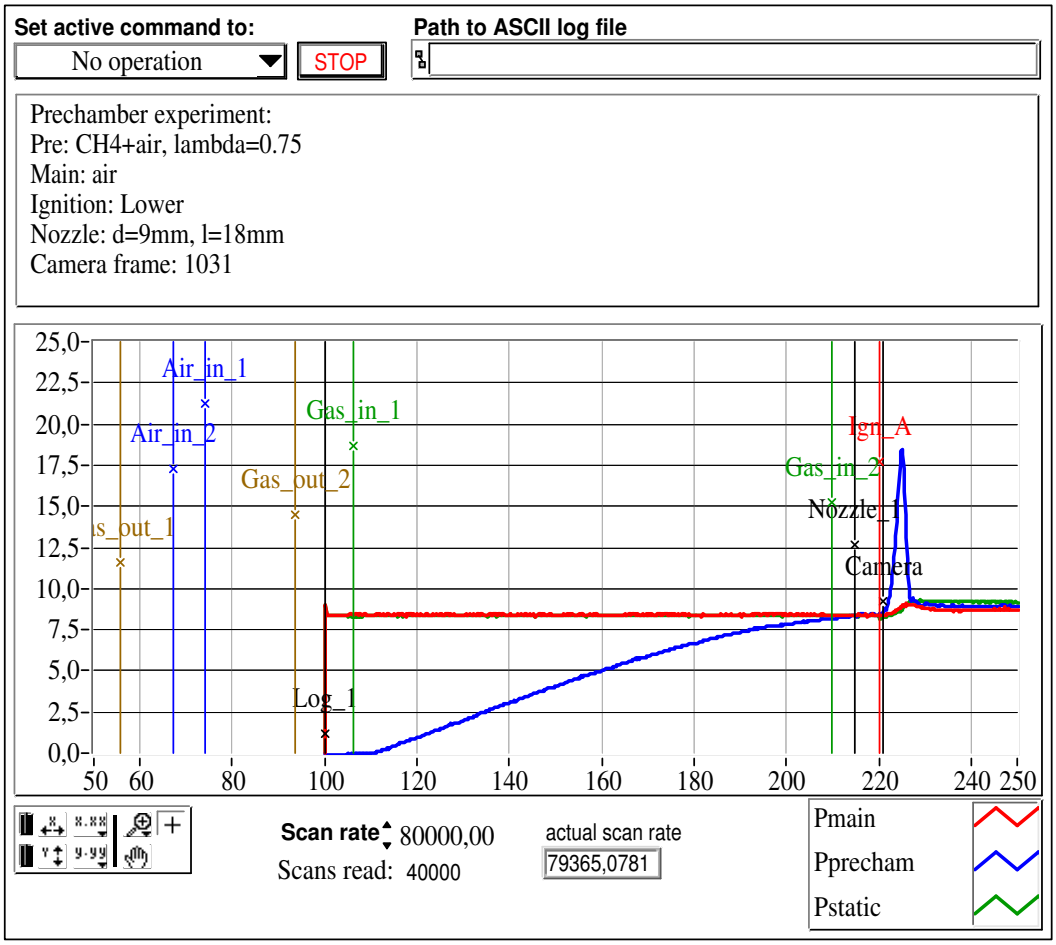

Figure E.7: Operating sequence giving high (but unknown) turbulence in the prechamber, the filling of the prechamber ends 10 ms before ignition.

E.5 Experiment 3, lower ignition point

Gas "EM2" (rich C2H4+air), lower ignition point, nozzle n9/18, operating sequence is shown in figure E.7. The difference from the previous experiment is the location of the ignition.

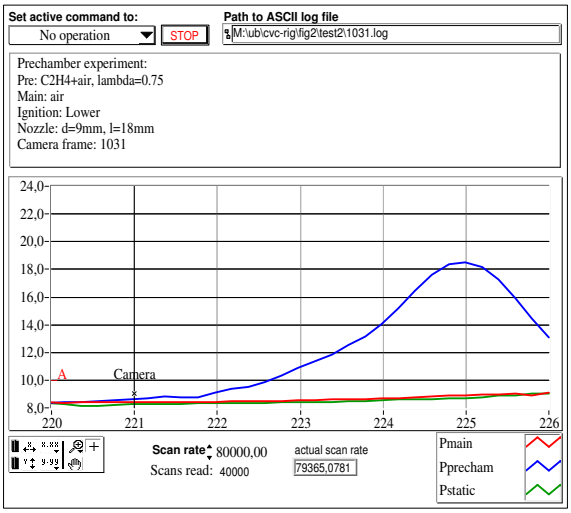
Set active command to:
No operation
STOP
Path to ASCII log file
M:\ub\cvc-rig\fig2\test2\1031.log
Prechamber experiment:
Pre: C2H4+air, lambda=0.75
Main: air
Ignition: Lower
Nozzle: d=9mm, l=18mm
Camera frame: 1031
24,0
22,0
20,0
18,0
16,0
14,0
12,0
10,0
8,0
A
Camera
220
221
222
223
224
225
226
Scan rate 80000,00
Scans read: 40000
actual scan rate
79365,0781
Pmain
Pprecham
Pstatic

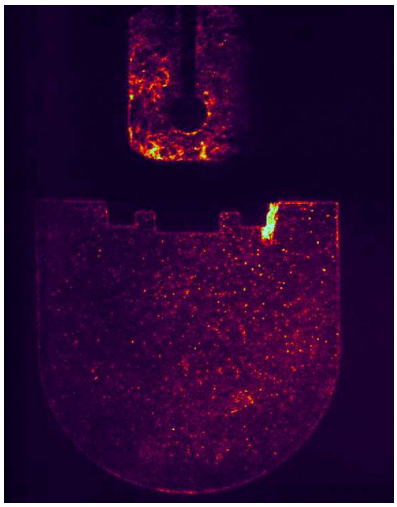

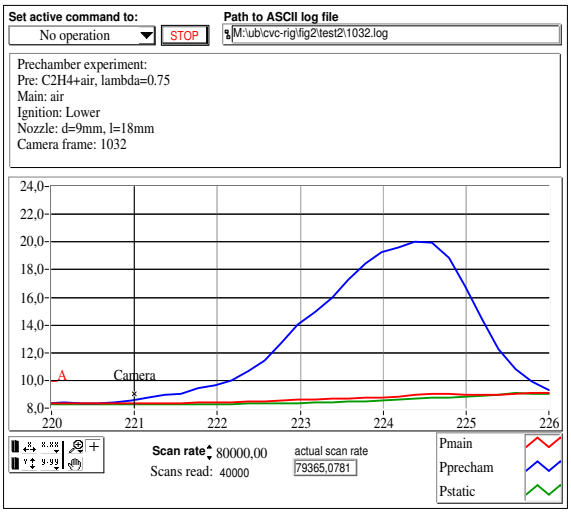
Set active command to:
No operation
STOP
Path to ASCII log file
M:\ub\cvc-rig\fig2\test2\1032.log
Prechamber experiment:
Pre: C2H4+air, lambda=0.75
Main: air
Ignition: Lower
Nozzle: d=9mm, l=18mm
Camera frame: 1032
24,0
22,0
20,0
18,0
16,0
14,0
12,0
10,0
8,0
A
Camera
220
221
222
223
224
225
226
Scan rate 80000,00
Scans read: 40000
actual scan rate
79365,0781
Pmain
Pprecham
Pstatic

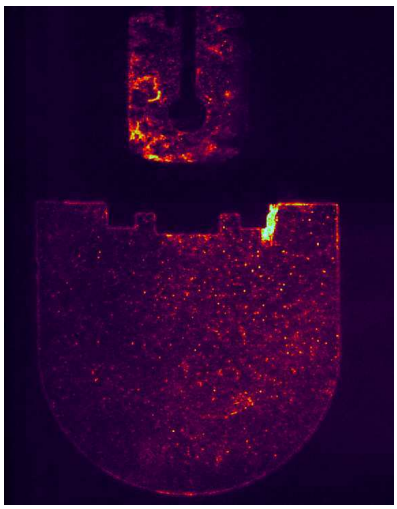

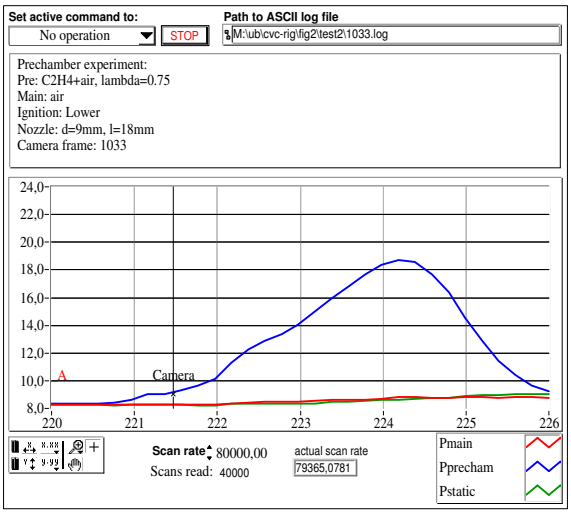
Set active command to:
No operation
STOP
Path to ASCII log file
M:\ub\cvc-rig\fig2\test2\1033.log
Prechamber experiment:
Pre: C2H4+air, lambda=0.75
Main: air
Ignition: Lower
Nozzle: d=9mm, l=18mm
Camera frame: 1033
24,0
22,0
20,0
18,0
16,0
14,0
12,0
10,0
8,0
A
Camera
220
221
222
223
224
225
226
Scan rate 80000,00
Scans read: 40000
actual scan rate
79365,0781
Pmain
Pprecham
Pstatic

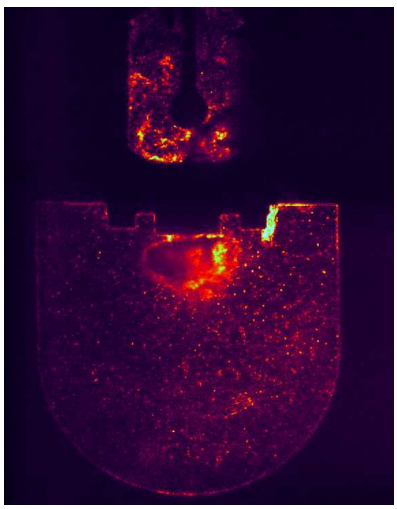

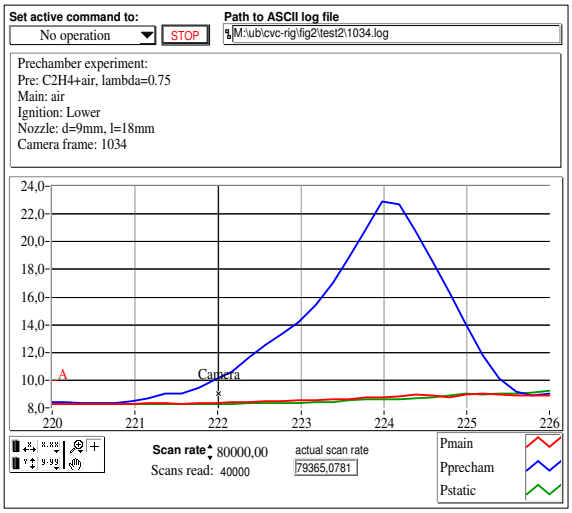
Set active command to:
No operation
STOP
Path to ASCII log file
M:\ub\cvc-rig\fig2\test2\1034.log
Prechamber experiment:
Pre: C2H4+air, lambda=0.75
Main: air
Ignition: Lower
Nozzle: d=9mm, l=18mm
Camera frame: 1034
24,0
22,0
20,0
18,0
16,0
14,0
12,0
10,0
8,0
A
Camera
220
221
222
223
224
225
226
Scan rate 80000,00
Scans read: 40000
actual scan rate
79365,0781
Pmain
Pprecham
Pstatic

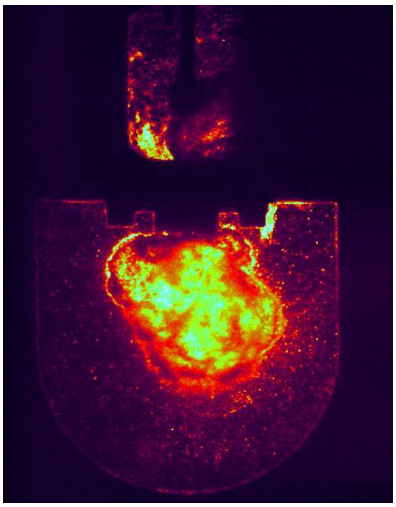

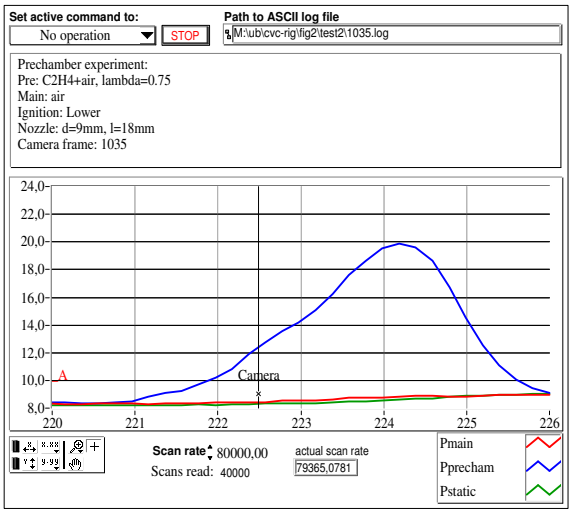
Set active command to:
No operation
STOP
Path to ASCII log file
M:\ub\cvc-rig\fig2\test2\1035.log
Prechamber experiment:
Pre: C2H4+air, lambda=0.75
Main: air
Ignition: Lower
Nozzle: d=9mm, l=18mm
Camera frame: 1035
24,0
22,0
20,0
18,0
16,0
14,0
12,0
10,0
8,0
A
Camera
220
221
222
223
224
225
226
Scan rate 80000,00
Scans read: 40000
actual scan rate
79365,0781
Pmain
Pprecham
Pstatic

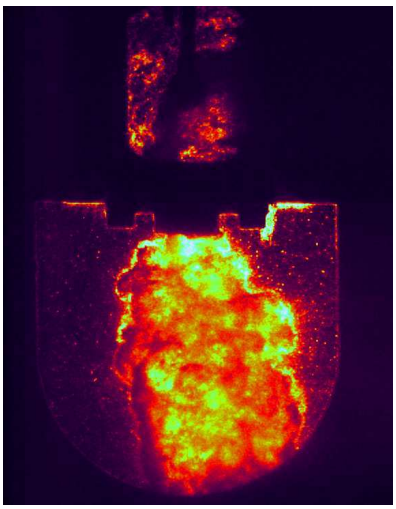

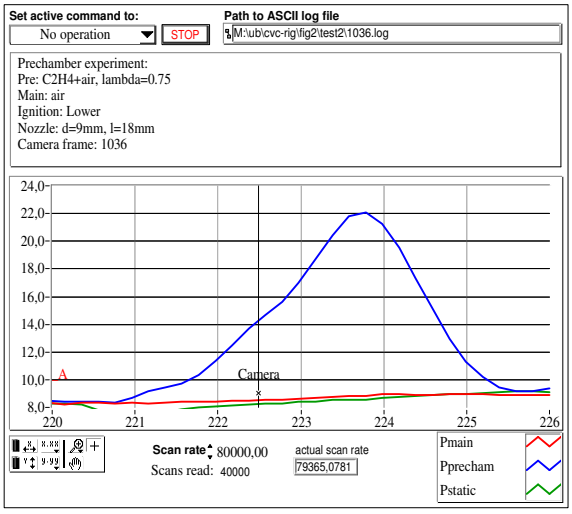
Set active command to:
No operation
STOP
Path to ASCII log file
M:\ub\cvc-rig\fig2\test2\1036.log
Prechamber experiment:
Pre: C2H4+air, lambda=0.75
Main: air
Ignition: Lower
Nozzle: d=9mm, l=18mm
Camera frame: 1036
24,0
22,0
20,0
18,0
16,0
14,0
12,0
10,0
8,0
A
Camera
220
221
222
223
224
225
226
Scan rate 80000,00
Scans read: 40000
actual scan rate
79365,0781
Pmain
Pprecham
Pstatic

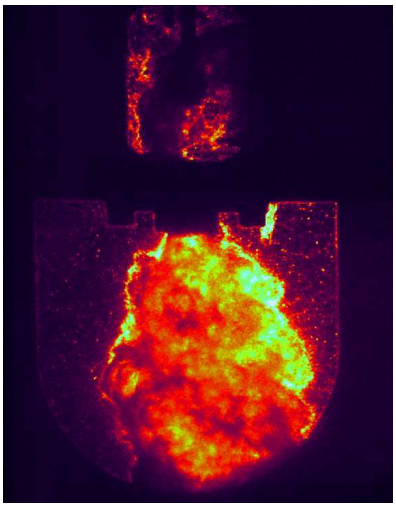

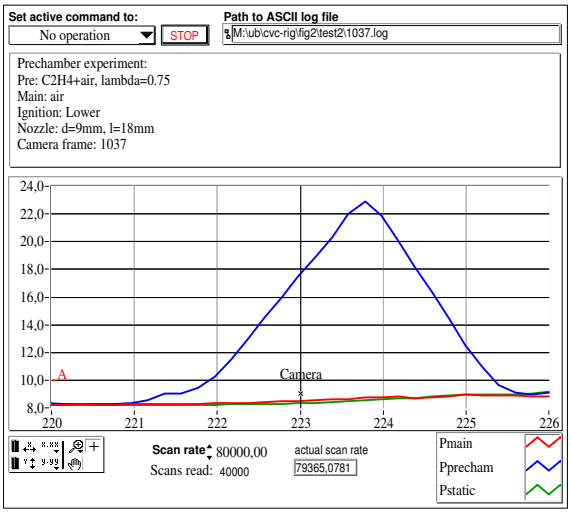
Set active command to:
No operation
STOP
Path to ASCII log file
M:\ub\cvc-rig\fig2\test2\1037.log
Prechamber experiment:
Pre: C2H4+air, lambda=0.75
Main: air
Ignition: Lower
Nozzle: d=9mm, l=18mm
Camera frame: 1037
24,0
22,0
20,0
18,0
16,0
14,0
12,0
10,0
8,0
A
Camera
220
221
222
223
224
225
226
Scan rate 80000,00
Scans read: 40000
actual scan rate
79365,0781
Pmain
Pprecham
Pstatic

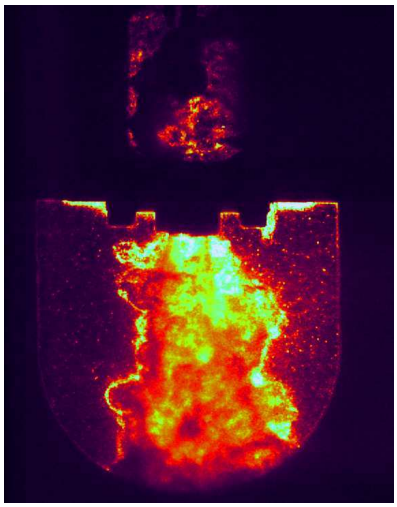

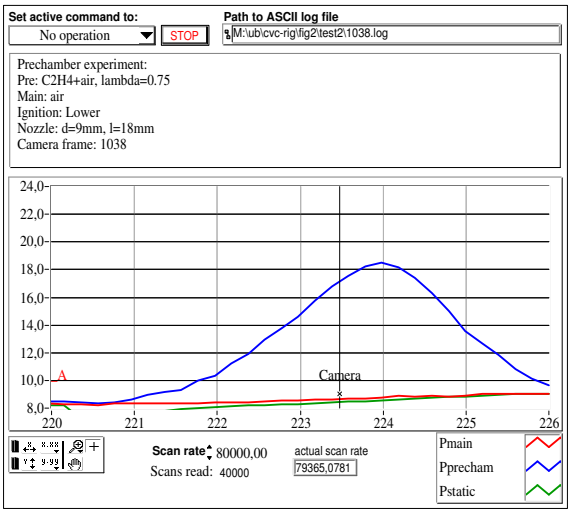
Set active command to:
No operation
STOP
Path to ASCII log file
M:\ub\cvc-rig\fig2\test2\1038.log
Prechamber experiment:
Pre: C2H4+air, lambda=0.75
Main: air
Ignition: Lower
Nozzle: d=9mm, l=18mm
Camera frame: 1038
24,0
22,0
20,0
18,0
16,0
14,0
12,0
10,0
8,0
A
Camera
220
221
222
223
224
225
226
Scan rate 80000,00
Scans read: 40000
actual scan rate
79365,0781
Pmain
Pprecham
Pstatic

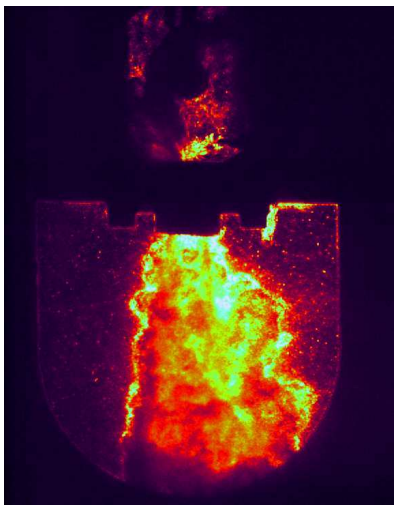

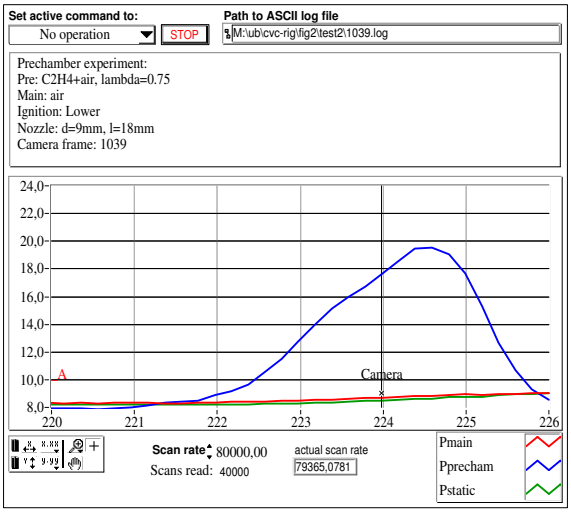
Set active command to:
No operation
STOP
Path to ASCII log file
M:\ub\cvc-rig\fig2\test2\1039.log
Prechamber experiment:
Pre: C2H4+air, lambda=0.75
Main: air
Ignition: Lower
Nozzle: d=9mm, l=18mm
Camera frame: 1039
24,0
22,0
20,0
18,0
16,0
14,0
12,0
10,0
8,0
A
Camera
220
221
222
223
224
225
226
Scan rate 80000,00
Scans read: 40000
actual scan rate
79365,0781
Pmain
Pprecham
Pstatic

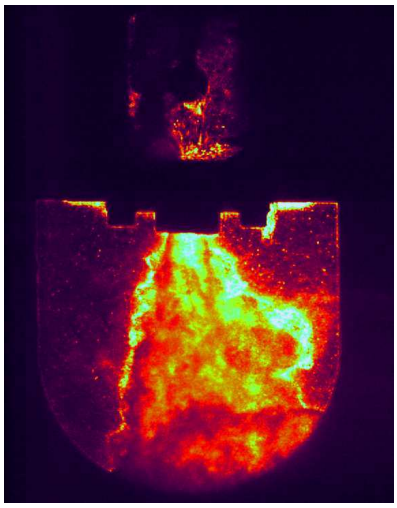

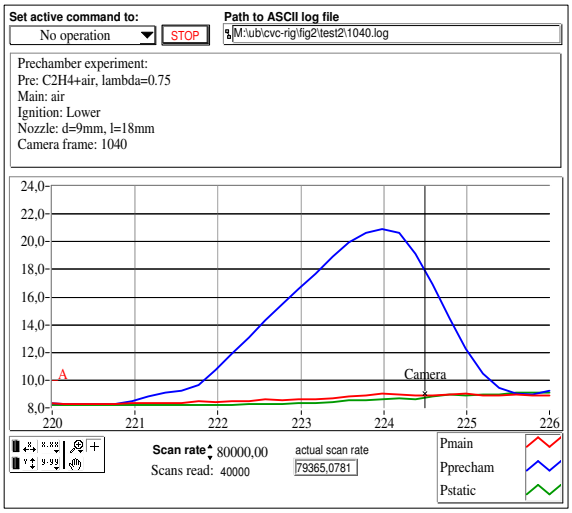
Set active command to:
No operation
STOP
Path to ASCII log file
M:\ub\cvc-rig\fig2\test2\1040.log
Prechamber experiment:
Pre: C2H4+air, lambda=0.75
Main: air
Ignition: Lower
Nozzle: d=9mm, l=18mm
Camera frame: 1040
24,0
22,0
20,0
18,0
16,0
14,0
12,0
10,0
8,0
220
221
222
223
224
225
226
A
Camera
Scan rate 80000,00
Scans read: 40000
actual scan rate
79365,0781
Pmain
Pprecham
Pstatic

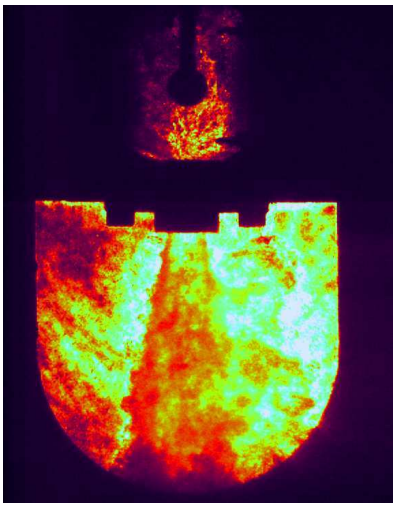

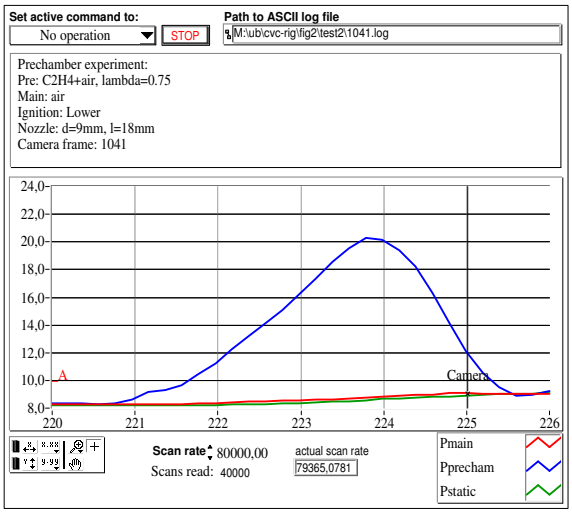
Set active command to:
No operation
STOP
Path to ASCII log file
M:\ub\cvc-rig\fig2\test2\1041.log
Prechamber experiment:
Pre: C2H4+air, lambda=0.75
Main: air
Ignition: Lower
Nozzle: d=9mm, l=18mm
Camera frame: 1041
24,0
22,0
20,0
18,0
16,0
14,0
12,0
10,0
8,0
220
221
222
223
224
225
226
A
Camera
Scan rate 80000,00
Scans read: 40000
actual scan rate
79365,0781
Pmain
Pprecham
Pstatic

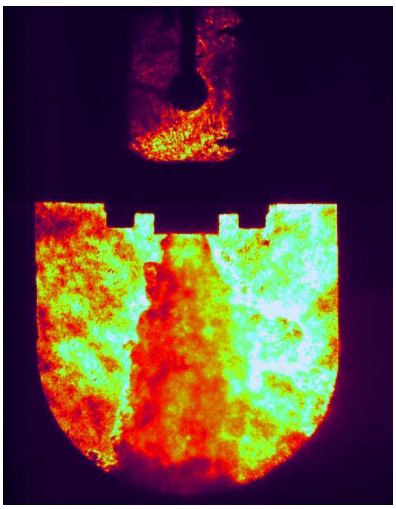

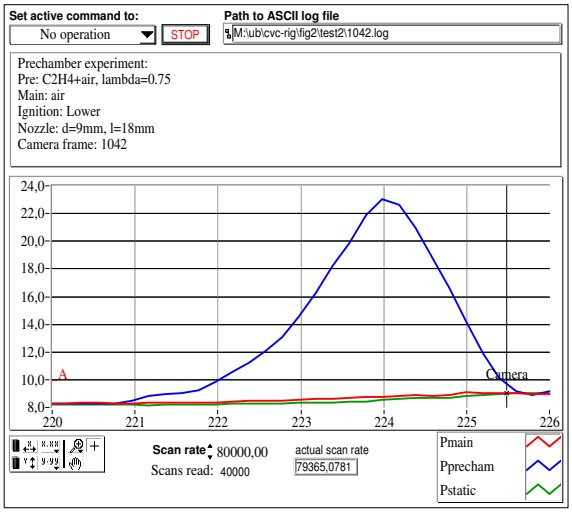
Set active command to:
No operation
STOP
Path to ASCII log file
M:\ub\cvc-rig\fig2\test2\1042.log
Prechamber experiment:
Pre: C2H4+air, lambda=0.75
Main: air
Ignition: Lower
Nozzle: d=9mm, l=18mm
Camera frame: 1042
24,0
22,0
20,0
18,0
16,0
14,0
12,0
10,0
8,0
220
221
222
223
224
225
226
A
Camera
Scan rate 80000,00
Scans read: 40000
actual scan rate
79365,0781
Pmain
Pprecham
Pstatic

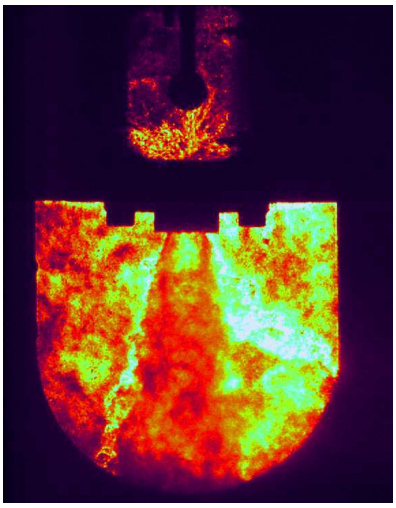

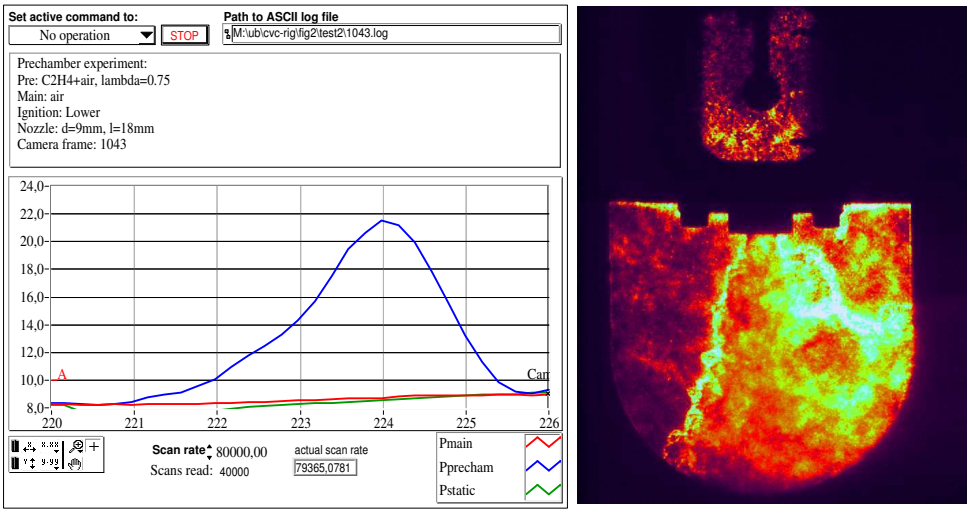

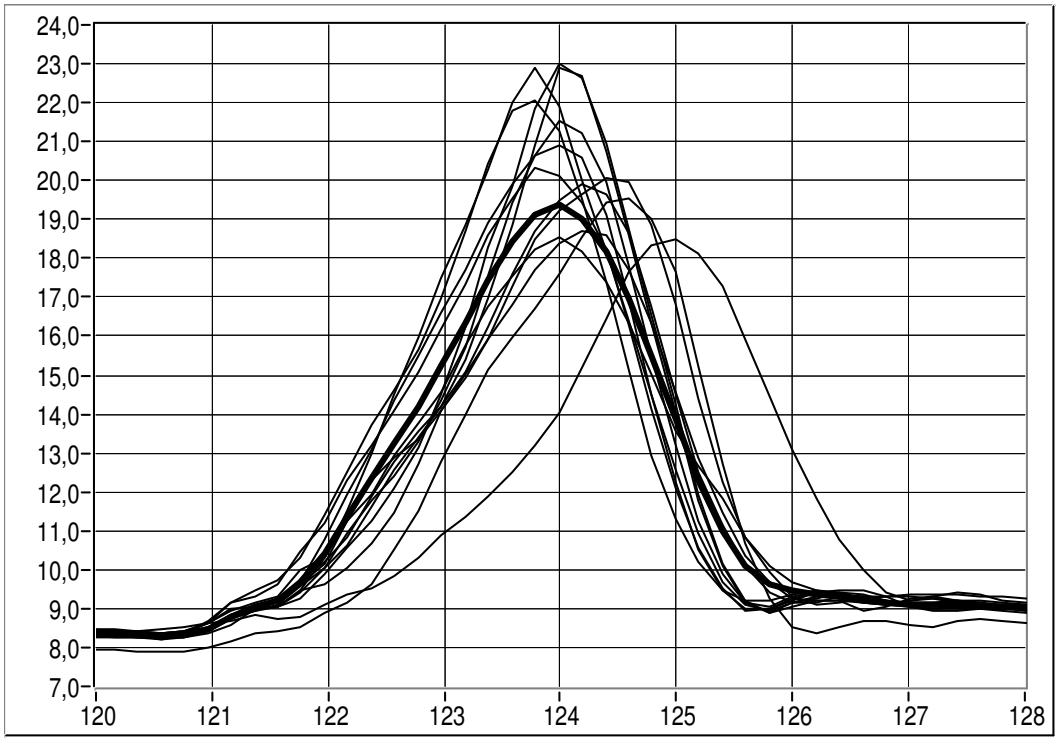

Figure E.8: Prechamber pressures from several combustions collected into one graph.

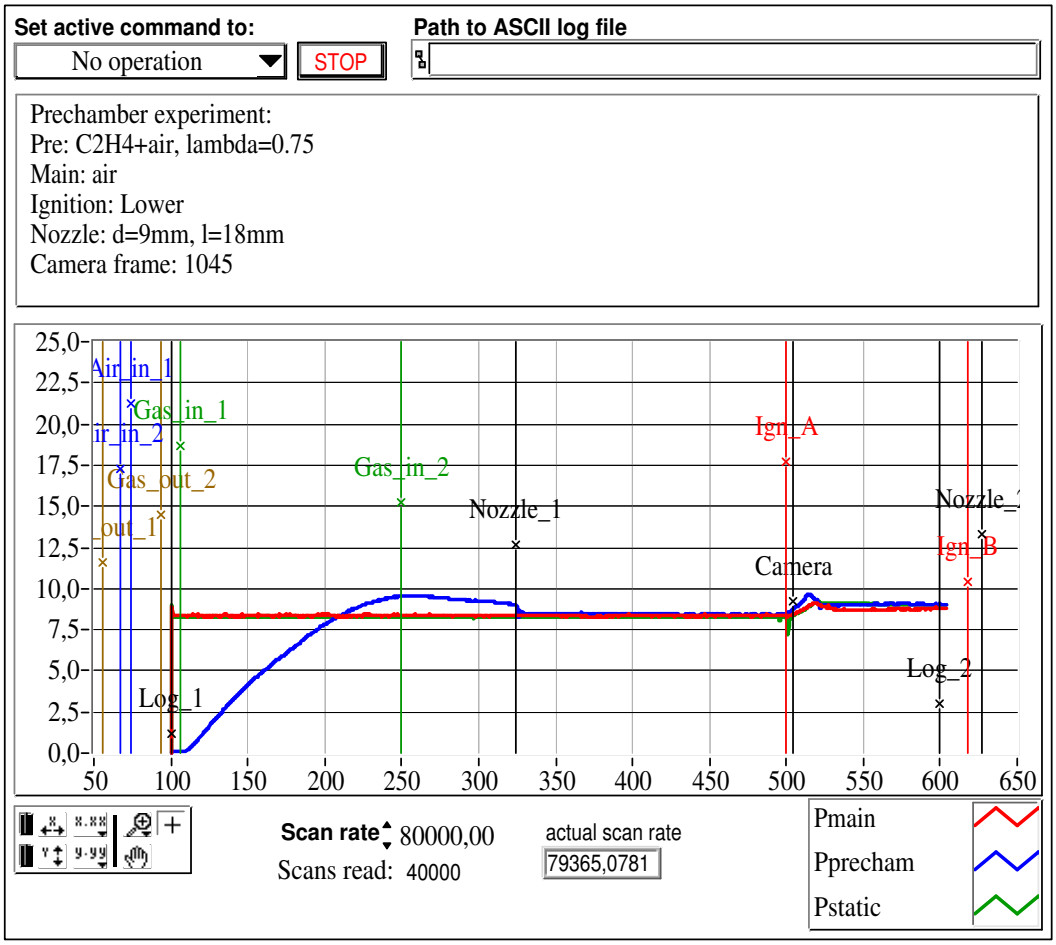

Figure E.9: Operating sequence

E.6 Experiment 4, less turbulence, lower ignition point

Gas "EM2" (rich C2H4+air), lower ignition point, nozzle n9/18. Operating sequence is shown in figure E.9. The filling of the prechamber ends 250 ms before ignition, giving low turbulence and slow combustion. The main difference compared to experiment 1, is the location of the ignition.

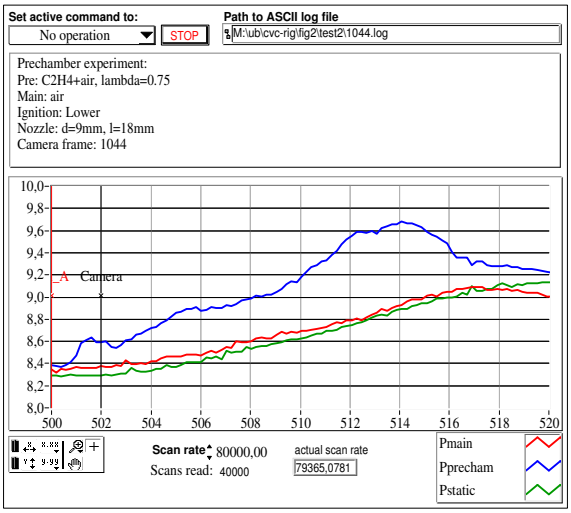
Set active command to:
No operation
STOP
Path to ASCII log file
M:\ub\cvc-rig\fig2\test2\1044.log
Prechamber experiment:
Pre: C2H4+air, lambda=0.75
Main: air
Ignition: Lower
Nozzle: d=9mm, l=18mm
Camera frame: 1044
10,0
9,8
9,6
9,4
9,2
9,0
8,8
8,6
8,4
8,2
8,0
A
Camera
500 502 504 506 508 510 512 514 516 518 520
Scan rate 80000,00
Scans read: 40000
actual scan rate
79365,0781
Pmain
Pprecham
Pstatic

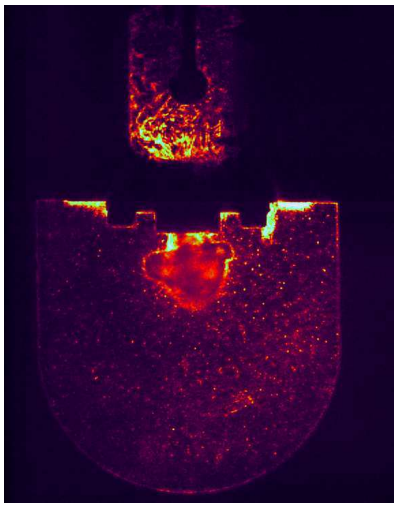

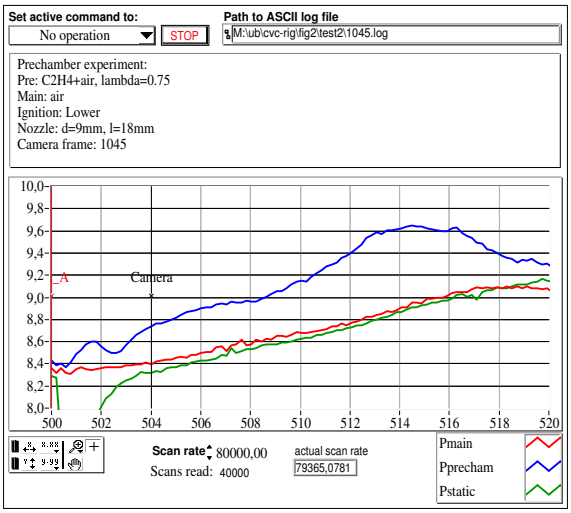
Set active command to:
No operation
STOP
Path to ASCII log file
M:\ub\cvc-rig\fig2\test2\1045.log
Prechamber experiment:
Pre: C2H4+air, lambda=0.75
Main: air
Ignition: Lower
Nozzle: d=9mm, l=18mm
Camera frame: 1045
10,0
9,8
9,6
9,4
9,2
9,0
8,8
8,6
8,4
8,2
8,0
A
Camera
500 502 504 506 508 510 512 514 516 518 520
Scan rate 80000,00
Scans read: 40000
actual scan rate
79365,0781
Pmain
Pprecham
Pstatic

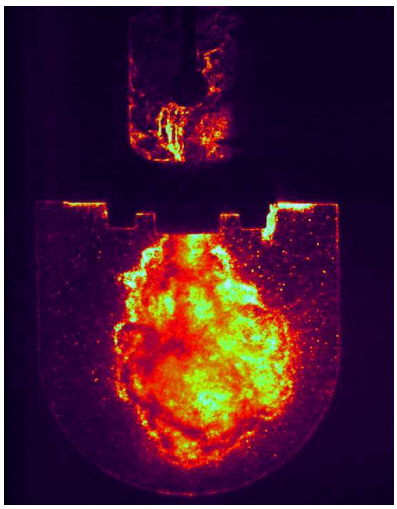

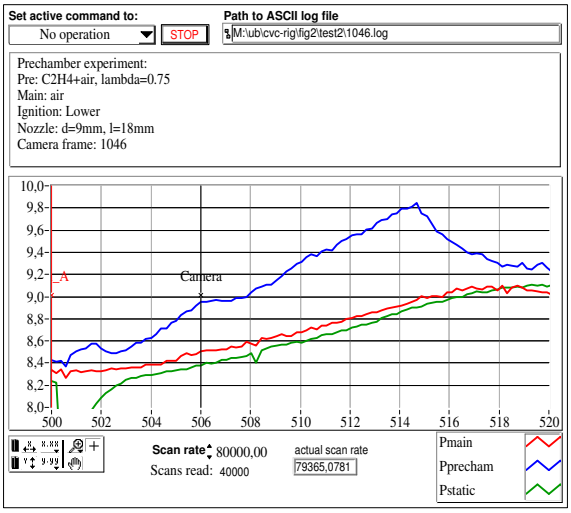
Set active command to:
No operation
STOP
Path to ASCII log file
M:\ub\cvc-rig\fig2\test2\1046.log
Prechamber experiment:
Pre: C2H4+air, lambda=0.75
Main: air
Ignition: Lower
Nozzle: d=9mm, l=18mm
Camera frame: 1046
10,0
9,8
9,6
9,4
9,2
9,0
8,8
8,6
8,4
8,2
8,0
A
Camera
500 502 504 506 508 510 512 514 516 518 520
Scan rate 80000,00
Scans read: 40000
actual scan rate
79365,0781
Pmain
Pprecham
Pstatic

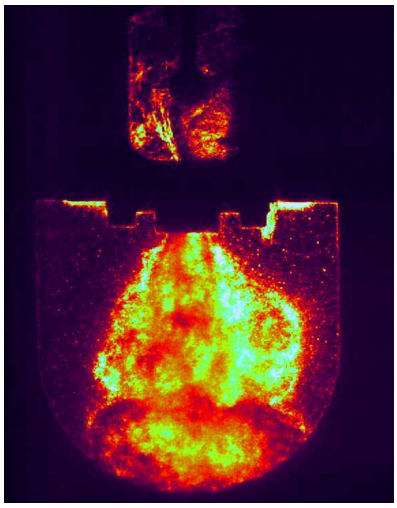

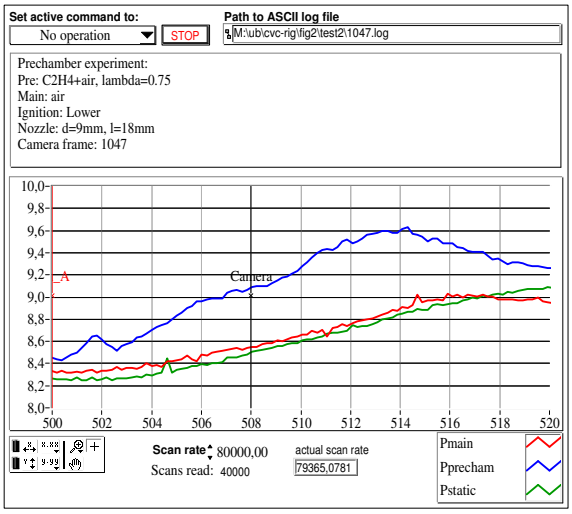
Set active command to:
No operation
STOP
Path to ASCII log file
M:\ub\cvc-rig\fig2\test2\1047.log
Prechamber experiment:
Pre: C2H4+air, lambda=0.75
Main: air
Ignition: Lower
Nozzle: d=9mm, l=18mm
Camera frame: 1047
10,0
9,8
9,6
9,4
9,2
9,0
8,8
8,6
8,4
8,2
8,0
A
Camera
500 502 504 506 508 510 512 514 516 518 520
Scan rate 80000,00
Scans read: 40000
actual scan rate
79365,0781
Pmain
Pprecham
Pstatic

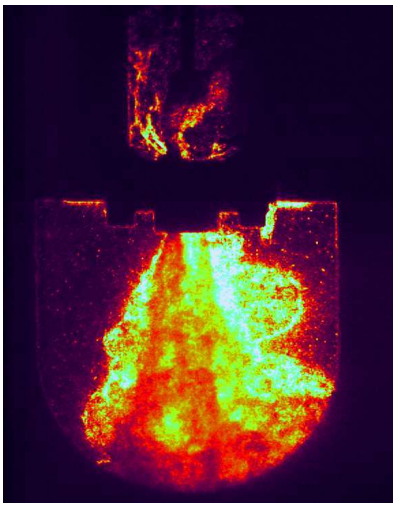

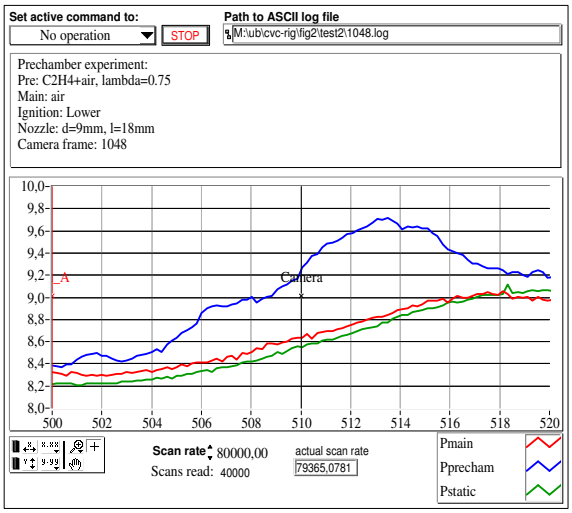
Set active command to:
No operation
STOP
Path to ASCII log file
M:\ub\cvc-rig\fig2\test2\1048.log
Prechamber experiment:
Pre: C2H4+air, lambda=0.75
Main: air
Ignition: Lower
Nozzle: d=9mm, l=18mm
Camera frame: 1048
10,0
9,8
9,6
9,4
9,2
9,0
8,8
8,6
8,4
8,2
8,0
A
Camera
500 502 504 506 508 510 512 514 516 518 520
Scan rate 80000,00
Scans read: 40000
actual scan rate
79365,0781
Pmain
Pprecham
Pstatic

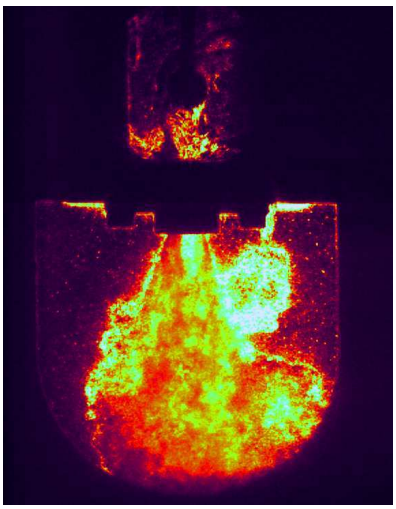

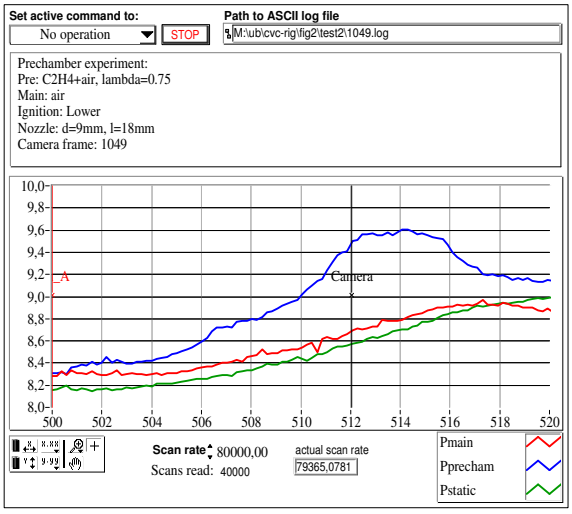
Set active command to:
No operation
STOP
Path to ASCII log file
M:\ub\cvc-rig\fig2\test2\1049.log
Prechamber experiment:
Pre: C2H4+air, lambda=0.75
Main: air
Ignition: Lower
Nozzle: d=9mm, l=18mm
Camera frame: 1049
10,0
9,8
9,6
9,4
9,2
9,0
8,8
8,6
8,4
8,2
8,0
A
Camera
500 502 504 506 508 510 512 514 516 518 520
Scan rate 80000,00
Scans read: 40000
actual scan rate
79365,0781
Pmain
Pprecham
Pstatic

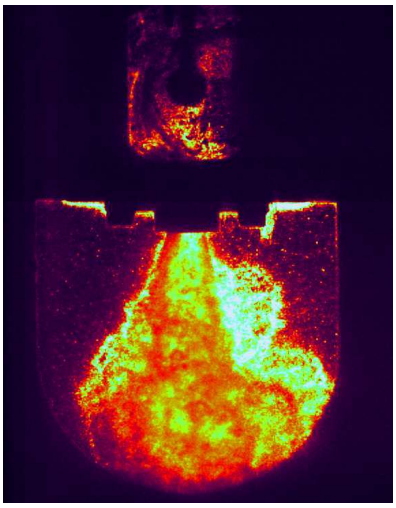

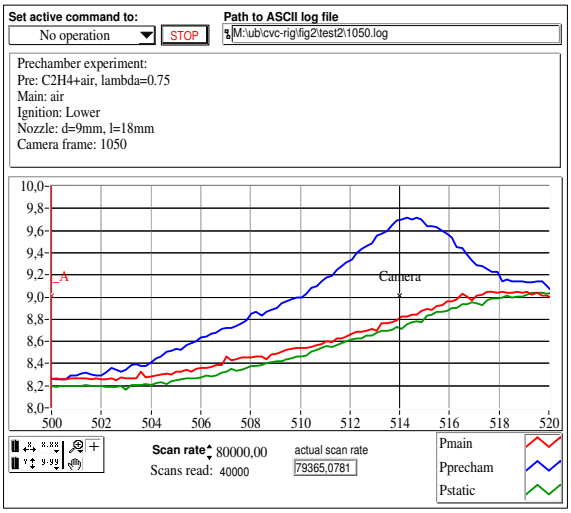
Set active command to:
No operation
STOP
Path to ASCII log file
M:\ub\cvc-rig\fig2\test2\1050.log
Prechamber experiment:
Pre: C2H4+air, lambda=0.75
Main: air
Ignition: Lower
Nozzle: d=9mm, l=18mm
Camera frame: 1050
10,0
9,8
9,6
9,4
9,2
9,0
8,8
8,6
8,4
8,2
8,0
A
Camera
500 502 504 506 508 510 512 514 516 518 520
Scan rate 80000,00
Scans read: 40000
actual scan rate
79365,0781
Pmain
Pprecham
Pstatic

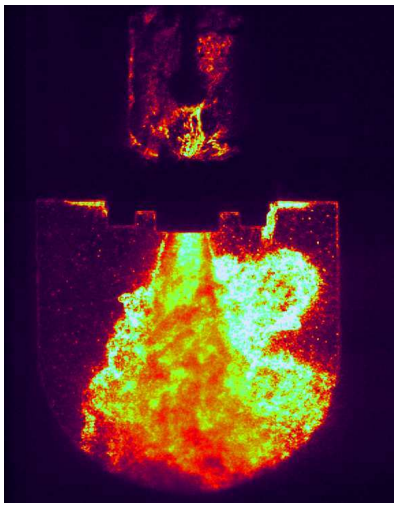

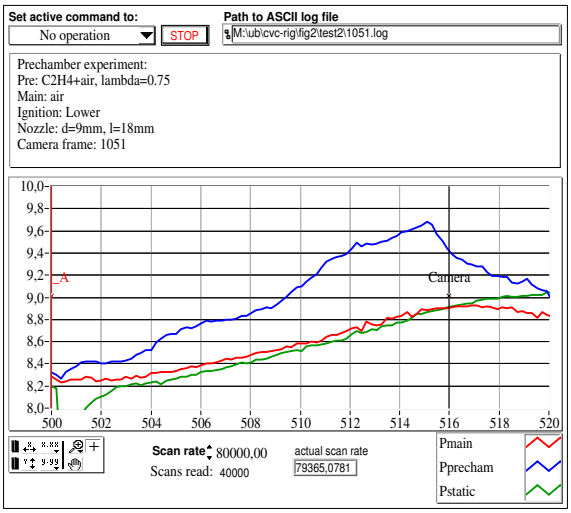
Set active command to:
No operation
STOP
Path to ASCII log file
M:\ub\cvc-rig\fig2\test2\1051.log
Prechamber experiment:
Pre: C2H4+air, lambda=0.75
Main: air
Ignition: Lower
Nozzle: d=9mm, l=18mm
Camera frame: 1051
10,0
9,8
9,6
9,4
9,2
9,0
8,8
8,6
8,4
8,2
8,0
A
Camera
500 502 504 506 508 510 512 514 516 518 520
Scan rate 80000,00
Scans read: 40000
actual scan rate
79365,0781
Pmain
Pprecham
Pstatic

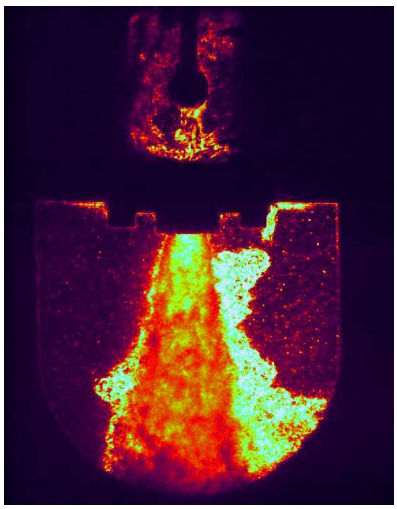

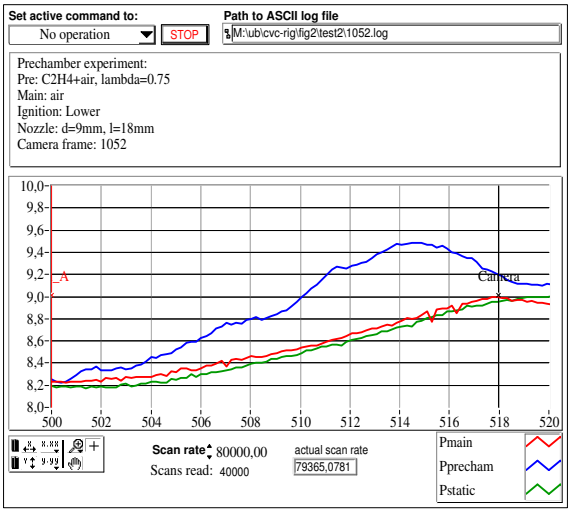
Set active command to:
No operation
STOP
Path to ASCII log file
M:\ub\cvc-rig\fig2\test2\1052.log
Prechamber experiment:
Pre: C2H4+air, lambda=0.75
Main: air
Ignition: Lower
Nozzle: d=9mm, l=18mm
Camera frame: 1052
10,0
9,8
9,6
9,4
9,2
9,0
8,8
8,6
8,4
8,2
8,0
A
Camera
500 502 504 506 508 510 512 514 516 518 520
Scan rate 80000,00
Scans read: 40000
actual scan rate
79365,0781
Pmain
Pprecham
Pstatic

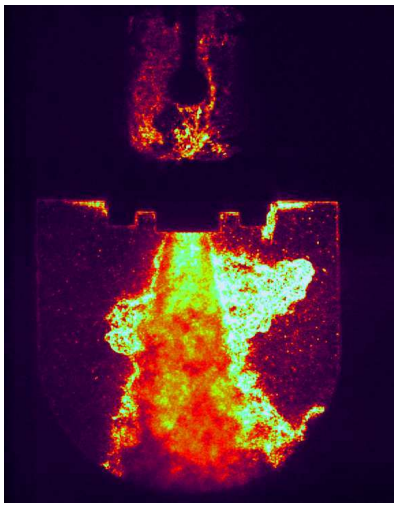

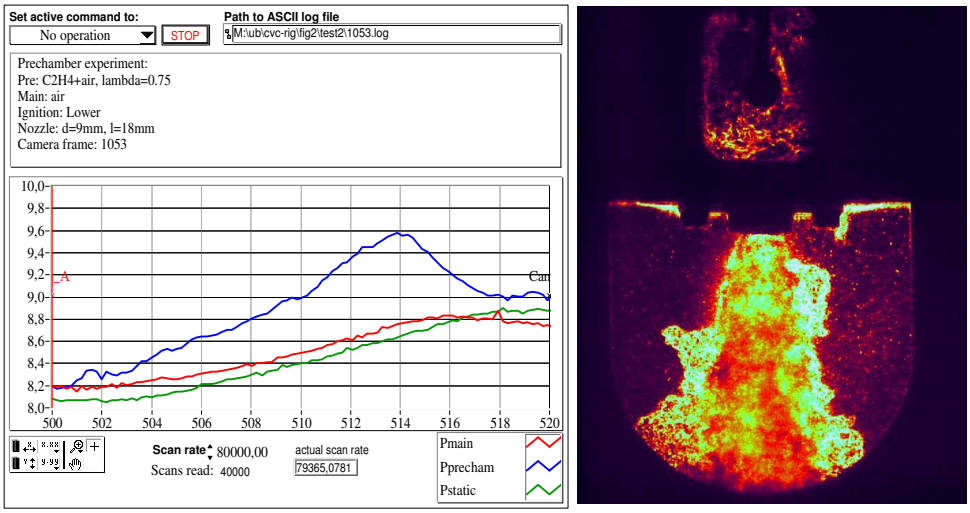

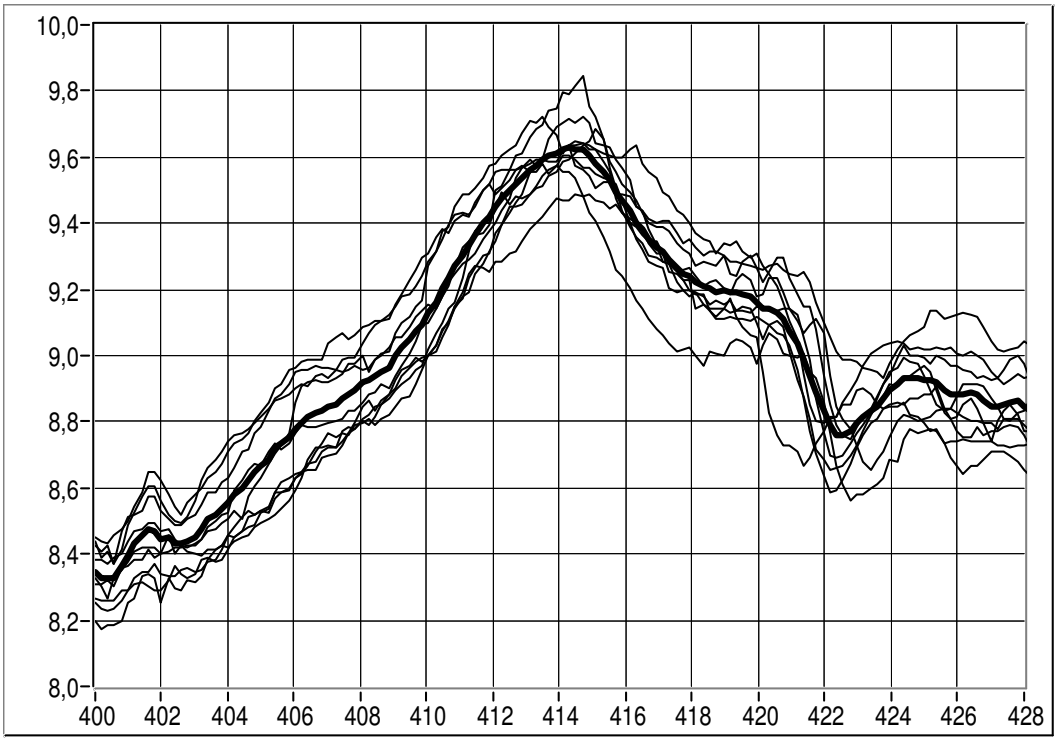

Figure E.10: Prechamber pressures from several combustions collected into one graph.

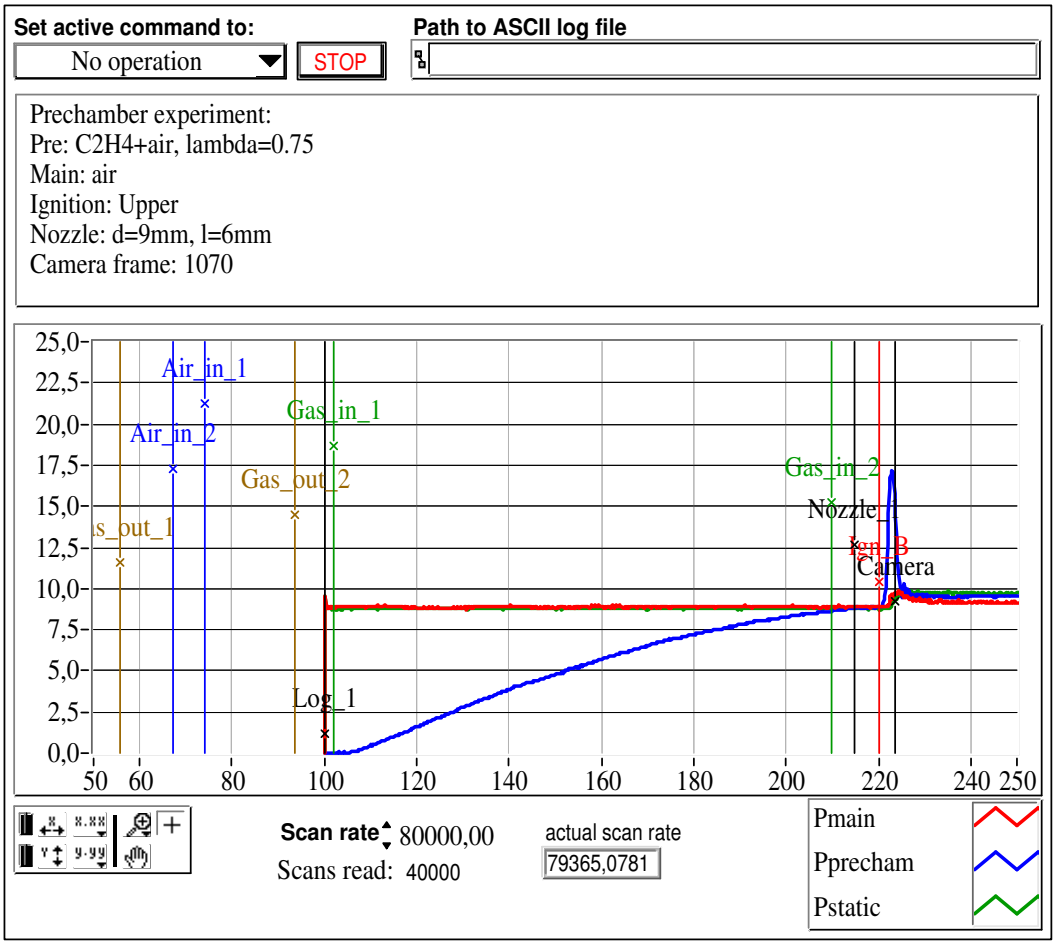

Figure E.11: Operating sequence

E.7 Experiment 5, short nozzle

Gas "EM2" (rich C2H4+air), upper ignition point, nozzle n9/6. Operating sequence is shown in figure E.11. The sequence is the same as in experiment 2, the only main difference is the shorter nozzle.

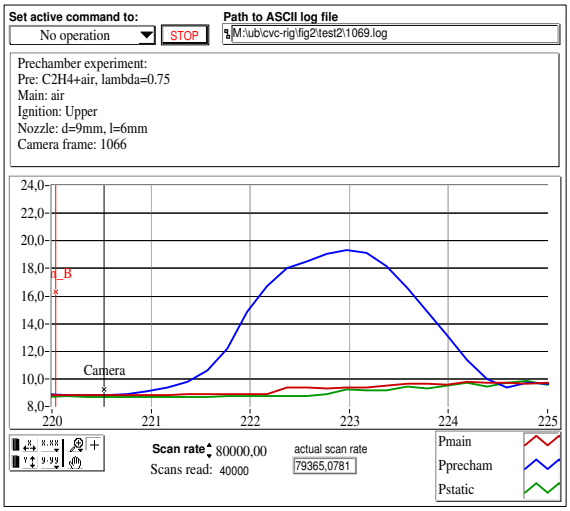
Set active command to:
No operation
STOP
Path to ASCII log file
M:\ub\cvc-rig\fig2\test2\1069.log
Prechamber experiment:
Pre: C2H4+air, lambda=0.75
Main: air
Ignition: Upper
Nozzle: d=9mm, l=6mm
Camera frame: 1066
24,0
22,0
20,0
18,0
16,0
14,0
12,0
10,0
8,0
n_B
Camera
220
221
222
223
224
225
Scan rate 80000,00
Scans read: 40000
actual scan rate
79365,0781
Pmain
Pprecham
Pstatic

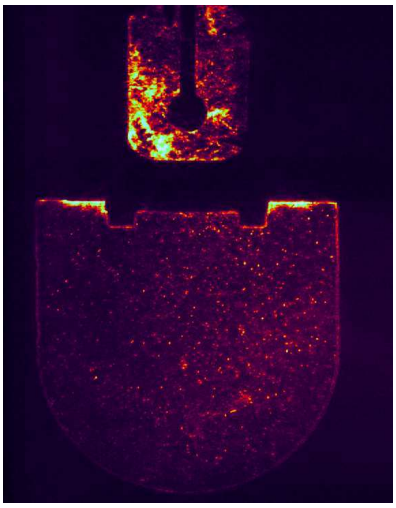

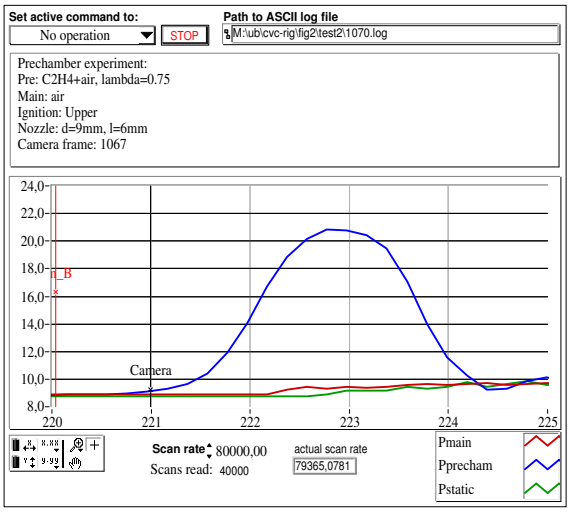
Set active command to:
No operation
STOP
Path to ASCII log file
M:\ub\cvc-rig\fig2\test2\1070.log
Prechamber experiment:
Pre: C2H4+air, lambda=0.75
Main: air
Ignition: Upper
Nozzle: d=9mm, l=6mm
Camera frame: 1067
24,0
22,0
20,0
18,0
16,0
14,0
12,0
10,0
8,0
n_B
Camera
220
221
222
223
224
225
Scan rate 80000,00
Scans read: 40000
actual scan rate
79365,0781
Pmain
Pprecham
Pstatic

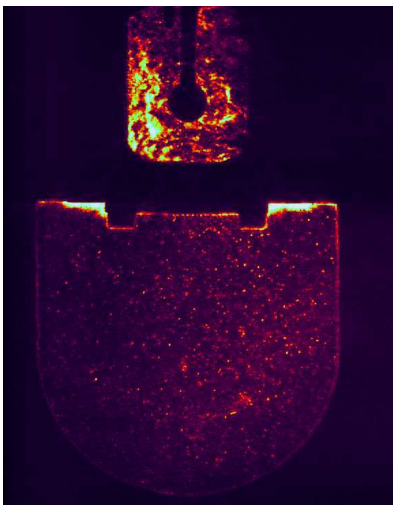

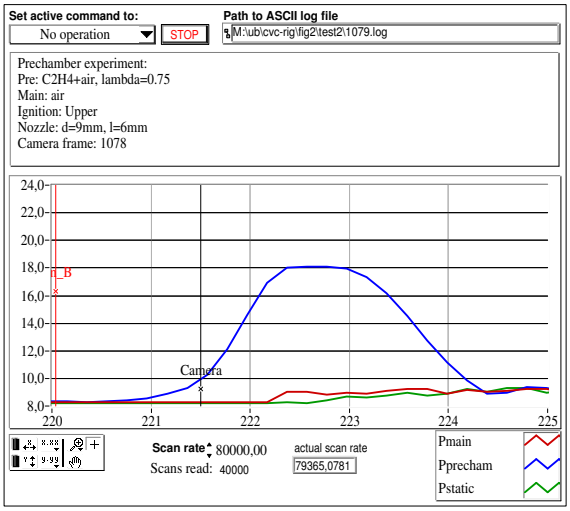
Set active command to:
No operation
STOP
Path to ASCII log file
M:\ub\cvc-rig\fig2\test2\1079.log
Prechamber experiment:
Pre: C2H4+air, lambda=0.75
Main: air
Ignition: Upper
Nozzle: d=9mm, l=6mm
Camera frame: 1078
24,0
22,0
20,0
18,0
16,0
14,0
12,0
10,0
8,0
n_B
Camera
220
221
222
223
224
225
Scan rate 80000,00
Scans read: 40000
actual scan rate
79365,0781
Pmain
Pprecham
Pstatic

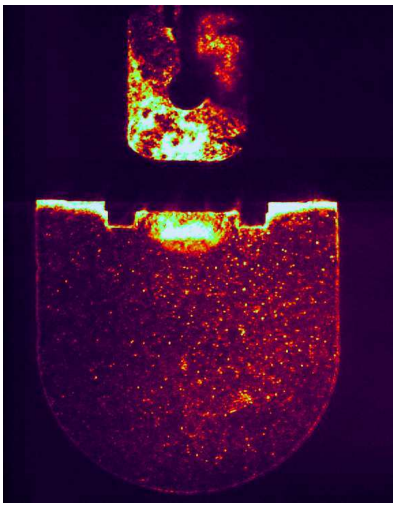

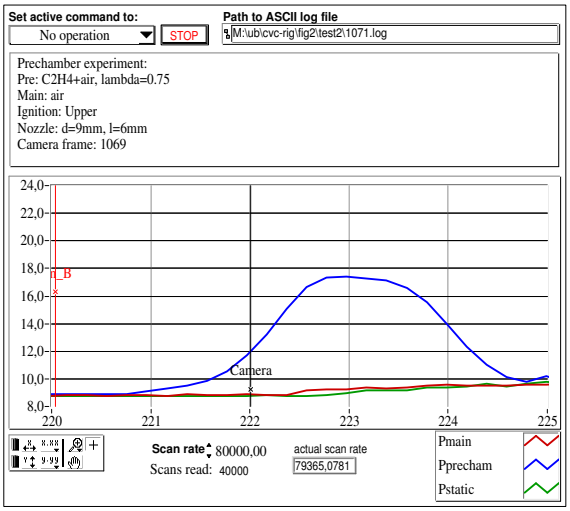
Set active command to:
No operation
STOP
Path to ASCII log file
M:\ub\cvc-rig\fig2\test2\1071.log
Prechamber experiment:
Pre: C2H4+air, lambda=0.75
Main: air
Ignition: Upper
Nozzle: d=9mm, l=6mm
Camera frame: 1069
24,0
22,0
20,0
18,0
16,0
14,0
12,0
10,0
8,0
n_B
Camera
220
221
222
223
224
225
Scan rate 80000,00
Scans read: 40000
actual scan rate
79365,0781
Pmain
Pprecham
Pstatic

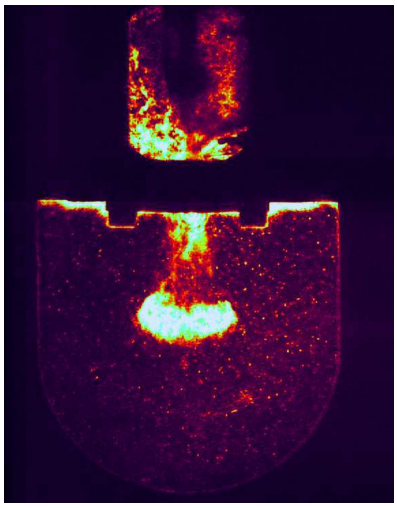

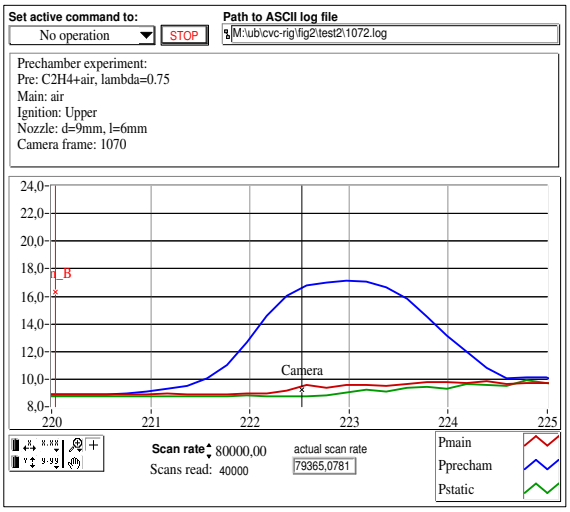
Set active command to:
No operation
STOP
Path to ASCII log file
M:\ub\cvc-rig\fig2\test2\1072.log
Prechamber experiment:
Pre: C2H4+air, lambda=0.75
Main: air
Ignition: Upper
Nozzle: d=9mm, l=6mm
Camera frame: 1070
24,0
22,0
20,0
18,0
16,0
14,0
12,0
10,0
8,0
n_B
Camera
220
221
222
223
224
225
Scan rate 80000,00
Scans read: 40000
actual scan rate
79365,0781
Pmain
Pprecham
Pstatic

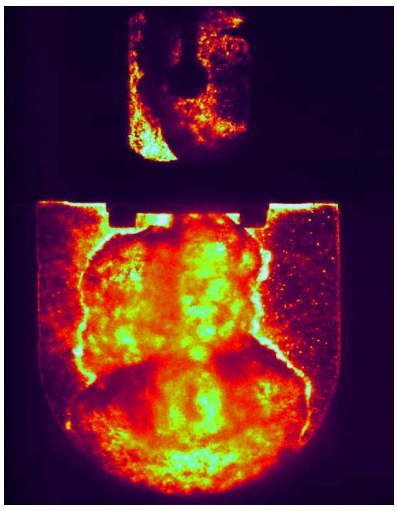

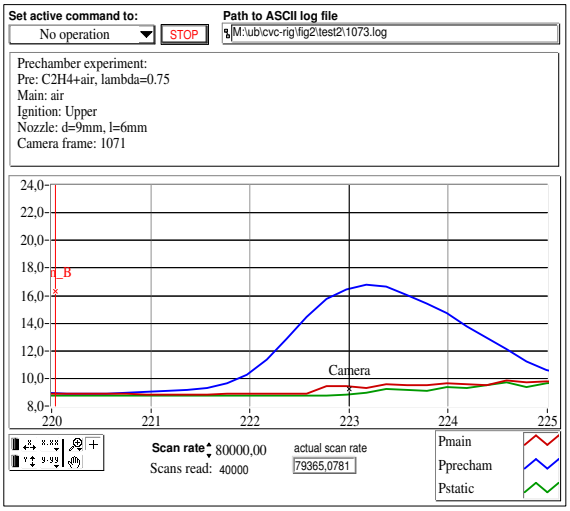
Set active command to:
No operation
STOP
Path to ASCII log file
M:\ub\cvc-rig\fig2\test2\1073.log
Prechamber experiment:
Pre: C2H4+air, lambda=0.75
Main: air
Ignition: Upper
Nozzle: d=9mm, l=6mm
Camera frame: 1071
24,0
22,0
20,0
18,0
16,0
14,0
12,0
10,0
8,0
n_B
Camera
220
221
222
223
224
225
Scan rate 80000,00
Scans read: 40000
actual scan rate
79365,0781
Pmain
Pprecham
Pstatic

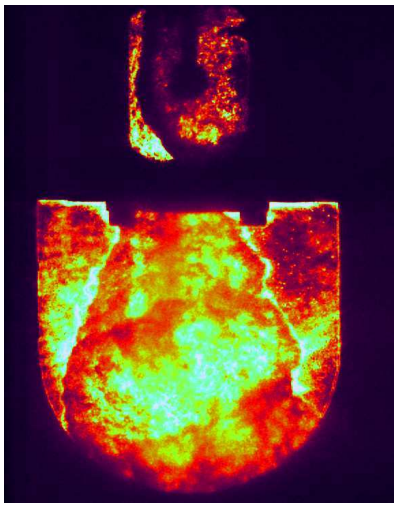

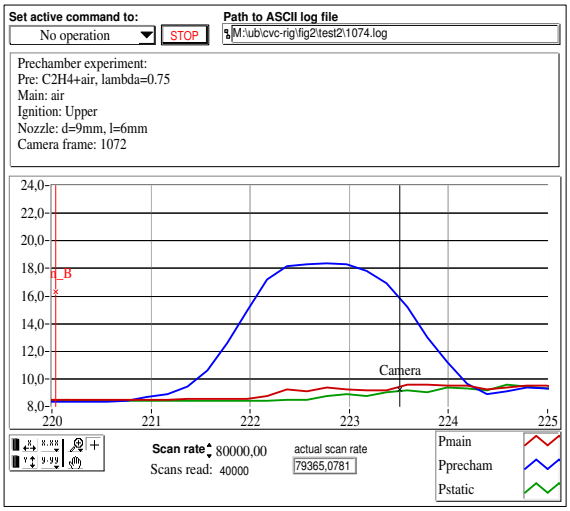
Set active command to:
No operation
STOP
Path to ASCII log file
M:\ub\cvc-rig\fig2\test2\1074.log
Prechamber experiment:
Pre: C2H4+air, lambda=0.75
Main: air
Ignition: Upper
Nozzle: d=9mm, l=6mm
Camera frame: 1072
24,0
22,0
20,0
18,0
16,0
14,0
12,0
10,0
8,0
n_B
Camera
220
221
222
223
224
225
Scan rate 80000,00
Scans read: 40000
actual scan rate
79365,0781
Pmain
Pprecham
Pstatic

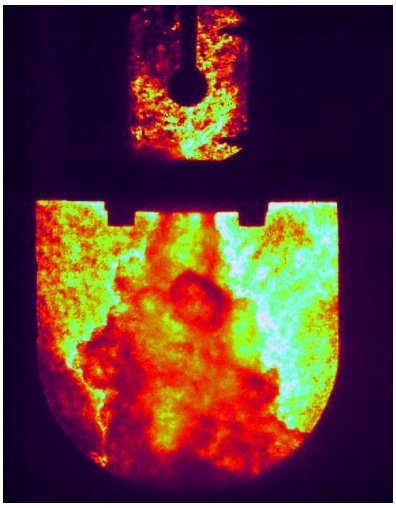

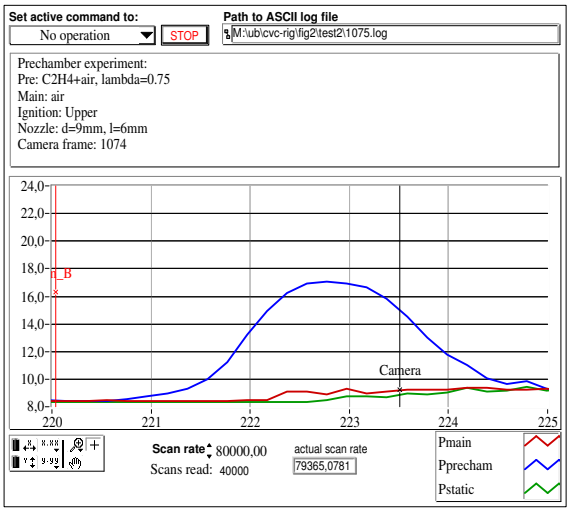
Set active command to:
No operation
STOP
Path to ASCII log file
M:\ub\cvc-rig\fig2\test2\1075.log
Prechamber experiment:
Pre: C2H4+air, lambda=0.75
Main: air
Ignition: Upper
Nozzle: d=9mm, l=6mm
Camera frame: 1074
24,0
22,0
20,0
18,0
16,0
14,0
12,0
10,0
8,0
n_B
Camera
220
221
222
223
224
225
Scan rate 80000,00
Scans read: 40000
actual scan rate
79365,0781
Pmain
Pprecham
Pstatic

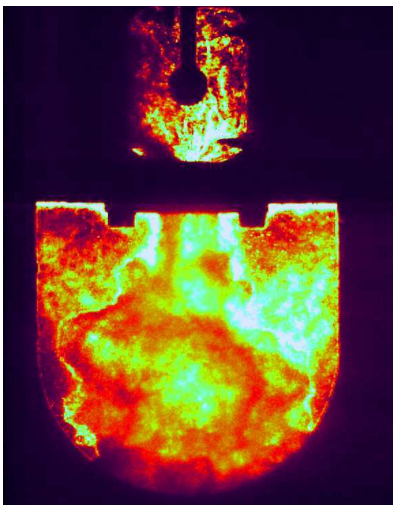

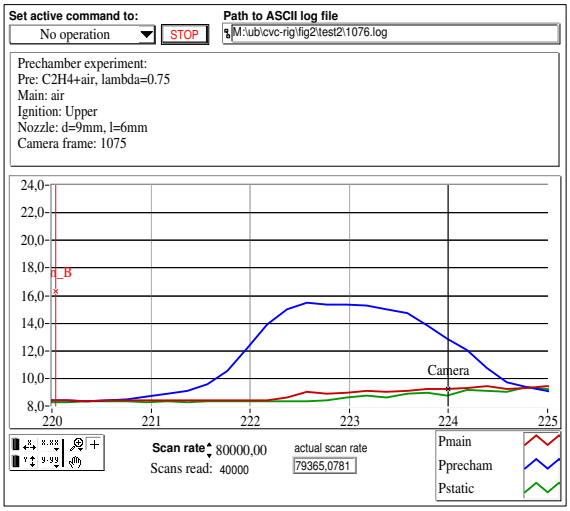
Set active command to:
No operation
STOP
Path to ASCII log file
M:\ub\cvc-rig\fig2\test2\1076.log
Prechamber experiment:
Pre: C2H4+air, lambda=0.75
Main: air
Ignition: Upper
Nozzle: d=9mm, l=6mm
Camera frame: 1075
24,0
22,0
20,0
18,0
16,0
14,0
12,0
10,0
8,0
n_B
Camera
220
221
222
223
224
225
Scan rate 80000,00
Scans read: 40000
actual scan rate
79365,0781
Pmain
Pprecham
Pstatic

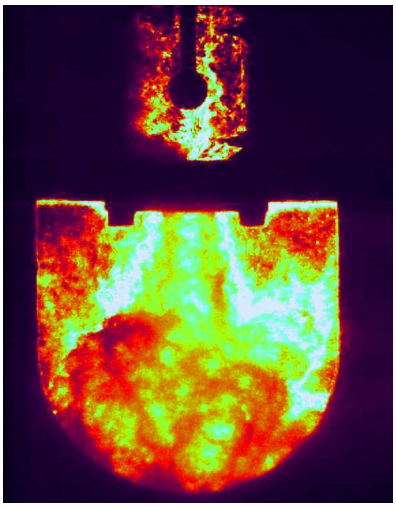

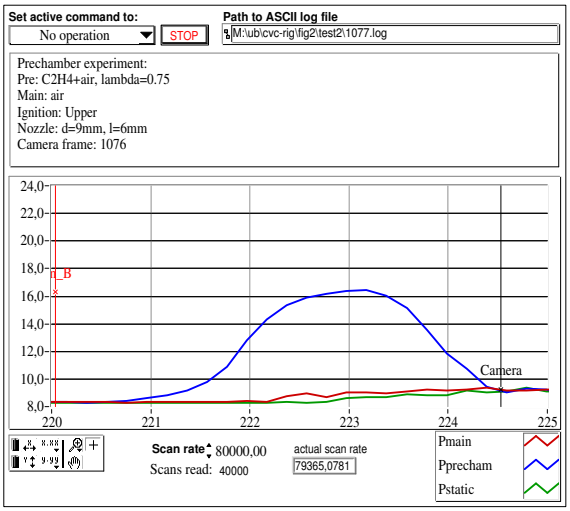
Set active command to:
No operation
STOP
Path to ASCII log file
M:\ub\cvc-rig\fig2\test2\1077.log
Prechamber experiment:
Pre: C2H4+air, lambda=0.75
Main: air
Ignition: Upper
Nozzle: d=9mm, l=6mm
Camera frame: 1076
24,0
22,0
20,0
18,0
16,0
14,0
12,0
10,0
8,0
n_B
Camera
220
221
222
223
224
225
Scan rate 80000,00
Scans read: 40000
actual scan rate
79365,0781
Pmain
Pprecham
Pstatic

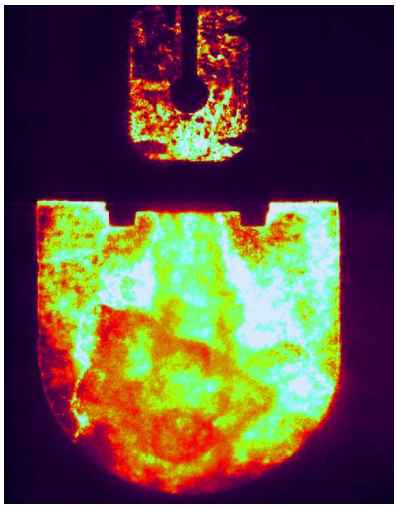

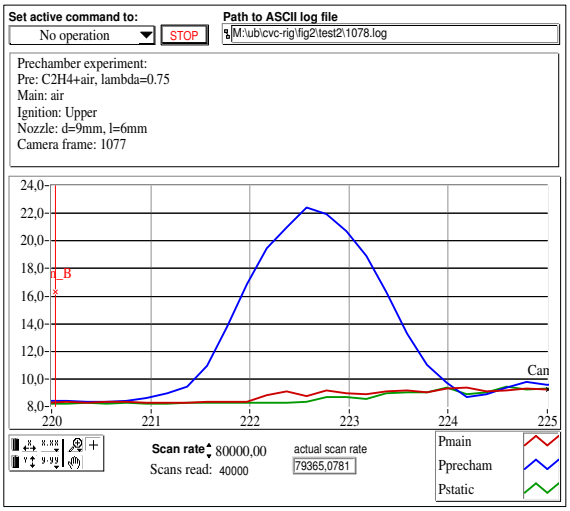
Set active command to:
No operation
STOP
Path to ASCII log file
M:\ub\cvc-rig\fig2\test2\1078.log
Prechamber experiment:
Pre: C2H4+air, lambda=0.75
Main: air
Ignition: Upper
Nozzle: d=9mm, l=6mm
Camera frame: 1077
24,0
22,0
20,0
18,0
16,0
14,0
12,0
10,0
8,0
n_B
Can
220
221
222
223
224
225
Scan rate 80000,00
Scans read: 40000
actual scan rate
79365,0781
Pmain
Pprecham
Pstatic

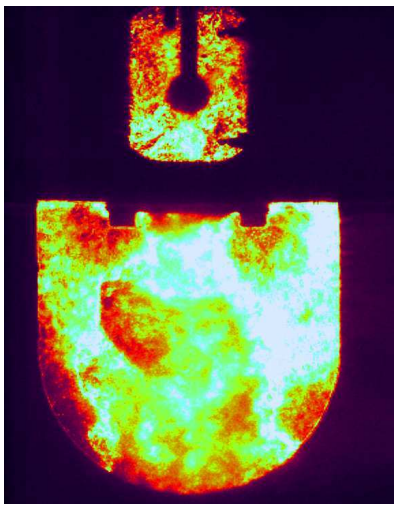

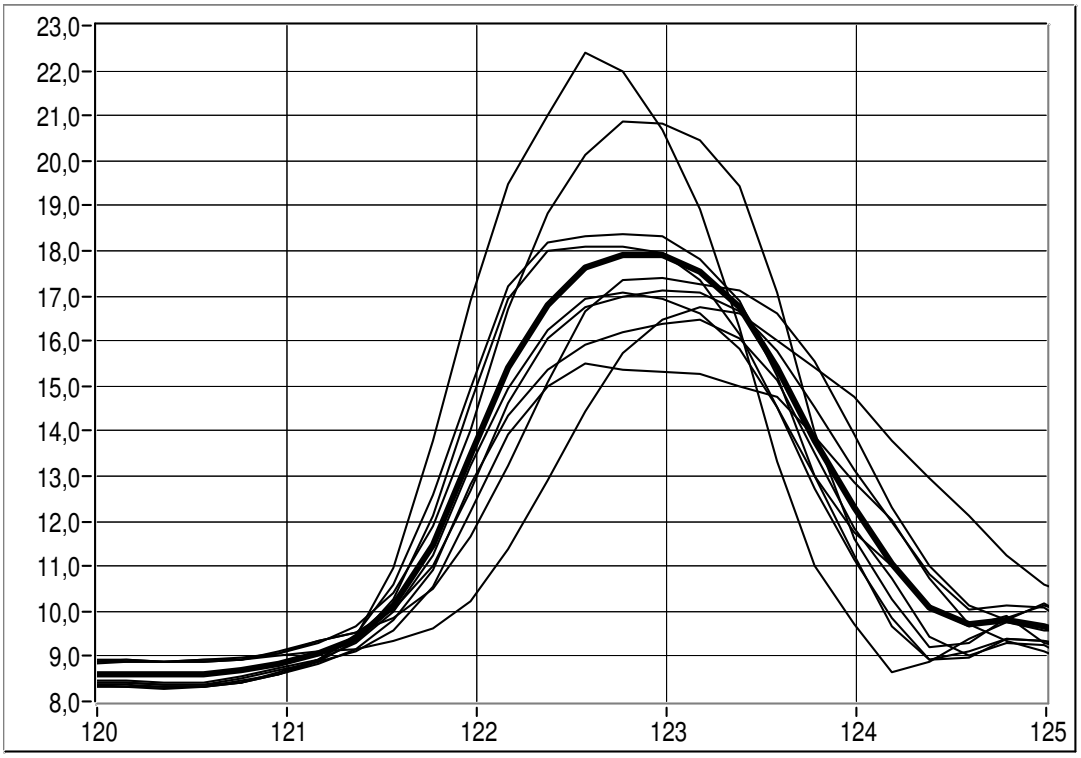

Figure E.12: Prechamber pressures from several combustions collected into one graph.

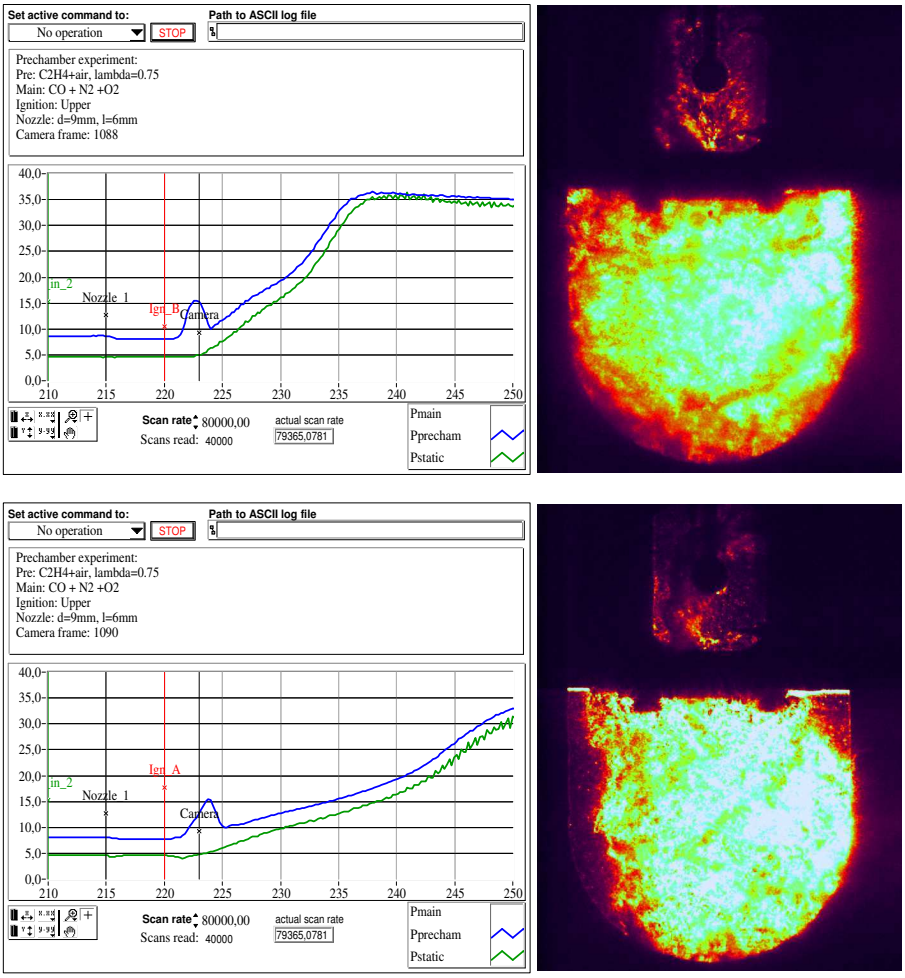

E.7.1 Experiment 6, filling also the main chamber

Same operation sequence as in experiment 5. These experiments takes much longer time, as the main chamber must be flushed and filled. Between each combustion, the rig is flushed with air for a couple of minutes in order to cool it down.

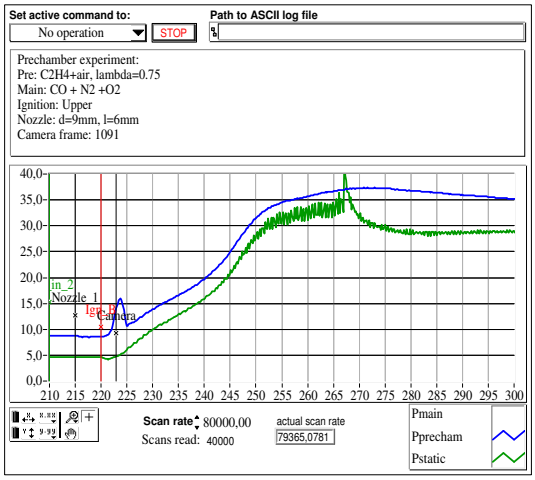
Set active command to:
No operation
STOP
Path to ASCII log file
Prechamber experiment:
Pre: C2H4+air, lambda=0.75
Main: CO + N2 +O2
Ignition: Upper
Nozzle: d=9mm, l=6mm
Camera frame: 1091
40,0
35,0
30,0
25,0
20,0
15,0
10,0
5,0
0,0
210 215 220 225 230 235 240 245 250 255 260 265 270 275 280 285 290 295 300
in_2
Nozzle_1
Ign_1
Camera
Scan rate 80000,00
Scans read: 40000
actual scan rate
79365,0781
Pmain
Pprecham
Pstatic

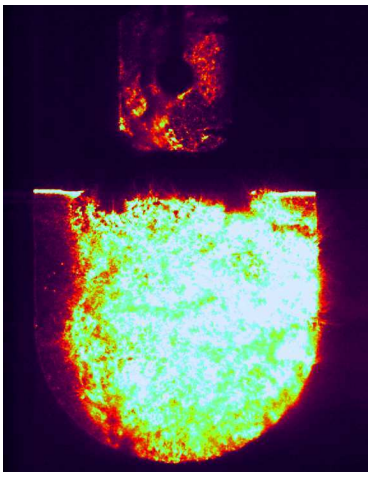

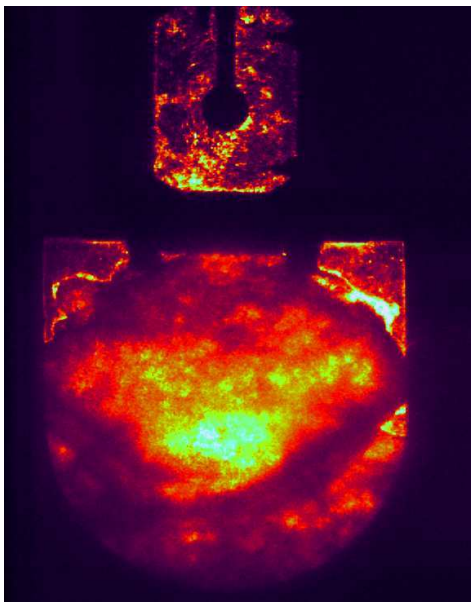

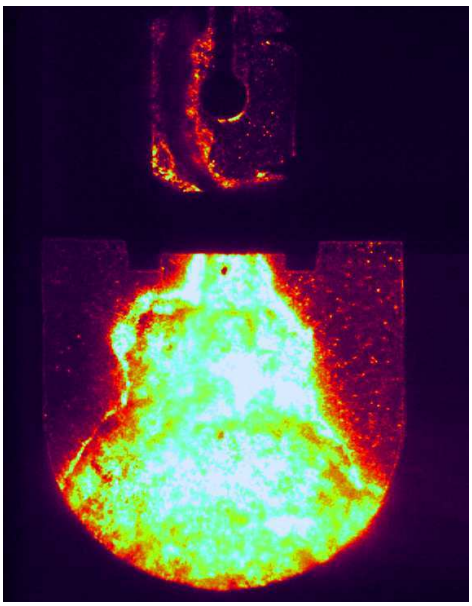

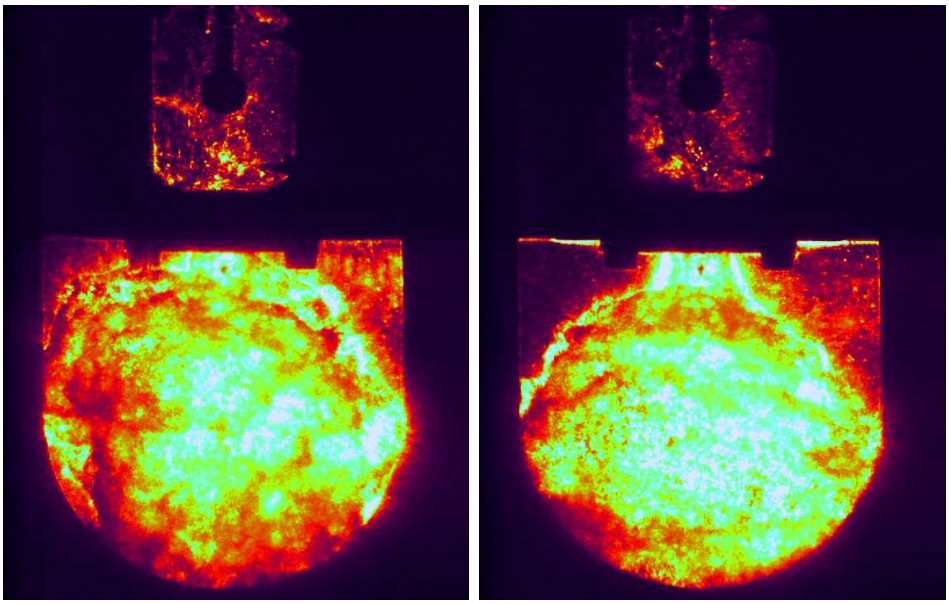

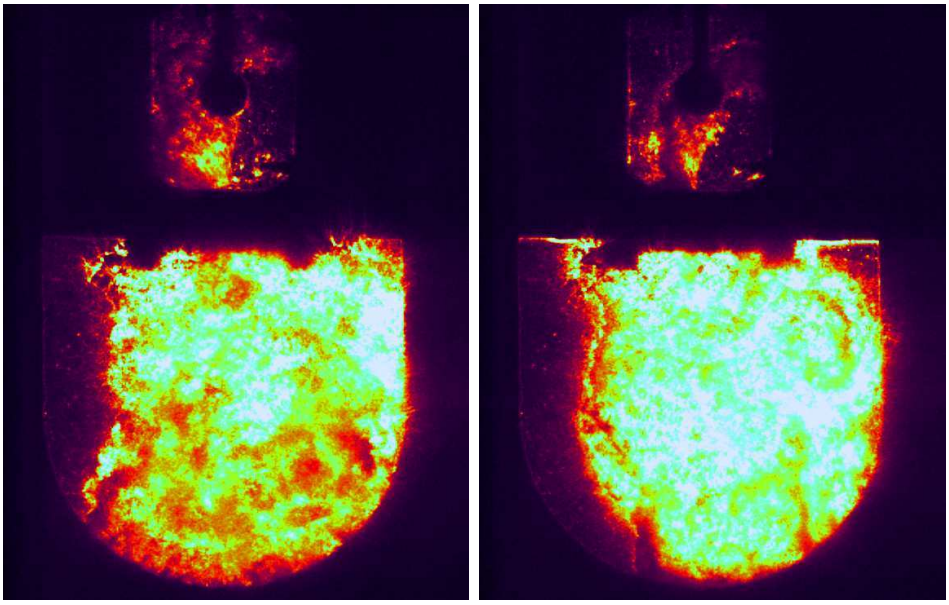

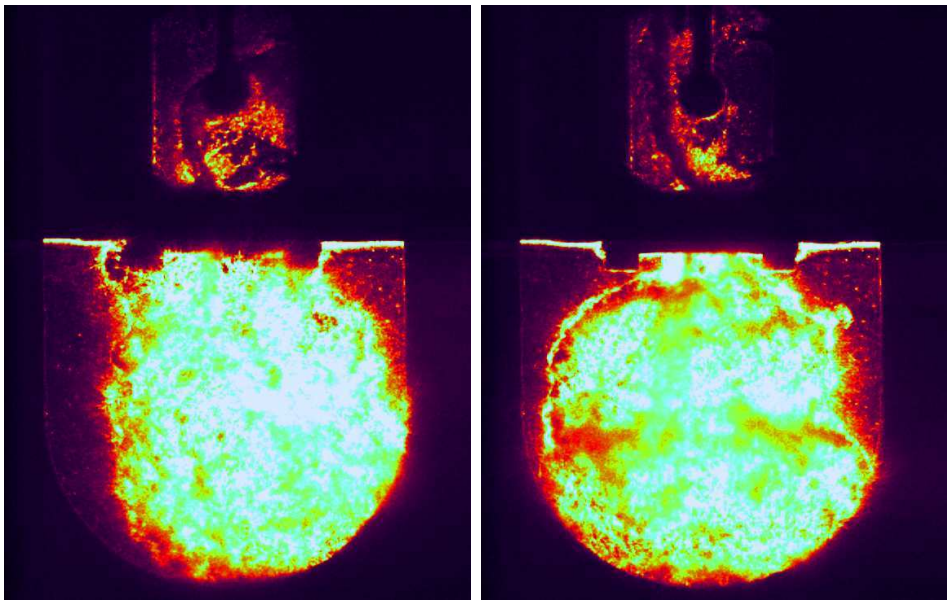

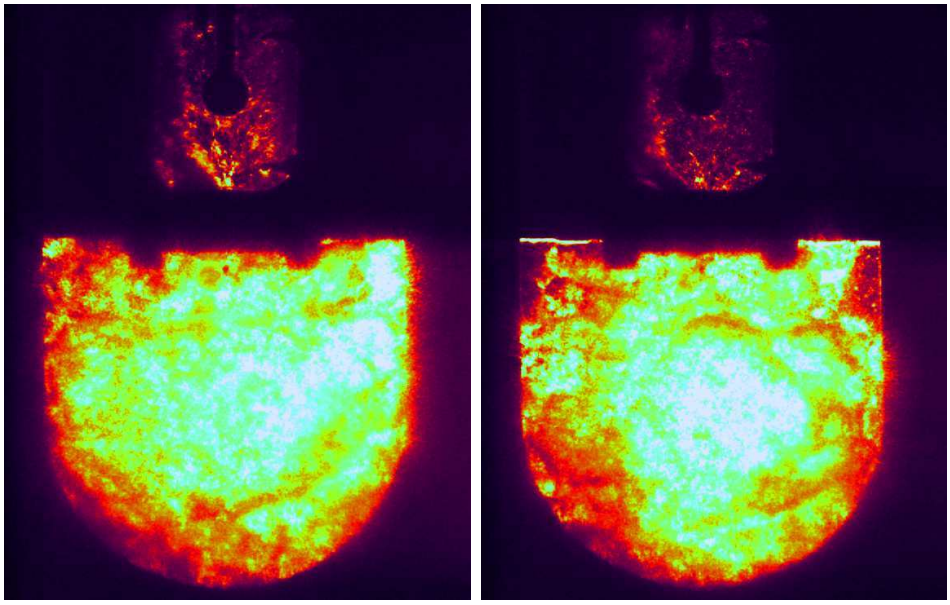

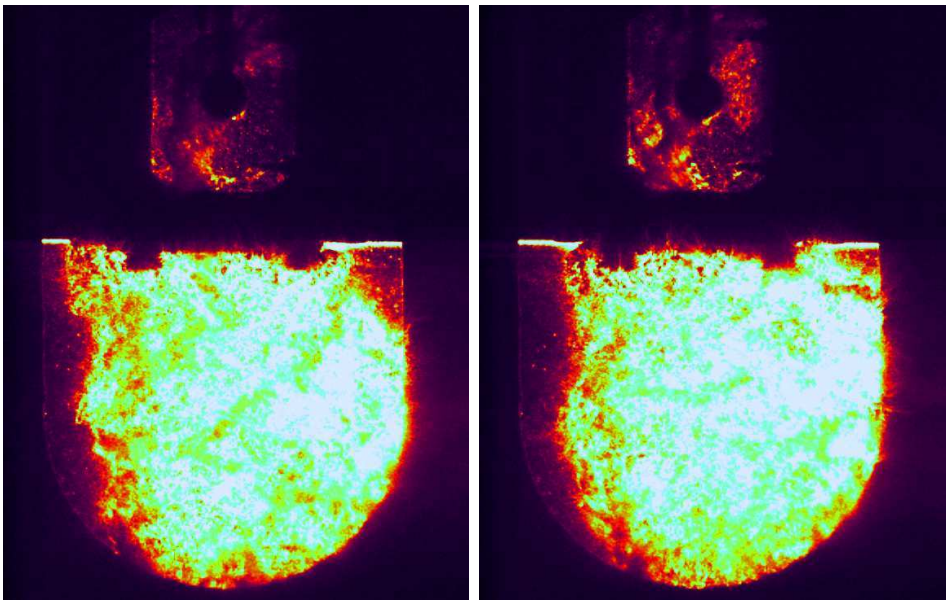

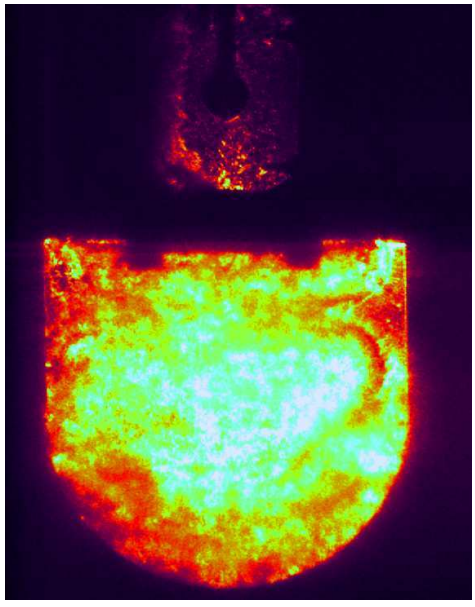

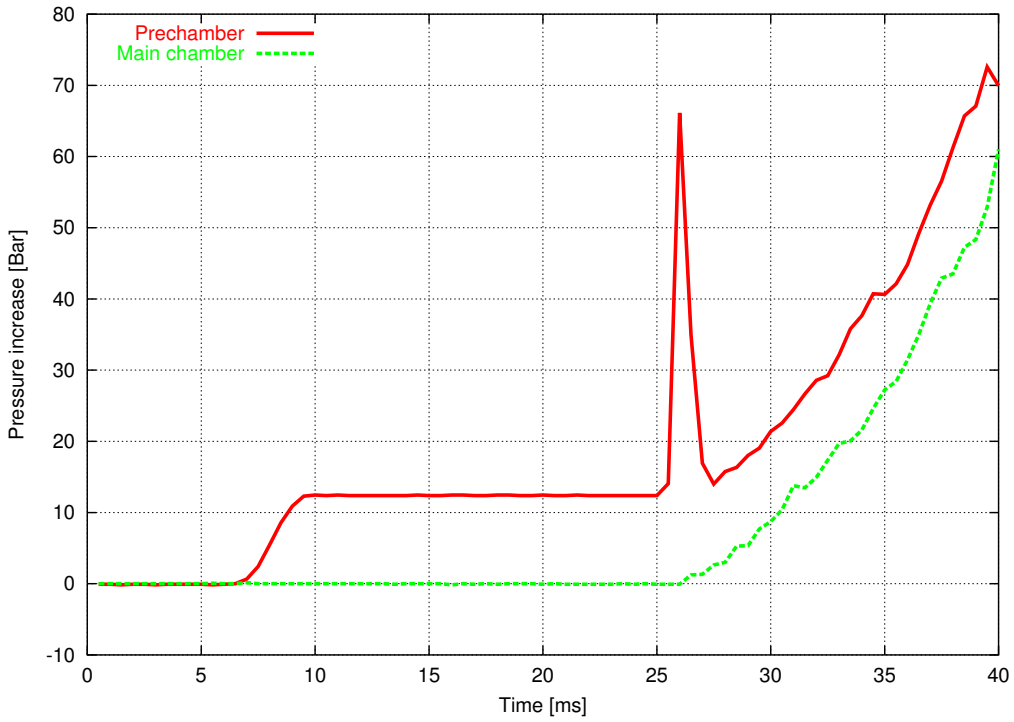

Figure E.13: Pressure increase in prechamber and main chamber during an attempt to create engine-like conditions.

E.8 Experiment attempting to make "engine like" conditions

The smallest prechamber (C22/30) is filled with C_2H_4 at 1 atmosphere pressure. The main chamber is filled with lean mixture of air and C_2H_4 at 15 bar pressure. The nozzle between the two chambers (nozzle n6/6, — 6 mm diameter and 6 mm length) is opened 15 ms before ignition with upper ignition point. The pressure difference between the two chambers create a violent in-flow and turbulence that prevails during the the combustion.

This operation sequence is made in order to make somewhat engine-like conditions in the prechamber at the time of ignition — an in-homogeneous charge with a high turbulence level and high combustion speed.

The pressure increase during the experiment can be seen in figure E.13. The first bump on the prechamber pressure is when the nozzle opens, then there is a spike up to 67 bar during combustion in the prechambers, then the pressure of both chambers increase up to 70 bar.

Note that the peak pressure ratio over the nozzle during the combustion

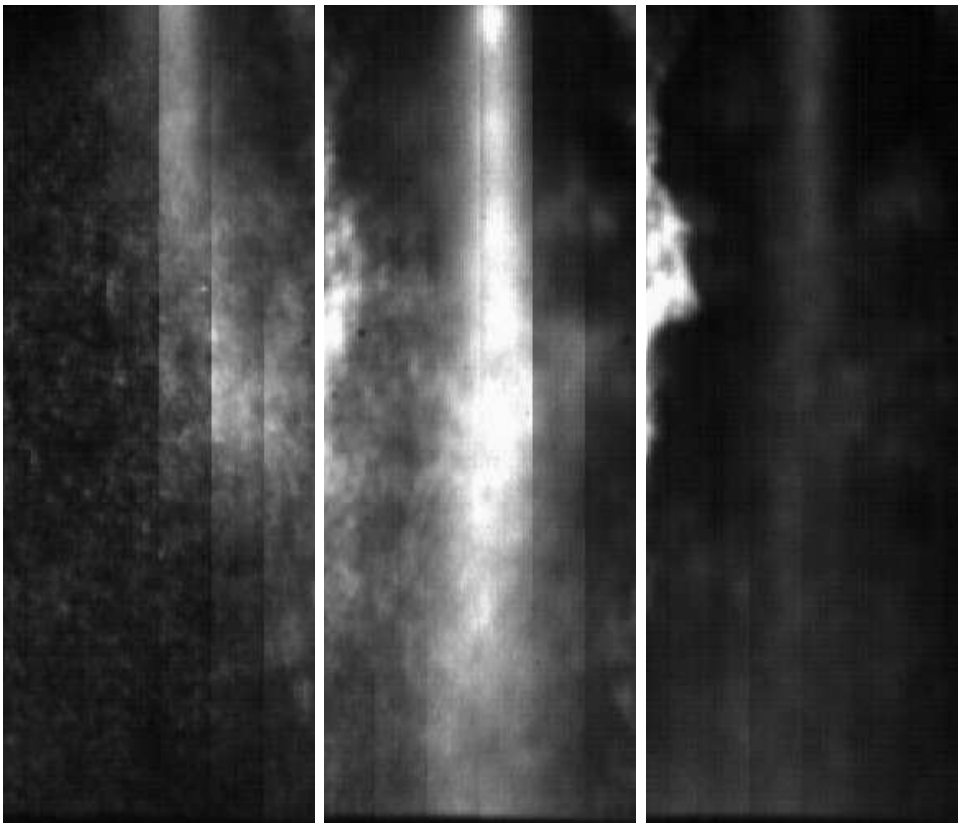

Figure E.14: Pictures from an attempt to create engine-like conditions. The pictures are taken with high speed video at 2000 frames per second. The jet speed is clearly faster than the scan rate of the left picture as the jet is not visible on the left side of the picture, but already reaches the full length of the picture when the last section of the picture is scanned.

in the prechamber is so high as $67/15 = 4.5$, while it may reach about 2 in an engine. This means that the jet may not perform as in an engine — the jet reaches sonic speed in this experiment.

The resulting jet and combustion in main chamber is captured with high speed video at 2000 frames per second (not as single shot pictures as in the other experiments). Unfortunately, the shutter speed of the video camera was insufficient for the high flow velocities, so the jet pictures are unclear.

E.9 Discussion/summary of the results

E.9.1 Validation of numerical models

Measured pressure from a combustion was used as input to a two zone calculation model with ROHR and jet length as output. It was (to a small extent) possible to compare the calculated jet length with observed jet length.

It is difficult estimate the volume fraction combusted from the pictures, it was therefore not attempted to compare it with the calculated volume fraction combusted.

It is difficult to measure the hot jet length from the presented pictures because:

- Both the cold jet (before flame reaches nozzle) and the hot jet is shown when Schlieren method is used.
- The jet reaches further than the visible area — sometimes before the flame reaches the nozzle. The window is too small compared to the size of the prechamber.

For better comparison of jet length, one need to use a smaller prechamber (or a larger combustion rig) or else the jet will reach past the window too soon. The duration of the hot jet is very small, one needs an accuracy and resolution with respect to time better than 10 μs in order to observe the length of the hot jet.

The calculated ROHR is lower than expected value. The net heat release inside the prechamber was only 0.6 MJ/kg charge. This may be due to physical (real) effects like incomplete combustion or heat transfer to the walls.

E.9.2 Experiments with turbulence.

The experiments presented here indicates that turbulence is essential. With too low turbulence, a reasonable burn rate can not be obtained. Snyder et al. [1988] also mention that the reproduction of engine like flow and turbulence through the filling of the prechamber is essential when testing prechambers for use in engines. The question is then: How to generate a repeatable and measurable turbulence, and what is the optimum turbulence?

Turbulence may also lead to cycle to cycle variations and misfire. These effects were not observed during this series of experiments. The reason may be: a) A relatively low pressure. b) Powerful ignition sources. c) Low turbulence.

E.9.3 Location of ignition source

Ignition close to the nozzle gives: a) longer duration of the prechamber combustion. b) Lower pressure in the prechamber. When the nozzle is kept closed, then the prechamber is symmetric and either ignition source gives the same combustion pressure.

E.9.4 Experiments with increased oxygen pressure.

During one experiment, the glue sealing the ignition electrodes was oxidated, resulting that hot oxygen-rich flames blasted out of the prechamber and cutting away a few cm^3 of iron from prechamber on the way. The result was a glowing spray out of the CVC-rig, plastering the surrounding parts with iron oxide.

If increased oxygen pressure is to be used, then the CVC-rig must be made of stainless steel or other materials that will resist oxidation. Also: The sealing must be very carefully made so that no sealing material other than stainless steel and ceramics is exposed to the flames.

Appendix F

Schlieren methods

F.1 Introduction

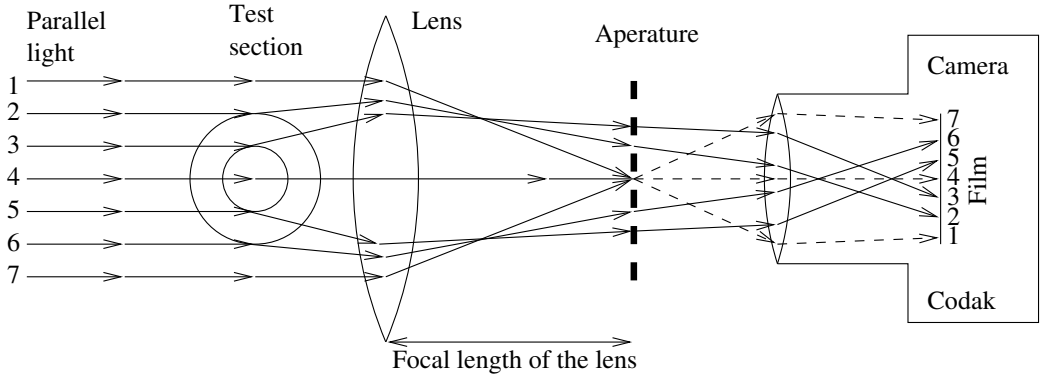

Figure F.1: Schematic Schlieren setup with lenses.

Schlieren techniques are photographic techniques for recording directional changes of light through a test section. The test section may for example be a gas jet, a fuel spray, a flame or a gas with temperature gradient.

One or more beams of parallel light are sent through the test section. After passing through the test section, the light passes through a focusing lens or is reflected on a focusing mirror. The lens (or mirror) will focus the light which have the same direction out of the test section as into the test section, while the light which has been bent off through the test section will not be focused. An aperture placed in the focal point allows only the light one wish to record to pass into the camera. Examples of apertures are shown in figure F.2.

Note the path of the seven marked light rays and where they end up on the film in figure F.1. If the camera is focused on the test section, then the

Figure F.2: Examples of apertures to be placed in the focal point of a Schlieren setup.

position on the film will be independent of the bending of the ray through the test section.

F.2 Fundamental optics

Not much knowledge of optics is needed to understand how a Schlieren system works, these basic concepts should suffice:

- A lens focuses parallel light in a focal point. The distance between the lens and the focal point is called "focal length". Figure F.1 illustrates this.
- A camera is in focus when the light arriving at a single point on the film comes from ("from" as in emitted, reflected or passing trough) a single point in the target. In other words: Light emitted from or passing through a point in the target may hit only a single point on the film. Figure F.1 illustrates this also as light rays passing through the test section at equal distances end up on equal distances on the film even if they are bent off though the test section.

Considerably more knowledge is needed if one wishes to use Schlieren systems for measuring the angle the light has been bent off in each point of the picture. Hallvard Paulsen presents in his Dr.Ing. thesis Paulsen [1995] how to use a Schlieren system for such measurements .

F.3 Example setup

A Schlieren setup with lenses have been used by several people at Marintek and faculty of Marine Engineering, NTNU. The setup is sketched in figure F.3 and consists of:

- Laser: type: He-Ne, power: 5 mW, wavelength: 633 nm.

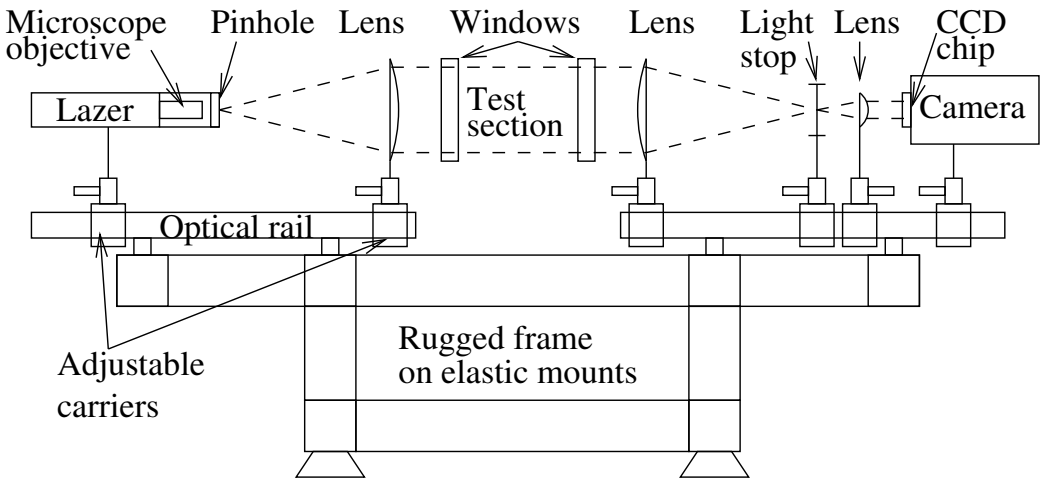

Figure F.3: Schematic Schlieren setup with lenses.

- Microscope objective for the laser. type ?????
- Pinhole, 10μm mounted on the laser in the focus point of the microscope objective.
- Two large lenses. Diameter = 125 mm, focal length = 1000 mm.
- Two glass windows for use in the CVC-rig.
  Diameter = 125 mm, thickness = 25 mm.
- Selection of apertures.
- Selection of camera lenses, a lens of 20 mm diameter and 80 mm focal length gives full view of the glass windows.
- CCD video camera with "line rate" accuracy trigger and shutter speed of $1/20,000$ s.
- Mounting gear: Optical rails, adjustable carriers and a rugged frame.

Installation procedure

1. Align up optical mounting rails on each side of the test section.
2. Mount the laser on the rail end and adjust the angles so that the laser beam is parallel with the mounting rails and also goes through the middle of the test section.

3. Mount each lens and window, starting with the one closes to the laser. Adjust the angles and positions so that the reflecting laser light from the device hit directly back into the laser. A lens which is out of center will cast two reflections.

4. Mount the microscope objective and pin hole on the laser and adjust the the axial position of the large lenses until a small focusing point is achieved. If the large lens closest to the laser is not positioned exactly, then the peripheral light will not focus in the same distance from the lens as the light passing close to the center.

5. Mount the camera and adjust the focus and zoom. Focus on for example a candle light or a bolt placed in the middle of the test section.

6. Mount the light stop aperture.

References

All citations in this document are referenced by name of first author and year of publication. The reference list below is sorted with respect to name of first author.

Tor Øyvind Ask. *Ignition and Flame Growth in Lean Gas-Air Mixtures, an Experimental Study with a Schlieren System.* Dr.Ing. marine engineering, Norges Tekniske Høgskole, 1992.

T. Chikahisa and T. Murayama. Theory and experiments on air-entrainment in fuel sprays and their application to interpret diesel combustion processes. *SAE 950447*, 1995.

B. M. Chrisman and P. D. Freen. Development of the 2400G stationary gas engines. *Heavy duty engines: a look at the future. ASME*, 22:37–47, 1994.

M. E. Crane and S. R. King. Emmision reduction through precombustion chamber design in a natural gas, lean burn engine. *Transactions of the SNAME*, 114:466–474, July 1992.

J. C. Dent. A basis for the comparation of various experimental methods for studying spray penetration. *SAE 710571*, 1971.

S. G. Dexter and C. Ennemoser. Fire not misfire in pre-chamber gas engines. *CIMAC*, page D45, May 1995.

Irvin Glassman. *Combustion.* Academic Press, third edition, 1996.

J. F. Griffiths and J. A. Barnard. *Flame and Combustion.* Blackie Academic & Professional, Glasgow, third edition, 1995.

L. A. Gussak, G. V. Evart, and D. A. Ribinsky. Carburettor type internal combustion engine with prechamber. *U. S. Patent 3,092,088*, 1963.

John B. Heywood. *Internal Combustion Engine Fundamentals.* Automotive technology series. McGraw-Hill, Reading, Massachusetts, 1988.

S. D. Hires, A. Ekchian, J. B. Heywood, R. J. Tabaczynski, and J. C. Wall. Performance and NO_x emmisions modelling of a jet ignition prechamber stratified charge engine. *SAE 760161*, 1976.

H. Hiroyasu and M. Arai. Fuel spray penetration and spray angle in diesel engines. *Trans. of the SAE of Japan*, 21:5–11, 1980.

Jacques Lavy, Jean-Charles Dabadie, Christian Angelberger, Pierre Duret, Jürgen Willand, Andreas Juretzka, Jochen Schäflein, Yvane Lendresse, Arnaud Satre, Christo Schulz, Heinz Kreämer, Hya Zhao, and Len Damiano. Innovative ultra-low NO_x controlled auto-ignition combustion process for gasoline engines: the 4-space project. *SAE011837*, 2000.

Rune Nordrik. *Investigation of spark ignition and autoignition in methane and air using computational fluid dynamics and chemical reaction kinetics. A numerical study of ignition process in internal combustion engines.* Dr.Ing. marine engineering, Norges Tekniske Høgskole, 1993.

Rune Nordrik, Hallvard Paulsen, and Harald Valland. Arbeidsnotat: Numerisk beregning av strømning og blanding i forkammeret på Bergen Diesel's gassmotor. MARINTEK A/S og Institutt for Marint Maskineri, NTH, July 1989.

Hallvard Paulsen. *A study of transient jet and spray using a Schlieren method and digital image processing.* Dr. Ing. marine engineering, Norges Tekniske Høgskole, 1995.

H. Phillips. Ignition in a transient turbulent jet of hot inert gas. *Combustion and flame*, 19:187–195, 1972.

Harry R. Ricardo. Recent work on the internal-combustion engine. In *SAE Transactions*, volume 17. SAE, May 1922.

Peter Schihl, Walter Bryzik, and Arvind Atreya. Analysis of current spray penetration models and proposal of a phenomenological cone penetration model. In *Fuel spray technology and applications*, volume SP-1132, chapter 960773, pages 41–50. SAE, 1996.

P. H. Schweitzer. Penetration of oil sprays. *Pennsylvania State College Bulletin*, 46, 1937.

W. E. Snyder and S. G. Dexter. Looking into a lean burn spark ignited gas engine. Presented at the annual energy-sources technology conference and exhibition, New Orleans, Lousiana, January 1990.

W. E. Snyder, M. R. Wright, and S. G. Dexter. A natural gas engine combustion rig with high-speed photography. *Transaction of the ASME*, 110 (3), July 1988.

Harald Valland. Simulering av forbrenning med gassutblåsning gjennom et konstant utløpsareal. Technical report, Norges Tekniske Høgskole, 1984.

Y. Wakuri, M. Fujii, t. Amitani, and R. Tsuneya. Studies on the penetration of fuel spray in a diesel engine. *Bulletin of JSME*, 13(9), 1960.

D Wolff, M Tamura, H Tai, and T Sakurai. Looking into the prechamber of a lean-burn gas engine. *JSME INTERNATIONAL JOURNAL SERIES B-FLUIDS AND THERMAL ENGINEERING - ISSN: 1340-8054*, 40(2): 320–327, 1997.

Dirk Wunsch, Stefan Heyne, Jan-Bernard Vos, and Daniel Favrat. Numerical flow simulation of a natural gas engine equipped with an unscavanged autoignition prechamber. *European Combustion Meeting ECM 2007, Chania, Greece, 11-13 April 2007*, 2007.

Friedemann Zacharias. *Analytische Darstellung der thermodynamischen Eigenschaften von Verbrennungsgasen.* PhD thesis, TU Berlin, 1966.

Vilmar Æsøy. *Hot surface assisted compression ignition in a direct injection natural gas engine.* Dr.Ing. marine engineering, Norges Teknisk-Naturvitenskapelige Universitet, 1996.

Jan M. Øverli. *Strømningsmaskiner*, volume 3 of *Termiske maskiner*. Tapir forlag, 1992.

R A P P O R T E R
UTGITT VED
INSTITUTT FOR MARIN TEKNIKK
(tidligere: FAKULTET FOR MARIN TEKNIKK)
NORGES TEKNISK-NATURVITENSKAPELIGE UNIVERSITET

UR-79-01 Brigt Hatlestad, MK:	The finite element method used in a fatigue evaluation of fixed offshore platforms. (Dr.Ing. Thesis)
UR-79-02 Erik Pettersen, MK:	Analysis and design of cellular structures. (Dr.Ing. Thesis)
UR-79-03 Sverre Valsgård, MK:	Finite difference and finite element methods applied to nonlinear analysis of plated structures. (Dr.Ing. Thesis)
UR-79-04 Nils T. Nordsve, MK:	Finite element collapse analysis of structural members considering imperfections and stresses due to fabrication. (Dr.Ing. Thesis)
UR-79-05 Ivar J. Fylling, MK:	Analysis of towline forces in ocean towing systems. (Dr.Ing. Thesis)
UR-80-06 Nils Sandsmark, MM:	Analysis of Stationary and Transient Heat Conduction by the Use of the Finite Element Method. (Dr.Ing. Thesis)
UR-80-09 Sverre Haver, MK:	Analysis of uncertainties related to the stochastic modelling of ocean waves. (Dr.Ing. Thesis)
UR-85-46 Alf G. Engseth, MK:	Finite element collapse analysis of tubular steel offshore structures. (Dr.Ing. Thesis)
UR-86-47 Dengody Sheshappa, MP:	A Computer Design Model for Optimizing Fishing Vessel Designs Based on Techno-Economic Analysis. (Dr.Ing. Thesis)
UR-86-48 Vidar Aanesland, MH:	A Theoretical and Numerical Study of Ship Wave Resistance. (Dr.Ing. Thesis)
UR-86-49 Heinz-Joachim Wessel, MK:	Fracture Mechanics Analysis of Crack Growth in Plate Girders. (Dr.Ing. Thesis)
UR-86-50 Jon Taby, MK:	Ultimate and Post-ultimate Strength of Dented Tubular Members. (Dr.Ing. Thesis)
UR-86-51 Walter Lian, MH:	A Numerical Study of Two-Dimensional

Nov. 2007, IMT

	Separated Flow Past Bluff Bodies at Moderate KC-Numbers. (Dr.Ing. Thesis)
UR-86-52 Bjørn Sortland, MH:	Force Measurements in Oscillating Flow on Ship Sections and Circular Cylinders in a U-Tube Water Tank. (Dr.Ing. Thesis)
UR-86-53 Kurt Strand, MM:	A System Dynamic Approach to One-dimensional Fluid Flow. (Dr.Ing. Thesis)
UR-86-54 Arne Edvin Løken, MH:	Three Dimensional Second Order Hydrodynamic Effects on Ocean Structures in Waves. (Dr.Ing. Thesis)
UR-86-55 Sigurd Falch, MH:	A Numerical Study of Slamming of Two-Dimensional Bodies. (Dr.Ing. Thesis)
UR-87-56 Arne Braathen, MH:	Application of a Vortex Tracking Method to the Prediction of Roll Damping of a Two-Dimension Floating Body. (Dr.Ing. Thesis)
UR-87-57 Bernt Leira, MR:	Gaussian Vector Processes for Reliability Analysis involving Wave-Induced Load Effects. (Dr.Ing. Thesis)
UR-87-58 Magnus Småvik, MM:	Thermal Load and Process Characteristics in a Two-Stroke Diesel Engine with Thermal Barriers (in Norwegian). (Dr.Ing. Thesis)
MTA-88-59 Bernt Arild Bremdal, MP:	An Investigation of Marine Installation Processes - A Knowledge - Based Planning Approach. (Dr.Ing. Thesis)
MTA-88-60 Xu Jun, MK:	Non-linear Dynamic Analysis of Space-framed Offshore Structures. (Dr.Ing. Thesis)
MTA-89-61 Gang Miao, MH:	Hydrodynamic Forces and Dynamic Responses of Circular Cylinders in Wave Zones. (Dr.Ing. Thesis)
MTA-89-62 Martin Greenhow, MH:	Linear and Non-Linear Studies of Waves and Floating Bodies. Part I and Part II. (Dr.Techn. Thesis)
MTA-89-63 Chang Li, MH:	Force Coefficients of Spheres and Cubes in Oscillatory Flow with and without Current. (Dr.Ing. Thesis)
MTA-89-64 Hu Ying, MP:	A Study of Marketing and Design in Development of Marine Transport Systems. (Dr.Ing. Thesis)

MTA-89-65 Arild Jæger, MH:	Seakeeping, Dynamic Stability and Performance of a Wedge Shaped Planing Hull. (Dr.Ing. Thesis)
MTA-89-66 Chan Siu Hung, MM:	The dynamic characteristics of tilting-pad bearings.
MTA-89-67 Kim Wikstrøm, MP:	Analysis av projekteringen for ett offshore projekt. (Licenciat-avhandling)
MTA-89-68 Jiao Guoyang, MR:	Reliability Analysis of Crack Growth under Random Loading, considering Model Updating. (Dr.Ing. Thesis)
MTA-89-69 Arnt Olufsen, MK:	Uncertainty and Reliability Analysis of Fixed Offshore Structures. (Dr.Ing. Thesis)
MTA-89-70 Wu Yu-Lin, MR:	System Reliability Analyses of Offshore Structures using improved Truss and Beam Models. (Dr.Ing. Thesis)
MTA-90-71 Jan Roger Hoff, MH:	Three-dimensional Green function of a vessel with forward speed in waves. (Dr.Ing. Thesis)
MTA-90-72 Rong Zhao, MH:	Slow-Drift Motions of a Moored Two-Dimensional Body in Irregular Waves. (Dr.Ing. Thesis)
MTA-90-73 Atle Minsaas, MP:	Economical Risk Analysis. (Dr.Ing. Thesis)
MTA-90-74 Knut-Aril Farnes, MK:	Long-term Statistics of Response in Non-linear Marine Structures. (Dr.Ing. Thesis)
MTA-90-75 Torbjørn Sotberg, MK:	Application of Reliability Methods for Safety Assessment of Submarine Pipelines. (Dr.Ing. Thesis)
MTA-90-76 Zeuthen, Steffen, MP:	SEAMAID. A computational model of the design process in a constraint-based logic programming environment. An example from the offshore domain. (Dr.Ing. Thesis)
MTA-91-77 Haagensen, Sven, MM:	Fuel Dependant Cyclic Variability in a Spark Ignition Engine - An Optical Approach. (Dr.Ing. Thesis)
MTA-91-78 Løland, Geir, MH:	Current forces on and flow through fish farms. (Dr.Ing. Thesis)
MTA-91-79 Hoen, Christopher, MK:	System Identification of Structures Excited by Stochastic Load Processes. (Dr.Ing. Thesis)

MTA-91-80 Haugen, Stein, MK:	Probabilistic Evaluation of Frequency of Collision between Ships and Offshore Platforms. (Dr.Ing. Thesis)
MTA-91-81 Sødahl, Nils, MK:	Methods for Design and Analysis of Flexible Risers. (Dr.Ing. Thesis)
MTA-91-82 Ormberg, Harald, MK:	Non-linear Response Analysis of Floating Fish Farm Systems. (Dr.Ing. Thesis)
MTA-91-83 Marley, Mark J., MK:	Time Variant Reliability under Fatigue Degradation. (Dr.Ing. Thesis)
MTA-91-84 Krokstad, Jørgen R., MH:	Second-order Loads in Multidirectional Seas. (Dr.Ing. Thesis)
MTA-91-85 Molteberg, Gunnar A., MM:	The Application of System Identification Techniques to Performance Monitoring of Four Stroke Turbocharged Diesel Engines. (Dr.Ing. Thesis)
MTA-92-86 Mørch, Hans Jørgen Bjelke, MH:	Aspects of Hydrofoil Design: with Emphasis on Hydrofoil Interaction in Calm Water. (Dr.Ing. Thesis)
MTA-92-87 Chan Siu Hung, MM:	Nonlinear Analysis of Rotordynamic Instabilities in High-speed Turbomachinery. (Dr.Ing. Thesis)
MTA-92-88 Bessason, Bjarni, MK:	Assessment of Earthquake Loading and Response of Seismically Isolated Bridges. (Dr.Ing. Thesis)
MTA-92-89 Langli, Geir, MP:	Improving Operational Safety through exploitation of Design Knowledge - an investigation of offshore platform safety. (Dr.Ing. Thesis)
MTA-92-90 Sævik, Svein, MK:	On Stresses and Fatigue in Flexible Pipes. (Dr.Ing. Thesis)
MTA-92-91 Ask, Tor Ø., MM:	Ignition and Flame Growth in Lean Gas-Air Mixtures. An Experimental Study with a Schlieren System. (Dr.Ing. Thesis)
MTA-86-92 Hessen, Gunnar, MK:	Fracture Mechanics Analysis of Stiffened Tubular Members. (Dr.Ing. Thesis)
MTA-93-93 Steinebach, Christian, MM:	Knowledge Based Systems for Diagnosis of Rotating Machinery. (Dr.Ing. Thesis)

MTA-93-94 Dalane, Jan Inge, MK:	System Reliability in Design and Maintenance of Fixed Offshore Structures. (Dr.Ing. Thesis)
MTA-93-95 Steen, Sverre, MH:	Cobblestone Effect on SES. (Dr.Ing. Thesis)
MTA-93-96 Karunakaran, Daniel, MK:	Nonlinear Dynamic Response and Reliability Analysis of Drag-dominated Offshore Platforms. (Dr.Ing. Thesis)
MTA-93-97 Hagen, Arnulf, MP:	The Framework of a Design Process Language. (Dr.Ing. Thesis)
MTA-93-98 Nordrik, Rune, MM:	Investigation of Spark Ignition and Autoignition in Methane and Air Using Computational Fluid Dynamics and Chemical Reaction Kinetics. A Numerical Study of Ignition Processes in Internal Combustion Engines. (Dr.Ing. Thesis)
MTA-94-99 Passano, Elizabeth, MK:	Efficient Analysis of Nonlinear Slender Marine Structures. (Dr.Ing. Thesis)
MTA-94-100 Kvålsvold, Jan, MH:	Hydroelastic Modelling of Wetdeck Slamming on Multihull Vessels. (Dr.Ing. Thesis)
MTA-94-102 Bech, Sidsel M., MK:	Experimental and Numerical Determination of Stiffness and Strength of GRP/PVC Sandwich Structures. (Dr.Ing. Thesis)
MTA-95-103 Paulsen, Hallvard, MM:	A Study of Transient Jet and Spray using a Schlieren Method and Digital Image Processing. (Dr.Ing. Thesis)
MTA-95-104 Hovde, Geir Olav, MK:	Fatigue and Overload Reliability of Offshore Structural Systems, Considering the Effect of Inspection and Repair. (Dr.Ing. Thesis)
MTA-95-105 Wang, Xiaozhi, MK:	Reliability Analysis of Production Ships with Emphasis on Load Combination and Ultimate Strength. (Dr.Ing. Thesis)
MTA-95-106 Ulstein, Tore, MH:	Nonlinear Effects of a Flexible Stern Seal Bag on Cobblestone Oscillations of an SES. (Dr.Ing. Thesis)
MTA-95-107 Solaas, Frøydis, MH:	Analytical and Numerical Studies of Sloshing in Tanks. (Dr.Ing. Thesis)
MTA-95-108 Hellan, øyvind, MK:	Nonlinear Pushover and Cyclic Analyses in Ultimate Limit State Design and Reassessment of Tubular Steel Offshore Structures. (Dr.Ing. Thesis)

MTA-95-109 Hermundstad, Ole A., MK:	Theoretical and Experimental Hydroelastic Analysis of High Speed Vessels. (Dr.Ing. Thesis)
MTA-96-110 Bratland, Anne K., MH:	Wave-Current Interaction Effects on Large-Volume Bodies in Water of Finite Depth. (Dr.Ing. Thesis)
MTA-96-111 Herfjord, Kjell, MH:	A Study of Two-dimensional Separated Flow by a Combination of the Finite Element Method and Navier-Stokes Equations. (Dr.Ing. Thesis)
MTA-96-112 Æsøy, Vilmar, MM:	Hot Surface Assisted Compression Ignition in a Direct Injection Natural Gas Engine. (Dr.Ing. Thesis)
MTA-96-113 Eknes, Monika L., MK:	Escalation Scenarios Initiated by Gas Explosions on Offshore Installations. (Dr.Ing. Thesis)
MTA-96-114 Erikstad, Stein O., MP:	A Decision Support Model for Preliminary Ship Design. (Dr.Ing. Thesis)
MTA-96-115 Pedersen, Egil, MH:	A Nautical Study of Towed Marine Seismic Streamer Cable Configurations. (Dr.Ing. Thesis)
MTA-97-116 Moksnes, Paul O., MM:	Modelling Two-Phase Thermo-Fluid Systems Using Bond Graphs. (Dr.Ing. Thesis)
MTA-97-117 Halse, Karl H., MK:	On Vortex Shedding and Prediction of Vortex-Induced Vibrations of Circular Cylinders. (Dr.Ing. Thesis)
MTA-97-118 Igland, Ragnar T., MK:	Reliability Analysis of Pipelines during Laying, considering Ultimate Strength under Combined Loads. (Dr.Ing. Thesis)
MTA-97-119 Pedersen, Hans-P., MP:	Levendefiskteknologi for fiskefartøy. (Dr.Ing. Thesis)
MTA-98-120 Vikestad, Kyrre, MK:	Multi-Frequency Response of a Cylinder Subjected to Vortex Shedding and Support Motions. (Dr.Ing. Thesis)
MTA-98-121 Azadi, Mohammad R. E., MK:	Analysis of Static and Dynamic Pile-Soil-Jacket Behaviour. (Dr.Ing. Thesis)
MTA-98-122 Ulltang, Terje, MP:	A Communication Model for Product Information. (Dr.Ing. Thesis)
MTA-98-123 Torbergsen, Erik, MM:	Impeller/Diffuser Interaction Forces in Centrifugal Pumps. (Dr.Ing. Thesis)

MTA-98-124 Hansen, Edmond, MH:	A Discrete Element Model to Study Marginal Ice Zone Dynamics and the Behaviour of Vessels Moored in Broken Ice. (Dr.Ing. Thesis)
MTA-98-125 Videiro, Paulo M., MK:	Reliability Based Design of Marine Structures. (Dr.Ing. Thesis)
MTA-99-126 Mainçon, Philippe, MK:	Fatigue Reliability of Long Welds Application to Titanium Risers. (Dr.Ing. Thesis)
MTA-99-127 Haugen, Elin M., MH:	Hydroelastic Analysis of Slamming on Stiffened Plates with Application to Catamaran Wetdecks. (Dr.Ing. Thesis)
MTA-99-128 Langhelle, Nina K., MK:	Experimental Validation and Calibration of Nonlinear Finite Element Models for Use in Design of Aluminium Structures Exposed to Fire. (Dr.Ing. Thesis)
MTA-99-129 Berstad, Are J., MK:	Calculation of Fatigue Damage in Ship Structures. (Dr.Ing. Thesis)
MTA-99-130 Andersen, Trond M., MM:	Short Term Maintenance Planning. (Dr.Ing. Thesis)
MTA-99-131 Tveiten, Bård Wathne, MK:	Fatigue Assessment of Welded Aluminium Ship Details. (Dr.Ing. Thesis)
MTA-99-132 Søreide, Fredrik, MP:	Applications of underwater technology in deep water archaeology. Principles and practice. (Dr.Ing. Thesis)
MTA-99-133 Tønnessen, Rune, MH:	A Finite Element Method Applied to Unsteady Viscous Flow Around 2D Blunt Bodies With Sharp Corners. (Dr.Ing. Thesis)
MTA-99-134 Elvekrok, Dag R., MP:	Engineering Integration in Field Development Projects in the Norwegian Oil and Gas Industry. The Supplier Management of Norne. (Dr.Ing. Thesis)
MTA-99-135 Fagerholt, Kjetil, MP:	Optimeringsbaserte Metoder for Ruteplanlegging innen skipsfart. (Dr.Ing. Thesis)
MTA-99-136 Bysveen, Marie, MM:	Visualization in Two Directions on a Dynamic Combustion Rig for Studies of Fuel Quality. (Dr.Ing. Thesis)
MTA-2000-137 Storteig, Eskild, MM:	Dynamic characteristics and leakage

	performance of liquid annular seals in centrifugal pumps. (Dr.Ing. Thesis)
MTA-2000-138 Sagli, Gro, MK:	Model uncertainty and simplified estimates of long term extremes of hull girder loads in ships. (Dr.Ing. Thesis)
MTA-2000-139 Tronstad, Harald, MK:	Nonlinear analysis and design of cable net structures like fishing gear based on the finite element method. (Dr.Ing. Thesis)
MTA-2000-140 Kroneberg, André, MP:	Innovation in shipping by using scenarios. (Dr.Ing. Thesis)
MTA-2000-141 Haslum, Herbjørn Alf, MH:	Simplified methods applied to nonlinear motion of spar platforms. (Dr.Ing. Thesis)
MTA-2001-142 Samdal, Ole Johan, MM:	Modelling of Degradation Mechanisms and Stressor Interaction on Static Mechanical Equipment Residual Lifetime. (Dr.Ing. Thesis)
MTA-2001-143 Baarholm, Rolf Jarle, MH:	Theoretical and experimental studies of wave impact underneath decks of offshore platforms. (Dr.Ing. Thesis)
MTA-2001-144 Wang, Lihua, MK:	Probabilistic Analysis of Nonlinear Wave-induced Loads on Ships. (Dr.Ing. Thesis)
MTA-2001-145 Kristensen, Odd H. Holt, MK:	Ultimate Capacity of Aluminium Plates under Multiple Loads, Considering HAZ Properties. (Dr.Ing. Thesis)
MTA-2001-146 Greco, Marilena, MH:	A Two-Dimensional Study of Green-Water Loading. (Dr.Ing. Thesis)
MTA-2001-147 Heggelund, Svein E., MK:	Calculation of Global Design Loads and Load Effects in Large High Speed Catamarans. (Dr.Ing. Thesis)
MTA-2001-148 Babalola, Olusegun T., MK:	Fatigue Strength of Titanium Risers - Defect Sensitivity. (Dr.Ing. Thesis)
MTA-2001-149 Mohammed, Abuu K., MK:	Nonlinear Shell Finite Elements for Ultimate Strength and Collapse Analysis of Ship Structures. (Dr.Ing. Thesis)
MTA-2002-150 Holmedal, Lars E., MH:	Wave-current interactions in the vicinity of the sea bed. (Dr.Ing. Thesis)
MTA-2002-151 Rognebakke, Olav F., MH:	Sloshing in rectangular tanks and interaction with ship motions. (Dr.Ing. Thesis)

MTA-2002-152 Lader, Pål Furset, MH:	Geometry and Kinematics of Breaking Waves. (Dr.Ing. Thesis)
MTA-2002-153 Yang, Qinzheng, MH:	Wash and wave resistance of ships in finite water depth. (Dr.Ing. Thesis)
MTA-2002-154 Melhus, Øyvin, MM:	Utilization of VOC in Diesel Engines. Ignition and combustion of VOC released by crude oil tankers. (Dr.Ing. Thesis)
MTA-2002-155 Ronæss, Marit, MH:	Wave Induced Motions of Two Ships Advancing on Parallel Course. (Dr.Ing. Thesis)
MTA-2002-156 Økland, Ole D., MK:	Numerical and experimental investigation of whipping in twin hull vessels exposed to severe wet deck slamming. (Dr.Ing. Thesis)
MTA-2002-157 Ge, Chunhua, MK:	Global Hydroelastic Response of Catamarans due to Wet Deck Slamming. (Dr.Ing. Thesis)
MTA-2002-158 Byklum, Eirik, MK:	Nonlinear Shell Finite Elements for Ultimate Strength and Collapse Analysis of Ship Structures. (Dr.Ing. Thesis)
IMT-2003-1 Chen, Haibo, MK:	Probabilistic Evaluation of FPSO-Tanker Collision in Tandem Offloading Operation. (Dr.Ing. Thesis)
IMT-2003-2 Skaugset, Kjetil Bjørn, MK:	On the Suppression of Vortex Induced Vibrations of Circular Cylinders by Radial Water Jets. (Dr.Ing. Thesis)
IMT-2003-3 Chezhian, Muthu	Three-Dimensional Analysis of Slamming. (Dr.Ing. Thesis)
IMT-2003-4 Buhaug, Øyvind	Deposit Formation on Cylinder Liner Surfaces in Medium Speed Engines. (Dr.Ing. Thesis)
IMT-2003-5 Tregde, Vidar	Aspects of Ship Design: Optimization of Aft Hull with Inverse Geometry Design. (Dr.Ing. Thesis)
IMT-2003-6 Wist, Hanne Therese	Statistical Properties of Successive Ocean Wave Parameters. (Dr.Ing. Thesis)
IMT-2004-7 Ransau, Samuel	Numerical Methods for Flows with Evolving Interfaces. (Dr.Ing. Thesis)
IMT-2004-8 Soma, Torkel	Blue-Chip or Sub-Standard. A data interrogation

	approach of identity safety characteristics of shipping organization. (Dr.Ing. Thesis)
IMT-2004-9 Ersdal, Svein	An experimental study of hydrodynamic forces on cylinders and cables in near axial flow. (Dr.Ing. Thesis)
IMT-2005-10 Brodtkorb, Per Andreas	The Probability of Occurrence of Dangerous Wave Situations at Sea. (Dr.Ing. Thesis)
IMT-2005-11 Yttervik, Rune	Ocean current variability in relation to offshore engineering. (Dr.Ing. Thesis)
IMT-2005-12 Fredheim, Arne	Current Forces on Net-Structures. (Dr.Ing. Thesis)
IMT-2005-13 Heggernes, Kjetil	Flow around marine structures. (Dr.Ing. Thesis)
IMT-2005-14 Fouques, Sebastien	Lagrangian Modelling of Ocean Surface Waves and Synthetic Aperture Radar Wave Measurements. (Dr.Ing. Thesis)
IMT-2006-15 Holm, Håvard	Numerical calculation of viscous free surface flow around marine structures. (Dr.Ing. Thesis)
IMT-2006-16 Bjørheim, Lars G.	Failure Assessment of Long Through Thickness Fatigue Cracks in Ship Hulls. (Dr.Ing. Thesis)
IMT-2006-17 Hansson, Lisbeth	Safety Management for Prevention of Occupational Accidents. (Dr.Ing. Thesis)
IMT-2006-18 Zhu, Xinying	Application of the CIP Method to Strongly Nonlinear Wave-Body Interaction Problems. (Dr.Ing. Thesis)
IMT-2006-19 Reite, Karl Johan	Modelling and Control of Trawl Systems. (Dr.Ing. Thesis)
IMT-2006-20 Smogeli, Øyvind Notland	Control of Marine Propellers. From Normal to Extreme Conditions. (Dr.Ing. Thesis)
IMT-2007-21 Storhaug, Gaute	Experimental Investigation of Wave Induced Vibrations and Their Effect on the Fatigue Loading of Ships. (Dr.Ing. Thesis)
IMT-2007-22 Sun, Hui	A Boundary Element Method Applied to Strongly Nonlinear Wave-Body Interaction Problems. (PhD Thesis, CeSOS)
IMT-2007-23 Rustad, Anne Marthine	Modelling and Control of Top Tensioned Risers. (PhD Thesis, CeSOS)

IMT-2007-24 Johansen, Vegar	Modelling flexible slender system for real-time simulations and control applications.
IMT-2007-25 Wroldsen, Anders Sunde	Modelling and control of tensegrity structures. (PhD Thesis, CeSOS)
IMT-2007-26 Aronsen, Kristoffer Høye	An experimental investigation of in-line and combined in-line and cross flow vortex induced vibrations. (Dr.avhandling, IMT)
IMT-2007-27 Zhen, Gao	Stochastic response analysis of mooring systems with emphasis on frequency-domain analysis of fatgue due to wide-band processes. (PhD-thesis CeSOS).
IMT-2007-28 Thorstensen, Tom Anders	Lifetime Profit Modelling of Ageing Systems Utilizing Information about Technical Condition. Dr.ing. thesis, IMT.
IMT-2008-39 Refsnes, Jon Erling Gorset	Nonlinear Model-Based Control of Slender Body AUVs, PhD-Thesis, IMT
IMT-2008-30 Pákozdi, Csaba	A Smoothed Particle Hydrodynamics Study of Two-dimensional Nonlinear Sloshing in Rectangular Tanks. Dr.ing.thesis, IMT.
IMT-2008-31 Berntsen, Per Ivar B.	Structural Reliability Based Position Mooring. PhD-Thesis, IMT.
IMT-2008-32 Ye, Naiquan	Fatigues Assessment of Aluminium Welded Box stiffener Joints in ships. Dr.ing.-Thesis, IMT.
IMT-2008-33 Radan, Damir	Integrated Control of Marine Electrical Power Systems. PhD-Thesis, IMT.
IMT-2008-34 Thomassen, Paul	Methods for Dynamic Response Analysis and Fatigue Life Estimation of Floating Fish Cages. PhD-thesis, IMT.